STRUCTURAL CONTROLS OF Ni-Cu-PGE ORES AND MOBILIZATION OF METALS AT THE GARSON MINE, SUDBURY

By

JOSHUA MUKWAKWAMI

Thesis submitted in partial fulfillment
of the requirements for the degree of
Doctor of Philosophy (PhD)
in
Mineral Deposits and Precambrian Geology

School of Graduate Studies
Laurentian University
Sudbury, Ontario

Abstract

The Garson Ni-Cu-PGE deposit is located on the South Range of the 1850 Ma Sudbury structure along the contact between the Sudbury Igneous Complex (SIC) and the underlying metasedimentary and metavolcanic rocks of the Paleoproterozoic Huronian Supergroup. It comprises four ore bodies that are hosted by E-W-trending shear zones that dip steeply to the south. The shear zones formed as south-directed D_1 thrusts in response to flexural-slip during regional buckling of the SIC. They imbricated the ore zones, the SIC norite, the underlying Huronian rocks and they emplaced slivers of Huronian rocks and anatectic breccia into the overlying Main Mass norite. Coexisting garnet-amphibole pairs yielded syn-D_1 amphibolite facies metamorphic temperatures ranging from ~550°C to 590°C. The shear zones were coeval with the moderately south-dipping South Range and Thayer Lindsley shear zones, which formed to accommodate the strain in the hinge zone as the SIC tightened with progressive D_1 shortening. The SE limb of the SIC was overturned together with the D_1 thrusts, which were then reactivated as steeply south-dipping reverse shear zones during syn-D_2 greenschist metamorphism. Syn-D_2 metamorphic titanite yield a U-Pb age of ca. 1849 ± 6 Ma, suggesting that D_1 and D_2 are part of a single progressive deformation event that occurred immediately after crystallization of the SIC during the Penokean Orogeny.

The ore bodies plunge steeply to the south parallel to the colinear L_1 and L_2 stretching mineral lineations. Ore types consist mainly of pyrrhotite-pentlandite-chalcopyrite breccia ores, but also include pyrrhotite-pentlandite-chalcopyrite disseminated sulfide mineralization in norite, and syn-D_2 quartz-calcite-chalcopyrite-pyrrhotite-pentlandite

veins. In the breccia ores, matrix sulfides surround silicate rock fragments that have a strong shape-preferred orientation defining a pervasive foliation. The fragments are highly stretched parallel to the mineral lineations in wall rocks, suggesting that the ore bodies are zones of high strain. Pyrrhotite and chalcopyrite occur in piercement structures, in boudin necks between fragments, in fractures in wall rocks and in fold hinges, suggesting that the sulfides were mobilized by ductile plastic flow. Despite evidence of high strain in the ore zones, the sulfide matrix in D_1 and D_2 breccia ores show little evidence of strain as they consist predominantly of polygonal pyrrhotite aggregates, suggesting that they recrystallized during, or immediately after D_1 and D_2. However, rare elongate pyrrhotite grains aligned parallel to S_2 are locally preserved only in D_2 breccia ores. Exsolution of pentlandite loops along grain boundaries of elongate pyrrhotite formed S_2-parallel pentlandite-rich layers in D_2 breccia ores, whereas the pentlandite loops are multi-oriented in D_1 contact breccia as they were exsolved along grain boundaries polygonal pyrrhotite. Because exsolution of pentlandite post-date D_1 and D_2, and that individual pentlandite grains neither have a shape-preferred orientation nor show evidence for cataclastic flow, the sulfides reverted to, and were mobilized as a homogeneous metamorphic monosulfide solid solution *(mss)* during D_1 and possibly D_2. This is in agreement with predictions from phase equilibria as the average Garson composition plots within the *mss* field in Fe-Ni-S ternary diagram at temperatures above ~400°C.

Disseminated and breccia ores at Garson have similar mantle-normalized multi-element chalcophile patterns as undeformed contact-type disseminated and massive ore,

respectively, at the well known Creighton mine in the South Range. This suggests that the Garson ores are magmatic in origin and that their compositions were not significantly altered by hydrothermal fluids and deformation. The lack of variations in Ni tenors between the disseminated and breccias ores suggest that the R-factor was not the process controlling metal tenors because the disseminated sulfides do not consistently have higher metal tenors than the breccia ore. The breccia ores are enriched in Rh-Ru-Ir and are depleted in Cu-Pd-Pt-Au, in contrast to footwall-type ore at the nearby Garson Ramp mine which is enriched in the same metals. When Ni_{100}, Rh_{100}, Ir_{100}, Pt_{100} and Pd_{100} are plotted against Cu_{100}, the breccia and footwall-type ore analyses plot along model *mss* fractionation and sulfide melt model curves, suggesting that these two ore types are related by *mss* fractionation.

In summary, the Garson breccia ores are *mss* cumulates that settled quickly at the base of the SIC via a gravity filtration process, and were mobilized as a metamorphic *mss* by ductile plastic flow during D_1 and D_2. Despite minor local hydrothermal mobilization of some metals, the study confirms findings from other studies that highly deformed Ni-Cu-PGE deposits, such as the Garson deposit, can provide important information on the genesis of the deposits.

For my wife, son, and daughter

Tendai, Emmanuel, and Deborah-Hakhesa

"….there is a friend who sticks closer than a brother." Prov. 18[24]

Acknowledgements

This research project was funded by a Vale Ltd.-Natural Sciences and Engineering Council of Canada (NSERC)-Collaborative Research and Development grant to Drs. B. Lafrance and C.M. Lesher, NSERC Discovery grants to Drs. B. Lafrance and C.M. Lesher, and a Society of Economic Geology Foundation Canada grant to J. Mukwakwami. Geochronology work was done under the Targeted Geoscience Initiative Phase 4 program of the Geological Survey of Canada led by D. Ames. Laurentian University provided a full fee waiver in my fifth year, after the expiry of my scholarship.

I am very grateful for my supervisors, Drs. B. Lafrance and C.M. Lesher, for providing me the opportunity to do this project. Their continual mentorship and intellectual insight are greatly appreciated. Our numerous discussions and allowing me the opportunity to exercise my mind helped me become a better a research geologist and scientist.

Vale Ltd. is thanked for providing access to geological data, mine exposures, and diamond drill cores. Although many individuals in Vale Ltd. have been very helpful in this project, I would like to extend special thanks to S. Lowen and D. Hodder for providing transport to and from the mine, and together with C. Gauld, S. Kedzierski, L. Desjardins, D. Butt, B. Gauvreau, D. Bellefeuille, and J. Letto, they provided logistical assistance and many beneficial discussions on the geology of the Garson Mine.

Dr. P.J. Jugo is thanked for discussions and encouragement as a member of the supervising committee during the early stages of the project. Dr. D. Burrows read the thesis and prompted some useful corrections. I benefited significantly from discussions

with members of faculty in the Geology Department at Laurentian, in particular, Drs. D.G.F. Long, D.K. Tinkham, B. Kamber, D.J. Kontak, A.M. McDonald, T. Ulrich and P.C. Thurston. Dr. H.L. Gibson is thanked for constant and persistent encouragement. Roxane and Edda are thanked for their kindness. W. Desjardins, A. Gladu, J. Byron, and W. Zhe are thanked for their technical support. The encouragement and kindness of my colleagues are sincerely appreciated. To mention a few: Claire Somers, Guillaume Perrette Mike Babachuk, Robert Lodge, Kate Rubingh, Nicholas Tonnelier, Kirk Ross, Caroline Mealin, Taus Jorgensen, Edward Nelles, Lindsay Richan, Geoffrey Baldwin, Dele Olaniyan, Craig Stewart and Fabio Cafagna. Special thanks to M. Adibpour and family for their hospitality. My first days in Canada would not have been any better without their support.

D. Crabtree, John Hechler and Sandra Clarke of the Ontario Geological Survey are thanked for helping with the microprobe and SEM analyses, and N. Rayner of the Geological Survey of Canada in Ottawa is thanked for dating my samples.

The Zimbabwean community and the Seventh Adventist Church in Sudbury were a great blessing and source of comfort for my family. I am thankful to each one of them and their families. Foremost among these are C. Nyabeze, G. Nyabeze, P. Stevens, N. Stevens, Y. Gwekwerere, E. Mbvaimbvai, M. Mbvaimbvai, A. Dune, T. Nyabeze, S. Ngindi, P. Ngindi, R. Nyereyemhuka and T. Mhende.

I am thankful to my wife, Tendai Mangure Mukwakwami for taking most of the parental care upon her shoulders during the past 5 years. Emmanuel and Deborah were so inspiring.

Table of Contents

List of Figures

List of Tables

Chapter 1: Introduction to the Thesis

1.1 Introduction

The Garson Ni-Cu-platinum group elements (PGE) mine is owned by Vale Ltd., and is located within the town limit of the city of Greater Sudbury, about 15 km SE of the city center. The mine opened in 1907 and up until the end of 2007 (the last year for which public domain information is available) had produced 57,233,535 tonnes of ore containing 763,434 tonnes of Cu and 926,868 tonnes of Ni at average grades of 1.33% Cu and 1.62% Ni.

The Garson deposit occurs on the South Range of the 1850 Ma Sudbury impact structure (Krogh, 1984), which comprises the Sudbury Igneous Complex (SIC) and radial and concentric quartz diorite dikes, underlying footwall anatectic breccias, pseudotachylitic Sudbury breccias, and overlying impact fall-back- and phreatomagmatic breccias and sedimentary rocks of the Whitewater Group (Dressler, 1984; Lightfoot et al., 1997; Ames, 1999, Grieve et al., 2010). The Sudbury structure is one of the largest Ni-Cu-PGE mining camps in the world, which has a combined past production and resources of over 1,648 million metric tons grading ~1.2 percent Ni and ~1.0 percent Cu (Naldrett and Lightfoot, 1993). Three main types of magmatic Ni-Cu-PGE mineralization are recognized in the Sudbury mining camp: (1) Fe-Ni–rich, Pt-Pd–poor contact-type mineralization that occurs within embayments along the footwall contact of the SIC, (2) Cu-Ni-Pt-Pd–rich mineralization hosted by quartz-diorite offset dikes, and (3) Cu-Ni-Pt-Pd–rich mineralization that occurs in brecciated footwall rocks below the embayments (e.g., Naldrett, 1984a, b; Farrow and Lightfoot, 2002; Ames and Farrow, 2007).

Whereas deposits in the North Range are relatively undeformed, the Garson deposit and many others in the South Range underwent at least two deformation events during which they were deformed along south-dipping shear zones (e.g., Davidson, 1948; Lochhead, 1955; Owen and Coats, 1984; Shanks and Schwerdtner, 1991a & b; Binney et al., 1994; Bailey et al., 2004, Riller, 2005 Mukwakwami et al., 2012). These deformation events resulted in folding of the SIC, overturning of the SIC in the vicinity of Garson mine, and development of the folding-induced southeast-dipping reverse shear zones, i.e., the South Range and Thayer Lindsley shear zones during the 1.9-1.8 Ga Penokean Orogeny (Shanks and Schwerdtner, 1991a, b; Riller, 2005; Riller et al., 2010). Other orogenic events such as the ca. 1.7–1.6 Ga Mazatzal-Labradorian event (Bailey et al., 2004; Piercey et al., 2007), ca. 1.4 Ga Chieflakian event (Fueten and Redmond, 1997; Szentpéteri, 2009) and ca. 1.3-1.0 Ga Grenville Orogeny (Brocoum and Dalaziel, 1974; Rivers, 1997) may have affected the Sudbury impact structure but their effects are not well understood.

1.2 Research Problems

The main research problem at Garson Mine focuses on understanding how massive Ni-Cu deposits deform and how metals/sulfides are mobilized during deformation and metamorphism. Although the Ni-Cu-(PGE) deposits formed by primary magmatic processes, post-magmatic processes such as deformation, metamorphism, and hydrothermal alteration are known to change the geometry of the ore deposits, redistribute massive sulfides within secondary structures, alter the compositions of the ores, and modify primary massive sulfide textures (e.g., Barrett et a., 1977; McQueen, 1987; Duuring et al., 2007; Almeida et al., 2007). Because the Garson ores are deformed, and because the Sudbury structure was affected by at least two post-SIC deformation events, it is important to establish the architecture, kinematics, and relative timing of the shear zones in order to determine how these shear zones affected the primary magmatic Ni-Cu-(PGE) mineralization at the mine. Understanding the structures at the mine is paramount in constraining the timing of sulfide/metal mobilization, because sulfides/metals could have been mobilized during more than one phase of deformation and metamorphism.

Although the contact-type, footwall-type, and offset-type deposits associated with the SIC have been the subjects of many publications and are reasonably well understood, the mechanisms that produced the deformed contact ores and how the various metals fractionated during deformation and metamorphism are less well understood. Bailey et al. (2006) have shown that Ni was mobilized during amphibolite-grade metamorphism at the Thayer Lindsley mine, which is located ~10 km west of the Garson Mine, but no observation or data were provided on the mobility of other metals. Several mine levels (4800, 4900, 5000 and 5100 ft levels) at Garson were active at the timing of mapping, which provided access to excellent exposures of the geology, ore, and structures that are essential for characterizing the mineralogy, texture and geochemistry of the deformed ores and addressing processes of sulfide mobilization (magmatic vs. mechanical vs. metamorphic-hydrothermal).

1.3 Objectives of the Thesis

The objectives of the thesis are to:

- Present a structural interpretation of the Garson mine at the mine scale and regional tectonic scale.
- Determine the relative importance of partial melting versus mechanical and hydrothermal mobilization of metals and sulfides during deformation of the ore zones.
- Characterize the effect of mobilization processes on the geochemistry of the deposit.
- Constrain the absolute timing of deformation and sulfide mobilization.
- Determine the structural and lithological controls on Ni-Cu-PGE mineralization at the Garson Mine and implications for ongoing exploration at the mine and in the South Range of the Sudbury structure.

1.4 Methodology

In order to achieve the above objectives, the following methods were used.

1.4.1 Underground Mapping

Accessible underground exposures on the 3560, 4800, 4900, 5000, and 5100 levels were mapped at a mine scale of 1″ to 20′ between July 2007 and May 2009 for a total of 157 days. This was done to determine the relative timing and kinematics of the shear zones, and the effects of these structures on the ore zones. An additional 6 days were spent doing some follow-up underground work between January and March, 2010. Two days were spent on surface outcrops. Oriented samples were collected to further characterize the kinematics of the shear zones, their metamorphic evolution and microstructures of the ore zones. The mapping was complemented by compilation of existing underground maps, sections, and drill core logs. Microprobe analysis of amphibole, plagioclase, ilmenite, epidote and garnet (Appendices A-E) were done at the Ontario Geoscience Laboratories to constrain the temperatures of sulfide mobilization. Two hundred and thirty-nine thin sections from ore and rock samples were examined, including 19 thin sections of metabreccia obtained from Vale Ltd.

1.4.2 Geochemical Studies

Sixty-five representative samples of all the mineralization types and 9 samples of unmineralized rocks were collected for whole-rock major and trace element geochemical analysis. The analyses (Appendix G) were done at the Ontario Geoscience Laboratories and the analytical methods are described in the manuscripts. Complete geochemical data with precision and accuracy values for individual elements are given in electronic Appendix H (mineralized samples) and electronic Appendix I (unmineralized samples). Where available, the ore geochemical data were complimented by data from the mine database.

1.4.3 Geochronology

Two gabbro samples and one SIC norite sample were collected from D_2 shear zones for geochronology. The candidate established the structural setting of titanite, crushed and pulverized the samples. Titanite analyses were obtained using a Zeiss EVO-50 SEM equipped with EDS detectors in the Ontario Geoscience Laboratories in Sudbury

(Appendix F). Mineral separation and preliminary ID-TIMS U-Pb titanite dating were done by N. Rayner at the Geological Survey of Canada in Ottawa.

1.5 Structure of the Thesis

The thesis comprises an introductory chapter (Chapter 1), three self-contained manuscripts (Chapters 2, 3 and 4) already published or ready for publication in peer-reviewed scientific journals, and a concluding chapter (Chapter 5). Chapters 2-4 overlap, to some degree, so that they can be published as stand-alone individual journal manuscripts. Chapter 1 introduces the reader to the research problems, the objectives of the research and the methods used to achieve those objectives.

Chapter 2 is written as a manuscript entitled "Back-thrusting and Overturning of the Southern Margin of the 1.85 Ga Sudbury Igneous Complex at the Garson Mine, Sudbury, Ontario" (published 2012, Precambrian Research 196–197, 81–105). It provides the first comprehensive description of the main rock types at the mine, the mesoscopic and microscopic fabrics of two major deformation events (D_1 and D_2) in the shear zones. A working mine-scale model is presented to explain the effects of deformation on the current geometry of the ore bodies at the mine. As the Garson shear zones have similar amphibolite-grade fabrics but opposite senses of shear to the contiguous Thayer Lindsley and South Range shear zones, a regional model was proposed in which the Garson shear zones are interpreted as south-directed back-thrusts that formed during the same orogenic event, the 1.7-1.6 Ga Mazatzal-Labradorian Orogeny of Bailey et al. (2004).

Chapter 3 is written as a manuscript entitled "Fabrics and Textures of Deformed and Metamorphosed Ni-Cu-PGE Sulfide Ores at Garson Mine and their Implications for Sulfide Mobilization Processes." The manuscript is to be submitted to *Mineralium Depo*sita. It presents the first Penokean U-Pb titanite ages from shear zones at the base of the SIC, the first temperature estimates for post-impact syn-D_1 amphibolite facies metamorphism in the South Range using the average T method (Holland and Blundy, 1994) and the Fe-Mg exchange (Ravna, 2000) geothermometers for coexisting garnet-amphibole pairs in metabasalt, and a detailed description of the major sulfide mineralogy, textures and internal meso- and microscopic fabrics within the main ore zones. In addition, microstructures in quartz are used to constrain syn-D_2 greenschist facies metamorphic temperatures. Together with phase equilibria considerations, they form the basis for evaluating the significance of the three mechanisms of sulfide mobilization: ductile plastic flow, partial metamorphic anatexis of the ore zones, and metamorphic hydrothermal mobilization (e.g., Cox, 1987; Marshall and Gilligan, 1987; Tomkins et al., 1987).

Remark: In Chapter 2 (Mukwakwami et al., 2012), D1 occurred during the 1.7-1.6 Ga Mazatzal-Labradorian Orogeny as explained above. However, ID-TIMS U-Pb metamorphic titanite data, presented in chapter 3, constrain D_2 to 1849 ± 0.6 Ma, suggesting that D_1 and D_2 are part of a progressive Penokean deformation event that occurred immediately after crystallization of the SIC. The discrepancy in the timing of D_1 in the 2 manuscripts arose because the U-Pb titanite ages were only obtained after the first paper (Mukwakwami et al., 2012) had been published. Funds for geochronology became available later, through a TGI grant to D. Ames.

Chapter 4 is written as a manuscript entitled “Geochemistry of Deformed Magmatic Ni-Cu-PGE Ore at Garson Mine, Sudbury, Ontario.” The manuscript focuses on the geochemistry of the deformed pyrrhotite-pentlandite-chalcopyrite disseminated/breccia ores and hydrothermal quartz-calcite-sulfide veins at the Garson mine, as well as chalcopyrite-pyrrhotite-pentlandite footwall-type ore at the adjacent Garson Ramp mine. The geochemistry of the disseminated and breccia ores are compared to that of undeformed disseminated and contact-type massive sulfide ores at Creighton. As the ores from the two deposits show similar multi-element chalcophile element patterns, the disseminated and breccia ores at Garson are interpreted to have a magmatic origin, i.e., they were not mobilized by hydrothermal fluids. The breccia ores are enriched in Ir-Ru-Rh and depleted in Cu-Pt-Pd-Au, which are depleted and enriched, respectively, in footwall-type ores. The breccia ores are interpreted as monosulfide solid solution cumulates that are related to the footwall-type ore by fractional crystallization.

Chapter 5 presents the overall conclusions of the research project.

1.6 Statement of Original Contributions

The candidate did the underground mapping, collected the ore samples, characterized their microstructures, did the microprobe mineral analyses, submitted samples for whole rock geochemistry, interpreted all the data, and wrote the three manuscripts. B. Lafrance and C.M. Lesher supervised all aspects of the projects and they edited the manuscripts and the thesis. Dave Crabtree assisted with electron probe microanalyses, and John Hechler and Sandra Clarke assisted with the SEM work. Discussions with D. Kontak helped towards establishing the structural setting of titanite. D.K. Tinkham performed the geothermometric calculations using the average T method and provided guidance in all the geothermometric calculations. N. Rayner did the mineral separation and the ID-TIMS U-Pb dating of metamorphic titanite. The geochronology work was done under the Targeted Geoscience Initiative Phase 4 program of the Geological Survey of Canada led by D. Ames.

Chapter 2: Back-Thrusting and Overturning of the Southern Margin of the 1.85 Ga Sudbury Igneous Complex at the Garson Mine, Sudbury, Ontario

JOSHUA MUKWAKWAMI, BRUNO LAFRANCE and C. MICHAEL LESHER

Mineral Exploration Research Centre, Department of Earth Sciences, Laurentian University, 933 Ramsey Lake Road, Sudbury, Ontario P3E 2C6, Canada

2.1 Abstract

The Garson deposit is one of several deformed magmatic Ni-Cu-platinum group element (PGE) deposits in the South Range of the 1.85 Ga Sudbury structure. The deposits occur along the southeast limb of the folded Sudbury Igneous Complex (SIC), at the contact between the SIC basal norite and underlying Paleoproterozoic metabasalt and metasedimentary rocks of the Huronian Supergroup. At the Garson deposit inclusion-rich breccia and disseminated Ni-Cu-PGE sulfide ores are hosted by steeply south-dipping shear zones and splays that underwent two major ductile deformation events (D_1 and D_2). D_1 is characterized by a steeply, south-dipping, S_1 foliation and a down-dip L_1 mineral stretching lineation defined by ferrotschermakite in metabasalt and by magnesiohornblende in norite. Coexisting ferrotschermakite and oligoclase in metabasalt indicate amphibolite facies conditions during D_1. The shear zones formed along or near the SIC-Huronian contact during the 1.7-1.6 Ga Mazatzal-Labradorian Orogeny. They formed as layer-parallel, north-dipping, north-over-south thrusts in response to flexural

slip during buckling of the SIC. As the general transport direction was from south to north during the Mazatzal-Labradorian Orogeny, the D_1 shear zones are back-thrusts with opposite transport direction. The thrusts imbricated the SIC, underlying Huronian rocks, and ore zones, and emplaced slivers of Huronian rocks into the overlying norite. In contrast to the D_1 shear zones at Garson, the Thayer Lindsley and the regional South Range shear zones, which transgress the SIC-Huronian contact at a high angle, formed as moderately SE-dipping reverse shear zones as a result of localization of folding-induced strain near the hinge zone in order to accommodate further flattening and tightening of the SIC with progressive D_1 shortening. Together with the southeast limb of the SIC, the D_1 shear zones were overturned into their present steep southerly dips and were reactivated as south-over-north shear zones either later during the Mazatzal-Labradorian Orogeny or during the 1.5-1.45 Ga Chieflakian event, which was coeval with accretion of juvenile Andean-style, calc-alkaline magmatic arcs along the entire southeastern margin of Laurentia. During this D_2 reactivation event, S_1 was transposed and locally preserved in crenulations bounded by a S_2 chloritic shear foliation, which has a strong down-dip L_2 mineral chlorite lineation and parallel L_2 ductile slickenlines.

2.2 Introduction

The ca. 1850 Ma Sudbury structure (Krogh et al., 1984) is one of the oldest, largest, and best-exposed terrestrial impact structures, containing an entire stratigraphic section of impactites including shocked and melted basement rocks overlain by an impact melt sheet, and post-impact sedimentary rocks (Fig. 2.1; see reviews by Farrow and Lightfoot, 2002; Ames and Farrow, 2007; Grieve et al., 2008). The Garson deposit, located along the SE margin of the structure, is one of many magmatic Ni-Cu-PGE deposits that formed along the basal contact of the impact melt sheet. However, after cooling and crystallization of the melt sheet, the deposit and many other footwall contact deposits in the South Range (e.g., Falconbridge, East mine and Thayer Lindsley) were offset and deformed by shear zones that transect the South Range (Fig. 2.2: e.g., Davidson, 1948; Lochhead, 1955; Owen and Coats, 1984; Binney et al., 1994; Bailey et al., 2004; Ames and Farrow 2007).

Despite several decades of mining and research on Ni-Cu PGE deposits in the South Range, the effects of deformation on the distribution of the ores in the deposits remain poorly understood. Three models have been proposed to explain the deformation and distribution of ores in the South Range: 1) injection of sulfide melt into pre-existing faults prior to solidification of the SIC (Lochhead, 1955; Lee and Siddorn, 2006; Siddorn and Ham, 2006), 2) south-over-north faulting of S-dipping ore-bearing contacts (Binney et al., 1994; Bailey et al., 2004), and 3) north-over-south thrusting of N-dipping ore-bearing contacts followed by rotation and S-directed reverse faulting (Davidson, 1948; Lee and Siddorn, 2006; Siddorn and Ham, 2006; Snelling, 2009). These models have important implications for exploration not only on mine-scale, but for the entire South Range. In order to understand the effects of deformation on the Garson deposit and test these models, we compiled all existing geological information for the mine, mapped all exposures of the #1 and # 4 shear zones on the 3560, 4800, 4900, 5000, and 5100 levels, and examined selected samples in thin section to establish their structural and metamorphic history. These data form the basis for a structural interpretation of the

Garson deposit. Our results suggest that the ore zones, SIC norite, and underlying Huronian rocks were imbricated along shear zones that formed as back-thrusts in response to south-directed flexural slip during regional folding of the Sudbury structure during the 1.7-1.6 Ga Mazatzal-Labradorian Orogeny, that the contact was overturned, and that the shear zones were later reactivated as high angle reverse, south-over-north shear zones during the Mazatzal-Labradorian or the Chieflakian orogenies. Our model for the Garson mine shows that progressive folding of a large igneous complex such as the SIC can produce back-thrusts by flexural slip adjacent to the contact between the complex and the surrounding country rocks and that the back-thrusts can imbricate the base of the igneous complex.

2.3 Geological Setting

The Sudbury structure formed as a circular ~150-250 km peak-ring impact structure, which was flattened during subsequent orogenic events and eroded during the Pleistocene glaciation (see review by Grieve et al., 2008). The current 60 by 30 km elliptical structure exposure straddles the boundary between the Archean Superior Province and the Paleoproterozoic Southern Province, and is bordered by the Grenville Province, south of Sudbury (Fig. 2.1). The Sudbury structure comprises the 2.5 - 3 km thick layered SIC and associated radial and concentric quartz dioritic 'offset' dikes, underlying anatectic footwall breccias and pseudotachylitic Sudbury breccias, and overlying Whitewater Group (Dressler, 1984; Lightfoot et al., 1997; Ames et al., 2002; Ames and Farrow, 2007). Whereas the northern and eastern portions of the SIC overlie granitic, gneissic, and granulitic basement rocks of the Superior Province, the southern portion overlies metasedimentary supracrustal and metavolcanic rocks of the Huronian Supergroup of the Southern Province (Fig. 2.1).

The SIC consists of a layered body of norite, quartz gabbro, and granophyre, called the Main Mass, underlain by a discontinuous lower layer, the Sublayer norite, which is present within footwall embayment structures at the base of the SIC and within the 'throats' of radial offset dikes that extend from embayment structures (Fig. 2.2; Lightfoot et al., 2001). The ores formed at a relatively early stage during the cooling and crystallization history of the SIC (Lightfoot et al., 2001; Keays and Lightfoot, 2004) and occur as disseminations in Sublayer, as semi-massive to massive accumulations in Sublayer, and in brecciated and partially-melted rocks underlying the SIC (footwall breccia, metabreccia) along the base of the SIC ('contact ores'). They also occur as veins in underlying Sudbury Breccias ('footwall ores') and as disseminations and semi-massive to massive accumulations in quartz diorite offset dikes ('offset ores'). The SIC is overlain by the Onaping Formation, which was initially deposited as a ~200m thick sequence of suevitic and fallback breccias (Peredery, 1972) and which continued to grow through explosive phreatomagmatic fragmentation of the impact melt sheet caused by the infiltration of sea water from a shallow ocean that covered the impact structure (Ames, 1999; Ames et al., 2002; Grieve et al., 2010). Post-impact marine sedimentation buried the Onaping Formation under a blanket of calcareous argillite and siltstone of the Onwatin Formation and turbiditic sandstone of the Chelmsford Formation (Long, 2004; Ames et al., 2006).

The rocks of the Southern Province were affected by the pre-impact ~2.4-2.2 Ga Blezardian Orogeny (Stockwell, 1982; Riller and Schwerdtner, 1997), the pre- to post-impact 1.89-1.83 Ga Penokean Orogeny (Sims et al., 1989), the post-impact 1.7-1.6 Ga Mazatzal-Labradorian Orogeny (Bailey et al., 2004; Piercey et al., 2007), the 1.45 Chieflakian event (Fueten and Redmond, 1997; Szentpéteri, 2009), and the 1.2-1.0 Ga Grenvillian Orogeny (Rivers, 1997). The effects of each of these orogenies on the 1.85 Ga SIC remain a subject of controversy due to the paucity of geochronological constraints on the timing of deformation and metamorphism. Overprinting of major regional folds in the Southern Province by ~2.2 Ga Nipissing diabase intrusions (Card et al., 1972, 1984; U-Pb age by Corfu and Andrews, 1986) suggests that the pre-impact Blezardian deformation of the South Range occurred between ~2.4 Ga, the depositional age of the rhyolitic Copper Cliff Formation of the Huronian Supergroup of the Southern Province (Krogh et al., 1984), and 2.2 Ga, the age of the crosscutting Nipissing intrusions. Changes from the assumed original circular shape of the Sudbury structure (Grieve et al., 1991) to its current elliptical geometry has been largely attributed to folding and displacement along the moderately southeast-dipping, reverse South Range Shear Zone during the Penokean Orogeny (Fig. 2.2: Shanks and Schwerdtner, 1991a, b; Milkereit et al., 1992, Cowan and Schwerdtner, 1994; Boerner and Milkereit, 1999; Cowan et al., 1999, Riller et al., 2010). This deformation also resulted in intrafolding of the Whitewater Group over the SIC, steepening of the SIC in the South Range, and overturning of the SIC in the vicinity of the Garson Mine (Milkereit et al., 1992, Cowan and Schwerdtner 1994; Szabó and Halls, 2006; Klimczak et al., 2007).

Penokean tectonism at its type locality in the southern Lake Superior region of Wisconsin, Minnesota, and Michigan was associated with the development of nappes and overthrusts and is well-constrained between 1.89 Ga and 1.83 Ga by the emplacement of voluminous suites of syn- and post-tectonic igneous rocks in the Wisconsin magmatic terrane (Sims et al., 1989). Evidence for magmatism at 1.9 Ga in the Sudbury region has only been inferred from Nd model ages of rocks of the Grenville Province (Dickin and McNutt, 1989), but geochronologic data do not provide conclusive evidence for the presence of a Proterozoic juvenile arc terrane or a crustal suture zone of Penokean age (Davidson et al., 1992; Riller et al., 1999; Piercey et al., 2007; Carr et al., 2000).

Davidson et al. (1992) questioned the validity of attributing post-impact deformation in the South Range to the Penokean Orogeny because Rb-Sr and K-Ar metamorphic ages cluster around 1.75-1.70 Ga and are therefore younger than the Penokean Orogeny. These metamorphic ages are coeval with widespread magmatism in the Southern Province and the adjacent Grenville Province, and are closer in age to the accretion of juvenile Andean-style, calc-alkaline magmatic arcs along the southeastern margin of Laurentia during the 1.71-1.61 Ga Yavapai and Mazatzal Orogenies (Davidson et al., 1992; Rivers, 1997; Carr et al., 2000). This led Davidson et al. (1992) to suggest that major deformation, magmatism, and metamorphism in the Southern Province in Ontario occurred during the Yavapai and Mazatzal orogenies. Recently, a syn-deformation, U-Pb zircon age of 1658 ± 68 Ma was reported for a south-dipping reverse shear zone within the SIC at the Thayer Lindsley mine (Bailey et al., 2004). Because the Thayer Lindsley shear zone has similar orientation, amphibolite-grade fabrics, and sense of displacement as the South Range shear zone (Fig. 2.2), they suggested that the two shear zones are coeval and that they formed during a single episode of southeast-over-northwest thrusting that was synchronous with the Mazatzal Orogeny in the southwest USA (Van Schmus et al., 1993) and the Labradorian Orogeny in Labrador (Rivers, 1997).

Fueten and Redmond (1997) mapped southeast-dipping reverse shear zones that cut the Chief Lake Complex, which is a multi-phase intrusive complex containing both ~1750 Ma and ~1460 Ma felsic intrusions (Sullivan and Davidson, 1993; Davidson and van Breemen, 1994; Krogh, 1994) along the Grenville Front Tectonic Zone immediately south of Sudbury (Fig. 2.1). They constrained the age of these shear zones to 1453 to 1445 Ma and suggested that this ca. 1.45 Ga orogenic event, later called the Chieflakian event (Corfu and Easton, 2000), also affected the Southern Province and was likely coeval with large-scale thrusting across the South Range Shear Zone. Their study, however, predated that of Bailey et al. (2004) who obtained an age of ca. 1658 Ma for southeast-over-northwest reverse faulting in the South Range. More recently, Szentpéteri (2009) reported 1450-1480 Ma K/Ar and $^{40}Ar/^{39}Ar$ biotite/muscovite ages for chlorite-rich, S to SE-dipping reverse shear zones in the vicinity of the Victoria mine (Fig. 2.2). The shear zones are sub-parallel to and merge with the South Range Shear Zone, suggesting that they may be peripheral segments of the South Range Shear Zone, and hence, that major deformation in the South Range of the SIC was synchronous with the 1.45 Ga Chieflakian event (Szentpéteri, 2009). However, they may also reflect resetting of the K/Ar and $^{40}Ar/^{39}Ar$ isotope systems during post-orogenic cooling of the South Range, as observed at the Thayer Lindsley shear zone (Bailey et al., 2004) or they may reflect the effect of ca. 1.5-1.45 Ga felsic magmatism, which was widespread across the Southern and Grenville provinces (Davidson et al., 1992; Krogh, 1994; Rivers 1997; Bailey et al, 2004, Piercey et al., 2007). This magmatism occurred during ca. 1.5-1.45 Ga arc accretion in the Pinware Terrane of the Grenville Province in SE Labrador (Davidson et al., 1992; Tucker and Gower, 1994; Rivers, 1997; Wasteneys et al., 1997) and in southwestern USA (Bowring and Karlstrom, 1990; Read et al., 1999), suggesting the existence of an Andean-type magmatic arc along the full length of the southern seaboard of Laurentia between 1.5 and 1.45 Ga (Rivers, 1997).

The 1.2-1.0 Ga Grenville Orogeny is the youngest major tectonic event in the Sudbury area. It is characterized by polyphase deformation, intense metamorphism, and voluminous magmatic activity. Despite its proximity to the Grenville Front Tectonic Zone, the SIC and its Ni-Cu-PGE deposits have not been affected by the Grenville Orogeny (Brocoum and Dalaziel, 1974; Boerner and Milkereit, 1999). Unstrained olivine diabase dikes of the ~1240 Ma Sudbury swarm (Krogh et al., 1987; Dudás et al., 1994) transect major shear zones overprinting the SIC, but are truncated at the Grenville Front (Bethune, 1997), suggesting that the SIC did not undergo major deformation after ~1240 Ma. Furthermore, the magnetic remanence acquired by the Huronian Supergroup and younger dykes during the Grenville Orogeny does not extend beyond 2-8 km north of the Grenville Front (Palmer et al., 1977, Stupavsky and Symons, 1982), well south of the SIC, which is located at least 8 km north of the front. This suggests that the Grenville Orogeny had minimal or no effect on the shape, deformation, and metamorphism of the SIC and its deposits (Szabó and Halls, 2006).

The SIC is cut by brittle, NW to NNW-trending, steeply-dipping Neotectonic faults of the Onaping set (Fig. 2.2), which include the Fecunis Lake and the Sandcherry Creek faults that sinistrally displaced the SIC-basement contact in the North Range (Fig. 2.2: Rousell, 1984; Coats and Snajdr, 1984; Buchan and Ernst, 1993). These faults host 5-13 Ma (Rb-Sr) galena-sphalerite-calcite-quartz-chlorite veins (Marshal et al. 1999), indicating hydrothermal activity as young as the Miocene in Sudbury.

2.4 Geology of the Garson Mine

In 100 years of mining (1907-2007, currently operating), the Garson deposit produced 57,233,535 tonnes of ore containing 763,434 tonnes of Cu and 926,868 tonnes of Ni at average grades of 1.33% Cu and 1.62% Ni. Mine level maps and cross sections were originally done in feet, and for consistency, mine level maps will be referred by their depth in feet from surface (e.g., 4000 level).

The deposit occurs at the contact between the SIC and the Paleoproterozoic Elsie Mountain Formation of the Elliot Lake Group of the Huronian Supergroup (Young et al., 2001; Long, 2004; Ames, 2005). The Elsie Mountain Formation is locally brecciated into an up to 65m thick unit called metabreccia next to this contact above the 4000 level. The SIC-Huronian contact at Garson is overturned, dips steeply (73-88°) to the south (Fig. 2.4) and is sheared for a strike distance and depth of at least 2 km (Cochrane, 1991) and 1.6 km, respectively. The Elsie Mountain Formation consists mostly of metabasalt that is flanked by pelitic schist to the south (Figs. 2.3a-d, 2.4). Whereas the pelitic schist is thinly-laminated, metabasalt is generally massive, but is penetratively foliated along the margins of ore bodies and at the contact with the SIC. The metabasalt is interleaved with minor lenses of metawacke, pelitic schists and quartzite that trend east-west and dip steeply to the south, parallel to sub-parallel to the SIC-Huronian contact (Figs. 2.3a-d, 2.4). Norite is the main SIC unit at the mine. It is generally massive, but is strongly foliated near its contact with metabasalt and metasedimentary rocks of the Elsie Mountain Formation. Lenses of norite locally occur along the #4 shear zone.

The deposit comprises four principal ore zones, each coincident with shear zones, i.e., #1, #2, #3 and #4 shear zones, after which they are named (Figs. 2.3, 4). Ore zones are generally bounded by sheared wall rocks with a strongly-developed schistose foliation that laterally extends over ~50 cm to ~5m into the wall rocks. The #1 shear zone occurs along the sheared contact between basement rocks and either the SIC norite or metabreccia and can be traced for ~1280m down-dip from surface. Below this depth (~1220m), the #1 shear zone diverges from the sheared SIC-Huronian contact and continues into the Huronian rocks (Fig. 2.4). The #2 and #3 shear zones are splays from the #1 shear zone and they truncate the SIC norite (Figs. 2.3, 4). At surface, the #2 shear ore body occurs along the SIC-Huronian Supergroup contact near the northwestern corner of the map and extends eastwards into the Main Mass SIC norite (Fig. 2.3a). It converges and merges with the #1 shear ore body below the 1000 level. The #3 shear ore body exclusively occurs within the Main Mass SIC norite, and it can be traced from below 1600 level to above the 2800 level where it merges with the #1 shear ore body below 2200 level. The #4 shear ore body truncates the Main Mass SIC norite above the 4000 level, converges towards the #1 shear zone to within ~50m on the 4000 level, and extends into Huronian rocks below the 4000 level, where it is sub-parallel to the #1 shear ore body (Figs. 2.3c, d). Slivers of metabreccia, Huronian metabasalt and metasedimentary rocks occur in association with the #2, #3, and #4 ore bodies within the Main Mass SIC norite. The slivers trend east-west parallel to sub-parallel to the SIC-Huronian contact.

2.4.1 Description of Rock Types

In hand specimen, *metabasalt* is composed of prismatic black amphibole grains that are up to 3 mm in length and are embedded in a medium to dark green, fine to very fine-grained matrix of amphibole-quartz-biotite-plagioclase-ilmenite ± garnet. Two generations of amphiboles with different textures and compositions are present: 1) large black prismatic magnesiohornblende that is brown in thin section and locally occurs as veinlets in massive metabasalt, and 2) optically continuous, strongly pleochroic blue-green ferrotschermakite that occurs as rims on brown magnesiohornblende (Figs. 2.5a, 2.6a) and as elongated grains coexisting with very small (<0.5 mm) plagioclase grains of oligoclase composition (Fig. 2.5b). Small (~1mm) twinned plagioclase porphyroclasts are rare in the rock matrix.

Metawacke is massive, fine-grained, and dark gray in hand specimen. It consists of 60-70% quartz, 10-20% plagioclase, and 15-25% blue-green ferrotschermakite (Fig. 2.6b) intergrown with biotite. Quartz grains have sutured grain boundaries and locally exhibit undulose optical extinction and subgrains. *Pelitic schist* is medium gray in color, very fine-grained, and consists primarily of muscovite and quartz with < 5% biotite and chlorite, defining a schistose foliation.

Metabreccia is not exposed in the current mine workings. Thin sections obtained from Vale archives show that metabreccia consists of euhedral plagioclase laths, quartz, amphibole, biotite, and accessory titanite. It has a meta-igneous texture characterized by a poikilitic texture, in which large quartz grains enclose numerous plagioclase laths and amphibole (Fig. 2.6c), similar to that of footwall breccia in contact with the SIC in the North Range (Lakomy, 1990; McCormick et al., 2002). The similar textures, together with the location of metabreccia near the base of the SIC at Garson mine (Fig. 2.4), suggest that the metabreccia may represent an anatectic footwall breccia that formed by partial melting of the underlying Huronian rocks beneath the cooling SIC, as observed elsewhere within the Sudbury structure (e.g., Dressler 1984; Lakomy, 1990).

Main Mass norite occurs as a medium- to coarse-grained, grayish-green rock containing amphibole, biotite, plagioclase, quartz, ilmenite, chlorite, and titanite with accessory zircon and apatite (Fig. 2.6d). Plagioclase grains are up to 4 mm in length, zoned, and exhibit a brown to gray coloration, similar to South Range igneous plagioclase described by Naldrett et al. (1970). They are labradorite (An_{50-57}: Fig. 2.5b) locally rimmed by oligoclase (An_{20-23}: Fig. 2.5b). Two generations of amphiboles are present: 1) coarse (up to 3 mm) dark brown magnesiohornblende and 2) optically-continuous dark green and light green to colorless magnesiohornblende that occurs as rims around brown magnesiohornblende, as randomly oriented grains in massive norite, and as elongate neoblasts that define a foliation in foliated norite (Fig. 2.6d). The dark brown magnesiohornblende is commonly blocky and near-equant in shape and contains several inclusions of plagioclase with magmatic andesine to labradorite composition (An_{43-57}:

2.5b), suggesting that the brown amphibole is a pseudomorph of magmatic pyroxene that enclosed primary plagioclase chadacrysts. Biotite occurs in association and is commonly intergrown with green magnesiohornblende.

Olivine diabase dikes trend NW and truncate the Huronian rocks, shear zones, SIC norite, and ore bodies (Fig. 2.3b). Two types of olivine diabase dikes occur at the Garson mine: 1) thick (20-60m) equigranular dikes, and 2) thin (<1m) plagioclase-porphyritic dikes. The thick equigranular dikes are fine to medium-grained, dark gray in hand specimen, and are composed of plagioclase laths (45%) in a matrix of hourglass-zoned titanaugite (35%), olivine (15%), and magnetite (5%; Fig. 2.6e). The plagioclase-phyric dikes contain strongly-zoned, resorbed plagioclase phenocrysts (up to 10 cm wide) surrounded by an aphanitic to very fine-grained black matrix composed of titanaugite, olivine, plagioclase, and magnetite. The dikes within the ore zones are locally faulted and broken-up into discontinuous rectangular blocks and they are intensely altered to dark green and colorless amphiboles that replace olivine and titanaugite (Fig. 2.6f). The relative age relationship between the two types of diabase dikes is not known. However, as they have similar trends, mineralogy, and trace element geochemistry as the Sudbury dike swarm (Table 2.3, Fig. 2.7), which also locally contain large plagioclase phenocrysts (Bethune, 1997), the two textural types of diabase dikes at the Garson mine are interpreted as intrusions of the Sudbury dike swarm, which was emplaced at 1240 Ma (Krogh et al., 1987; Dudás et al., 1994) across the Southern and Superior provinces.

2.4.2 Amphibole Chemistry

Amphiboles from metabasalt, Main Mass SIC norite, and norite inclusions in massive sulfide ore, were analyzed to determine if they are igneous or metamorphic in origin. Because aluminum in tetrahedral coordination sites (Al^{IV}) and Ti contents of calcic amphiboles increase with temperature and aluminum in octahedral coordination sites (Al^{VI}) increases with pressure, high temperature magmatic and low- to medium grade metamorphic amphiboles can be distinguished on plots of Al^{IV} vs Al^{VI} and Ti vs Al^{IV} (e.g., Leake, 1971; Fleet and Bernett, 1978; Zenk and Schulz, 2004). Brown magnesiohornblende in SIC norite at Garson mine and the Elsie Mountain Formation metabasalt near Kirkwood mine (see Fig. 2.2 for location) have higher Al^{IV}/Al^{VI} ratios than green magnesiohornblende and ferrotschermakite and they plot in or near the field of unaltered igneous amphiboles (Fig. 2.8a). They are enriched in Ti, which ranges 0.14-0.24 atoms per formula unit, and show a strong positive linear correlation on the Ti vs Al^{IV} diagram (Fig. 2.8b). The trends are similar to those of calcic amphiboles in high temperature magmatic rocks (Fleet and Barnett, 1978; Rubio Pascual et al., 2002; Zenk and Schulz, 2004). In contrast, green magnesiohornblende and ferrotschermakite exhibit a strong positive correlation between Al^{IV} and Al^{VI} and they plot within the field of metamorphic amphiboles (Fig. 2.8a). The Ti contents of green magnesiohornblende and ferrotschermakite are low and do not exceed 0.05 atoms per formula unit (Fig. 2.8b).

The high Ti content and high Al^{IV}/Al^{VI} ratios in brown magnesiohornblende (Fig. 2.8) are consistent with calcic amphiboles crystallizing at low pressure, high temperature conditions, e.g., magmatic or low pressure granulite-grade conditions (Raase, 1974;

Hammarstrom and Zen, 1986). As the SIC was not metamorphosed to granulite-grade, the mineral chemistry suggests a magmatic–origin for brown magnesiohornblende in Main Mass SIC norite, consistent with textural observations, i.e., the blocky and near-equant crystal habits in some brown magnesiohornblende. They crystallized or replaced pyroxenes under sub-solidus conditions in the presence of a late-magmatic exsolved fluid (Chivas 1981; Pe-piper 1988). Brown magnesiohornblende in metabasalt are either of magmatic origin or they formed at high temperatures by contact metamorphism within the contact auriole of the SIC (Thompson et al., 1985). Thus, brown magnesiohornblende did not form during a regional metamorphic event preceding the growth of the metamorphic green and blue-green amphiboles.

2.4.3 Ni-Cu-PGE Sulfide Mineralization

The 4 principal ore zones, i.e., #1, #2, #3 and #4 shear ore bodies (Figs. 2.3, 2,4), consist predominantly of inclusion-rich breccia ore comprising rock fragments in a sulfide matrix (50-80%), but they also include disseminated (up to 10%) sulfides in norite lenses within the ore zones, in the norite wallrocks to the massive sulfides, and to a lesser extent in slivers of norite enclosed by metabasalt. The ore minerals within both the breccia ore and disseminated sulfides zones consist predominantly of pyrrhotite (80-90 %), pentlandite (5-15%), chalcopyrite (5-10%), and magnetite (< 5%), and minor quantities of gersdorffite and cobaltite, trace amounts of niccolite, and rare sperrylite (Gammell et al., 2004). Chalcopyrite-rich portions (≥85%) locally occur on the margins of breccia ore zones and margins of silicate rock inclusions in breccia ore. Breccia ores can contain up to 50% inclusions of Huronian rocks (metabasalt, metawacke, pelitic schist, and quartzite), norite, and metabreccia. Inclusions of Huronian rocks are ubiquitous, but those of norite are localized within thicker segments of the #1 and #4 shear ore bodies between the 4800 and 5100 levels and near the intersections of the #1/#2 and #1/#3 shear ore bodies (Fig. 2.4), where norite inclusions locally constitute up to 90% of the total inclusion population.

Norite inclusions in massive sulfide in the #1 and #4 shear ore bodies are medium gray to black, medium- to coarse-grained, and sub-angular to rounded with diameters ranging from ~1 cm to 15m (Fig. 2.9a). They contain disseminations and blebs of pyrrhotite-pentlandite-chalcopyrite. The inclusions are generally weakly deformed, but strongly metamorphosed. In thin section, the inclusions consist of very small, 100 to 200 µm wide recrystallized plagioclase (An_{29-31}) replacing igneous plagioclase, ferrotschermakite rimming patches of colorless and weakly pleochroic brownish amphiboles, biotite, quartz, ilmenite, and accessory zircon. Rare, less metamorphosed inclusions have a cumulate texture consisting of approximately equal proportions of igneous orthopyroxene and clinopyroxene, and recrystallized plagioclase (Fig. 2.9b). Plagioclase is bytownitic to anorthitic (An_{84-91}) in composition. It is different in composition from andesitic-labradoritic (An_{45-65}) plagioclase in Main Mass norite, but is similar to the anorthitic (An_{90}) composition of plagioclase in cumulus norite inclusions within the South Range Sublayer (Naldrett et al., 1984).

2.4.4 Structural Geology

Detailed underground mapping of the #1 and # 4 shear zones where they were accessible at the time of the study on the 3560, 4800, 4900, 5000, and 5100 levels, together with mine sections (Fig. 2.4) and underground level maps (Figs. 2.3, 2.4, 2.10), form the basis for our structural interpretation. The deformation events, which are denoted D_1 to D_3, are specific to the Garson mine because the sequence of deformation events that occurred in the South Range is yet to be firmly established. The sequence of deformation events and structures is summarized in Table 2.4.

The earliest deformation (D_1) that affected the Garson deposit resulted in an east-west trending, steeply south-dipping to vertical, penetrative mylonitic S_1 foliation and a down-dip L_1 lineation (Figs. 2.11a, c, e). The structures are well preserved along the sheared SIC-Huronian contact. Norite and metabasalt are typically massive, but are strongly foliated within a distance of 15m and 3 m, respectively, of the SIC-Huronian contact. S_1 and L_1 are defined by green to colorless magnesiohornblende in norite and by ferrotschermakite in metabasalt. The amphiboles are intergrown with minor biotite (Figs. 2.6a, d). Microlithons consisting of elongate quartz ribbons and quartz grains are aligned parallel to the foliation. Ilmenite occurs as anhedral, elongate, disseminated, opaque grains parallel to S_1. S_1 wraps around plagioclase and brown magnesiohornblende porphyroclasts in sheared norite and metabasalt (Figs. 2.6a, d). Fine-grained, untwinned, recrystallized plagioclase grains (An_{24-28}) occur in quartz-rich layers in metabasalt, which also contain rare euhedral garnet porphyroblasts in stable grain contact with ferrotschermakite. Coexisting ferrotschermakite-oligoclase-biotite-quartz-ilmenite-(garnet) in metabasalt suggests syn-D_1 amphibolite facies metamorphic conditions (Spear, 1993). In thin section, S_1 locally appears as a composition foliation consisting of an older foliation (S-fabric) that is dragged into the orientation of a younger foliation (C-fabric,

Fig. 2.12a). Similarly, in an exposed underground face near the SIC-Huronian contact, a schistose foliation defined by green magnesiohornblende in norite is dragged in a clockwise manner into S_1 (Fig. 2.12b). These structural relationships suggest that S_1 formed during north-over-south shearing parallel to the SIC-Huronian contact.

The most prominent D_2 structures are up to 8m wide, reverse south-over-north shear zones, which are superposed on the older D_1 shear zones. Near the SIC-Huronian contact, the shear zones transect S_1 as 50 cm to ~3m wide (Figs. 2.13a, b), E-W trending zones characterized by a steeply south-dipping, penetrative, schistose S_2 foliation, containing a down-dip L_2 lineation (Figs. 2.11a, d, f). S_2 and L_2 in sheared norite and metabasalt are defined by the shape-preferred orientation of chlorite, which bounds millimeter-scale microlithons of quartz and plagioclase. Along the mineralized #1 and #4 shear zones, S_1 is intensely transposed by S_2 such that the shear zones appear as D_2 structures, that is, the main structures in the shear zones are S_2 and L_2. Where S_1 is locally preserved within the shear zones, it is steeper than S_2 and it is dragged into the plane of D_2 shear zones, indicating reverse south-over-north shearing (Figs. 2.13a, b).

S_1 amphibole and biotite in D_2 shear zones are variably replaced by chlorite along grain boundaries and in boudin necks of boudinaged amphibole grains (Fig. 2.13f). These minerals and ilmenite are generally completely replaced by chlorite and titanite, respectively, along S_2 foliation planes, suggesting that S_2 and L_2 formed under greenschist facies metamorphic conditions. In thin section, isolated, tight, crenulations defined by S_1 amphibole are bounded by S_2 chlorite foliation planes, indicating that S_1 has been transposed parallel to S_2 during greenschist facies metamorphism (Figs. 2.13c, d).

Surfaces exposed by parting along S_2 are shiny, appear polished and contain 'ridge-in-groove' striae (Means, 1987: Fig. 2.13e), which are parallel to L_2. The grooves are generally shallow, not exceeding 1 mm in depth. Individual ridges and grooves are between 1 mm and 5 mm wide and are up to 3 cm long. Rough congruous steps, which are up to 1 mm high, are well developed and they are oriented consistently perpendicular to the striae, indicating reverse south-over-north shearing.

Granitic dikes and quartz veins within the D_2 shear zones are folded into isoclinal to tight folds with thick hinges and attenuated limbs (Figs. 2.14a, b). Their sub-horizontal fold axes trend east-west (Fig. 2.11d). S_2 is axial planar to the folds, suggesting that the folds are syn-D_2 (Figs. 2.14a, b). S_2 is folded by asymmetrical drag folds with axes perpendicular to L_2. The folds consistently verge to the north suggesting reverse slip (Fig. 2.14c). Abundant kinematic indicators, such as shear offsets (Fig.13 a), dragged S_1 foliation (Figs. 13a, b), congruous steps cutting across 'ridge-in-groove' striae (Fig. 2.13e), shear bands and back-rotated boudins (Fig. 2.14d), consistently indicate reverse, south-over-north displacement during D_2. S_2 is truncated by 20 to 60m thick olivine diabase dikes, indicating that D_2 predates the emplacement of the 1240 Ma Sudbury dike swarm (Krogh et al., 1987; Dudás et al., 1994).

D_3 is characterized by brittle to ductile, steeply south-dipping, discrete faults and foliated fault zones that are up to 50 cm wide. The foliation is defined by chlorite associated with quartz, epidote, calcite, and minor titanite, suggesting greenschist to sub-greenschist facies metamorphic conditions during D_3. Dragging of S_2 into D_3 fault zones suggest north-over-south slip during D_3 (Fig. 2.14e). The deformation of plagioclase-phyric dikes within the #4 shear ore body (Fig. 2.14f) may have occurred during this event. The dikes are locally broken-up, faulted, and folded into open, upright and, sub-horizontal, east-trending folds. As other similar dikes of the Sudbury dike swarm cut across all shear zones and rock units at Garson, this suggests that the ore zones were only locally modified during D_3.

The youngest structure at the mine is a 50m wide zone of closely-spaced (cm to m), sub-vertical, NW- to NNW-trending fractures, called the 2500 structure, which cuts across the #1 shear ore body on the 5000 and 5100 ft levels without significantly displacing the ore zone. Individual fractures are persistent over distances of up to 10m, locally contain fault gouge and are coated by sub-horizontal, calcite-quartz slickenfibers indicating sinistral slip along the fractures. Galena-sphalerite and chalcopyrite that are up to 5 cm wide occur in association with calcite-quartz veins along the fractures. The brittle nature of the 2500 structure, its NW trend, and sinistral strike-slip indicators suggest that the structure is most likely coeval with the regional, NW-trending, Onaping fault set (Cochrane, 1991).

2.4.5 Metamorphic Hydrothermal Veins

Two sets of hydrothermal quartz-calcite veins are associated with D_2 shear zones. The veins vary in thickness from <1 cm to ~1m and are locally mineralized with chalcopyrite and minor pyrrhotite and pentlandite. The first vein set consists of steeply south-dipping, S_2-parallel veins in the margins of the ore bodies and in their sheared wall rocks. Steps cutting across quartz and calcite slickenfibers coating the vein walls suggest that the veins formed as reverse shear veins, which is consistent with D_2 movement in the host shear zones.

The second vein set consists of sub-horizontal to gently-dipping tabular veins, which occur in massive metabasalt within 5m of the shear zone boundaries where they are folded into F_2 gentle upright folds. The veins also occur within the shear zones where they cut across S_2 and they are locally overprinted by isoclinal F_2 folds (Fig. 2.14a) and by pinch-and-swell boudinage structures oriented perpendicular to L_2.The veins have chlorite-quartz-epidote-calcite-titanite selvedges and massive to fibrous textures defined by blocky quartz fibers oriented roughly perpendicular to the vein walls. Some veins cut across the shear veins, whereas others are overprinted by the shear veins, suggesting that the two vein sets are contemporaneous. The veins margins are characterized by the same greenschist grade minerals that define S_2 in metabasalt. These observations collectively suggest that the sub-horizontal veins are extensional veins that formed during D_2 reverse faulting.

2.5 Discussion

2.5.1 Syn-SIC Sulfide Mobilization Model

Lochhead (1955) suggested that the fault zones that host the ore zones at the East and Falconbridge mines were pre-SIC faults that controlled the outer edge of the SIC and into which ore was emplaced in an “extremely mobile state”. Because the mineralization extended further along more brittle structures in rocks underlying the SIC than along more ductile structures in SIC norite, ore emplacement was interpreted to have occurred after only partial cooling of the SIC.

Lee and Siddorn (2006) and Siddorn and Ham (2006) favored a molten sulfide injection model for the Garson deposit, emphasizing observations that (1) semi-massive sulfide ores truncate tectonic fabrics in wall rocks, and (2) massive sulfide ores contain abundant schistose wall rock inclusions with contorted foliations, which they interpreted to indicate that the tectonic fabrics and the shear zones predate the mobility and crystallization of the sulfide ore and the tectonic fabrics became contorted during turbulent flow of a sulfide melt. They also noted that inclusion margins have recrystallized acicular amphibole grains, which they interpreted to indicate thermal disequilibrium between the inclusions and a liquid sulfide melt. They suggested that the Garson shear zones initially formed as either pre-impact or syn-impact faults that acted as channels for the injection of sulfide melts and precipitation of sulfide ores.

Injection of sulfides into rocks underlying the SIC at Sudbury is normally accompanied by strong fractional crystallization and enrichment in Cu-Pd-Pt-Au (e.g., Hawley, 1965), which would normally allow us to reject this model as most of the displaced ores are not significantly enriched in chalcopyrite, but most of the mineralization in these environments occurs relatively close to the SIC contact where only minor fractionation would be expected. Although the high degree of superimposed deformation does not allow us to completely discount this model, the presence of para-autochthonous slivers of rocks underlying the SIC along sub-solidus, amphibolite-grade shear zones within the Main Mass SIC norite (Figs. 2.3, 4) at Garson indicates that the SIC and basement rocks were imbricated after crystallization of the SIC in that area.

2.5.2 Post-SIC South-Over-North Thrusting Model

Most models for post-SIC deformation along the South Range have emphasized reverse, southeast-over-northwest slip (e.g., Shanks and Schwerdtner, 1991a; Brocoum and Dalaziel, 1974; Bailey et al., 2004). Because the nearby Thayer Lindsley deposit (Fig. 2.2) was clearly deformed by south-over-north reverse shear zones (Bailey et al., 2004), we tested a similar model (Figs. 2.15a-c) involving a single stage south-over-north shearing event. If correct, the model must explain the net slip displacement of 450m to 700m necessitated by the emplacement of metabasalt and metabreccia slivers in SIC norite along the #3 and #4 shear zones (Figs. 2.3b-d, 2.4) during a single south-over-north D_2 shearing event (Fig. 2.15c). In such a model, south-over-north slip could only occur after the SIC-Huronian contact had been steepened or overturned through folding of the SIC (Fig. 2.15b). However, south-over-north faulting would simply offset the SIC-Huronian contact without imbricating or tectonically emplacing slivers of rocks underlying the SIC into the Main Mass SIC norite (Fig. 2.15c). Moreover, thrust faults with dips well under 45° are expected to develop in regions of horizontal compression (Anderson, 1905) and steep shear zones, such as those observed at Garson, likely formed either by reactivation of old normal faults or by reactivation of thrust faults that were steepened during the same deformation (Sibson et al., 1988).

2.5.3 Post-SIC North-Over-South Thrusting Model

Davidson (1948), Lee and Siddorn (2006), and Siddorn and Ham (2006) considered north-over-south thrusting and imbrication of the SIC-Huronian contact and rocks underlying the SIC as an alternative to their sulfide injection model. Our work suggests that a north-over-south shearing and thrusting working model better explains available geological and structural information at Garson and thus our working model is built upon that scenario.

The strong degree of deformation and incomplete access to mine exposures hampers interpretations of the original geometry of the SIC-Huronian contact at Garson, but local and regional geological relationships provide some general constraints. The underlying Huronian rocks were deformed during the Blezardian Orogeny prior to the Sudbury impact event and emplacement of the SIC (Stockwell, 1982; Riller, 2005) and were later compressed and displaced during the same event. Thus, the Huronian rocks were most likely tilted to some degree prior to D_1 (Fig. 2.16a). As impact structures larger than a few tens of kilometers in diameter have relatively flat crater floors (Grieve, 1987), the SIC is thought to have been emplaced as a sub-horizontal melt sheet (Fig. 2.16a: e.g., Golightly, 1994; Therriault et al., 2002). The current sub-parallelism of lithologic contacts and structural grain of the Huronian rocks to the SIC in the South Range in general (Cowan and Schwerdtner, 1994), and at Garson mine in particular (Fig. 2.3), was probably attained during folding of the Sudbury structure because oblique units can become near-concordant during folding (Ramsay, 1967; p. 491-517).

After impact, the superheated melt would have thermomechanically eroded rocks at the base of the SIC (e.g., Prevec and Cawthorn, 2002). Less deformed deposits on the South Range (e.g., Little Stobie #1: Davis, 1984) occur in footwall embayments that are lined by Sublayer norite and underlain by footwall breccia or metabreccia. Thus, the presence of metabreccia along the #3 shear ore body from the 1600 to ~2200 levels and along the base of the SIC near the junctions of the #1 with the #2 and #3 shear ore bodies from ~500 to 1200 level and from ~2200 and 2600 level, respectively (Figs. 2.3b, 2.4), suggest that these areas may represent original embayments, which were partly transported and imbricated into the SIC along the #1 and #3 shear zones. Within the deformed Garson ore zones, abundant norite inclusions in breccia ore have similar bytownitic to anorthitic plagioclase compositions similar to that in Sublayer elsewhere in the South Range (see Naldrett et al., 1984), further suggesting that the deformed Garson ores were originally emplaced in an embayment as Sublayer-hosted ore. In summary, the presence of metabreccia and Sublayer in the ore environment at Garson suggests that the ores were originally localized in an embayment along the SIC-Huronian contact, but that the initial geometry of the embayment is not preserved due to later deformation.

Sulfide ores are more ductile than silicate rocks at amphibolite-grade conditions (Barrett et al., 1977; Cox, 1987). The presence of more ductile massive sulfide ore at the SIC/Huronian contact facilitated the nucleation of the main #1 shear zone along the SIC-Huronian contact (Figs. 2.16b, c). The #2, #3 and #4 shear zones formed as splays that accommodated strain in the more competent Main Mass SIC norite as the deformation progressed (Figs. 2.16c-e). D_1 thrusting imbricated the SIC, underlying Huronian rocks, and massive sulfide ores (Figs. 2.16c-e), and transported slivers of norite and ductile sulfide ores into the Huronian rocks. Slivers of Huronian rocks along the #2-, #3- and #4 shear zones (Figs. 2.3a-d, 2.4), were dragged along these faults for distances of up to 700m. Despite strong deformation of inclusion-rich massive sulfide ore zones, norite and metabasalt are generally not penetratively deformed, indicating that strain was strongly partitioned into the shear zones. The distribution of the slivers at Garson provides constraints on the net displacements during D_1 and D_2 faulting. The imbrications of a narrow basalt sliver into the Main Mass norite (Fig. 2.4) indicate a minimum net slip of 450m to 700m.

The Garson D_1 shear zones, together with the SIC and basement rocks, were overturned to their present steep southerly dips (Fig. 2.16f). The D_1 Garson shear zones were then reactivated at greenschist-grade conditions as south-over-north shear zones during D_2. The coplanarity and colinearity of D_1 and D_2 structures suggest that they represent either 1) episodes of a single progressive deformation event that occurred during protracted cooling or 2) two different deformation events in which structures that formed during D_1 were reoriented parallel to D_2 structures during this younger deformation event (e.g., Bell, 1986; Ham and Bell 2004). Coplanar and composite foliations in high strain zones are often interpreted to develop as a result of superposition of fabrics by re-use and reactivation of a favorably oriented pre-existing foliation (e.g., Bell, 1986; Davis and Forde, 1994; Ham and Bell, 2004). Any pre-existing lineation can be rotated towards the youngest stretching lineation if the bulk shortening directions of the deformation events are similarly oriented (Davis and Forde, 1994), which could be the case at the Garson Mine because all deformation events (Mazatzal-Labradorian, Chieflakian, Grenville) that may have affected the Sudbury structure involved bulk NW-SE horizontal shortening (Brocoum and Dalaziel, 1974; Bailey et al., 2004 and references therein). Thus, early D_1 fabrics have similar orientations as D_2 fabrics, and any initial angular differences between the two generations of fabrics was attenuated by the rotation of D_1 fabrics into near-parallelism with D_2 fabrics.

During D_2, the Garson shear zones were steeply-dipping and they were therefore unfavorably oriented for reactivation under the then prevailing horizontal maximum compression direction. Under high fluid pressures that exceeded lithostatic pressure, as suggested by the presence of shallowly-dipping extensional quartz veins, the shear zones were reactivated as reverse brittle faults and hydrothermal minerals precipitated as shear veins with quartz slickenfibers along their margins (Sibson et al., 1988; Robert et al., 1995). Our reconstruction of the ore zones at Garson indicates that displacement during D_2 was minor and is in agreement with observed minor displacements in high angle reverse shear zones that host mesothermal gold deposits and that are misoriented for easy reactivation (Robert et al., 1995).

Displacements along D_3 normal faults were negligible on the scale of the Garson deposit and had no effect on the geometry of ore bodies. Because the Sudbury area was not affected by extensional deformation event after the impact, south-side-down normal slip during D_3 may have occurred as a result of either transient stress reversal after rupture of the faults and shear zones during D_2 (Pavlis et al., 1993; Robert et al., 1995) or it could be associated with late brittle faulting across the South Range (Buchan and Ernst, 1993).

2.5.4 Tectonic Implications and Timing of D1 and D2

The structural evolution of the Garson deposit provides valuable insight into processes and effects of post-impact deformation on the South Range of the Sudbury structure. The

Sudbury structure presently has the geometry of an asymmetrical non-cylindrical synformal fold (Fig. 2.2b), which formed during northwest-southeast bulk horizontal shortening (Shanks and Schwerdtner, 1991a). By comparing the folded Sudbury structure to folds produced in laboratory buckle fold experiments by Kuenen and de Sitter (1938), Cowan and Schwerdtner (1994) predicted that layer-parallel shear zones probably developed in the South Range in order to facilitate buckling of the SIC during progressive folding. The analogue model of Kuenen and de Sitter (1938) predicts that one limb deforms by solid body rotation and non-coaxial shear, whereas the other limb tilts slightly and records little strain (Figs. 2.17a-c). The steeply dipping southeast limb of the Sudbury structure (South Range) undoubtedly underwent a larger body rotation than the shallowly-dipping northwest limb (North Range). Because of strain incompatibilities between the Main Mass SIC norite and the underlying Huronian rocks during buckling, and given that the magnitude of layer-parallel slip and shear strain increases with increasing limb dip (Ramsay, 1974), propagation of layer parallel shear zones seems likely to have occurred in the southeastern portion of the SIC where the SIC-Huronian contact is sheared and overturned (Figs. 2.17b, c). The D_1 shear zones at Garson occur along or adjacent to the SIC-Huronian contact and they have a north-over-south sense of displacement, which is consistent with flexural slip along the SIC's southeast limb during buckling of the SIC. They formed due to strain localization along lithological contacts during flexural slip and they splayed into the Main Mass SIC norite to accommodate strain in the norite as the SE limb of the SIC progressively steepened and became overturned (Figs. 2.17b, c). As all known deformation events (Mazatzal-Labradorian, Chieflakian and Grenvillian) that may have affected the Sudbury structure involved south-over-north thrusting (Brocoum and Dalaziel, 1974; Fueten and Redmond, 1997; Bailey et al., 2004; Riller, 2005; Szentpéteri, 2009), the north-over-south Garson shear zones are interpreted as back-thrusts that formed at the base of the large SIC during buckling of the complex.

In contrast to the Garson D_1 shear zones, the regional, southeast-dipping, South Range Shear Zone (Fig. 2.2) and similar parallel shear zones such as the Thayer Lindsley shear zone, which have similar amphibolite grade fabrics but opposite senses of shear (southeast-over-northwest reverse slip) and shallower dips (45° to 50°) than the Garson D_1 shear zones, transgress and displace the SIC-Huronian contact (Figs. 2.2 (insert) and 2.18b). Their development is attributed to localization of folding-induced strain near the hinge zone to accommodate further flattening and tightening of the SIC with progressive D_1 shortening (Cowan and Schwerdtner, 1994; Riller et al., 2010). As the Thayer-Lindsley shear zone formed during the 1.7-1.6 Mazatzal-Labradorian Orogeny (Bailey et al., 2004) at similar amphibolite grade conditions as the D_1 Garson shear zones, the latter are interpreted to have formed during a progressive Mazatzal-Labradorian deformation event that began with buckling of the SIC, the formation of the north-over-south Garson shear zones during flexural slip (Fig. 2.17b), and south-over-north thrusting along the South Range and Thayer Lindsley shear zones during further shortening of the SIC (Fig. 2.17c).

The northwest limb of the folded SIC records little strain (Brocoum and Dalaziel; 1974; Cowan and Schwerdtner 1994), apart from moderately SE-dipping shear zones/faults along the SIC-Levack gneiss contact at the Levack-Longvack mines (see Fig. 2.2 for location: Coats and Snajdr, 1984) and in the vicinity of the Ministic offset dike (see Fig. 2.2 for location: Boast and Spray, 2006). These shear zones are interpreted as northwest-directed thrusts (Boast and Spray, 2006) which formed at the same time as the D_1 Garson shear zones because their sense of movement is consistent with flexural slip along the northwest limb of the folded SIC, or which formed later during D_1 during propagation of the South Range and Thayer Lindsley shear zones.

Reactivation of D_1 shear zones during D_2 as south-over-north shear zones only occurred after overturning the south east limb of the SIC, together with the shear zones. D_2 is poorly constrained between 1850 Ma and 1240 Ma, as the shear zones transect the 1850 Ma SIC (Krogh et al., 1984), but are truncated by the 1240 Ma olivine-diabase dikes of the Sudbury swarm (Krogh et al., 1987; Dudás et al., 1994). These shear zones and those in the vicinity of the Victoria mine (Fig. 2.2) are likely coeval as they both have greenschist-grade fabrics, south-over-north slip and are contiguous with the South Range Shear Zone. We therefore suggest that these shear zones, including the South Range Shear Zone, were reactivated during D_2 as south-over-north greenschist facies shear zones either later during the Mazatzal-Labradorian Orogeny or during the Chieflakian event, which was probably coeval with the 1500-1450 Ma Pinwarian orogenesis that records the accretion of juvenile Andean-style, calc-alkaline magmatic arcs along the entire southeastern margin of Laurentia (Rivers, 1997).

2.5.5 Comparisons with and Implications for Other Deposits on the South Range

The geologic setting of the Garson deposit is similar to that of the East, Falconbridge, and Thayer-Lindsley deposits along the east end of the South Range, and to that of the Creighton deposit along the west end of the South Range (see Fig. 2.2 for location). All comprise pyrrhotite-rich massive sulfide ores that occur along steeply south-dipping to vertical shear zones that coincide with or are parallel to the SIC-Huronian contact (Figs. 2.18a-c)). The kinematics of the shear zones at the Falconbridge and East mines are not well constrained and both north-over-south and south-over-north slips have been invoked (Davidson, 1948; Lochhead, 1955). Nevertheless, the SIC-Huronian contact at these mines is sheared over a combined strike distance of at least 3 km and a down-dip distance of over a kilometer (Fig. 2.18a), suggesting that the SIC-Huronian contact in the entire southeastern portion of the Sudbury structure is likely sheared.

Lochhead (1955) showed that in the upper parts of the Falconbridge deposit, where the sheared contact dips steeply north, mineralization was mobilized upward along steeply S-dipping (65-75°) splay faults into norite. If not attributable to injection of molten sulfide, as discounted above, the orientation of the splay faults suggests that they likely formed prior to overturning of the SIC during north-over-south shearing in a similar way as D_1 shear zones at Garson, as explained above. Thus, it is possible that the D_1 north-over-south shearing event recognized at Garson may have occurred but has been unrecognized in other parts of the South Range, which would have significant implications for the locations of mineralization along other parts of the SIC/Huronian contact. Because D_1

imbrication mobilizes contact-type massive sulfide into Main Mass norite, an environment that traditionally does not host deposits in the Sudbury camp, then shear zones that occur within the Main Mass close to the SIC-Huronian contact provide additional targets for exploration.

The Creighton deposit, which occurs ~30 km SW of Garson mine, is deformed by steeply NW-and N-dipping shear zones that accommodated a northwest-southeast and north-over-south slips, respectively (Fig. 2.18c; Snelling, 2009). Snelling (2009) suggested that the shear zones are part of a Riedel system that formed under NW-SE compression. As these shear zones occur along the SIC-Huronian contact and have steep dips, similar to those at Garson, they likely formed as back-thrusts during buckling of the SIC.

2.6 Conclusions

1) The Garson Ni-Cu-PGE deposit formed at the base of the SIC as contact Sublayer-hosted and footwall breccia-hosted ore and was deformed within shear zones that formed during the 1.7-1.6 Ga Mazatzal-Labradorian Orogeny.

2) D_1 shear zones propagated as south-directed back-thrusts that formed as a result of flexural slip along and near the SIC-Huronian contact during D_1 buckling of the SIC. The north-dipping thrusts imbricated the SIC norite, the underlying Huronian rocks, and the ore zones over distances of 400 to 700m.

3) D_1 shear zone were steepened and overturned during buckling of the SIC and the reverse, south-dipping, South Range and Thayer Lindsley shear zones propagated

across the South Range to accommodate further shortening and tightening of the Sudbury structure.

4) The D_1 shear zones and possibly the South Range Shear Zone were reactivated as D_2 south-over-north reverse shear zones either later during the Mazatzal-Labradorian Orogeny or during the ca. 1.45 Ga Chieflakian event.
5) Our model for the Garson mine shows that progressive deformation of large igneous complexes such as the SIC, which involved folding, followed by thrusting, can produce back-thrusts by flexural slip and these back-thrusts can imbricate the bases of the igneous complexes.

Acknowledgements

This paper is part of a PhD research undertaken by the first author at Laurentian University and has benefited from discussions with D. Tinkham (Laurentian University). The project was funded by a Vale-NSERC-CRD grant to BL and CML, NSERC Discovery grants to BL and CML, and an SEG Foundation Canada grant to JM. We are very grateful to Vale for providing access to geological data, mine exposures, and diamond drill cores, and to S. Lowen, D. Hodder, C. Gauld, S. Kedzierski, L. Desjardins, D. Butt, B.Gauvreau, and D. Bellefeuille for logistical assistance and many beneficial discussions on the geology of the Garson Mine. D. Crabtree of the Ontario Geological Survey helped with the microprobe analyses. We are very grateful to D.E. Ames and U. Riller for very constructive reviews that helped clarify our arguments. P.A. Cawood is thanked for editorial comments.

Table 2.1. Representative analyses of amphiboles in Garson metabasalt, Main Mass SIC norite, and norite inclusions in massive sulfide ores.

Sample #	**GA101**	**GA101**	**GA101**	**GA101**	**GA104**	**GA104**	**GA161**	**GA161**	**GA161**	**GA161**	**GA161**	**GA161**	**GA161**	**GA161**
Analysis	**1-1c**	**1-1r**	**1-2c**	**1-2r**	**10b-5**	**8-3**	**12-1c**	**12-1r**	**12-2c**	**12-2r**	**12-3c**	**12-3r**	**5-3**	**6-1**
Rock Type	**MB**	**MB**	**MB**	**MB**	**NI**	**NI**	**MMN**	**MMN**	**MMN**	**MMN**	**MMN**	**MMN**	**MMN**	**MMN**
Amph. Color	**Bl-Gr**	**Bl-Gr**	**Bl-Gr**	**Bl-Gr**	**Bl-Gr**	**Bl-Gr**	**Br**	**Br**	**Br**	**Gr**	**Gr**	**Gr**	**Gr**	**Gr**
SiO_2	40.8	42.1	41.2	40.7	41.7	41.1	46.2	46.7	51.9	51.2	53.0	54.7	47.8	53.11
TiO_2	0.3	0.2	0.3	0.4	0.2	0.2	2.2	2.1	0.2	0.2	0.1	0.1	0.3	0.1
Al_2O_3	16.9	16.1	16.0	17.6	17.6	17.7	8.5	8.3	5.7	6.2	4.2	3.0	9.9	2.7
Cr_2O_3	0.1	0.0	0.1	0.0	0.0	0.0	0.2	0.2	0.0	0.0	0.2	0.0	0.0	0.1
FeOt	21.6	20.4	21.7	20.8	17.7	18.8	13.0	13.1	13.2	13.5	12.9	11.6	14.4	12.4
MnO	0.2	0.2	0.2	0.2	0.3	0.2	0.3	0.2	0.3	0.3	0.3	0.2	0.3	0.3
MgO	5.4	6.3	5.4	5.3	7.2	6.6	13.7	13.6	14.7	14.0	15.2	16.4	12.2	15.8
CaO	11.3	11.0	11.3	11.1	11.3	11.3	11.7	11.5	12.3	12.1	12.0	12.3	11.6	12.0
Na_2O	1.3	1.6	1.2	1.6	1.5	1.5	0.8	0.9	0.5	0.7	0.4	0.3	1.1	0.3
K_2O	0.5	0.4	0.5	0.5	0.3	0.3	0.7	0.6	0.1	0.1	0.1	0.0	0.2	0.1
Total	98.3	98.2	97.9	98.2	97.9	97.8	97.3	97.3	98.9	98.2	98.5	98.6	97.7	97.6
							Structural formula on the basis of 23 oxygens							
Si	6.1	6.2	6.2	6.1	6.1	6.1	6.7	6.8	7.3	7.3	7.5	7.7	6.9	7.7
Ti	0.0	0.0	0.0	0.0	0.0	0.0	0.2	0.2	0.0	0.0	0.0	0.0	0.0	0.0
Al	3.0	2.8	2.8	3.1	3.0	3.1	1.5	1.4	0.9	1.0	0.7	0.5	1.7	0.4
Cr	0.0	0.0	0.0	0.0	0.0	0.0	0.0	0.0	0.0	0.0	0.0	0.0	0.0	0.0
Fe(III)	0.7	0.7	0.7	0.6	0.6	0.6	0.6	0.6	0.5	0.4	0.5	0.4	0.6	0.4
Fe(II)	2.0	1.8	2.1	2.0	1.6	1.7	0.9	1.0	1.1	1.2	1.0	1.0	1.2	1.0
Mn	0.0	0.0	0.0	0.0	0.0	0.0	0.0	0.0	0.0	0.0	0.0	0.0	0.0	0.0
Mg	1.2	1.4	1.2	1.2	1.6	1.5	3.0	2.9	3.1	3.0	3.2	3.4	2.6	3.4
Ca	1.8	1.7	1.8	1.8	1.8	1.8	1.8	1.8	1.9	1.8	1.8	1.8	1.8	1.8
Na	0.4	0.5	0.4	0.4	0.4	0.4	0.2	0.2	0.1	0.2	0.1	0.1	0.3	0.1
K	0.1	0.1	0.1	0.1	0.1	0.1	0.1	0.1	0.0	0.0	0.0	0.0	0.0	0.0
TOTAL	15.3	15.3	15.3	15.3	15.3	15.3	15.2	15.2	15.0	15.1	14.9	14.9	15.1	14.9
$Mg/(Mg+Fe^{2+})$	0.38	0.43	0.37	0.37	0.50	0.46	0.76	0.75	0.74	0.71	0.76	0.77	0.69	0.77

Oxides are in wt. %. FeOt: FeO total, r: rim, c: core, MB: metabasalt, NI: norite inclusion, MMN: Main Mass SIC norite.

Table 2.2. Representative analyses of plagioclase grains in Garson metabasalt, Main Mass SIC norite, and norite inclusions in massive sulfide ores.

Sample #	GA101	GA101	GA101	GA104	GA104	GA104	GA104	GA161	GA161	GA161	GA161	GA161	GA161	GA161
Analysis	**1-1c**	**1-2c**	**1-3a**	**8-1**	**10-1**	**10-2**	**10-3**	**12-1**	**12-2c**	**4-1**	**5-1c**	**13-1**	**13-2r**	**13-3r**
Rock Type	**MB**	**MB**	**MB**	**NI**	**NI**	**NI**	**NI**	**MMN**	**MMN**	**MMN**	**MMN**	**MMN**	**MMN**	**MMN**
SiO_2	62.4	61.5	62.5	60.8	45.3	61.6	45.5	54.0	55.7	57.2	54.2	55.1	62.6	63.2
TiO_2	0.0	0.0	0.0	0.0	0.0	0.0	0.0	0.0	0.0	0.0	0.0	0.0	0.0	0.0
Al_2O_3	23.3	24.1	23.6	24.7	34.4	24.1	33.7	28.6	27.0	26.6	28.5	28.1	23.3	22.7
MgO	0.0	0.0	0.0	0.0	0.0	0.0	0.0	0.0	0.3	0.0	0.0	0.0	0.0	0.0
CaO	5.0	5.8	5.2	6.5	18.4	6.0	16.9	11.1	9.3	9.1	11.1	10.5	4.8	4.3
MnO	0.0	0.0	0.0	0.0	0.0	0.0	0.0	0.0	0.0	0.0	0.0	0.0	0.0	0.0
FeO*	0.3	0.4	0.3	0.0	0.0	0.0	0.1	0.1	0.4	0.1	0.3	0.2	0.0	0.0
SrO	0.1	0.1	0.1	0.2	0.0	0.3	0.1	0.2	0.2	0.2	0.2	0.2	0.2	0.3
BaO	0.0	0.0	0.0	0.0	0.0	0.0	0.0	0.0	0.1	0.0	0.0	0.0	0.0	0.0
Na_2O	8.8	8.3	8.7	8.1	1.1	8.2	1.3	5.0	5.4	6.5	5.2	5.5	8.9	9.2
K_2O	0.1	0.1	0.1	0.0	0.0	0.0	0.3	0.2	0.9	0.1	0.1	0.1	0.1	0.1
Total	100	100	100	100	99	100	98	99	99	100	100	100	100	100
Structural formula on the basis of 8 oxygens														
Si	2.8	2.7	2.8	2.7	2.1	2.7	2.1	2.5	2.5	2.6	2.5	2.5	2.8	2.8
Ti	0.0	0.0	0.0	0.0	0.0	0.0	0.0	0.0	0.0	0.0	0.0	0.0	0.0	0.0
Al	1.2	1.3	1.2	1.3	1.9	1.3	1.9	1.5	1.4	1.4	1.5	1.5	1.2	1.2
Mg	0.0	0.0	0.0	0.0	0.0	0.0	0.0	0.0	0.0	0.0	0.0	0.0	0.0	0.0
Ca	0.2	0.3	0.2	0.3	0.9	0.3	0.9	0.5	0.5	0.4	0.5	0.5	0.2	0.2
Fe	0.0	0.0	0.0	0.0	0.0	0.0	0.0	0.0	0.0	0.0	0.0	0.0	0.0	0.0
Na	0.8	0.7	0.7	0.7	0.1	0.7	0.1	0.4	0.5	0.6	0.5	0.5	0.8	0.8
K	0.0	0.0	0.0	0.0	0.0	0.0	0.0	0.0	0.1	0.0	0.0	0.0	0.0	0.0
Total	5.0	5.0	5.0	5.0	5.0	5.0	5.0	5.0	5.0	5.0	5.0	5.0	5.0	5.0
Ab %	75.8	71.8	74.9	69.2	9.5	71.0	12.1	44.6	48.8	56.4	45.8	48.4	76.8	79.0
An %	23.8	27.8	24.7	30.6	90.5	28.8	86.4	54.3	46.2	43.2	53.6	51.0	22.7	20.4
Or %	0.4	0.4	0.4	0.2	0.0	0.2	1.5	1.1	5.1	0.4	0.6	0.6	0.5	0.5

Oxides are in wt. %. FeOt: FeO total, r: rim, c: core, MB: metabasalt, NI: norite inclusion, MMN: Main Mass SIC norite.

Table 2.3. Whole rock trace-element compositions (ppm) of equigranular and plagioclase-phyric diabase dikes.

Sample #	Cs	Tl	Rb	Ba	Th	W	U	Nb	Ta	La	Ce	Pr	Sr	Nd	Zr
GA001	0.4	0.1	23.4	667	2.3	0.2	0.6	14.9	0.9	27.5	63.0	8.4	407	36.6	239
GA003	0.6	0.1	22.2	655	2.1	0.1	0.6	13.6	0.8	27.5	61.7	8.2	477	35.5	217

	Hf	Sm	Eu	Gd	Tb	Dy	Ho	Er	Tm	Yb	Lu	Sc	Co	Cr	Ni
GA001	5.5	8.2	2.7	7.9	1.2	7.5	1.5	4.1	0.6	3.6	0.5	28.9	63.9	86.0	108
GA003	5.1	7.7	2.5	7.4	1.1	6.7	1.3	3.7	0.5	3.3	0.5	24.1	50.8	70.0	100

Table 2.4. Sequence of deformation events and structures at Garson mine.

Deformation Event	**Description**
D_3 Localized south-side-down normal shear zones	Steeply, south-dipping brittle-ductile shear zones with a schistose foliation defined by chlorite associated with epidote, quartz, calcite and titanite Metamorphism: Sub-greenschist to greenschist facies
D_2 south-over-north shear zones	L_2: Down-dip stretching lineation on S_2 foliation defined by chlorite S_2: Steeply, south-dipping schistose foliation defined by chlorite associated with quartz, epidote, calcite and titanite; axial planar to F_2 folds F_2: Isoclinal to tight folds with sub-horizontal E-W trending axes. Metamorphism: Greenschist facies
D_1 North- over-south shear zones	L_1: Down-dip stretching lineation defined by ferrotschermakite in metabasalt and green magnesiohornblende in sheared norite along S_1 S_1: Steeply, south-dipping foliation defined by ferrotschermakite in metabasalt and green magnesiohornblende in sheared norite, which are associated with quartz, oligoclase and ilmenite Metamorphism: Amphibolite facies

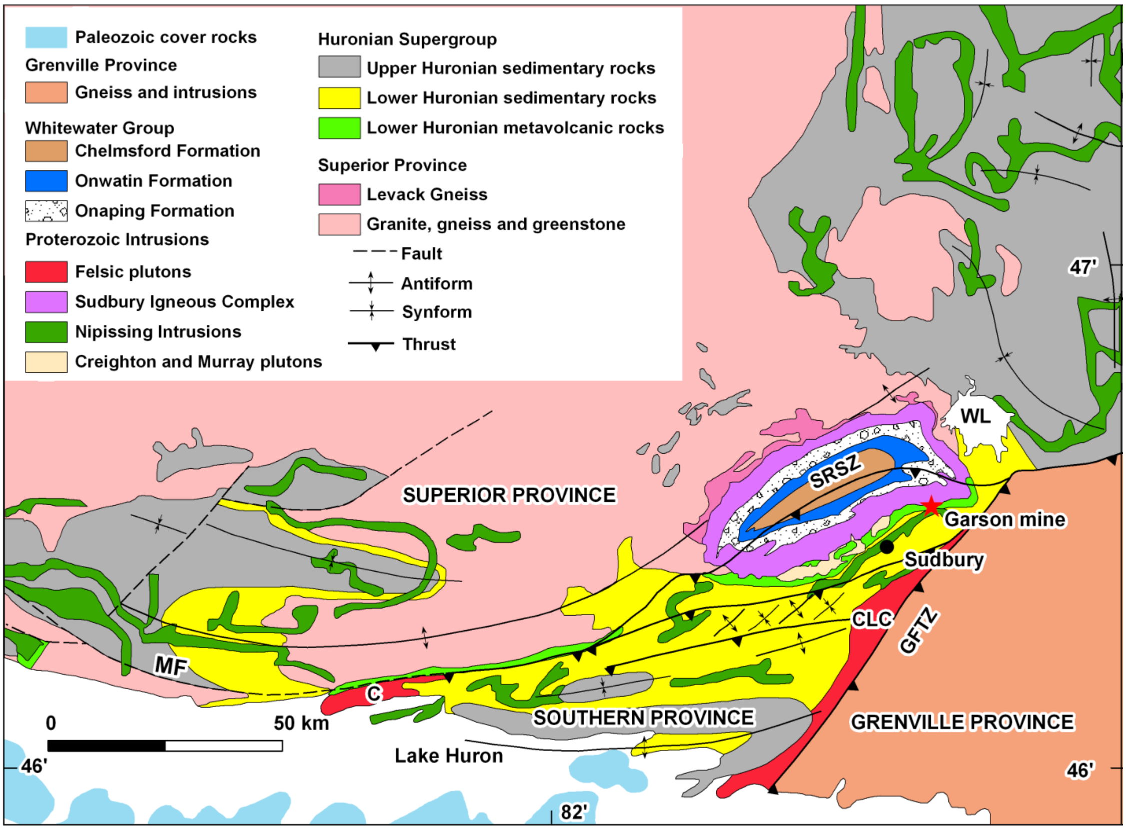

Figure 2.1. Simplified geological map (modified after Card et al., 1984; Riller, 2005; Ames et al., 2005) showing the Sudbury structure at the junction between the Archean Superior Province, Paleoproterozoic Southern Province, and Mesoproterozoic Grenville Province. SRSZ: South Range Shear Zone, GFTZ: Grenville Front Tectonic Zone, MF: Murray Fault, C: Cutler granite, CLC: Chief Lake Complex.

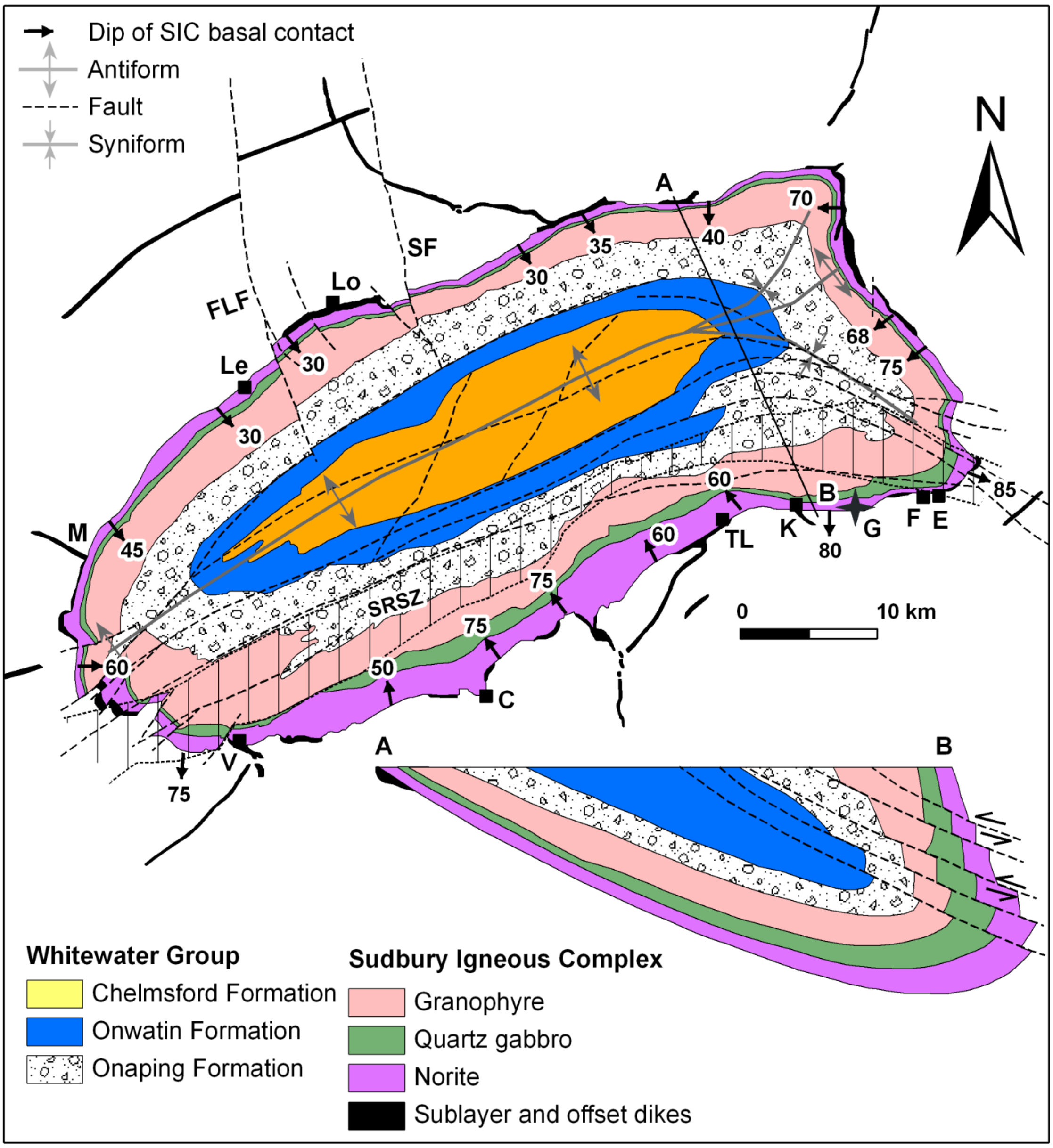

Figure 2.2. Simplified geological map and section (insert) of the Sudbury structure (modified after Dressler et al., 1991; Ames et al., 2005; Riller, 2005; Klimczak et al., 2007) showing the location of Garson mine and the distribution of the Main Mass, Sublayer, and offset dikes of the SIC and overlying formations of the Whitewater Group. SRSZ: South Range Shear Zone, TL: Thayer Lindsley Mine, K: Kirkwood Mine, G: Garson Mine, F: Falconbridge Mine, E: East Mine, V: Victoria Mine, Le: Levack Mine, Lo: Longvack Mine, C: Creighton Mine, M: Ministic offset dike, FLF: Fecunis Lake Fault, SF: Sandcherry Fault, HS: Huronian Supergroup.

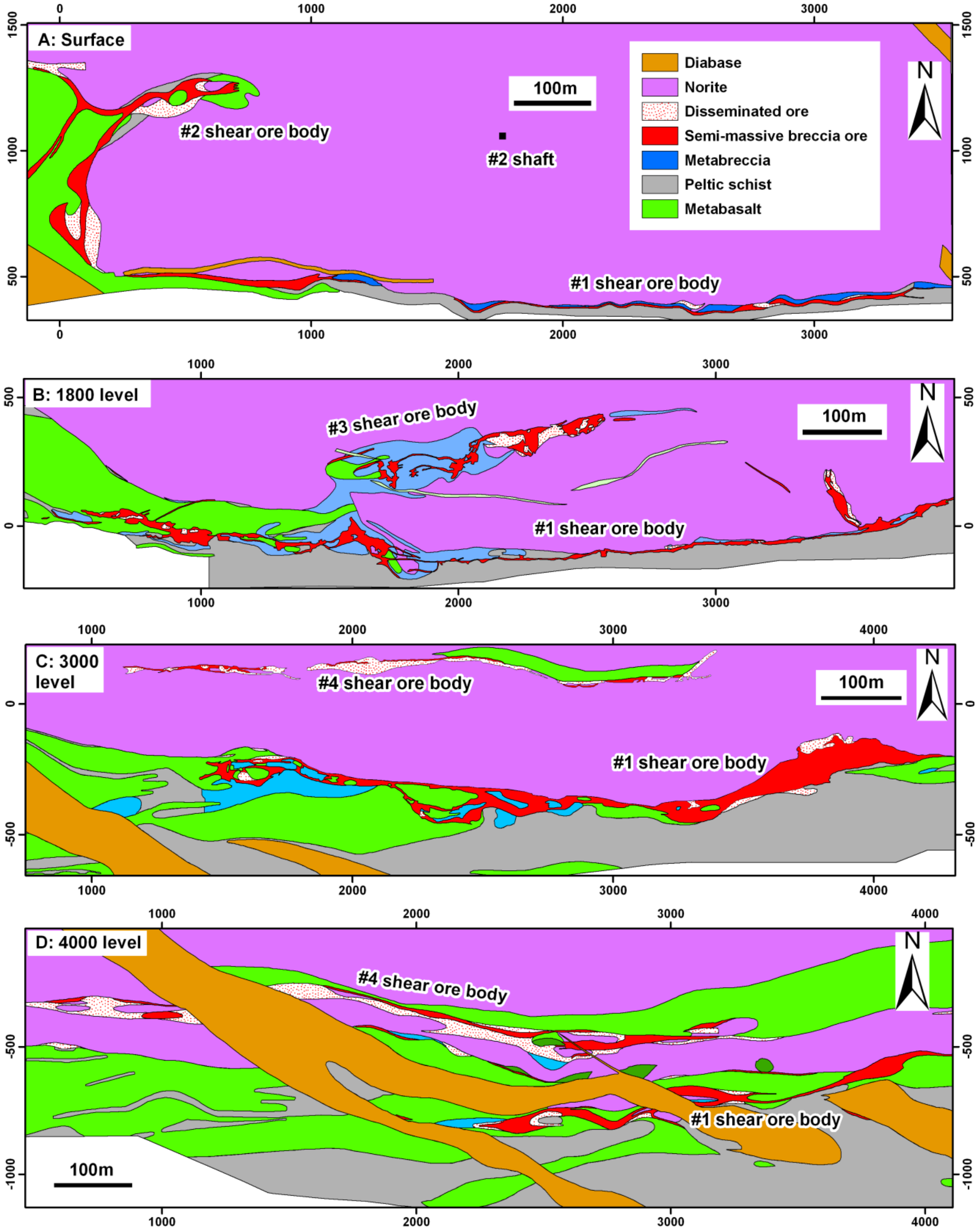

Figure 2.3. Maps of the Garson mine (modified after Aniol and Brown, 1979). (a) Surface, (b) 1800 level, (c) 3000 level, (d) 4000 level.

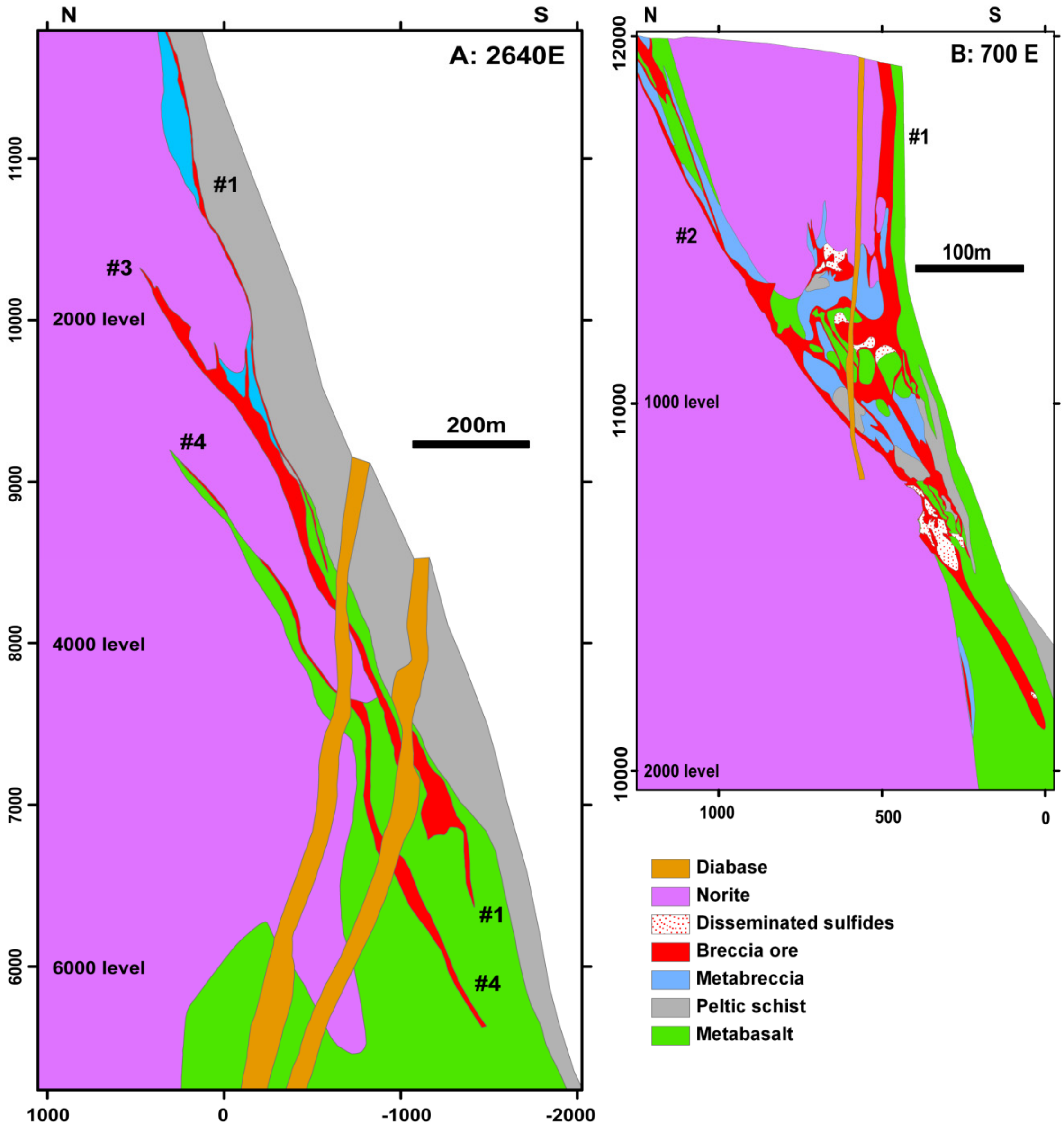

Figure 2.4. Cross section (looking east) of the Garson ore bodies (modified after Aniol and Brown, 1979) along sections (a) 2640 E and (b) 700E.

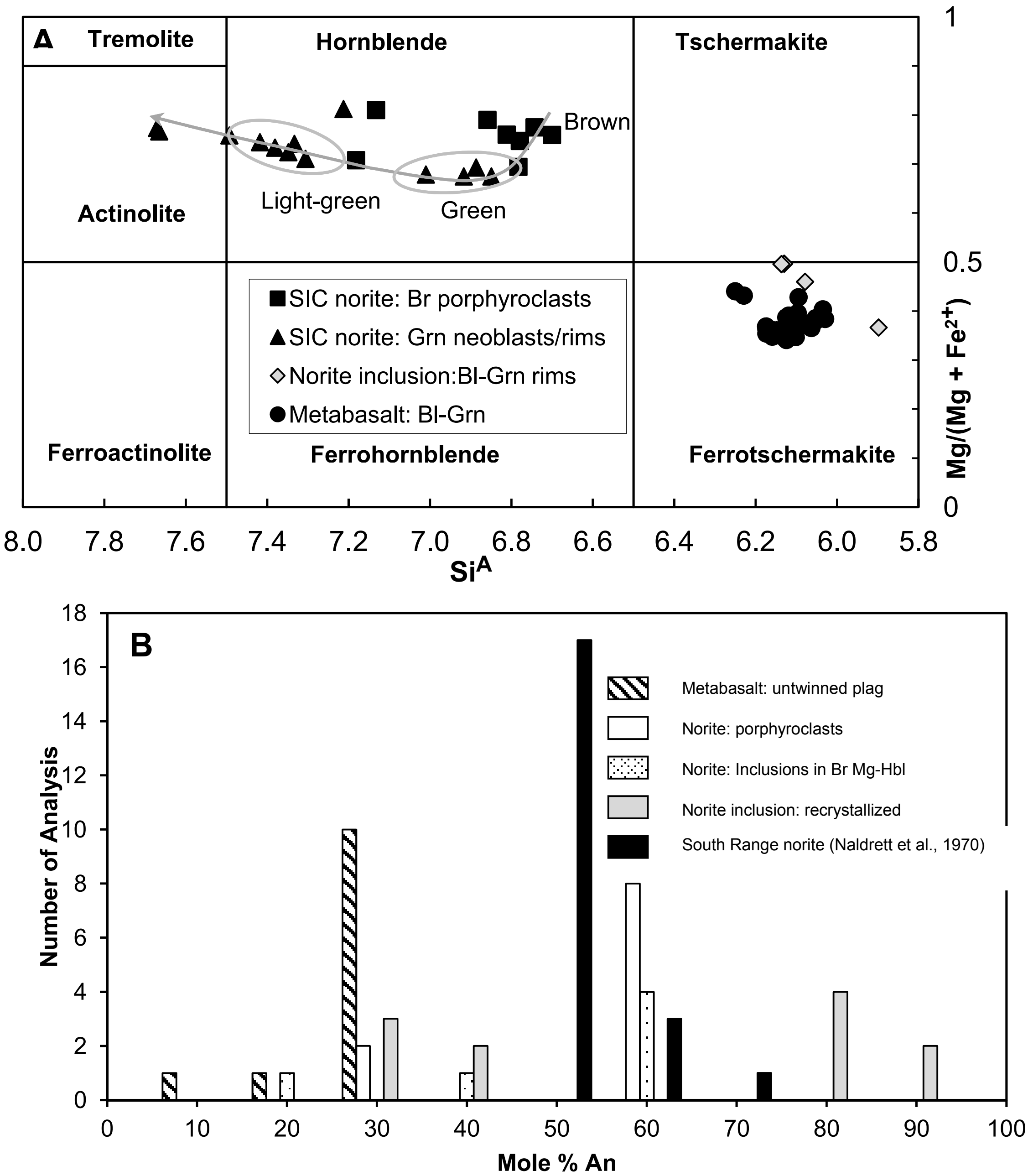

Figure 2.5. (a) Classification diagram (after Leake et al., 1997) for calcic amphiboles in metabasalt, sheared norite, and noritic inclusions in pyrrhotite-rich massive sulfide ore. The arrow indicates core-to-rim-zonation trend from brown amphibole to pale-green amphibole through green amphibole in norite. Representative amphibole analyses are given in Table 2.1. (b) Anorthite content (mole%) of plagioclase in metabasalt, norite, and norite inclusions. Representative amphibole analyses are given in Table 2.2. SiA: Si atoms per formula unit, Br: brown, Grn: green, Bl-Grn: blue green.

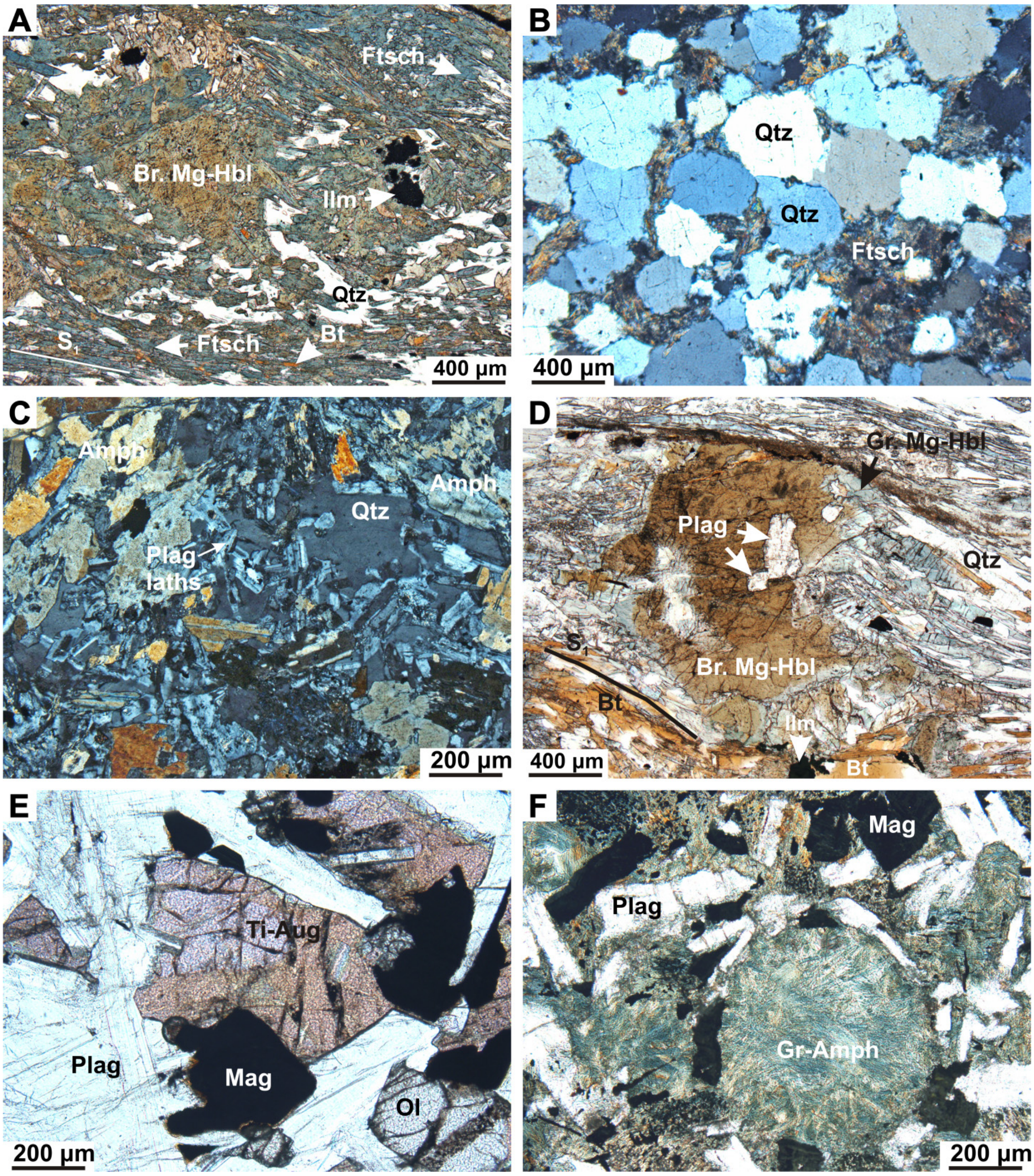

Figure 2.6. Photomicrographs of principal lithologies at Garson mine: (a) Weakly-foliated metabasalt, (b) Metawacke, (c) Metabreccia with poikilitic texture, (d) Sheared norite, (e) Intergranular texture in pristine equigranular olivine-diabase dike, (f) Altered plagioclase-phyric olivine-diabase dike. Ftsch: ferrotschermakite, Br. Mg-Hbl: brown magnesiohornblende, Gr. Mg-Hbl: green magnesiohornblende, Ilm: ilmenite, Bt: biotite, Chl: chlorite, Qtz: quartz, Ti-Aug: titan-augite, Mag: magnetite, Ol: olivine, Plag: plagioclase, Amph: amphibole.

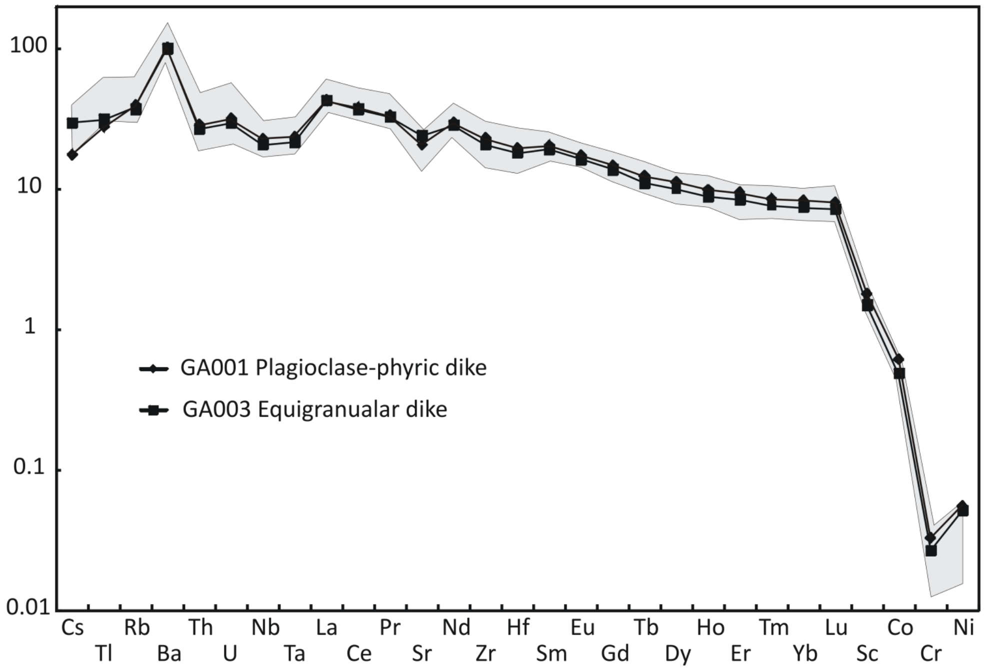

Figure 2.7. Multielement diagram normalized to primitive mantle for plagioclase-phyric and equigranular olivine-diabase dikes from the Garson mine. The gray field represents the pattern of 22 Sudbury dike swarm olivine-diabase dikes (Ernst and Buchan, 2010). Primitive mantle values from McDonough and Sun (1995).

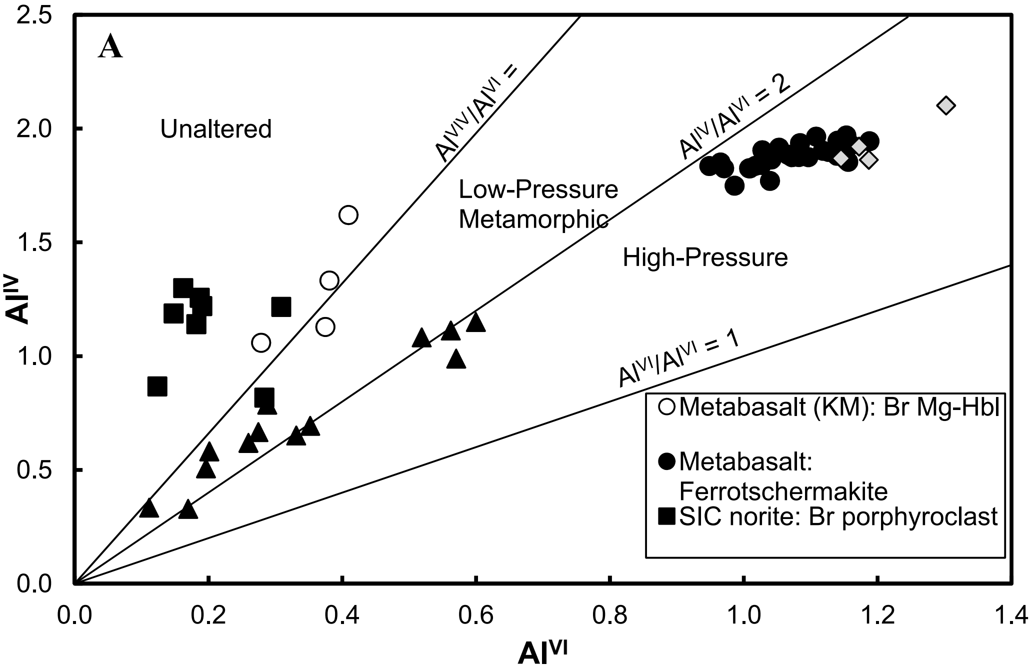

Figure 2.8. (a) Al^{IV}-Al^{VI} and (b) Ti-Al^{IV} diagrams of amphiboles in metabasalt, SIC norite, and norite inclusions in breccia ores.

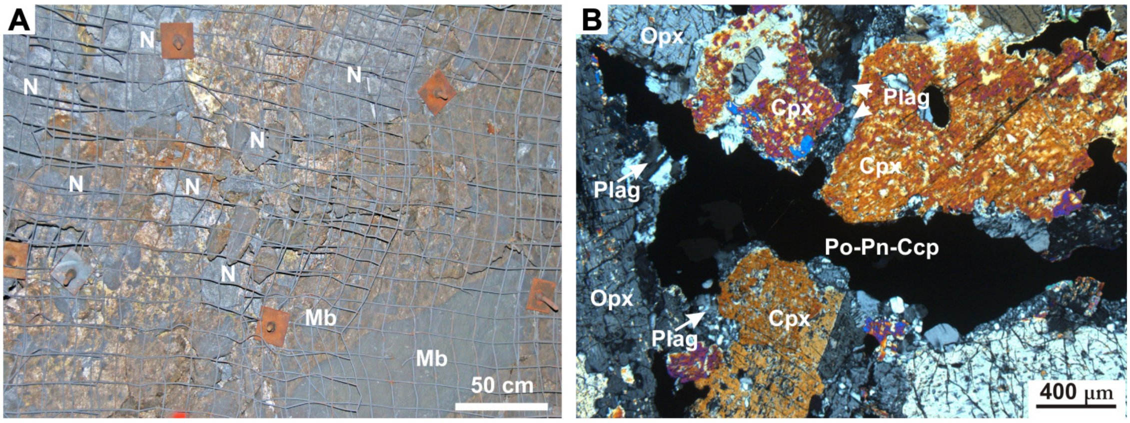

Figure 2.9. (a) Underground photograph showing abundant norite inclusions in pyrrhotite-rich breccia ore. (b) Photomicrograph (crossed polars) of norite inclusion in pyrrhotite-rich breccia ore. N: norite, Mb: metabasalt, Plag: plagioclase, Opx: orthopyroxene, Cpx: clinopyroxene, Po: pyrrhotite, Pn: pentlandite, Ccp: chalcopyrite.

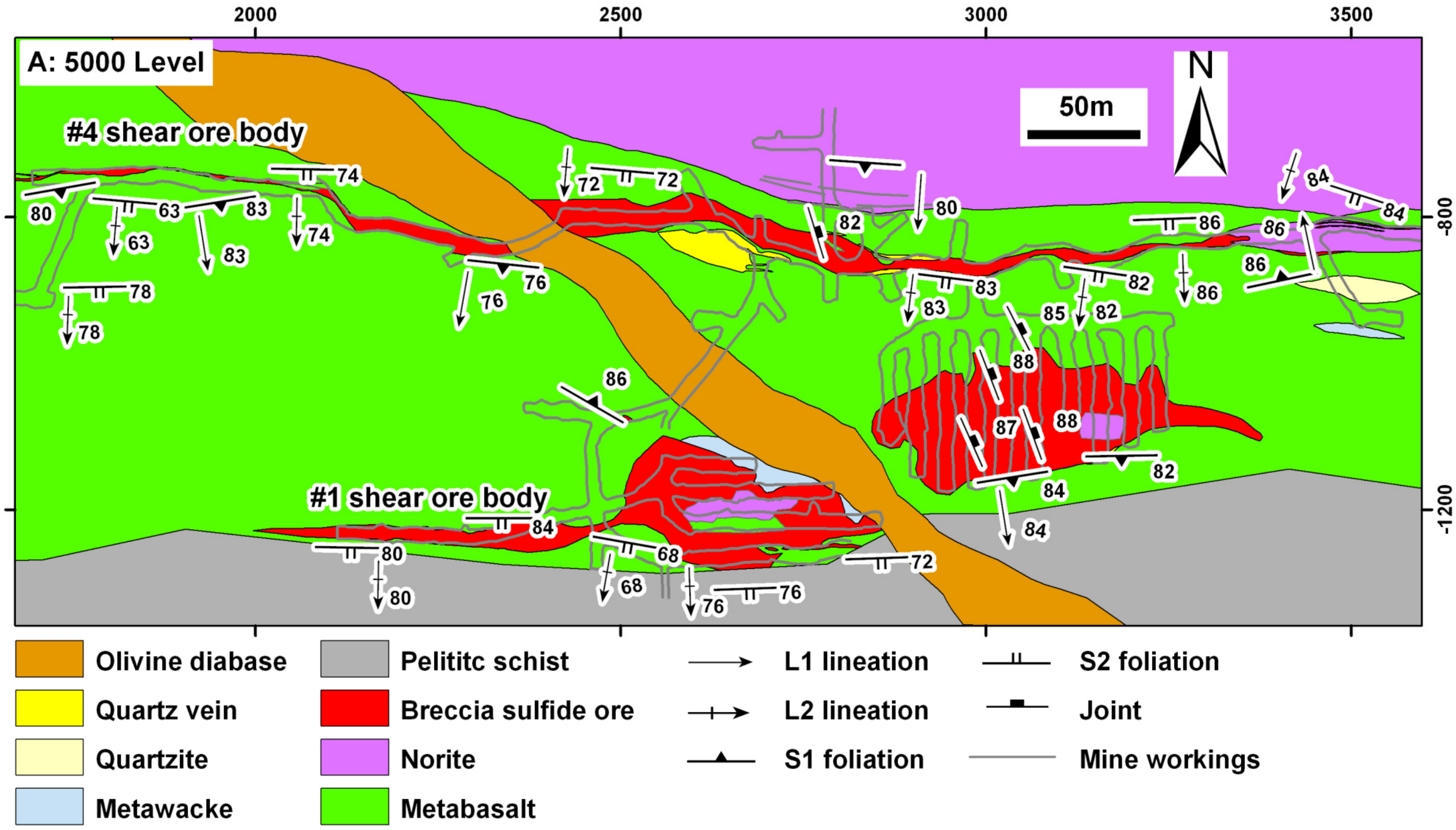A: 5000 Level
2000
2500
3000
3500
-800
-1200
50m
N
#4 shear ore body
#1 shear ore body
Olivine diabase
Quartz vein
Quartzite
Metawacke
Pelititc schist
Breccia sulfide ore
Norite
Metabasalt
L1 lineation
L2 lineation
S1 foliation
S2 foliation
Joint
Mine workings

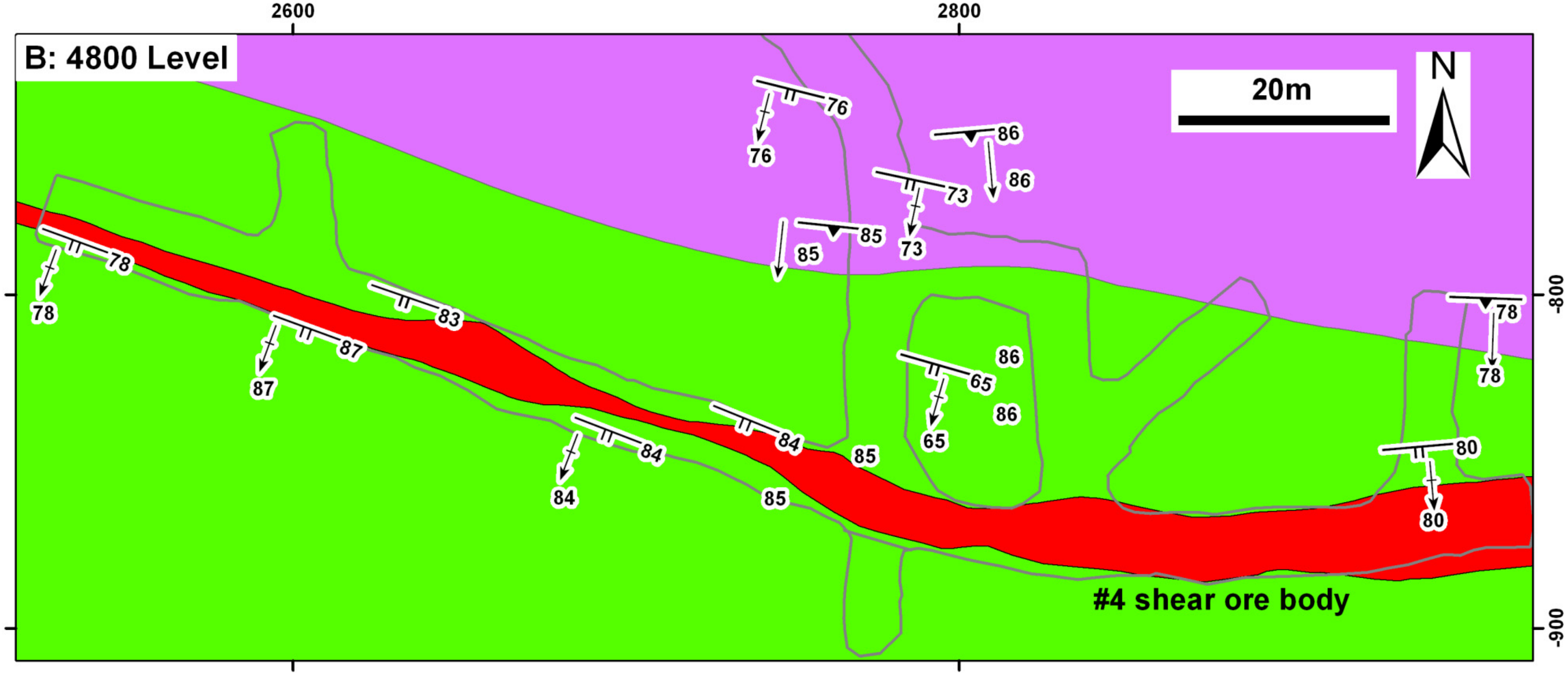

Figure 2.10. Geological maps of the (a) 5000 ft level and (b) 4800 ft level of the Garson Mine showing structures near the SIC-Huronian contact and the #4 and #1ore bodies.

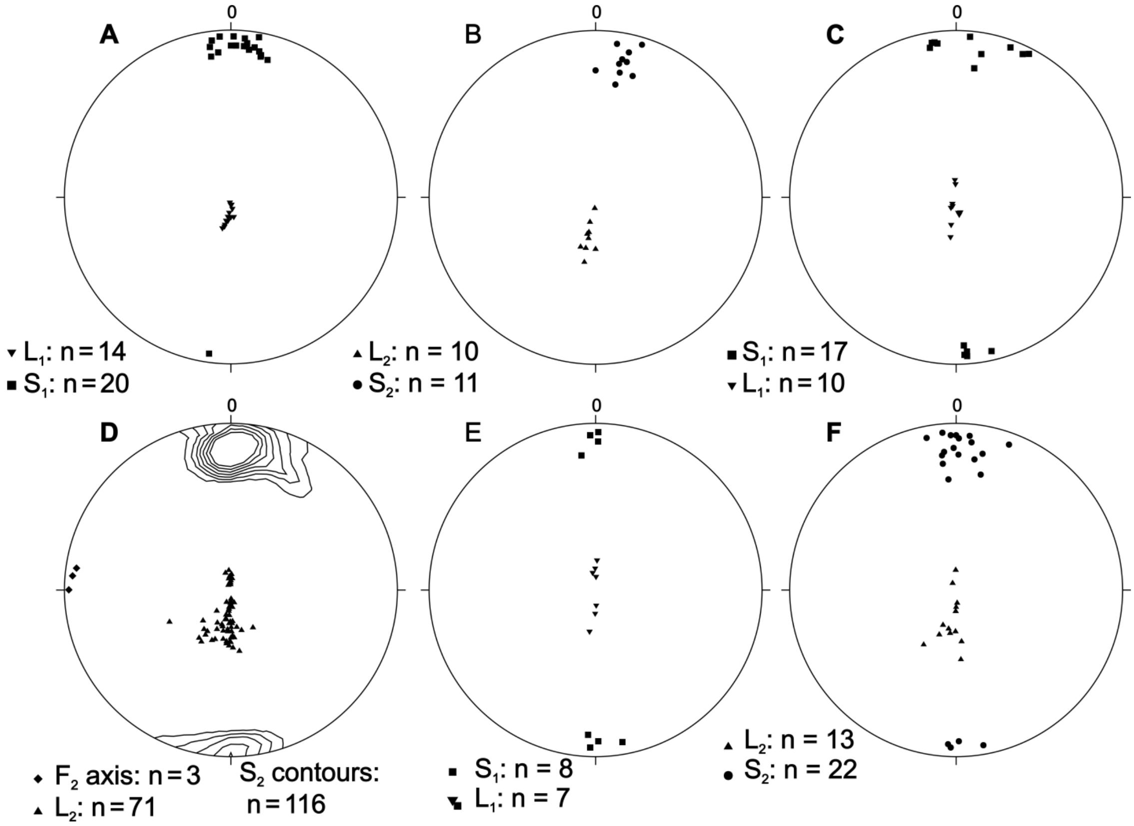

Figure 2.11. Equal area, lower hemisphere projections of (a) L_1 mineral lineation and poles to S1 foliation near the SIC-Huronian contact, (b) L_2 mineral lineation and poles to S_2 near the SIC-Huronian contact, (c) L_1 mineral lineation and poles to S_1 foliation along the #4 shear zone, (d) L_2 mineral lineation, F_2 fold axes and poles to S_2 foliation (contours are in 2 multiples of random distribution) along the #4 shear zone, (e) L_1 mineral lineation and poles to S_1 foliation along the #1 shear zone, (f) L_2 mineral lineation and poles to S_2 foliation along the #4 shear zone.

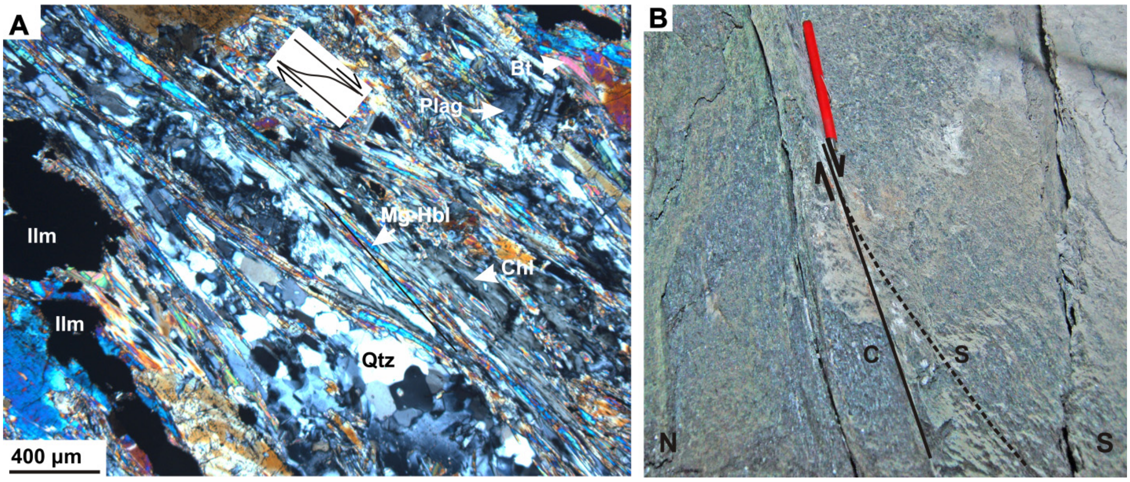

Figure 2.12. (a) Photomicrograph (cross-polarized light) of S_1 foliation in sheared norite near contact with metabasalt. S-C fabric in oriented thin section exhibit clockwise rotation, consistent with north-over-south shear, (b) Underground photograph of sheared norite near contact with metabasalt. S-C fabric indicates north-over-south slip. Qtz: quartz, Bt: biotite, Plag: plagioclase, Chl: chlorite, Ilm: ilmenite, Br. Mg-Hbl: brown magnesiohornblende, Gr. Mg-Hbl: green magnesiohornblende, Ftsch: ferrotschermakite.

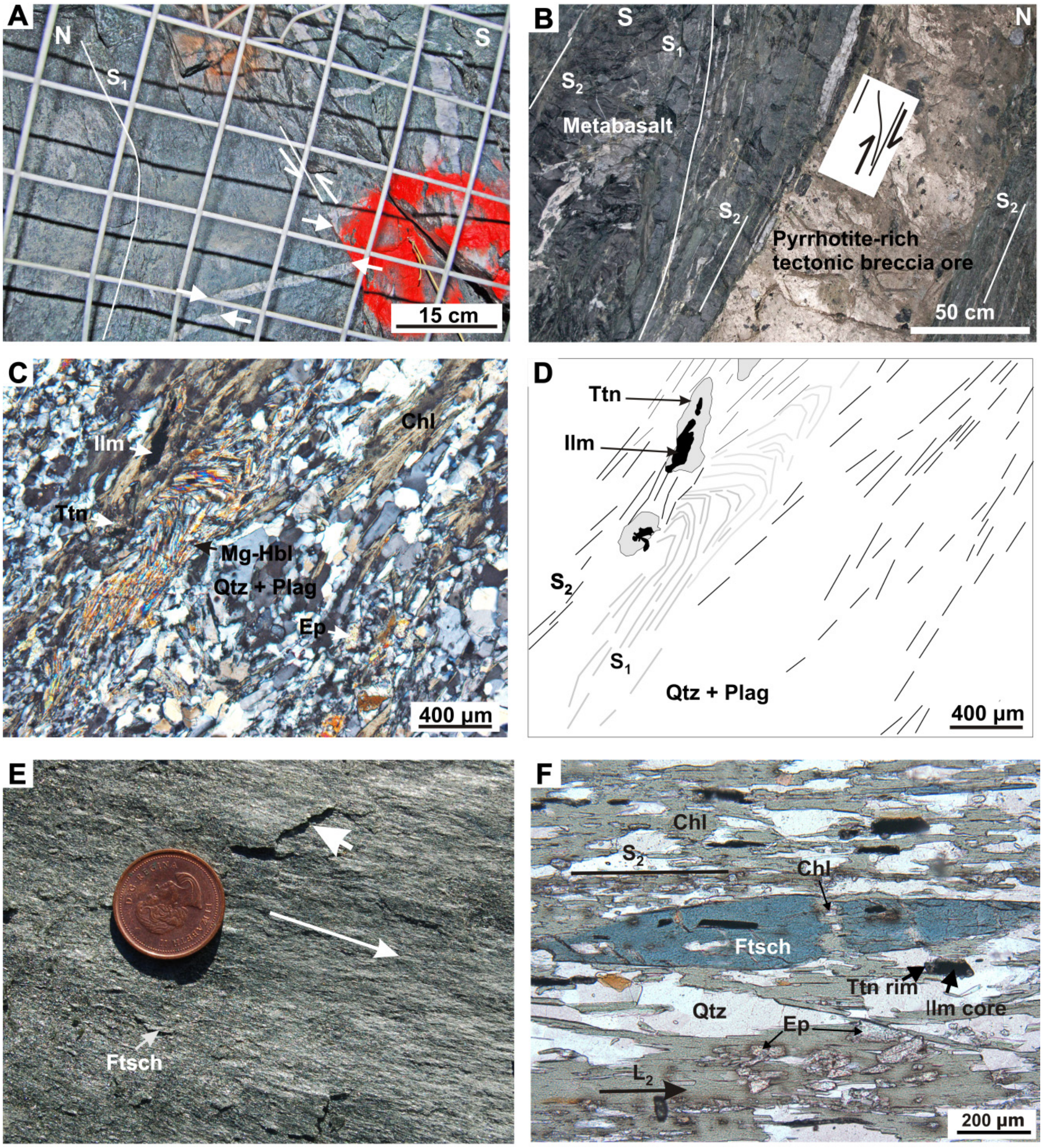

Figure 2.13. Underground photographs of (a) sheared norite near contact with metabasalt showing anticlockwise rotation of S_1 and displaced quartz veins (indicated by arrows) across a D_2 shear zone, indicating reverse slip and (b) sheared metabasalt along the #4 shear zone. S_1 foliation is dragged into the orientation of S_2, suggesting reverse shear. (c) Photomicrograph (cross-polarized light) of sheared norite near contact with metabasalt showing transposition of S_1 by S_2. S_1 magnesiohornblende in sheared norite defines an isolated tight crenulation hinge bounded by S_2 chlorite foliation planes and (d) Sketch of photomicrograph in (c). (e) Hand sample of sheared metabasalt from the #4 shear zone showing a ductile slickenline lineation exposed by parting the sample along a foliation

surface in a chlorite-rich metabasalt. Long arrow is parallel to the striations and points in the direction of movement (down-dip). The short white arrow indicates a congruous step. The mineral stretching lineation (L_2) and relict ferrotschermakite grains are aligned parallel to the slickenline lineation. (f) Photomicrograph (plane-polarized light) of sheared metabasalt from the #4 shear zone. Microboudinaged ferrotschermakite is aligned parallel to L_2 and S_2 and chlorite grows in microboudin necks. Ftsch: ferrotschermakite, Ilm: ilmenite, Qtz: quartz, Ttn: titanite, Chl: chlorite, Ep: epidote.

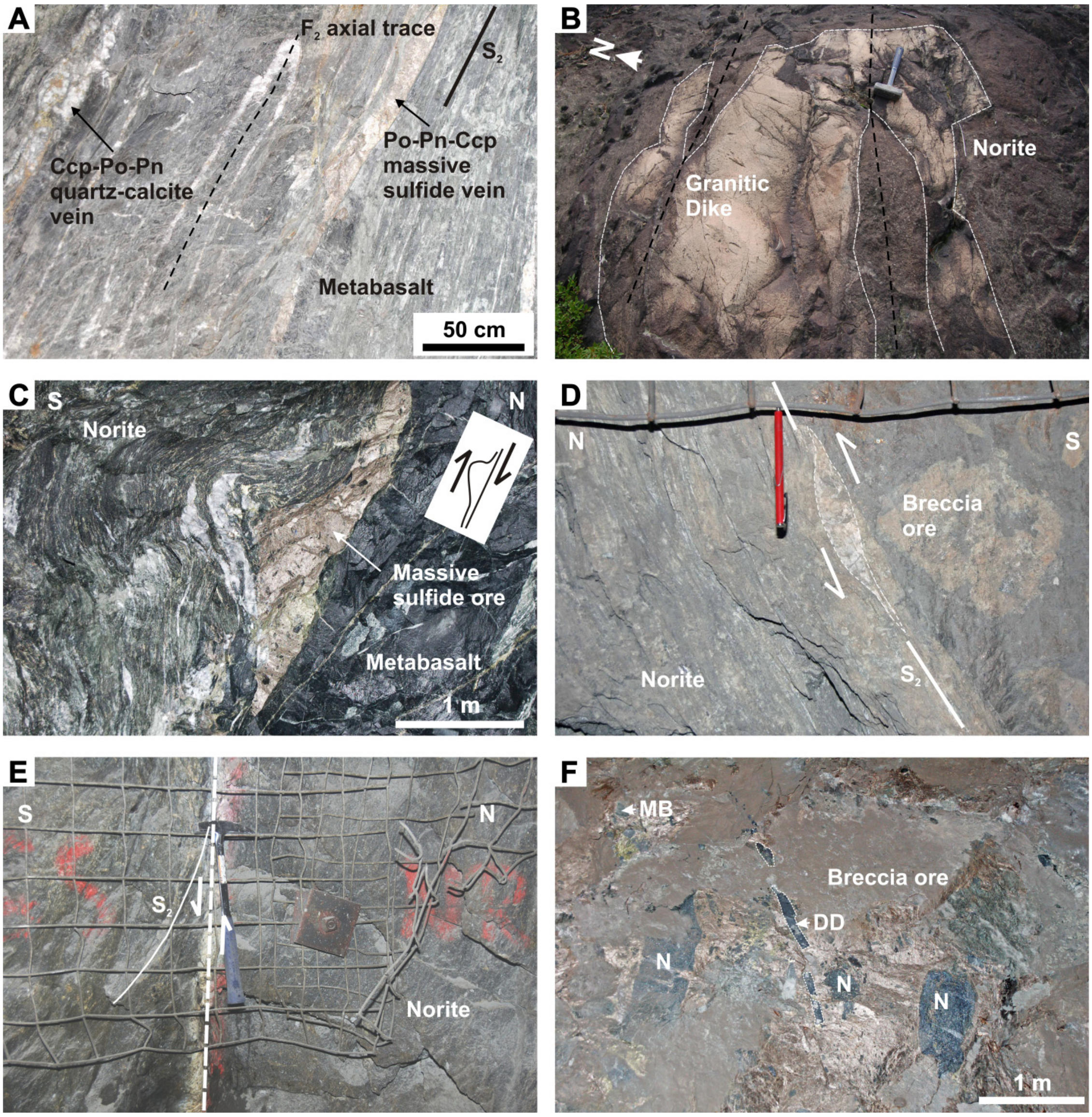

Figure 2.14. (a) Underground photograph of F_2 isoclinal folded quartz extension vein. (b) Surface photograph of granitic dike (outlined by white broken lines) folded into an isoclinal F_2 fold in sheared Main Mass norite, ~400 m northeast of #2 shaft (see Fig. 2.3a for location). The fold has an east-west trending axial planar S_2 chlorite foliation (outlined by black broken lines). Underground photographs of (c) north-verging asymmetric F_2 fold indicating reverse slip, (d) back-rotated quartz vein boudin indicating reverse slip during D_2, (e) D_3 fault indicating a south-side-down slip, and (f) broken-up plagioclase-phyric diabase dike in pyrrhotite-rich breccia ore. MB: metabasalt, N: norite, DD: plagioclase-phyric diabase dike.

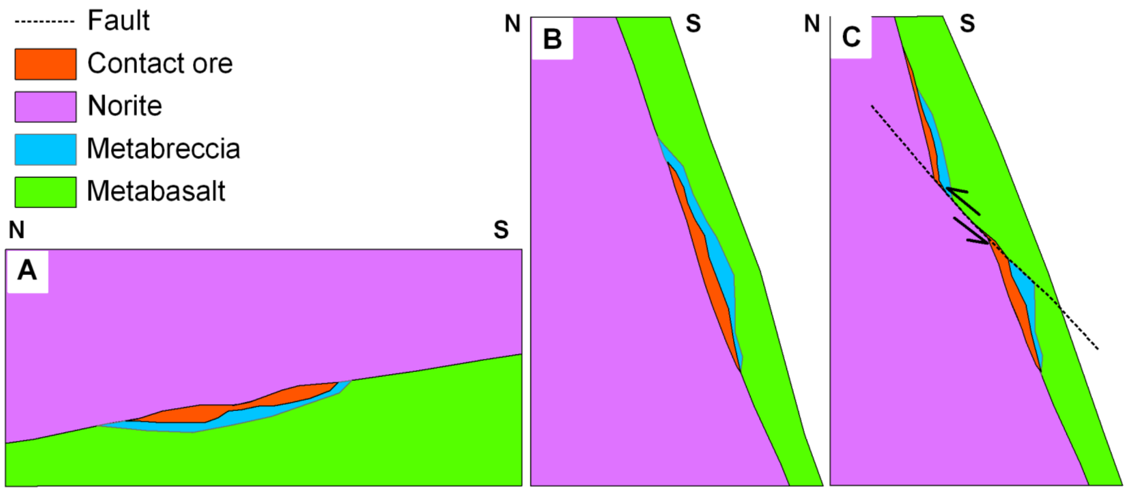

Figure 2.15. Schematic diagrams (not to scale) showing (a) emplacement of ore at the base of the SIC, (b) overturning of SIC, (c) north-over-south reverse shearing. This model is inconsistent with the observed displacements on the SIC contact at the Garson mine.

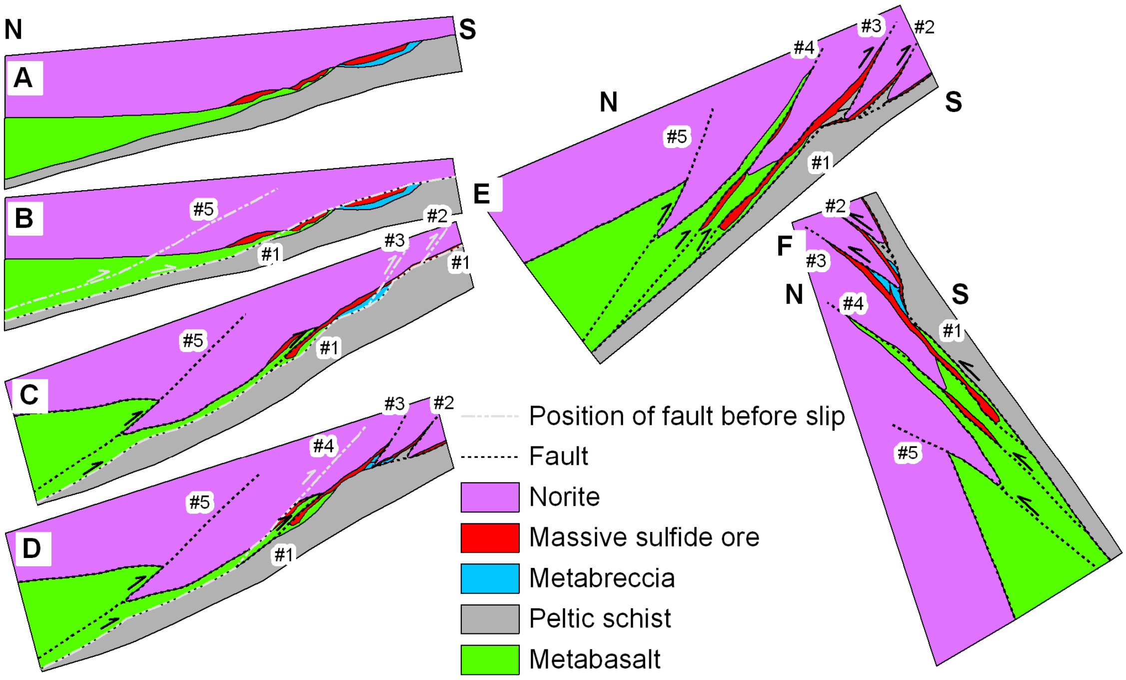

Figure 2.16. Model (facing east) showing the structural evolution of the Garson mine during NW-SE compression of the Sudbury structure. Dashed white lines represent the position of active faults before slip. (a) Initial geometry: emplacement of massive sulfide ore at the base of the SIC. (b) Position of #5 shear zone before slip. (c) Propagation of #5 north-dipping thrust, which transects the SIC, and imbrication of SIC norite/ore/footwall contact along the #1 shear zone during D_1 north-over-south slip. Positions of #2 and #3 shear zones before slip are also shown. (d) Continued D_1 imbrication of SIC norite/ore/footwall contact and tectonic transport of slivers of footwall rocks into main mass SIC norite along the #2 and #3 shear zones during D_1 north-over-south slip. Position of #4 shear zone before slip is also shown. (e) North-over-south slip along #4 shear zone transport slivers of metabasalt into main mass SIC norite. (f) Overturning of the SIC during D_1 followed by D_2 south-over-north slip along reactivated steeply south-dipping, overturned D_1 shear zones.

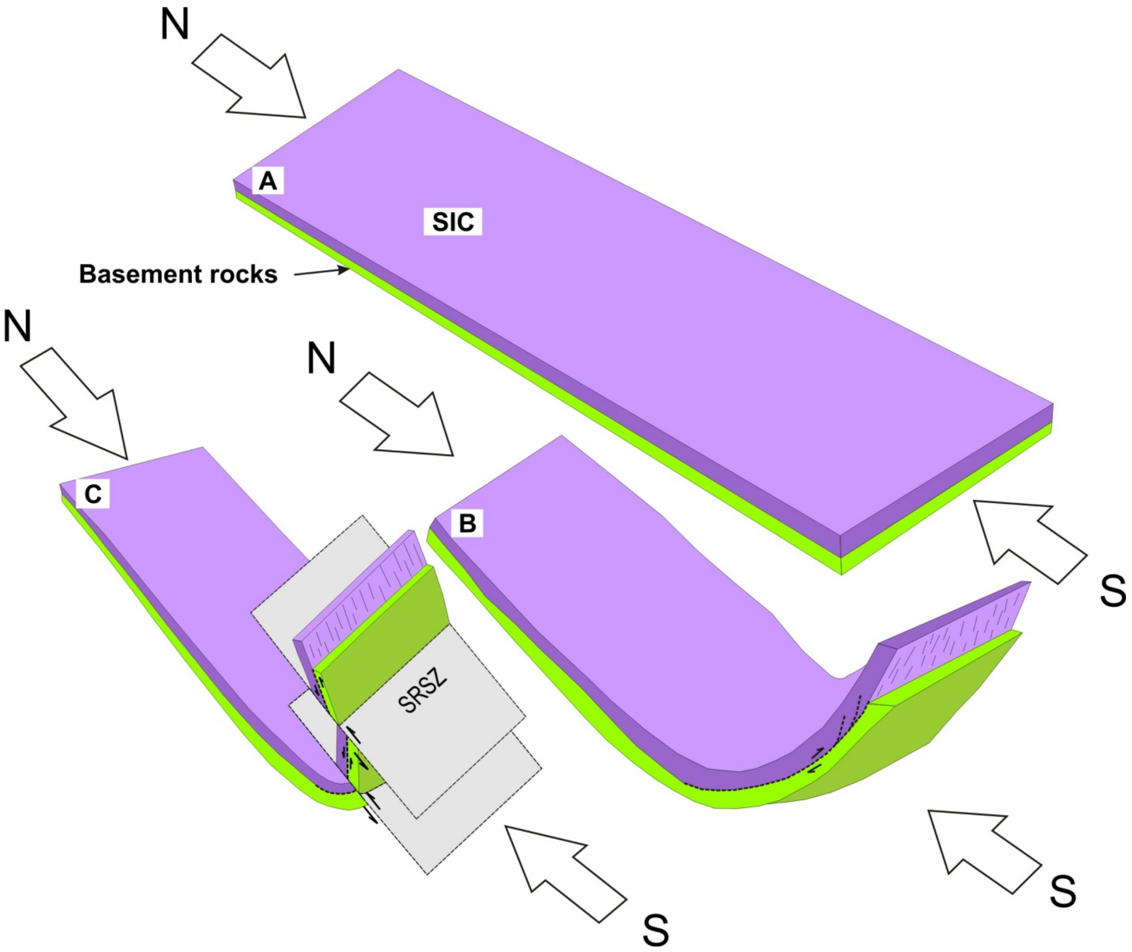

Figure 2.17. Schematic diagrams showing development of structures with progressive buckling along the South Range. (a) The SIC was emplaced as a sub-horizontal melt sheet overlying basement rocks. (b) Layer parallel north-dipping reverse shear zones formed in the south limb due to mechanical decoupling at the interface between the SIC and the underlying Huronian Supergroup footwall rocks during early D_1. (c) Formation of reverse, north-directed South Range Shear Zone late during D_1 and overturning of the southeast limb of the Sudbury structure.

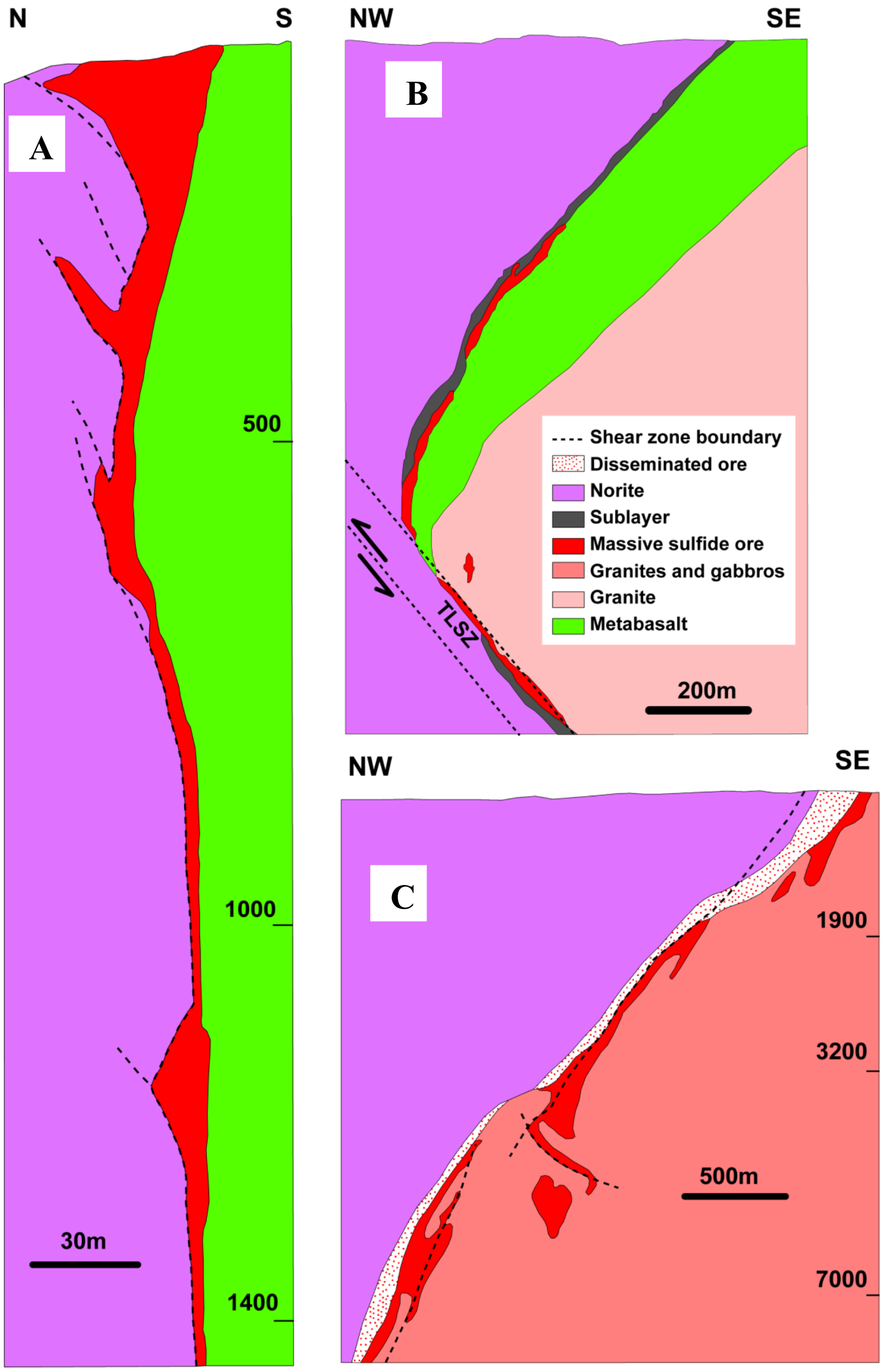

Figure 2.18. (a) N-S cross section of the Falconbridge mine (modified after Davidson, 1948; Lochhead, 1955; Owen and Coats, 1984). NW-SE cross sections of the (b) Thayer Lindsley mine (modified after Binney et al., 1994 and Bailey et al., 2004) and (c) Creighton mine (modified after Cochrane, 1991).

Chapter 3: Fabrics and Textures of Deformed and Metamorphosed Ni-Cu-PGE Sulfide Ores at Garson Mine and their Implications for Sulfide Mobilization Processes

JOSHUA MUKWAKWAMI[1], BRUNO LAFRANCE[1], C. MICHAEL LESHER[1], DOUGLAS K. TINKHAM[1], NICOLE RAYNER[2], AND DOREEN E. AMES[2]

1. Mineral Exploration Research Centre, Department of Earth Sciences, Laurentian University, 933 Ramsey Lake Road, Sudbury, Ontario P3E 2C6, Canada
2. Geological Survey of Canada, 601 Booth Street, Ottawa, Ontario K1A 0E8

3.1 Abstract

The Garson Ni-Cu-platinum group element (PGE) deposit is a deformed, overturned, low Ni tenor contact-type deposit along the contact between the Sudbury Igneous Complex and stratigraphically underlying rocks of the Huronian Supergroup in the South Range of the 1.85 Ga Sudbury structure. The ore bodies are coincident with steeply south-dipping, north-over-south D_1 shear zones, which imbricated the SIC, its ore zones, and underlying Huronian rocks during mid-amphibolite facies metamorphism. The shear zones were reactivated as south-over-north, reverse shear zones during D_2 at mid-greenschist facies metamorphism. Syn-D_2 metamorphic titanite yields an age of 1849 ± 6 Ma, suggesting that D_1 and D_2 occurred immediately after crystallization of the SIC during the Penokean Orogeny. The ore bodies plunge steeply to the south parallel to colinear L_1 and L_2 mineral lineations, suggesting strong structural controls on mineralization. Sulfide mineralization consists of breccia ores, with minor disseminated sulfides hosted in norite, and syn-D_2

quartz-calcite-sulfide veins. Mobilization by ductile plastic flow was the dominant mechanism of sulfide/metal mobilization during D_1 and D_2, with additional minor hydrothermal mobilization of Cu, Fe and Ni by hydrothermal fluids during D_2. A first generation of pentlandite overgrows a S_1 ferrotschermakite foliation in D_1 deformed ore zones. Pentlandite was exsolved from recrystallized polygonal pyrrhotite grains after cessation of D_1, which resulted in randomly distributed large pentlandite grains, and randomly-oriented pentlandite loops along grain boundaries of polygonal pyrrhotite within the breccias ore. A second generation of pentlandite overgrows a S_2 chlorite foliation in D_2 shear zones. Pyrrhotite recrystallized and was flattened during progressive D_2 deformation of breccia ore along narrow shear zones. Exsolution of pentlandite loops along the grain boundaries of these flattened grains produced a pyrrhotite-pentlandite layering that is not observed in D_1 deformed ore zones. The overprinting of the two foliations by pentlandite and exsolution of pentlandite along grain boundaries of flattened pyrrhotite grains suggests that the Garson ores reverted to a metamorphic monosulfide solid solution at temperatures ranging between 550 and 600°C during D_1, and continued to deform as a monosulfide solid solution during D_2.

3.2 Introduction

Primary magmatic processes typically account for the genetic and spatial association of magmatic Ni-Cu-platinum group elements (PGE) deposits and their mafic/ultramafic rocks worldwide (Naldrett, 2004). However, many deposits (e.g., Kambalda and Perseverance, Australia; Trojan, Zimbabwe, Sääksjärvi, Finland; Thompson, Canada) have been overprinted by deformation, greenschist to amphibolite facies metamorphism, and hydrothermal alteration (Barrett et al. 1977; Maiden et al., 1986; Bleeker, 1990; Menard et al., 1996; Mancini and Papunen, 2000; Liwanang, 2001; Layton-Mathews et al., 2007, Duuring et al., 2007, 2010). Some ore shoots were imbricated and show an elongation parallel to fold axes or to linear fabrics in surrounding rocks, suggesting a structural control on the geometry of the ore shoots (e.g., Barrett et al. 1977; McQueen 1987).

Although the contact-type, footwall-type, and offset-type deposits associated with the ca. 1850 Ma (U-Pb zircon age by Krogh et al., 1984; Davis, 2008) Sudbury Igneous Complex (SIC) have been the subjects of many publications and are reasonably well understood, the mechanisms that produced the present geometry and internal textures and structures of the deformed contact ores have received little attention. The Garson deposit and many others (e.g., Falconbridge, East, Creighton and Thayer Lindsley) in the South Range are overprinted by at least 2 post-impact tectono-metamorphic events, which imbricated ore-bearing contacts and mobilized ore into the hanging wall of high-angle reverse faults and thrust faults (Davidson, 1948; Lochhead, 1955; Owen and Coats, 1984; Binney et al., 1994; Bailey et al., 2004; Snelling, 2009; Mukwakwami et al., 2012). However, the role of sulfide mobilization processes, which include ductile plastic flow, partial metamorphic anatexis of the ore zones, and metamorphic-hydrothermal mobilization (Cox, 1987; Marshall and Gilligan, 1987, 1993; Gilligan and Marshall, 1987; Marshall et al., 2000; Tomkins, 2007; Tomkins et al., 2007), have not been determined in these deformed deposits. Understanding the importance of these mechanisms of sulfide/metal transport and deposition during deformation and metamorphism is critical for exploration, both on mine-scale, and on the scale of the entire South Range.

We describe the ore sulfide mineralogy, textures and internal meso- and microscopic fabrics within the main ore zones, and calculate the bulk composition of the Garson ores. These together with phase equilibria considerations in the Fe-Ni-S, and Cu-Fe-S systems, form the basis for our evaluation of the post-magmatic processes that affected the Garson ores. In addition, we present new ID-TIMS U-Pb metamorphic titanite ages that constrain the timing of metamorphism at Garson. Our study shows that ductile plastic flow was the dominant mechanism of sulfide/metal mobilization at Garson, and confirms that low Ni tenor Ni-Cu-PGE ores at Sudbury, reverted to metamorphic monosulfide solid solution during amphibolite facies metamorphism (~550-600°C). Although it has long been inferred that the SIC was deformed during the Penokean Orogeny (Brocoum and Dalziel, 1974; Card et al., 1984), our study presents the first Penokean U-Pb titanite ages from shear zones at the base of the SIC.

3.3 Geologic Setting

The regional geology and mine geology of the Garson mine are described in detail in Mukwakwami et al. (2012), and are only briefly described in this section. The terms D_1 and D_2 in this manuscript are specific to the Garson mine because the sequence of deformation events that affected the South Range is yet to be established.

The Garson Ni-Cu-PGE deposit is located in the South Range in the southeastern flank of the ca. 1850 Ma Sudbury structure (Fig. 3.1: Krogh et al., 1984; Davis, 2008), which comprises the SIC and its associated cogenetic radial and concentric quartz dioritic dikes, underlying anatectic footwall breccias and discontinuous pseudotachylitic Sudbury breccia belts (Dressler, 1984, Grant and Bite, 1984; Lightfoot et al., 1997), and overlying impact fall-back and phreatomagmatic breccias of the Onaping Formation (Peredery, 1972; Ames, 1999; Ames et al., 2002; Long, 2004; Grieve et al., 2010). The Onaping Formation is the lower formation of the Whitewater Group and it is in turn overlain by sedimentary rocks of the Onwatin and Chelmsford formations of the upper Whitewater Group. The main mass of the SIC consists of norite, quartz-gabbro and granophyre, and overlies discontinuous zones of inclusion-rich norite (Sublayer norite) and footwall breccias. The SIC hosts Ni-Cu-PGE deposits in three distinct environments: 1) within embayments along the footwall contact of the SIC, 2) within brecciated and veined footwall rocks, and 3) within quartz-diorite dikes. Whereas deposits in the North Range are relatively undeformed, those in the South Range (e.g., Garson, Falconbridge, East, Lockerby and Thayer Lindsley) were intensely deformed and offset by amphibolite-grade NE- to E-trending shear zones (e.g., Lochhead, 1955; Aniol and Brown, 1979; Shanks and Schwerdtner 1991a, b; Binney et al., 1994; Cowan and Schwerdtner, 1994, Riller et al., 1999, 2010; Bailey et al., 2004; Ames and Farrow, 2007; Mukwakwami et al., 2012).

The Garson deposit occurs on the southeastern limb of the folded SIC at the contact between the SIC Main Mass norite, footwall metabreccia, and interleaved metabasalt associated with metagabbro, metawacke, quartzite and pelitic schist of the Elliot Lake Group of the Huronian Supergroup (Figs. 3.2, 3.3). Metabreccia has an igneous texture characterized by euhedral plagioclase laths, interstitial quartz, amphibole, biotite, and accessory titanite. It likely formed by partial melting of the footwall rocks beneath the cooling SIC as suggested for footwall breccias in the less deformed North Range (Lakomy, 1990; McCormick et al., 2002). The deposit formed at the base of the SIC as contact ore hosted by Sublayer and metabreccia. It consists of four main sulfide ore bodies that are coincident with steeply south-dipping shear zones (#1, #2, #3, and #4 shear zones) after which they are named. The ore bodies consist predominantly of inclusion-rich breccia ore comprising rock fragments in a sulfide matrix (50-80%), but they also include minor disseminated sulfides (up to 10%) in norite lenses within the ore zones, in Main Mass norite, and to a lesser extent in slivers of norite enclosed by metabasalt (Mukwakwami et al., 2012). The #1 and #4 shear ore bodies are tabular, elongate bodies with down-dip plunges (Fig. 3.4). Norite and metabasalt within and adjacent to the shear zones were metamorphosed to amphibolite facies assemblages consisting of magnesiohornblende-quartz-oligoclase-biotite-ilmenite, and ferrotschermakite-quartz-oligoclase-biotite-ilmenite ± garnet, respectively. The pelitic schist unit, which flanks the metabasalt to the south, predominantly consists of muscovite and quartz and minor chlorite.

The Garson shear zones formed during D_1 and were later reactivated during D_2 at amphibolite and greenschist facies temperatures, respectively (Mukwakwami et al., 2012). D_1 shear zones are characterized by a steeply, south-dipping to sub-vertical, mylonitic S_1 foliation and by a down-dip L_1 mineral stretching lineation defined by ferrotschermakite in metabasalt and by magnesiohornblende in sheared norite. S_1 is transposed parallel to a shear-parallel foliation (S_2) along D_2-reactivated D_1 shear zones.

S_2 contains L_2 ductile slickenlines, which plunge steeply to the south down the dip of S_2, and is parallel to a L_2 chlorite mineral stretching lineation. The two L_1 and L_2 lineations are colinear and parallel to the plunge of the ore shoots (Fig. 3.4, insert). During D_1, the SIC was buckled into a regional ENE-trending fold and the Garson shear zones formed during north-over-south flexural slip at or near the contact between the SIC and underlying Huronian basement rocks. Slip along the shear zones displaced slivers of footwall basement rocks over distances of 400–700m and imbricated the SIC norite, the footwall rocks, and the ore zones into a north-dipping thrust stack. Later during D_1, the Garson shear zones were rotated to their present steep southerly dips during overturning of the southeastern limb of the SIC, and the south-over-north South Range Shear Zone (Fig. 3.1) cut through the hinge zone and south limb of the folded SIC to accommodate further shortening of the SIC (Cowan and Schwerdtner, 1994; Riller et al., 2010; Mukwakwami et al., 2012). South-over-north D_2 reactivation of the D_1 shear zones occurred during the same orogenic event as discussed below.

3.4 Metamorphism of the Deposit

3.4.1 Description of Sample and Mineral Chemistry

The metamorphic temperatures during D_1 can be estimated from a garnet-bearing, schistose, metabasalt sample from the #1 shear zone. In thin section the metabasalt consists of alternating quartz-rich and ferrotschermakite-rich domains. Quartz-rich domains locally contain minor epidote and rare, strongly zoned, anhedral plagioclase grains that rarely exceed 15 μm in size (Fig. 3.5a). The ferrotschermakite-rich domains contain minor epidote and ilmenite, as well as rare, euhedral, garnet porphyroblasts, which are 50 to 500 µm in size and which enclose ilmenite and quartz inclusion trails that are continuous with the external S_1 foliation in the matrix. Despite widespread syn-D_2 greenschist-grade retrogression in the shear zones (Mukwakwami et al., 2012), the sample lacks retrograde chlorite and titanite after ferrotschermakite and ilmenite, respectively, suggesting that it has not been affected by D_2 retrogression. The garnets are not resorbed or altered, and are in stable contact along straight grain boundaries with matrix ferrotschermakite (Fig. 3.5b), indicating that the two minerals are in textural equilibrium.

Qualitative X-ray maps of garnet and ferrotschermakite grains and quantitative analyses of their compositions were obtained using a Cameca SX-100 electron probe microanalyzer equipped with WDS detectors in the Ontario Geoscience Laboratories in Sudbury. Plagioclase grains were not analyzed because they are very small (<15 µm) and strongly zoned on a scale similar to that of the effective volume accessed by the electron beam diameter (10 µm). Operating conditions were 20 kV accelerating voltage and 20 nA beam current for quantitative analyses, and 20 kV accelerating voltage, 100 nA beam current and 20 ms/pixel dwell time (run in continuous mode) for qualitative X-ray maps. Between 15 and 20 analyses were collected along transects through the centre and rims of three garnet grains in order to obtain compositional profiles of the grains and assess possible retrograde diffusional modifications. Four to five point analyses were collected along the edge of several garnet grains in contact with ferrotschermakite grains to provide average garnet rim compositions, and four to six point analyses were collected in the rims and cores of these ferrotschermakite grains to obtain average rim and core compositions.

Amphibole grains showing some slight, grey-scale variations in backscattered images were analyzed to check if more than one type of amphibole was present. A few ilmenite grains were analyzed at their rims and cores. The ilmenite grains are homogeneous and they contain between 1.4 wt% and 2.4 wt% MnO. Garnet compositions were normalized to 12 oxygens and 8 cations, with Fe^{3+} estimated by recalculating the structural formula as in Ravna (2000), with $Fe^{3+} = 2 - (Al + Cr + Ti)$. Garnet is almandine-rich (X_{alm} = 0.56-0.61) with substantial grossular (X_{gr} = 0.23-0.28) and spessartine (X_{sps} = 0.13-0.14) components, and pyrope-poor (X_{py} = 0.02). Quantitative line scans across the centers of 3 garnet grains show near-flat Fe, Mn, Ca and Mg profiles with minor local fluctuations (Fig. 3.6). X-ray maps display small discrete off-center cores with slightly higher Mn and Fe, and lower Ca contents (Fig. 3.7). They also display an increase in Mn and a decrease in Ca along the rims of the euhedral grains (Figs. 3.7a, b). The lack of Fe-Mg zoning at the rims (Figs. 3.7c, d) suggests that the increase in Mn is a growth feature resulting from the possible breakdown of a Mn-bearing phase, most likely ilmenite, during the latter stages of garnet growth rather than late retrograde back-diffusion of Mn into garnet during consumption of these garnets (e.g., Hollister, 1966, 1969; Woodsworth, 1977). These maps together with the near-flat profiles of the grains, suggest incomplete homogenization of garnet due to diffusional re-equilibration at high temperatures during D_1, and absence of significant retrograde diffusional modification of the grains (e.g., Woodsworth, 1977; Spear, 1988; Daniel et al., 2003).

Amphibole analyses were normalized following the procedure and nomenclature of Leake et al. (1997). The amphibole composition from all analyses is ferrotschermakite and their major element composition does not vary significantly from grain to grain, suggesting that the slight grey-scale variations are likely due to some minor elements that were not analyzed and that they crystallized during a single D_1 event.

3.4.2 Temperature Calculations

Coexisting amphibole-garnet pairs in metabasalt were used to calculate the metamorphic temperatures using two different approaches to geothermometric calculations to estimate the syn-D_1 temperature conditions: 1) the average T method of Powell and Holland (1994) using the software THERMOCALC, dataset 5.5 (Holland and Powell, 1998), and 2) the calibrated garnet-hornblende geothermometer (Ravna, 2000). The garnet and amphibole activities for the average T method were calculated as in White et al. (2007) and Diener et al. (2007), respectively. Average T calculated using the average compositions of garnet rims and adjacent amphiboles at pressures between 1 and 8 kb range from 500 to 618°C (Fig. 3.8; Table 3.1) with standard deviations of 130 to 139°C.

We used Ravna's (2000) method for calculating the garnet structural formula, as explained above, whereas the amphibole structural formula was calculated using the empirical procedure of Schumacher (1991) as required by the calibrated garnet-hornblende geothermometer (Ravna, 2000). The calibrated garnet-hornblende geothermometer yielded T-values ranging between 558 and 588°C (Table 3.2) using the following geothermometric expression derived from experimental data:

$$T(°C) = \frac{1504+1784\left(X_{Ca}^{Grt}+X_{Mn}^{Grt}\right)}{In\, X_{D(Fe^{2+}/Mg)}^{Grt-Hbl}+0.720} - 273, \text{ where } In\, X_{D(Fe^{2+}/Mg)}^{Grt-Hbl} = \frac{(Fe^{2+}/Mg)^{Grt}}{(Fe^{2+}/Mg)_{M1-M3}^{Hbl}},$$

where $X_{Ca}^{Grt} = \frac{Ca}{Ca+Mn+Fe^{2+}+Mg}, and\ X_{Mn}^{Grt} = \frac{Mn}{Ca+Mn+Fe^{2+}+Mg}$.

3.5 Geochronology

3.5.1 Structural Setting and Chemistry of Titanite

Three sheared samples were collected from the #4 shear on the 4900 (sample GA187), 5000 (sample GA188), and 5100 (sample GA115) mine levels for U/Pb dating. Samples GA115 and GA188 are Huronian gabbro that are associated with metabasalt, and sample GA187 is norite. All samples have a strong S_2 foliation defined by chlorite after magnesiohornblende or ferrotschermakite (Mukwakwami et al., 2012; Fig. 3.9a). Titanite overgrows large, syn-D_1 ilmenite grains, which are parallel and continuous with the S_2 chlorite foliation (Figs. 3.9a, c). The titanite grains are subhedral to euhedral, they contain rare, tiny internal inclusions of ilmenite (Figs. 3.9b, d), and they occur along S_2 foliation planes. The euhedral grains have straight grain boundaries (Fig. 3.9a), suggesting that they are in textural equilibrium with chlorite.

Titanite grains from samples GA115 and GA187 were imaged and analyzed using a Zeiss EVO-50 SEM equipped with EDS detectors at the Ontario Geoscience Laboratories in Sudbury. Operating conditions were 20kV accelerating voltage, 0.75 nA beam current, and 50s count time. Between 1 and 4 analyses were collected from the core and rims of each grain. Back-scatter images show that all grains are homogeneous in composition and devoid of cores and/or overgrowths (Figs. 3.9b-d). Results of quantitative analyses are given in Fig. 3.10 and Appendix F. On a plot of SiO_2, CaO and FeO_{total} against TiO_2, the compositions of the rims and cores are indistinguishable in all the grains.

3.5.2 U-Pb Titanite Age

Titanite grains were separated by standard crushing, heavy-liquid, and magnetic-separation techniques at the Geological Survey of Canada Geochronology Laboratory in Ottawa, Ontario. They were analyzed in the same laboratory using isotope dilution-thermal ionization mass spectrometry (ID-TIMS), following the analytical procedures described by Parrish et al. (1992) and Davies et al. (1997). The U-Pb results are presented in Table 3.3 and on a concordia diagram in Fig. 3.11. The errors on the ratios and ages are 2σ.

All titanite grains are clear and colorless. At least three fractions, each composed of about ten titanite grains, were obtained from each sample. The multi-grain fractions are characterized by low U contents (2-64 ppm). Two fractions from sample GA187 and two from sample GA188 contained less than 1 ppm U, and were therefore unsuitable for geochronology. Two fractions (T1 and T3) from sample GA115 are concordant at 1859 ± 32 Ma and 1852 ± 6 Ma, whereas the third fraction is discordant (18%) with a ^{207}Pb/^{206}Pb age of 1810 ± 16 Ma. The only fraction that could be analyzed for sample GA187, as the other fractions did not contain uranium, yielded a ^{207}Pb/^{206}Pb age of 1791 ± 5 Ma (27% discordant). Four fractions from sample GA188 are discordant with ^{207}Pb/^{206}Pb ages of 1893 ± 74 Ma (3.7% discordant), 1869 ± 87 Ma (2.1% discordant), 1842 ± 43 Ma (9.7% discordant), and 1774 ± 19 Ma (24% discordant). Combining all data from all the three samples yield a good regression line (MSWD = 1.6) with upper and lower intercepts of 1850 ± 6 Ma and 266 ± 28 Ma, respectively. Regression through the four higher precision analyses, i.e., fractions with low common Pb-content, yields upper and lower intercepts of

1849 ± 6 Ma and 264 ± 28 Ma (MSWD = 2.3), respectively. This upper intercept is interpreted as the crystallization age of the titanite.

3.6 Fabrics and Textures of Metamorphosed and Deformed Ore

The Garson deposit comprises three types of Ni-Cu-PGE mineralization: (1) disseminated to matrix-textured sulfide mineralization, (2) breccia ore, and (3) quartz-calcite-sulfide veins. Their structures and textures are described below from underground exposures, polished slabs, and thin sections cut perpendicular to foliation and parallel to lineation.

3.6.1 Disseminated Sulfide Mineralization

Disseminated to matrix-textured mineralization occurs in metamorphosed, but weakly deformed to undeformed Main Mass norite, and in norite slivers along the #4 shear zone. It consists of 5 to 25% polycrystalline sulfide grains that fill interstices between labradorite rimmed by oligoclase, green magnesiohornblende, quartz, and biotite (Fig. 3.12a, b). The sulfide grains consist of pyrrhotite (80-90%), pentlandite (5-15%), and chalcopyrite (5-10%) in association with minor magnetite (<5%), trace gersdorffite, cobaltite and niccolite, and rare sperrylite (Gammell et al., 2004). Chalcopyrite-rich pods with irregular amoeboidal shapes are locally observed.

In moderately to strongly sheared norite, the sulfides occur as thin (≤5 mm wide), discontinuous and anastomosing pyrrhotite-rich bands parallel to S_1 or S_2 (Figs. 3.12c, d). Pyrrhotite and chalcopyrite were injected into fractures cutting through both magnesiohornblende and chlorite, suggesting that these sulfides behaved ductilely during both D_1 and D_2. Pentlandite occurs as rims around pyrrhotite and as irregular grains within pyrrhotite (Fig. 3.12d). Pentlandite appears to be undeformed as it is not cut by microfractures, and does not exhibit a shape-preferred orientation indicative of ductile flow. This suggests that exsolution of pentlandite from pyrrhotite either post-dates D_1 and D_2, or occurred late during these two deformation events.

3.6.2 Breccia Ore

Breccia ore contains up to 50% fragments of Huronian rocks (metabasalt, metawacke, pelitic schist, and quartzite), norite, and metabreccia surrounded by a pyrrhotite-rich matrix with similar mineralogy to that of disseminated to matrix-textured sulfides. It is subdivided into contact and fault breccia ores. Contact breccia ore occurs in thicker segments (8–50m wide) of the #1 and #4 shear ore bodies, whereas fault breccia ore occurs as tabular ore zones along narrow (~10 cm to 3m thick) segments of the ore bodies (Fig. 3.2). Contact breccia ore contains both D_1 and D_2 fabrics, whereas D_1 fabrics in fault breccia ore have been almost completely destroyed during D_2.

3.6.3 Contact breccia ore

Contact breccia ore is characterized by an abundance of norite inclusions (30-80%) together with metabasalt (20-60%) and other Huronian inclusions (Fig. 3.13a). The norite inclusions are sub-rounded to angular and they locally contain disseminations and blebs of pyrrhotite-pentlandite-chalcopyrite. They are generally weakly deformed, but strongly metamorphosed (Figs. 3.13b, c, f). Rare, less metamorphosed, norite inclusions have bytownitic to anorthitic plagioclase ($An_{84–91}$: Fig. 3.13c; Mukwakwami et al., 2012), similar to the anorthitic (An_{90}) composition of plagioclase in cumulus norite inclusions within the South Range Sublayer (Naldrett et al., 1984).

D_1 deformed ores contain norite and metabasalt fragments that are flattened and boudinaged parallel to S_1 (Figs. 3.13d, e), stretched parallel to L_1, and locally folded (Fig. 3.14a). Emanating from the #1 shear ore body are massive pyrrhotite-rich sulfide veins that extend at high angles into the wallrocks of the ore body for distances of up to 3m. The veins pinch and swell, and they are devoid of hydrothermal quartz or calcite (Fig. 3.14b), suggesting that they were emplaced as piercement veins during ductile plastic flow of the sulfides (e.g., Maiden et al., 1986). Chalcopyrite occurs in the distal part of the piercement structures (Fig. 3.14b), indicating greater ductility of chalcopyrite relative to pyrrhotite. Chalcopyrite and pyrrhotite occur in boudin necks between fragments (Figs. 3.13d, e), in fold hinges (Fig. 3.14a) and in fractures in silicate rock fragments (Fig. 3.13a), further attesting to ductile flow of these sulfides. Pentlandite occurs as very large (5-25 mm wide) irregular grains that are randomly distributed in a pyrrhotite-rich matrix and that overprint S_1. In thin section, norite fragments consist of clusters of actinolite–magnesiohornblende–magnesioriebekite rimmed by ferrotschermakite in contact with oligoclase (An_{29-31}: Mukwakwami et al., 2012), quartz, biotite, and ilmenite (Figs. 3.13b, c), indicative of amphibolite facies conditions during D_1. Sulfides overgrow S_1 defined by ferrotschermakite (Fig. 3.13f), and pyrrhotite occurs as anhedral grains with curved grain boundaries, coexisting with polygonal grains (0.2–3 mm in grain size; Figs. 3.14c, d) suggesting dynamic recrystallization by grain boundary migration (Ostwald and Lusk, 1978; Lusk and Ostwald, 1983; Cox and Etheridge, 1984; Cox, 1987). Pentlandite occurs as discontinuous loops rimming pyrrhotite (Figs. 3.14c, d), as fine exsolution lamellae along pyrrhotite cleavage planes (Fig. 3.14e), and as irregular coarse grains within pyrrhotite (Fig. 3.14f). Anhedral to subhedral magnetite is associated with pyrrhotite.

In D_2 deformed ores, norite and metabasalt fragments contain abundant chlorite after amphibole (Fig. 3.15a), and they are flattened parallel to a S_2 chlorite foliation. The fragments are boudinaged and boudin necks are filled with pyrrhotite and chalcopyrite (Figs. 3.15b, c), suggesting ductility of these sulfides during D_2. The ore consists primarily of pyrrhotite polygonal grains and, more rarely, elongate grains parallel to S_2 (Figs. 3.15f, 3.16a, b). The polygonal foam texture of the pyrrhotite grains likely formed during dynamic recrystallization or post-deformation static recrystallization of the grains (Ostwald and Lusk, 1978; Lusk and Ostwald, 1983; Cox and Etheridge, 1984). Pentlandite occurs as 2-10 mm size grains that overgrow the S_2 foliation (Figs. 3.15c-e). These grains are associated with a network of sub-millimeter, pentlandite loops that are generally oriented parallel to S_2 (Figs. 3.15e). In thin section, the pentlandite loops rim pyrrhotite grain boundaries (Figs. 3.15f, 3.16a, b). The pentlandite loops grew towards the center of pyrrhotite grains and coalesced to form irregular-shaped pentlandite grains, which are aligned parallel to S_2, and are continuous with these loops (Figs. 3.15c-e, 3.16a, b).

3.6.4 Fault breccia ore

In contrast to contact breccia ore, fault breccia ore contains no norite fragments, abundant metabasalt fragments (85 to 95%), and few (≤15%) fragments of metawacke, pelitic schist, and quartzite (Fig. 3.16c). Metabasalt in the wallrocks of the zones and fragments within the ore zones have well-developed greenschist chloritic S_2 and L_2 fabrics (Fig. 3.16d). Ore zones locally thicken in the hinges of north-verging F_2 folds (Fig. 3.16e), truncate S_2 (Fig. 3.16f), and flowed into wallrock fractures which resulted in the plucking of wallrock fragments and incorporation of these fragments into the ore zones (Fig. 3.17a). Chalcopyrite and minor pyrrhotite fill extensional fractures that are near-perpendicular to the stretching lineation in quartz boudins (Fig. 3.17b). Collectively, these observations indicate ductile flow of both pyrrhotite and chalcopyrite during D_2.

Pentlandite occurs as coarse, granoblastic grains varying in size from 2 mm to 7 mm, as discontinuous layers that are up to 3 mm thick and less than 3 cm in length, and as elongate grains oriented parallel to S_2 (Figs. 3.17c-e). In thin section, pyrrhotite forms polygonal grains and rare elongate grains (Figs. 3.17d, e). The elongate pyrrhotite grains have aspect ratios of 2 to 4 with dimensional long axes of 200 to 600 μm parallel to S_2. They have interlobate grain boundaries indicative of grain boundary migration, and faint, internal, low-angle boundaries with optical misorientations of 5-10° across them. These low-angle boundaries are interpreted as subgrain boundaries (e.g., Lusk and Ostwald, 1983) bounding subgrains varying in size from ~50-250 μm. Thus, the polygonal pyrrhotite likely formed by subgrain rotation and migration recrystallization of the deformed elongate grains (e.g., Lusk and Ostwald, 1983). Anhedral magnetite grains (150-500 μm in size) are cut by fractures filled with chalcopyrite and minor pyrrhotite (Fig. 3.17f). The fractures formed as tensile fractures perpendicular to the stretching lineation. This suggests that magnetite is more competent, and behaved brittlely during D_2 ductile plastic flow of pyrrhotite and chalcopyrite.

3.6.5 Quartz-Calcite-Sulfide Veins

Quartz-calcite-sulfide veins are observed in both D_2 deformed contact- and fault-breccia ores. They occur as gently-dipping, up to ~5m long, extensional veins that truncate S_2, and as laminated shear veins that are parallel to S_2 (Fig. 3.18a; Mukwakwami et al., 2012). The latter are up to 1 m thick and they are found along or near the ore zone margins as steeply south-dipping to sub-vertical veins that can be traced for up to 20m along strike. Both vein types are locally folded into isoclinal to tight folds transposed parallel to S_2, and they form pinch and swell structures parallel to S_2 and L_2. In thin section, quartz has a shape-preferred orientation parallel to S_2. Large grains have interlobate to amoeboid grain boundaries and they contain subgrains that are similar in size to surrounding smaller recrystallized grains (Fig. 3.18b), suggesting that the smaller grains formed by subgrain rotation and migration recrystallization during D_2 (Hirth and Tullis, 1992; Stipp et al., 2002).

The veins contain irregular pods (Fig. 3.18a) of chalcopyrite (80-90%), pyrrhotite (5-15%) and pentlandite (≤5%), and accessory sphalerite. The pods have rims of pyrrhotite with minor, coarse-grained, granular and flame pentlandite, and cores of chalcopyrite (Fig. 3.18c). Mineralized fragments of quartz-calcite veins occur within fault breccia ore, where they are stretched parallel to L_2 (Fig. 3.18d). S_2 is defined by foliated and flattened metabasalt fragments and it wraps around the vein fragments, which formed as shear and extensional veins that were brecciated during D_2.

3.7 Bulk Composition of the Garson Ores

Data used to calculate the bulk composition of the Garson ores are from the assay database of Vale Ltd. for diamond drill cores that intersected the #1 and #4 shear ore bodies between the 3000 and 6500 levels. The database does not contain assay data for the #2 and #3 shear ore bodies because they were mined out before the database was compiled. However, this data would not have changed the calculated average ore composition because the mineralogy of the main ore zones are similar (Aniol and Brown, 1979). The samples were analyzed at ALS Minerals, Sudbury, Ontario, as described in Mukwakwami et al. (submitted).

Over 20700 analyses from the drill hole database were used to calculate metal tenors using the method described by Naldrett (1981). Because most metals are assumed to be in the sulfide fraction, calculation of the metal tenor is important as it allows comparison of metal contents in samples with different proportions of sulfides (e.g., Ross and Keays, 1979; Naldrett et al., 1979; Barnes and Lightfoot, 2005). The method assumes that all chalcophile metals were originally dissolved in the sulfide melt. Cu is allocated to chalcopyrite, Ni is allocated to pentlandite, and the remainder is allocated to pyrrhotite. Sulfur is allocated to pentlandite and chalcopyrite, and the remainder is calculated as pyrrhotite. The total sulfide content of the sample is the sum of pentlandite, chalcopyrite and pyrrhotite. The tenors of those and other metals in 100% sulfides are then calculated by dividing the measured concentrations of the metal in the whole rock by the total sulfide content. In calculating the bulk composition of the Garson deposit, metal tenors were weighted by the sulfur content of each sample to ensure that the contribution of each sample to the average bulk composition is proportional to its sulfur content. The sulfur-weighted mean (S_{WMi}) for each metal (i) was obtained by summing the products of the metal tenor (T_i) and the measured sulfur content (S_i) divided by the total sum of measured sulfur from the entire sample population (S_t), i.e.,

$$S_{WMi} = \sum_{i=1}^{n}(T_i * \frac{S_i}{S_t}).$$

The average composition of Garson ores using this method is 3.92 wt.% Cu, 5.01 wt.% Ni, 37.7 wt.% S and 53.4 wt.% Fe, suggesting that it is a low Ni tenor deposit, i.e., Ni <8 wt.%, which is depleted in Cu relative to the ~4.6% Cu and ~4.8% Ni average of 490 South Range massive ores calculated from the data of Naldrett et al. (1999; see Table 3.4).

3.8 Discussion

The Garson deposit formed as a contact-type deposit at the base of the SIC because the ore bodies are closely associated with the SIC-Huronian contact, and the contact breccia contains norite fragments that are similar to Sublayer norite (Mukwakwami et al., 2012). The occurrence of the main ore bodies along shear zones, and the steep southerly plunge of the ore bodies parallel to the penetrative colinear L_1 and L_2 lineations (Fig. 3.4) suggest a structural control on the ore body configurations related to post-magmatic processes as observed in other deformed massive sulfide ore deposits world-wide (e.g., Wilson, 1973; Rickard and Zweifel, 1975; Barrett et al., 1977; McQueen, 1987; Lacroix and Darling, 1991; Belkabir and Hubert 1995; Davis, 2005, Duuring et al., 2010). The strong foliations in wall rocks enveloping the ore zones, together with internal fabrics in the ore zones, i.e., a strong shape-preferred orientation of silicate rock fragments defining pervasive foliations and stretching lineations, indicate that the main ore zones are themselves zones of high strain.

The mechanisms of sulfide/metal mobilization during deformation and metamorphism have been commonly classified into three main types 1) ductile plastic flow of sulfides, where strain is preferentially partitioned into relatively low-strength sulfides (e.g., Barrett et al., 1977; McQueen, 1979, 1981, 1987; Cox, 1987; Gilligan and Marshall, 1987; Marshall and Gilligan, 1987; Cowden and Archibald, 1987; Marshall et al., 2000), 2) metamorphic-hydrothermal mobilization that involves liquid-state transport through solutions and wet diffusion (e.g., Keays et al., 1982; Cox, 1987; Gilligan and Marshall, 1987; Marshall and Gilligan, 1987; Marshall et al., 2000), and 3) metamorphic partial anatexis that involves production of a partial sulfide melt and/or dissolution of ore minerals by a migrating silicate partial melt, and subsequent mobilization of the melt (e.g., Mavrogenes et al., 2001; Frost et al., 2002; Sparks and Mavrogenes, 2005; Baile and Reid, 2005; Tomkins et al., 2007).

At the low-to-medium metamorphic pressure conditions suggested for the South Range (e.g., Thompson et al., 1985; Fleet et al., 1987; Blonde, 1996; Easton et al., 2000), the Powell and Holland (1994) geothermometer yield metamorphic temperatures ranging from 550 to 596°C, assuming pressures between 3 and 6 kbar. The range is comparable to corresponding garnet-amphibole temperatures of 558 to 588°C obtained in this study using the calibration by Ravna (2000). Thus syn-D_1 metamorphic temperatures at Garson were likely in the ~550-600°C range, which is within error of the temperature of 580 ±

60°C (Blonde, 1996) estimated for amphibolite facies metamorphism in the Nippissing diabases, just SW of the SIC. Dynamic recrystallization of quartz in deformed veins, in quartz fragments in breccia ore, and in quartz-rich microlithons bounded by chlorite domains suggests metamorphic temperatures of at least ~280°C (Ströckhert et al., 1999; Stipp et al., 2002) during D_2. More specifically, subgrain rotation, which is the dominant mechanism of dynamic recrystallization, points to a higher minimum temperature of roughly 400°C (Hirth and Tullis, 1992; Stipp et al., 2002, 2010; Faleiros, 2010; Long et al., 2011).

3.8.1 Metamorphic Sulfide Anatexis

Frost et al. (2002) and Tomkins et al. (2007) suggested that small quantities of partial melts enriched in As, Cu, Sb, Pb, Sn, Bi, Te, Pd, Pt, Ag and Au can be produced at moderate to high metamorphic temperatures (~520-850°C) in volcanogenic massive sulfide deposits. Because of the low abundances of the above elements, the maximum amount of partial melt that can be generated from Ni-Cu-PGE magmatic deposits is less than 0.05 volume percent (Tomkins et al., 2007). The mineralogy of mobilized breccia ores (pyrrhotite-pentlandite-chalcopyrite) in the main shear zones would melt only at temperatures exceeding ~900°C (Kullerud et al., 1969), which are far higher than the calculated metamorphic temperatures of ~550-600°C during D_1. This suggests that sulfide mobilization at Garson was not caused by metamorphic sulfide anatexis.

3.8.2 Hydrothermal Mobilization

Metamorphic-hydrothermal fluids can modify the compositions of deformed sulfide ores through dissolution and consequent precipitation of sulfides/metals during or after post-metamorphic peak conditions (e.g., Gilligan and Marshall, 1987; Marshall and Gilligan, 1987; Marshall et al., 2000). Syn-D_2 quartz-calcite-sulfide veins (Figs. 3.18a, c) provide evidence for hydrothermal mobilization of sulfides and metals (e.g., Cook et al., 1993; Vokes and Craig, 1993). The veins have distinctly high Pd/Ir ratios compared to the disseminated to net-textured sulfides, and to contact- and fault breccia ores (Mukwakwami et al., submitted). The high Pd/Ir ratios of quartz-calcite-sulfide veins are consistent with their mobilization by hydrothermal fluids (e.g., Bavinton and Keays, 1978; Groves et al., 1979; Keays et al., 1982; Lesher and Keays, 1984; Farrow and Watkinson, 1997), but the consistent lower ratios for the other ore types suggest that these ore types were not significantly modified by hydrothermal fluids (Mukwakwami et al., submitted).

3.8.3 Mobilization by Ductile Plastic Flow

3.8.3.1 Deformation of Ore

Despite strong deformation of the massive sulfide ore zones, norite and metabasalt are only penetratively deformed adjacent to the ore zones, suggesting that strain was strongly partitioned into the shear zones (Mukwakwami et al., 2012). The strength of pyrrhotite and chalcopyrite decreases markedly at temperatures above 200°C and low pressures (<1kb) in laboratory experiments, and they undergo intracrystalline plastic deformation by deformation twinning, dislocation glide and then dislocation creep with increasing temperatures (Gill, 1969; Clark and Kelly, 1973; Artkinson, 1975; Kelly and Clark, 1975; Roscoe, 1975; Cox, 1987; Marshall et al., 2000). Pentlandite is a less ductile mineral, and it deforms brittlely at temperatures below 400°C at 1.5 kbar (McQueen, 1987). As experiments are conducted at strain rates that are orders of magnitude faster than natural strain rates, all sulfides deform ductilely at lower temperatures under natural conditions (Clark and Kelly, 1973; Cox, 1987). Thus, pyrrhotite-rich massive sulfides would readily yield by ductile plastic flow at the greenschist- to amphibolite facies temperatures recorded at Garson (e.g., Barrett et al., 1977; Cox and Etheridge, 1984; Cox, 1987; McQueen, 1987; Marshall et al., 2000).

Several lines of evidence suggest that the sulfide ore zones underwent ductile plastic flow on the microscopic and meter-scale during D_1 and D_2. These include: (1) the deformation of disseminated and net-textured sulfides into bands oriented parallel to S_1 and S_2 (Figs. 3.12c, d: e.g., Wakefield, 1976; Lacroix and Darling, 1991), (2) the ductile flow of sulfides into boudin necks and into pinches of boudinaged and flattened rock fragments that have necked but not broken through (Figs. 3.13d, 3.15b, c), (3) the sulfide infilling fractures cutting through magnetite, silicate grains, fragments, and foliations (Figs. 3.16c, f, 3.17a, b, f,), (4) the accumulation and flow of sulfides in fold hinges and other dilatant structures (Fig. 3.16e), (5) the elongation and shape-preferred orientation of pyrrhotite parallel to S_2 (Figs. 3.15f, 3.17d, e), and (6) the occurrence of isoclinally folded rock fragments within massive sulfide ore (Fig. 3.15c).

Abundant Sublayer and norite inclusions-bearing contact breccia ore suggests that the Garson ores initially formed within embayments or depressions at the base of the SIC and was later deformed during D_1 and D_2 (Mukwakwami et al., 2012). The shear zones propagated along the weak sulfide ore at the contact between overlying Main Mass norite and underlying metabasalt basement rocks, repeating this contact through thrusting and imbrication of the basement rocks and SIC norite. The #4 shear zone ramped up from that contact and propagated into massive, non-mineralized Main Mass SIC norite that is stratigraphically above the norite-metabasalt contact. Massive sulfide ore was extruded from the embayments by plastic ductile flow into the shear zone and then sheared into a thin tabular zone along the shear zones, resulting in formation of fault breccia ore devoid of norite inclusions. This explains why the #4 shear ore body is in a reverse stratigraphic position, with norite to the south and metabasalt to the north (Fig. 3.3a). Thus, mobilization of ore along the #4 shear zone occurred over a down-dip distance of up to 450 m from the ~2900 and 4300 levels (Fig. 3.3a). Mobilization of massive sulfides by ductile plastic flow on the scale of tens of meters to 100m have been suggested for most deformed Ni-Cu-PGE deposits (e.g., Barrett et al., 1977, McQueen, 1987; Bleeker, 1990; Lacroix and Darling, 1991; Marshall et al., 2000), but this provides evidence for ductile plastic mobilization of Ni-Cu massive sulfide ore over a distance of about 450m.

3.8.3.2 Timing of D_1 and D_2

Titanite is in textural equilibrium with chlorite (Fig. 3.9a), it overgrows syn-D_1 ilmenite (Figs. 3.9a, c), and contains internal inclusions of ilmenite (Figs. 3.9b, d), suggesting a syn-D_2 metamorphic origin for the titanite. The titanite fractions have low U content, typical of metamorphic titanite (e.g., Getty and Gromet, 1992; Corfu and Stone, 1998; Frost et al., 2000; Bailey et al., 2004). As the grains are clear and colorless, are devoid of overgrowths, and are chemically homogeneous (Fig. 3.10), they represent a single generation. Thus, the high precision analyses of four fractions provide the best estimate for the crystallization of metamorphic titanite at 1849 ± 6 Ma (Fig. 3.11) during D_2. The age is within error of the emplacement age of the SIC (1850 ± 1 Ma: Krogh et al., 1984) and correlate with the Penokean orogenic event, which occurred between 1890 Ma and 1830 Ma along strike of Sudbury in the southern Lake Superior region of Wisconsin, Minnesota, and Michigan (Van Schmus, 1976; Sims et al., 1989; Van Schmus et al., 1996). Although it has long been suspected that ductile fabrics in Sudbury formed during the Penokean Orogeny (e.g., Brocoum and Dalziel, 1974; Card, 1978; Card et al., 1984), these new ages provide the first conclusive evidence of the deformation of the Sudbury impact structure during the Penokean Orogeny. Because titanite grew during D_2 shortly after the emplacement of the SIC, this further suggests that D_1 and D_2 occurred during a progressive deformation event. Subsequent tectonic pulses, the 1.7 Ga–1.6 Ma Yavapai-Labradorian Orogeny (Davidson et al., 1992; Bailey et al., 2004; Piercey et al., 2007) and 1.45 Ga Chieflakian event (Fueten and Redmond, 1997; Szentpéteri, 2009) further affected the South Range, but their effects on the SIC are not clearly understood. The cause of discordance and the significance of the lower intercept of 264 ± 28 Ma is not clear, but may be due to radiogenic Pb loss by continuous diffusion (e.g., Tilton, 1960; Wasserburg, 1963), in which case, the lower intercept would have no geological significance.

During cooling of the SIC, deposition of the Onaping Formation continued from an initial ~200m-thick impact fall-back breccia deposited above the impact melt sheet into a ~1600m-thick sequence of phreatomagmatic breccias and syn-magmatic intrusions that formed due to interaction between the melt sheet (molten SIC) and water from an overlying ocean (Peredery, 1972; Muir and Peredery, 1984; Gibbins, 1994; Ames and Gibson, 1995; Ames, 1999; Ames et al., 2002; Grieve et al., 2010). Subsequently, laminated carbonaceous mudstones of the overlying, ~600m-thick Onwatin Formation were deposited in a sediment-starved deep anoxic basin over a period of 0.6 Ma to 600 Ma, assuming modern depositional rates of 0.001-0.060m/Ka (Long, 2004). Turbiditic sandstone of the Chelmsford Formation, which has a preserved thickness of ~850m (Roussell, 1984), was conformably deposited above the Onwatin Formation.

Thermal modeling assuming heat loss solely by conduction suggests that solidification of the SIC from a superheated impact melt sheet took ~500 Ka, and that temperatures at the SIC/footwall contact would reach ~400°C after at 1.1 Ma (Ivanov and Deutsch, 1999). Prevec and Cawthorn (2002) and Zieg and Marsh (2005) suggested that the SIC solidified after ~60 Ka with heat loss through both conduction and convection. There are few constraints on these thermal models, and none of the models included the effects of thermomechanical erosion and assimilation of footwall rocks that generated embayments and sulfide-inclusion-rich Sublayer (e.g., Prevec and Cawthorn, 2002; Lesher et al., 2009) or explosive phreatomagmatic activity and melting of the overlying Onaping Formation (e.g., Ames et al., 2002; Grieve et al., 2010), both of which would have accelerated heat loss from the melt sheet. So, it is likely that the SIC cooled and solidified in less than 60

Ka and that deposition of the Onwatin and Chelmsford formations and the lithification of these rocks, which occurred over a period greater than 0.6 Ma (see above) likely outlasted the cooling of the SIC. Any residual heat near the base of the SIC likely had dissipated by conduction through the floor by the start of D_1. The conformable contacts in the Whitewater Group (e.g., Rousell, 1984; Ames, 1999; Long, 2004) further suggests that D_1 started after deposition of the entire sequence of the Whitewater Group. Thus, temperatures and pressures began to increase during D_1 due to the crustal thickening that accompanied the formation of compressive regional ductile shear zones, folds and cleavage that affect all the formations overlying the SIC (Cowan and Schwerdtenr, 1994; Riller and Schwerdtner, 1997; Riller et al., 1999; Mukwakwami et al., 2012).

3.8.3.3 Ore Textures and Phase Equilibria Consideration

The phase equilibria in the Fe-Ni-Cu-S system have been reviewed by Naldrett (2004) and although data for the phase equilibria in the quaternary system are limited, data for the Fe-Ni-S and Fe-Cu-S ternary systems provide some constraints on the formation of the ore textures at Garson and on the behavior of sulfide minerals during deformation of Sudbury structure. Assuming that residual heat had dessipated at the base of the SIC at the start of D_1, pentlandite and pyrrhotite in the Garson ore would progressively break down to a monosulfide solid solution via metal diffusion between pentlandite and pyrrhotite at the metamorphic temperatures associated with D_1. This process begins at ~200°C and complete conversion to a homogeneous monosulfide solid solution is achieved at low to medium metamorphic grade conditions (~300-550°C) in ores with <8 wt.% Ni (Naldrett et al., 1967; Craig and Kullerud, 1969; Kullerud et al., 1969; Shewman and Clark, 1970; Ewers, 1972; Cabri, 1973; Craig, 1973; Misra and Fleet, 1973; Barrett et al., 1977; McQueen, 1979, 1987, Bleeker, 1990). When projected on to a Fe-Ni-S ternary diagram, the Garson ore bulk composition falls within, and towards the sulfur-rich side of the monosulfide solid solution field at metamorphic temperatures above 400°C (Figs. 3.19a, b). Thus, under equilibrium conditions, the low Ni tenor (~5.0 wt.%) Garson ores reverted to a homogeneous Ni-poor metamorphic monosulfide solid solution during D_1 (550°C-600°C). Upon cooling the monosulfide solid solution crystallized pyrrhotite, and exsolved pentlandite (Naldrett et al., 1967; Craig and Kullerud, 1969; Kullerud et al., 1969).

The monosulfide solid solution likely coexisted with a Cu-rich intermediate solid solution because pyrrhotite or the monosulfide solid solution can only resorb up to ~1 wt.% Cu in solid solution between ~500–590°C, and the amount of soluble Cu decreases with decreasing temperature (Naldrett et al., 1967; Kullerud et al., 1969; Cabri, 1973; Craig, 1973; McQueen, 1979). When projected on to the Cu-Fe-S ternary diagram at 500°C, the Garson composition falls within the field of cubanite solid solution + pyrite (Fig. 3.19c). The cubanite–pyrite tie-line changes to chalcopyrite–pyrite upon cooling below ~330°C, and hence, the Garson composition would be composed of pyrrhotite, chalcopyrite, and pyrite (e.g., Yund and Kullerud, 1966; Naldrett et al., 1967; Kullerud et al., 1969). However, pyrite, which is a common primary constituent of pyrrhotite-rich Sudbury ores (e.g. Hawley, 1962; Hawley and Stanton, 1962; Naldrett., 2004, p. 451-455; Bailey et al., 2006; Dare et al., 2010), is not present within the Garson ores. It was most likely completely consumed in a reaction involving pyrite and hexagonal pyrrhotite to produce monoclinic pyrrhotite upon cooling to temperatures below ~310°C (Craig and Kullerud, 1969; Kullerud et al., 1969). Craig and Kullerud (1969) suggested that such a reaction may have caused the resorption and roundedness of pyrite grains observed in some of the Sudbury ores (e.g., Hawley, 1962; Hawley and Stanton, 1962).

Although D_1-deformed contact breccia ore has a strong S_1 foliation defined by silicate rock fragments (Figs. 3.13d-f), pyrrhotite grains are generally polygonal (Figs. 3.14c, d), suggesting that they either underwent dynamic recrystallization during deformation or they underwent static recrystallization after deformation. Pentlandite formed after deformation because it occurs as irregular loops rimming polygonal pyrrhotite grains (Fig. 3.14d), as lamellae exsolved in pyrrhotite (Fig. 3.14e), or as large grains that are randomly distributed and overgrow S_1. Chalcopyrite occurs as discrete irregular pods or patches that flowed into dilational sites during deformation. These observations are consistent with the reversion of Garson ores during D_1 to a metamorphic monosulfide solid solution coexisting with blebs of a Cu-rich cubanite solid solution, as observed in laboratory experiments (e.g., Ewers, 1972; McQueen, 1979). Upon cooling, the monosulfide solid solution crystallized pyrrhotite and exsolved pentlandite either late during D_1 or shortly after, and blebs of the cubanite solid solution formed the chalcopyrite segregations, which occur within pyrrhotite-rich sulfides (Figs. 3.14a, 3.16f). Thus our observations are in agreement with predictions from phase equilibria. As displacements along the shear zones occurred mainly during D_1 (Mukwakwami et al., 2012), the ore was deformed and ductilely flowed as a homogeneous monosulfide solid solution, but was later affected by D_2 reactivation of the shear zones.

The three varieties of pentlandite (grains, loops and lamellae), observed in D_1-deformed contact breccia ore are also observed in D_2-deformed contact- and fault breccia ores. However, the pentlandite loops and grains define S_2-parallel layers that are interlayered with rare elongate pyrrhotite grains (Figs. 3.15c-f, 3.16a, b, 3.17c-e). Barrett et al. (1977) and McQueen (1987) suggested that the layering could form due to mechanical sorting of polymineralic aggregates or stress-induced exsolution during deformation. We discount these processes for Garson as pentlandite in D_2 contact- and fault breccia ores clearly post-dates deformation because the grains are granoblastic, they are not fractured, they overgrow S_2 (Figs. 3.15c-e), and the loops are exsolved along grain boundaries of flattened pyrrhotite grains (Figs. 3.15c-f, 3.16a, b). This suggests that the Garson ores deformed as a homogeneous monosulfide solid solution during D_2 ($T \geq\sim 400°C$). As the pentlandite loops and grains exsolved along pyrrhotite grain boundaries, their orientations are largely dependent on the shape fabric of the pyrrhotite grains that exsolved the pentlandite (e.g., Francis et al., 1976; Ostwald and Lusk, 1978; Lusk and Ostwald, 1983). This is further demonstrated by the absence of pentlandite layering in D_1 deformed contact breccia ore, where pyrrhotite grains have no shape-preferred orientation (Figs. 3.14c, d). The deformation of the Garson ores as a monosulfide solid solution during D_2 occurred during a decrease in temperatures from D_1 (500-600°C) as part of a progressive D_1-D_2 Penokean event. Ore samples collected between the ~3000 and 6500 levels have restricted ranges of Fe/Ni ratios and Ni tenors (~4 to 8 wt.%), which is consistent with mobilization of the ores as homogeneous monosulfide solid solutions during D_1 and D_2 (Mukwakwami et al., submitted). This is because deformation of polymineralic aggregates results in segregation of the more ductile pyrrhotite from pentlandite, which in turn leads to large-scale variations in Fe/Ni ratios and Ni tenors within an ore shoot (Barrett et al., 1977; McQueen, 1987).

3.9 Conclusions

1) Ore shoots have a southerly down-dip plunge parallel to L_1 and L_2 stretching lineations, indicating strong structural controls on the geometry of the Ni-Cu sulfide ore zones.

2) Geothermometric calculations using the average T method of Powell and Holland (1994) and the garnet-hornblende geothermometer of Ravna (2000) indicate amphibolite facies temperatures of 550-590°C during south-directed thrust imbrication of the SIC-basement contact during D_1. Dynamic recrystallization of quartz by subgrain rotation suggests greenschist facies temperatures of at least ~400°C during north-directed reactivation of D_1 shear zones during D_2.

3) Whereas magnetite deformed brittlely at greenschist facies metamorphic temperatures, pyrrhotite and chalcopyrite deformed by ductile plastic flow during D_1 and D_2.

4) Solid-state ductile plastic flow was the dominant mechanism of sulfide/metal mobilization during D_1 and D_2, but metamorphic hydrothermal fluids caused minor mobilization of Ni and Cu, as indicated by the presence of quartz-calcite-chalcopyrite veins with minor pyrrhotite and pentlandite.

5) Syn-D_2 metamorphic titanite yield a U-Pb crystallization age of ca. 1849 Ma, suggesting that D_1 and D_2 are part of a single progressive Penokean deformation event,

which occurred immediately after crystallization of the SIC. This is the first well constrained Penokean age for the deformation of the Sudbury impact structure.

6) Pentlandite formed during metamorphic cooling following cessation of deformation during D_1 and D_2, confirming that Ni-Cu-PGE ores with a low bulk Ni tenor, such as those in the South Range, deform and can revert to a homogeneous monosulfide solid solution during deformation at amphibolites facies (550–600°C). This is consistent with predictions from experimental phase relations in the Fe-Ni-S and Cu-Fe-S systems.
7) Exsolution of pentlandite along grain boundaries of flattened pyrrhotite formed a pentlandite foliation layering in breccia ores that underwent deformation under greenschist facies temperatures during D_2. This layering is absent in breccia ores that deformed under amphibolites facies temperatures during D_1, because pentlandite exsolved along grain boundaries of recrystallized pyrrhotite with polygonal or granoblastic shapes and textures.

3.10 Acknowledgements

This work is part of a Ph.D. project by J. Mukwakwami and was prepared under the supervision of B. Lafrance and C.M. Lesher, and benefited from discussions with D.G.F Long and D. Kontak. The research was supported by a Vale-NSERC-CRD grant to B. Lafrance and C.M. Lesher, NSERC Discovery grants to B. Lafrance and C.M. Lesher, and a Society of Economic Geology Foundation Canada grant to J. Mukwakwami. Geochronology work was done under the Targeted Geoscience Initiative Phase 4 program of the Geological Survey of Canada led by D. Ames. We thank Vale for providing access to geological data, mine exposures, and diamond drill cores, and to S. Lowen, D. Hodder, C. Gauld, S. Kedzierski, L. Desjardins, D. Butt, B. Gauvreau, and D. Bellefeuille for logistical assistance and many beneficial discussions on the geology of the Garson Mine. D. Crabtree, John Hechler and Sandra Clarke of the Ontario Geological Survey helped with the microprobe and SEM analyses.

Table 3.1. Garnet-amphibole thermometry results. Temperatures calculated using the average T method of Powell and Holland (1994), using dataset 5.5 (Holland and Powell, 1998).

P (kbar)	**Temperature (°C)**			
	Grt 1	**Grt 4**	**Grt 2-1**	**Grt 2-2**
1	527	500	537	540
2	539	511	548	551
3	550	522	560	563
4	561	533	571	574
5	572	544	582	585
6	583	554	593	596
7	594	565	604	607
8	605	575	615	618

Table 3.2. Parameters calculated from average analyses of coexisting garnet-amphibole pairs for the garnet–hornblende geothermometer (Ravna, 2000).

Sample	**Fe^{3+}) (Grt)**	**Fe^{2+} (Grt)**	**X_{Ca} (Grt)**	**X_{Mn} (Grt)**	**$(Fe^{2+}/Mg)^{Grt}$ (Grt)**	**Fe^{3+} (Amph)**	**Fe^{2+} (Amph)**	**$(Fe^{2+}/Mg)^{Amph}_{M1-M3}$**	**$K_{D(Fe^{2+}/Mg)}^{Grt-Hbl}$**	**T°C**
Grt 1	0.011	1.833	0.241	0.140	29.28	0.25	2.62	4.60	6.37	576
Grt 2-1	0.007	1.817	0.247	0.136	29.18	0.26	2.61	4.62	6.31	580
Grt 2-2	0.012	1.835	0.243	0.139	28.86	0.25	2.62	4.69	6.16	588
Grt 4	0.006	1.799	0.243	0.149	32.02	0.25	2.61	4.64	6.90	558

Table 3.3. Isotopic data for titanite fractions from two Huronian gabbros and one from SIC norite, Garson mine.

					Isotopic Ratios[6]								Ages (Ma)[8]						
Fraction[1]	U[2] ppm	Pb*[3] ppm	206Pb[4]/204Pb	Pb[5] pg	208Pb/206Pb	207Pb/235U	±1SE Abs	206Pb/238U	±1SE Abs	Corr.[7] Coeff.	207Pb/206Pb	±1SE Abs	206Pb/238U	±2SE	207Pb/235U	±2SE	207Pb/206Pb	±2SE	% Disc.
GA115: Huronian gabbro																			
T1 (8)	7	3	105	16	0.26	5.256	0.056	0.3355	0.0014	0.5601	0.1136	0.0010	1865	14	1862	18	1859	32	-0.4
T2 (9)	64	19	226	50	0.17	4.068	0.022	0.2666	0.0004	0.6806	0.1107	0.0005	1524	4	1648	9	1810	16	17.8
T3 (11)	24	10	580	9	0.31	5.283	0.011	0.3384	0.0005	0.6949	0.1132	0.0002	1879	5	1866	4	1852	6	-1.7
GA187: SIC norite																			
T3 (9)	88	24	666	20	0.22	3.552	0.007	0.2353	0.0002	0.7380	0.1095	0.0002	1362	3	1539	3	1791	5	26.6
GA188: Huronian gabbro																			
T1 (10)	9	3	81	26	0.13	4.640	0.066	0.2987	0.0020	0.5335	0.1126	0.0014	1685	20	1756	24	1842	43	9.7
T2 (10)	23	6	180	21	0.15	3.600	0.023	0.2406	0.0005	0.6194	0.1085	0.0006	1390	5	1550	10	1774	19	24.1
T3 (9)	4	2	55	21	0.36	5.249	0.131	0.3287	0.0027	0.5864	0.1158	0.0025	1832	26	1861	43	1893	74	3.7
T4 (10)	2	1	50	15	0.27	5.189	0.151	0.3293	0.0029	0.6053	0.1143	0.0028	1835	29	1851	50	1869	87	2.1

[1] T=titanite fraction. Number in brackets refers to the number of grains in the analysis.

[2] U ppm is approximate, based on estimated weight of fraction.

[3] Radiogenic Pb.

[4] Measured ratio, corrected for spike and fractionation.

[5] Total common Pb in analysis corrected for fractionation and spike.

[6] Corrected for blank Pb and U and common Pb, errors quoted are 1 sigma absolute; procedural blank values for this study: 1 pg U and 5 pg Pb. Pb blank isotopic composition is based on the analysis of procedural blanks; corrections for common Pb were made using Stacey-Kramers compositions.

[7] Correlation Coefficient.

[8] Corrected for blank and common Pb, errors quoted are 2 sigma in Ma. The error on the calibration of the GSC 205Pb-233U-235U spike utilized in this study is 0.22% (2s).

Table 3.4. Average Ni and Cu tenors of the Garson deposit and other South Range contact deposits (see Fig. 3.1 for location of deposits). The averages for other deposits, other than the Garson deposit, are from Naldrett (2004, p. 449-451), and the average South Range massive ore is an average of 490 samples from the data of Naldrett et al. (1999)

Deposit	**Ni wt. %**	**Cu wt.%**
Garson	5.0	3.9
Creighton	5.3	7.1
Little Stobie	5.9	3.8
Crean Hill	5.3	6.1
Getrude	4.7	2.4
Lindsley	4.0	3.9
South Range massive ore	4.8	4.6

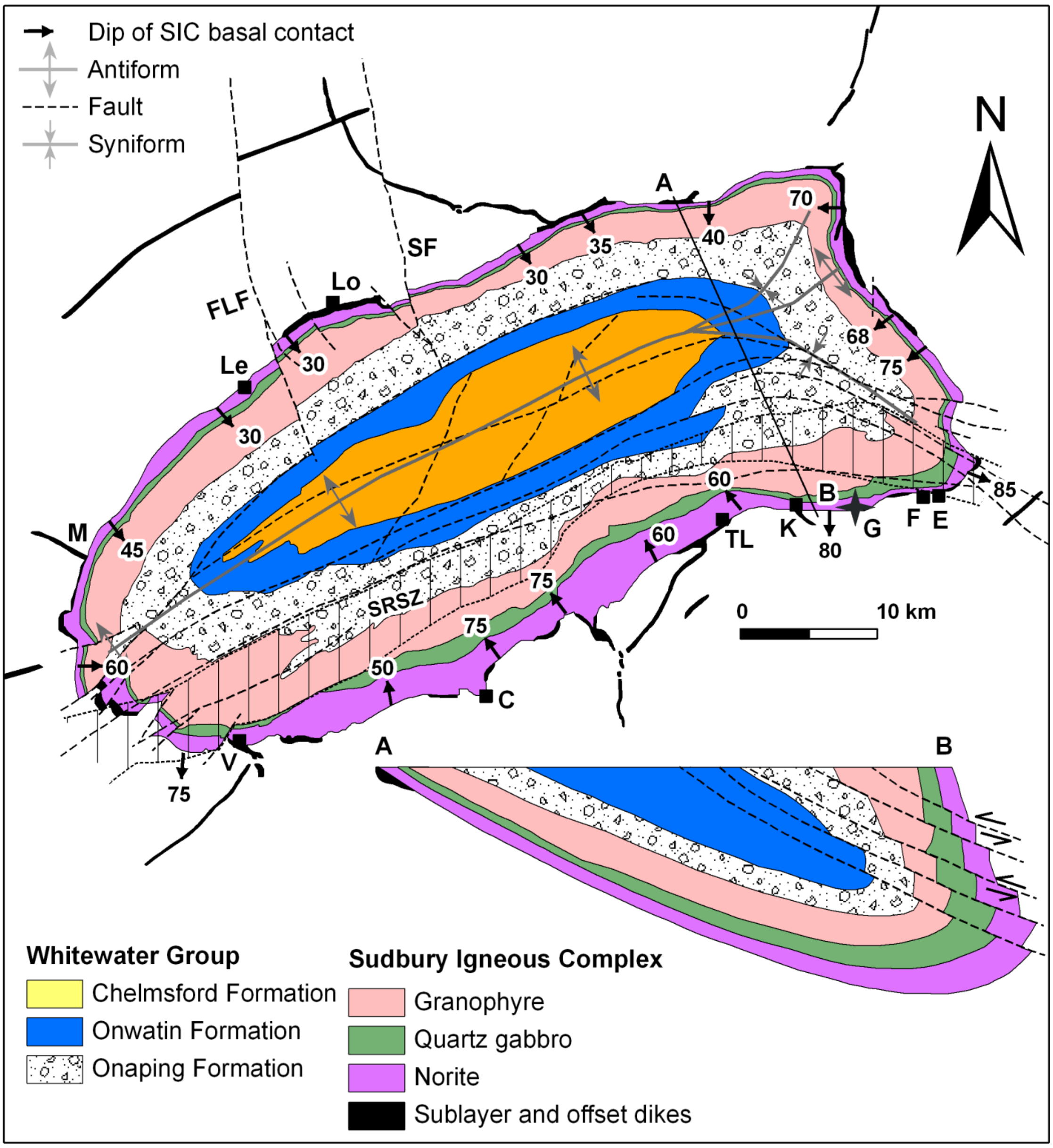

Figure 3.1. Simplified geological map of the Sudbury structure (modified after Dressler et al., 1991; Ames et al., 2005; Riller, 2005; Klimczak et al., 2007; Mukwakwami et al., 2012). Insert shows a cross section along A-B in Fig. 3.1. SRSZ: South Range Shear Zone, TL: Thayer Lindsley Mine, K: Kirkwood Mine, G: Garson Mine, F: Falconbridge Mine, E: East Mine, C: Creighton Mine, FLF: Fecunis Lake Fault, SF: Sandcherry Fault, HS: Huronian Supergroup.

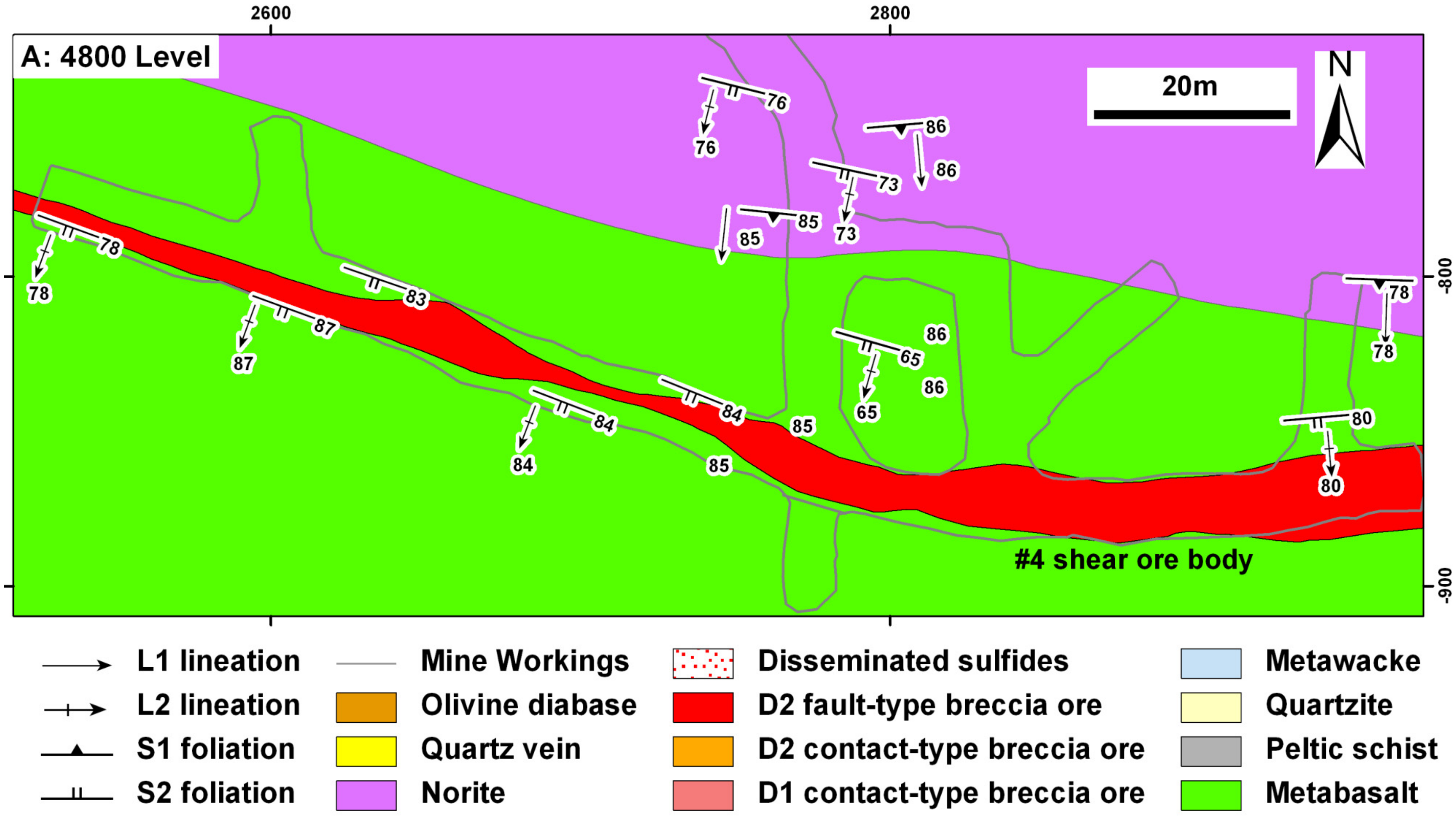
A: 4800 Level
2600
2800
-800
-900
20m
N
#4 shear ore body
78
87
83
84
85
76
86
73
65
80
L1 lineation
L2 lineation
S1 foliation
S2 foliation
Mine Workings
Olivine diabase
Quartz vein
Norite
Disseminated sulfides
D2 fault-type breccia ore
D2 contact-type breccia ore
D1 contact-type breccia ore
Metawacke
Quartzite
Peltic schist
Metabasalt

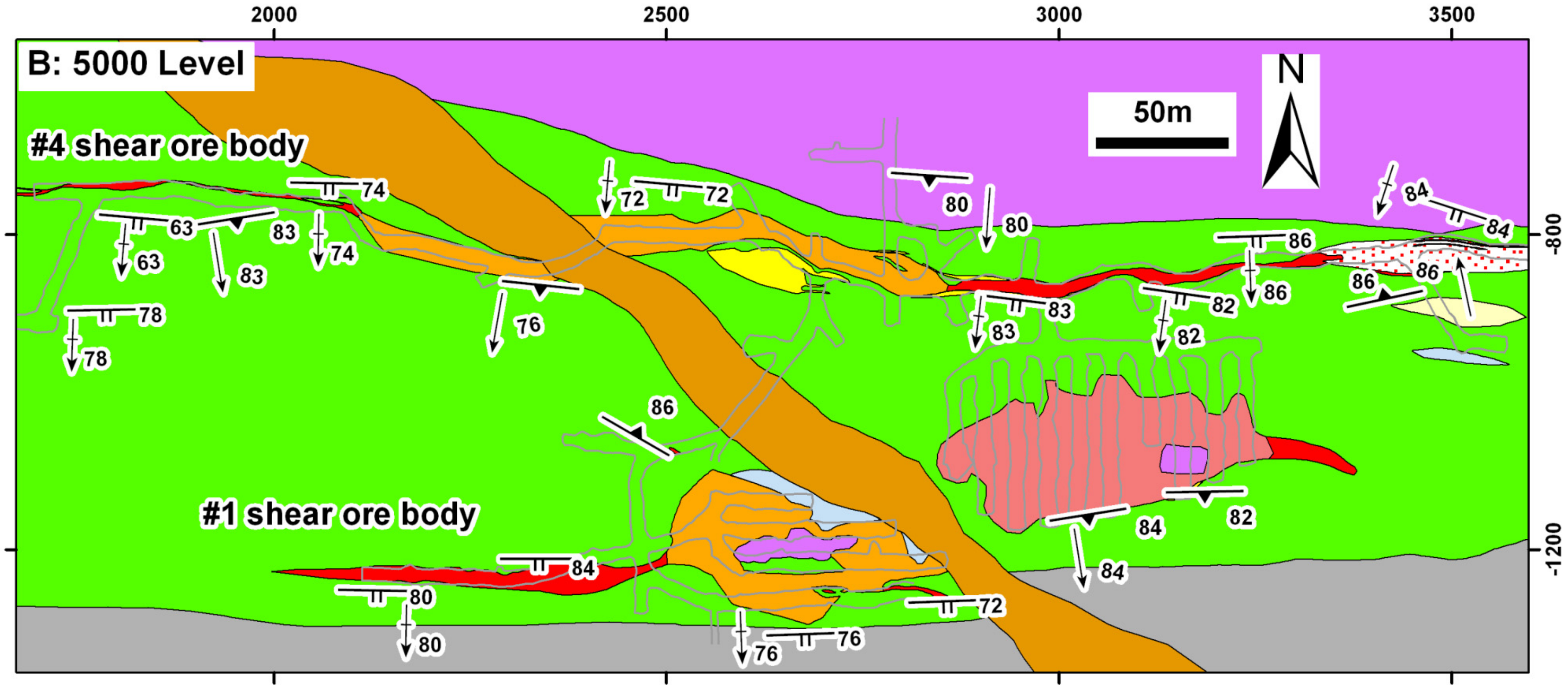

Figure 3.2. Geological maps showing the #1 and #4 ore bodies on the (a) 4800 ft level and (b) 5000 ft level of the Garson mine. Modified from Mukwakwami (2012).

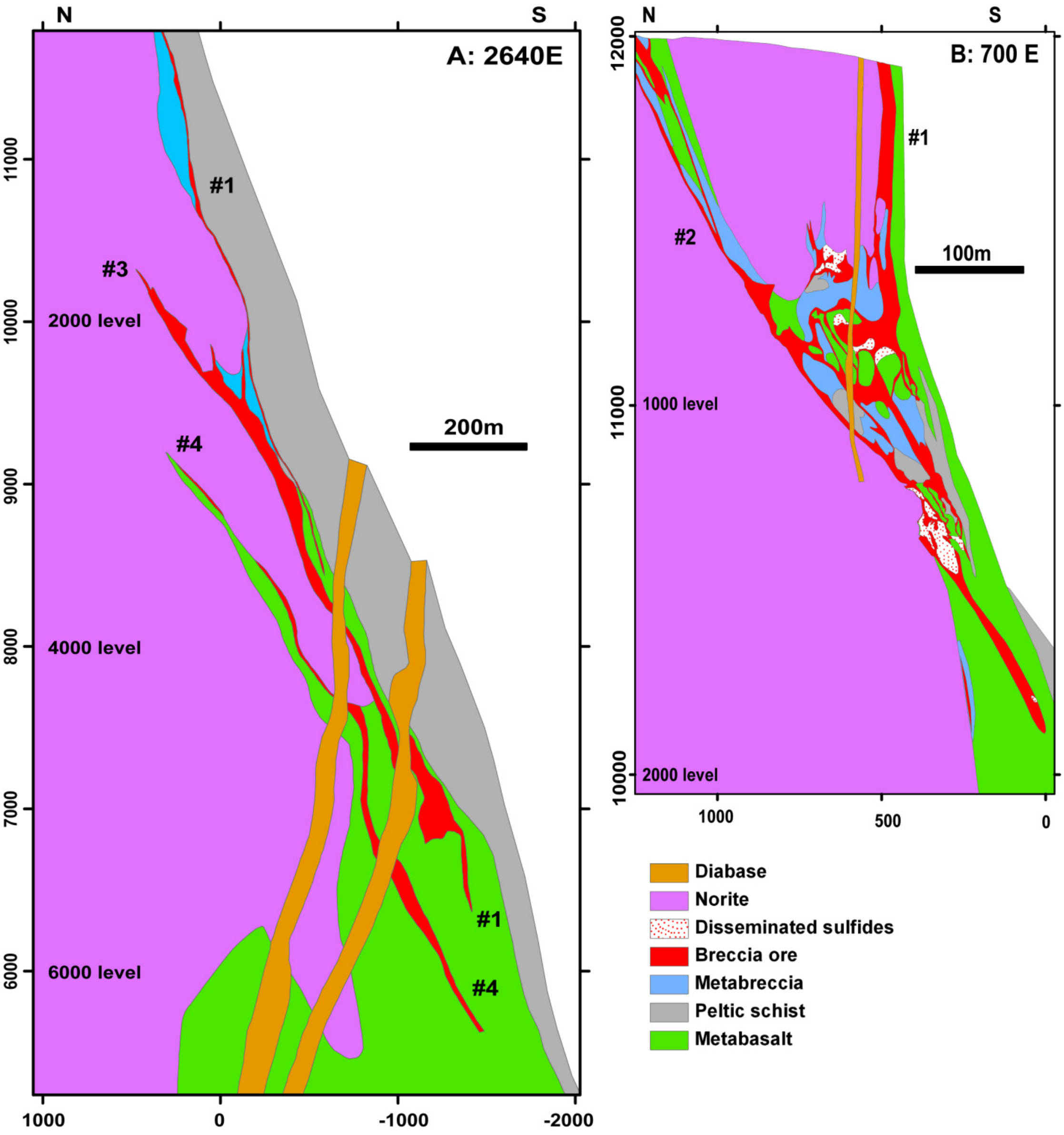

Figure 3.3. Cross sections (looking east) showing the #1, #2, #3 and #4 ore bodies at Garson mine (modified after Aniol and Brown, 1979) along sections (a) 2640 E and (b) 700E.

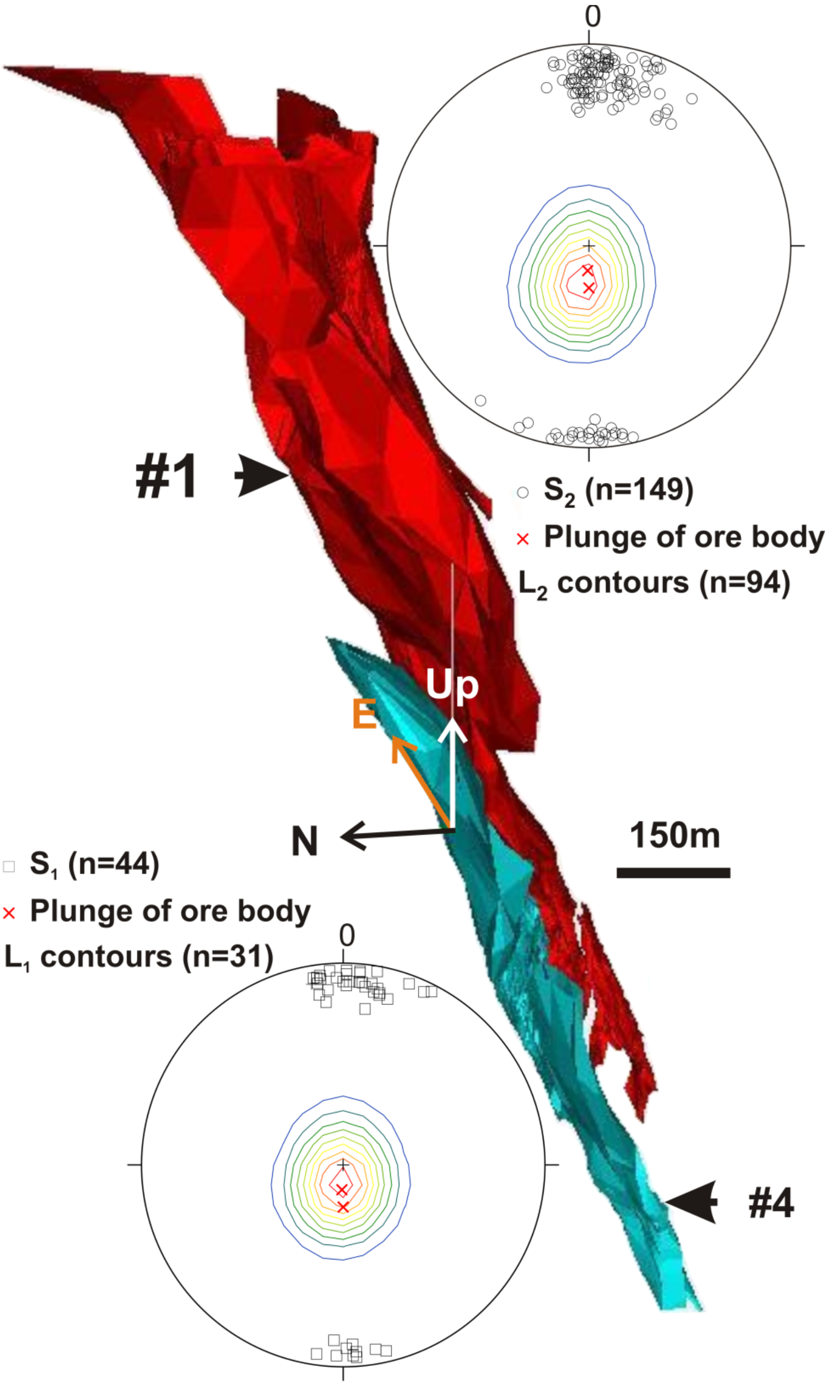

Figure 3.4. Wireframes showing 3-D geometry of the #1 and #4 shear ore bodies. Insert: equal area, lower hemisphere projections of L_1 and L_2 mineral lineations (contours are in 2 multiples of random distribution), average plunge of the #1 and #4 ore bodies, and poles to S_1 and S_2 foliations.

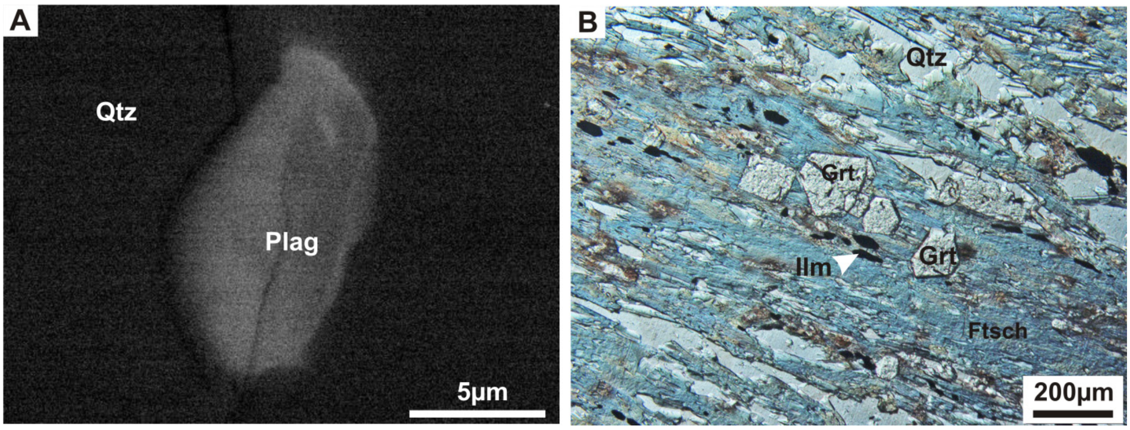

Figure 3.5. (a) Electron back-scatter image showing zoned plagioclase in a quartz-rich matrix in metabasalt. (b) Photomicrograph (crossed polars) of metabasalt showing euhedral garnets coexisting with ferrotschermakite.

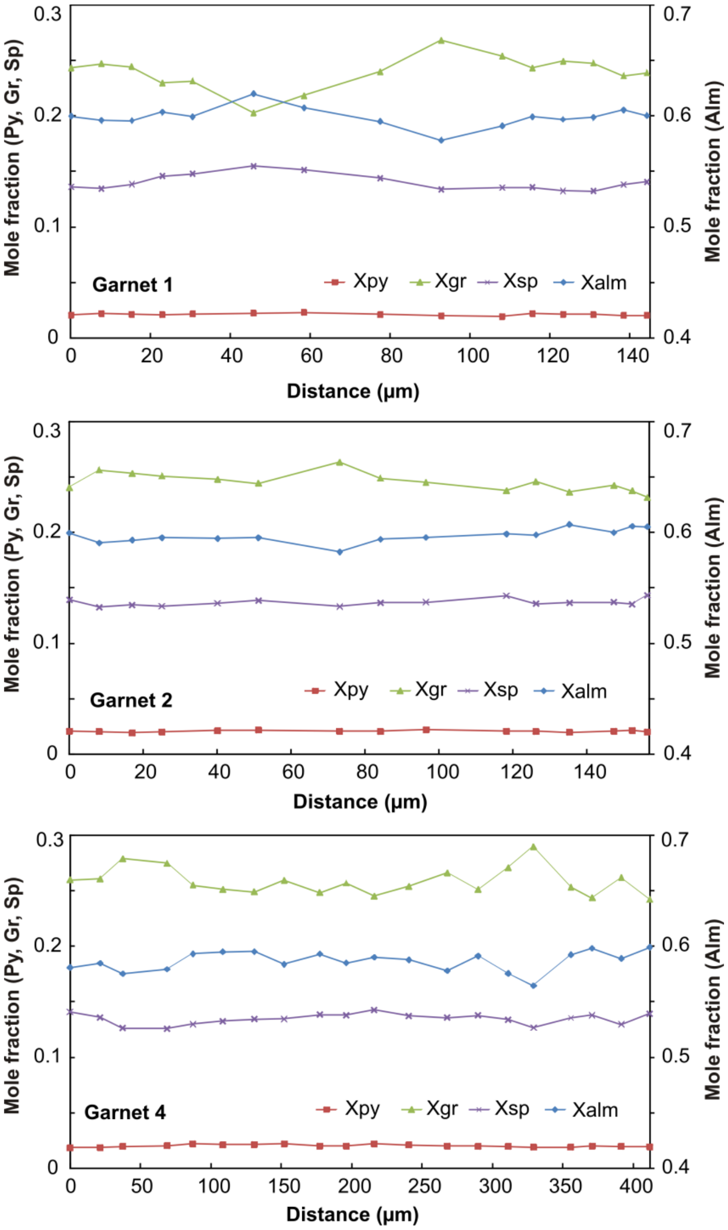

Figure 3.6. Compositional profiles across three garnet porphyroblasts from metabasalt. The distance (μm) is measured from one rim to the other. The position of the transect across garnet 4 is indicated by line A-B in X-Ray maps (Fig. 3.7).

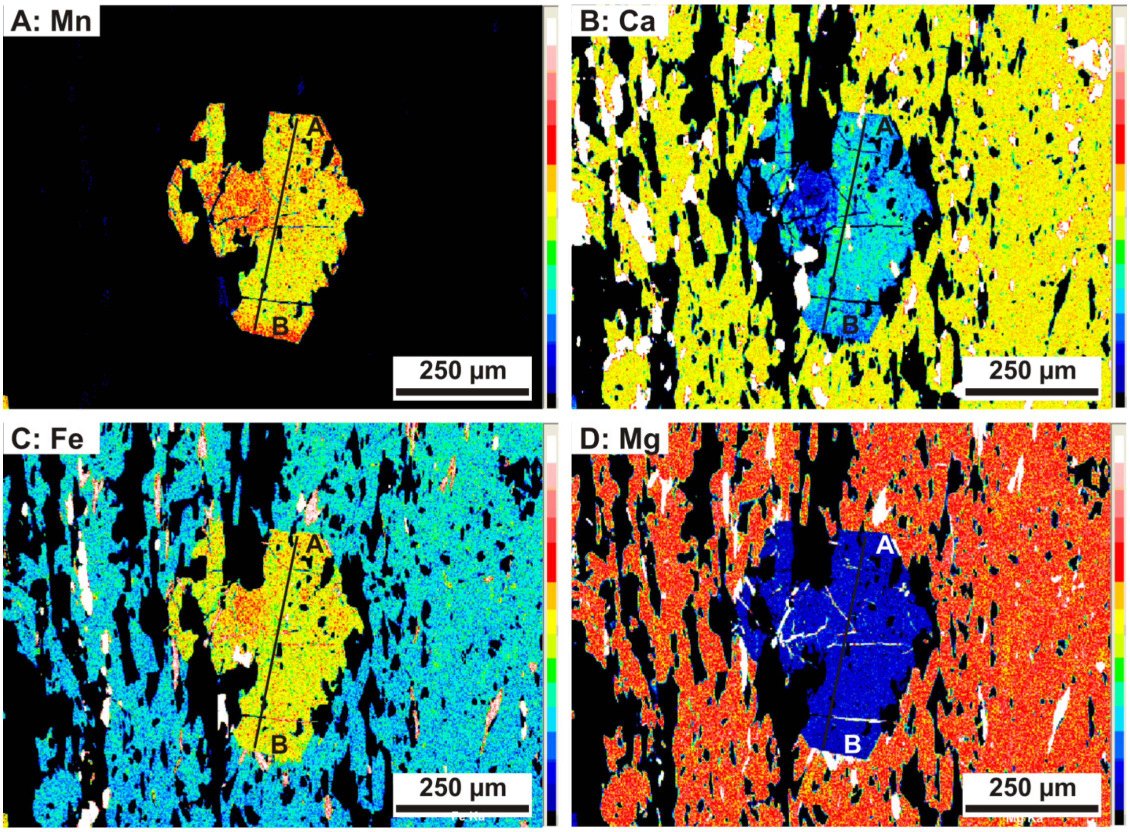

Figure 3.7. X-Ray maps of (a) Mn, (b) Ca, (c) Fe and (d) Mg for garnet 4 in Fig. 6 showing near-homogeneous porphyroblast in metabasalt. The position of the micrprobe transect across garnet 4 is indicated by line A-B.

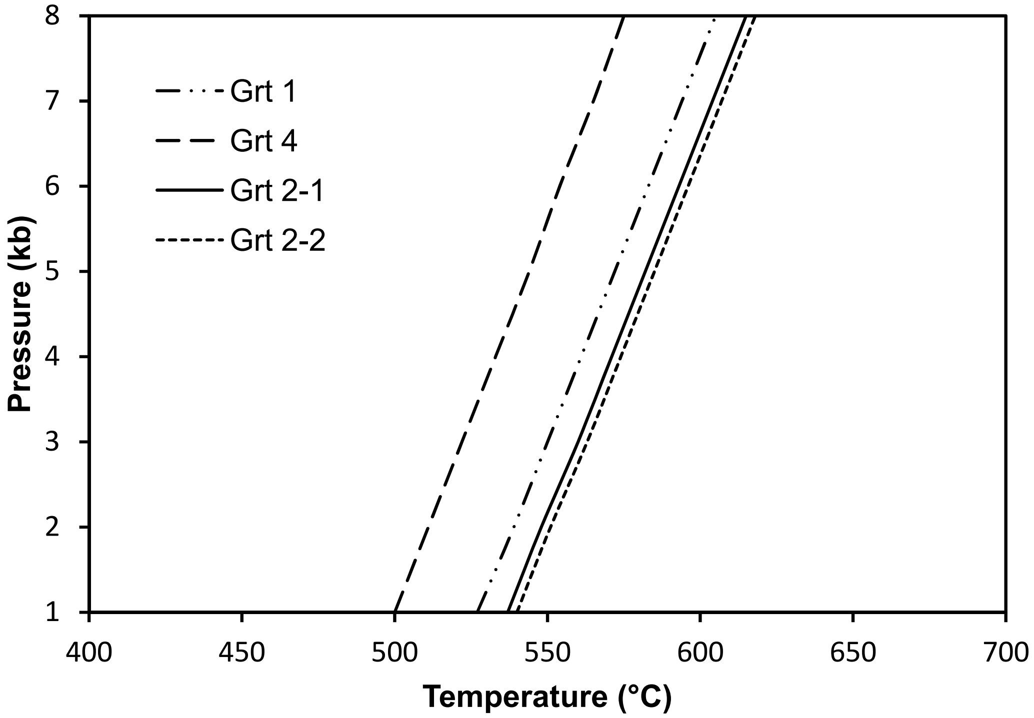

Figure 3.8. P-T diagram showing temperatures calculated using the average T method of Powell and Holland (1994) at pressures ranging from 1 to 8 kb.

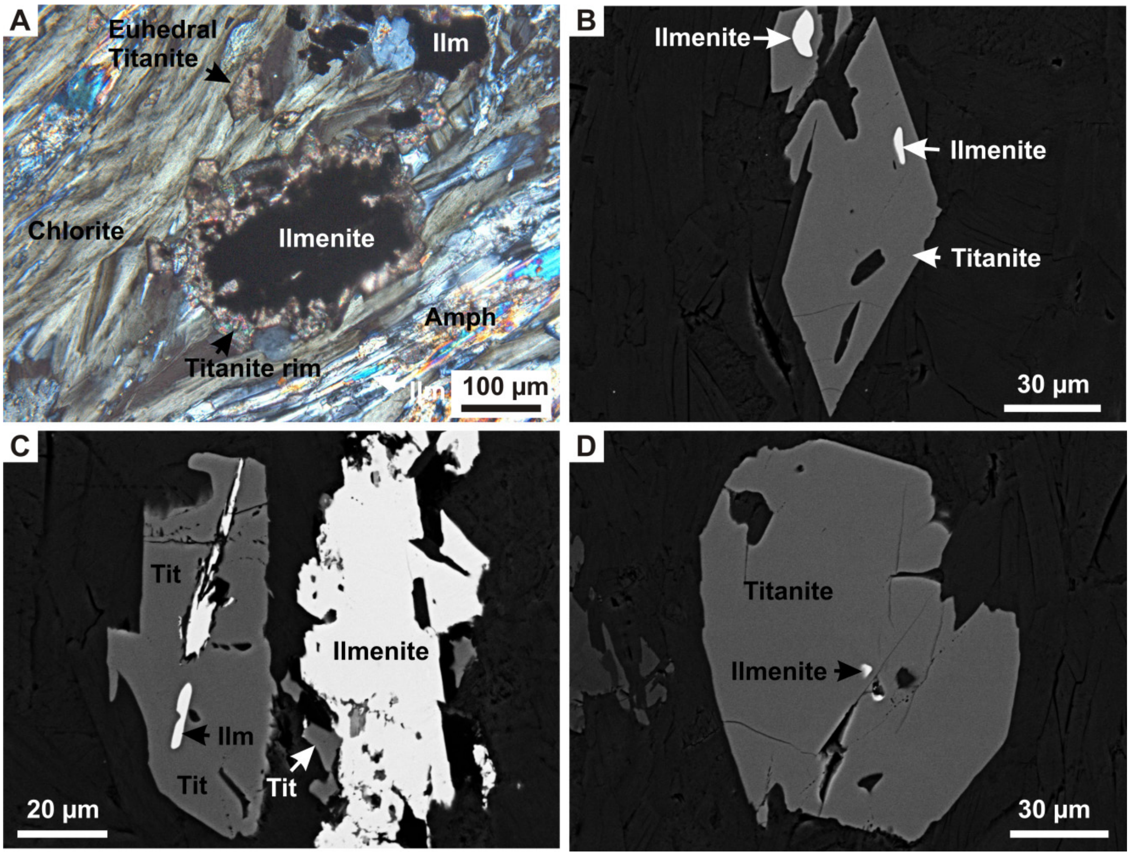

Figure 3.9. (a) Photomicrograph (crossed polars) of sheared norite showing euhedral titanite and titanite overgrowing ilmenite. Electron back-scatter images showing (b) homogeneous euhedral titanite with an ilmenite inclusion, (c) titanite replacing ilmenite grains, and (d) homogeneous subhedral titanite grain with an internal ilmenite inclusion.

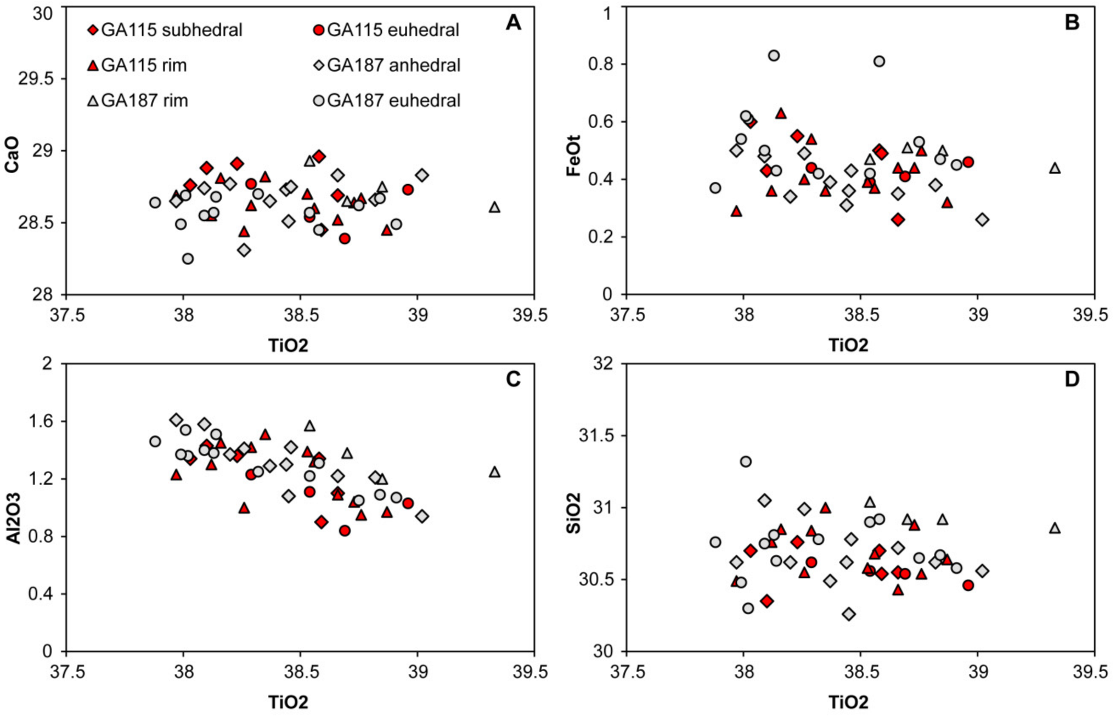

Figure 3.10. Analyses of euhedral and subhedral titanite, and titanite rims around ilmenite from Huronian metagabbro (GA115) and norite (GA187). (a) CaO vs TiO_2. (b) FeO_t vs TiO_2. (c) Al_2O_3 vs TiO_2. (d) SiO_2 vs TiO_2. FeO_t: FeO total.

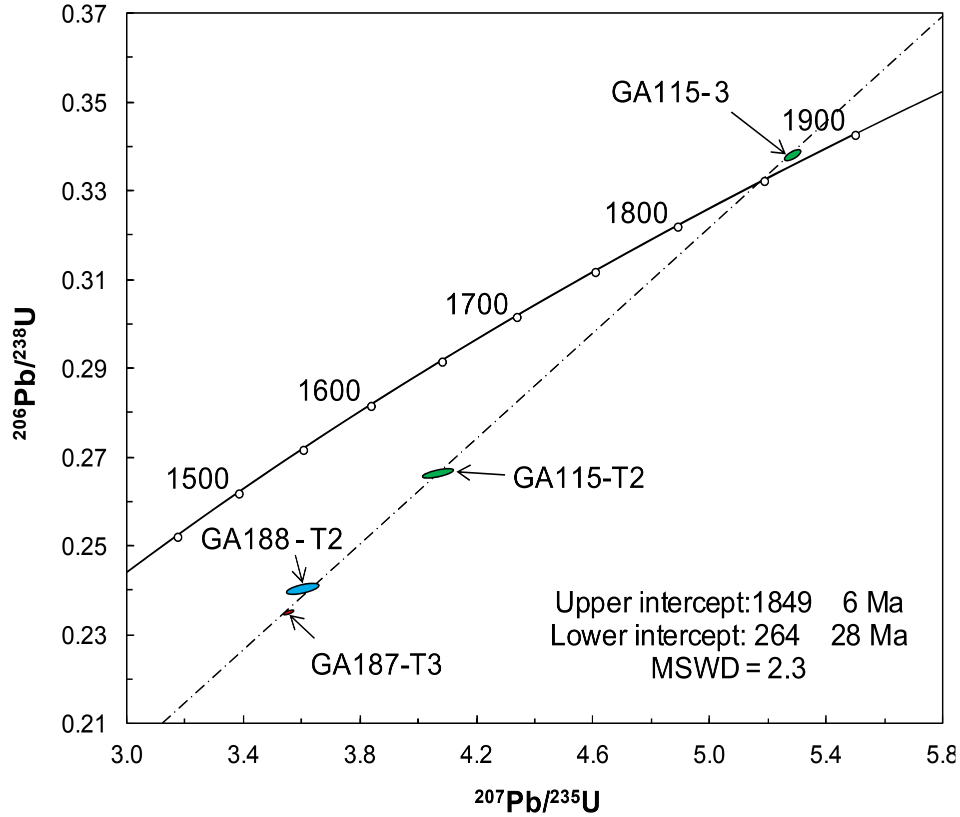

Figure 3.11. Isochron diagram for the U-Pb ID-TIMS analayses of titanite from gabbro and SIC norite. The sample and fraction numbers are indicated, e.g., GA115-T2.

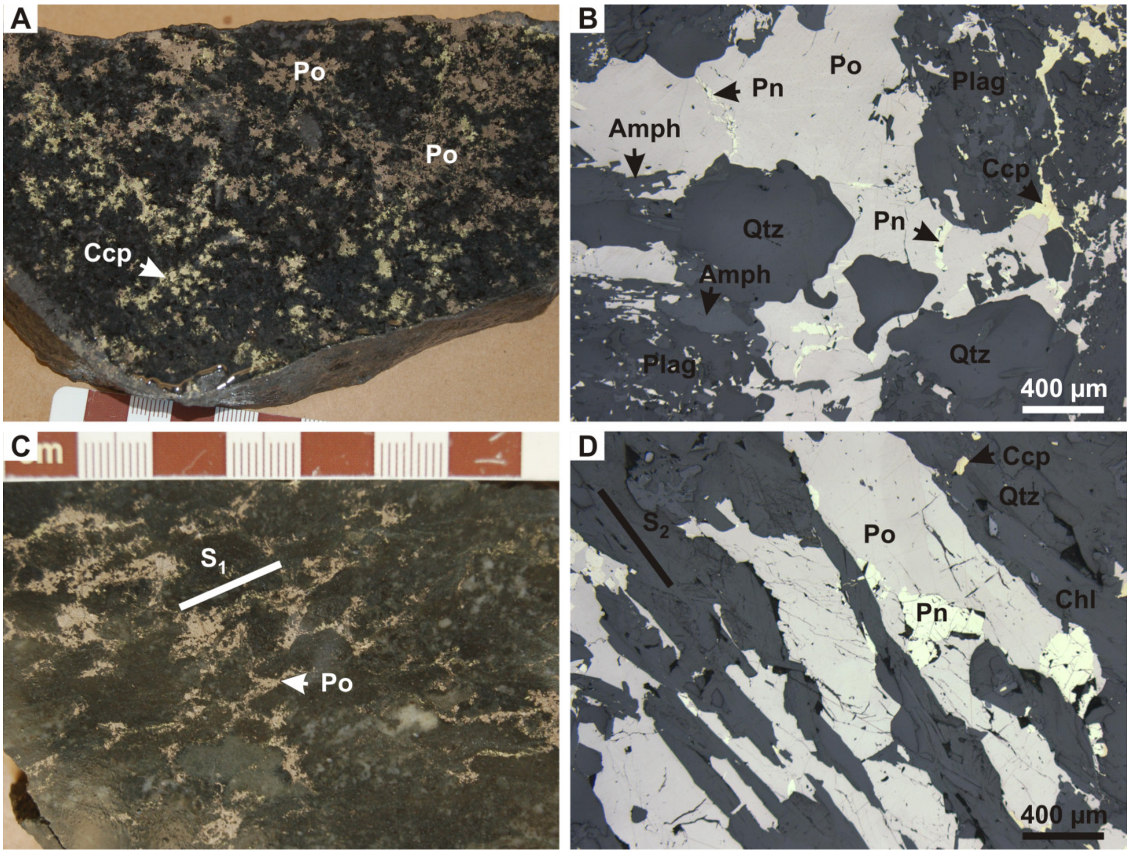

Figure 3.12. (a) Polished slab and (b) photomicrograph (reflected light) of undeformed disseminated to matrix textured sulfides. Sulfides are interstitial to silicate minerals. (c) Polished slab and (d) photomicrograph (reflected light) of deformed disseminated mineralization showing pyrrhotite-rich bands parallel to S_1 and S_2, resepctively. Po: pyrrhotite, Pn: pentlandite, Ccp: chalcopyrite, Chl: chlorite, Qtz: quartz, Amph: amphibole, Plag: plagioclase.

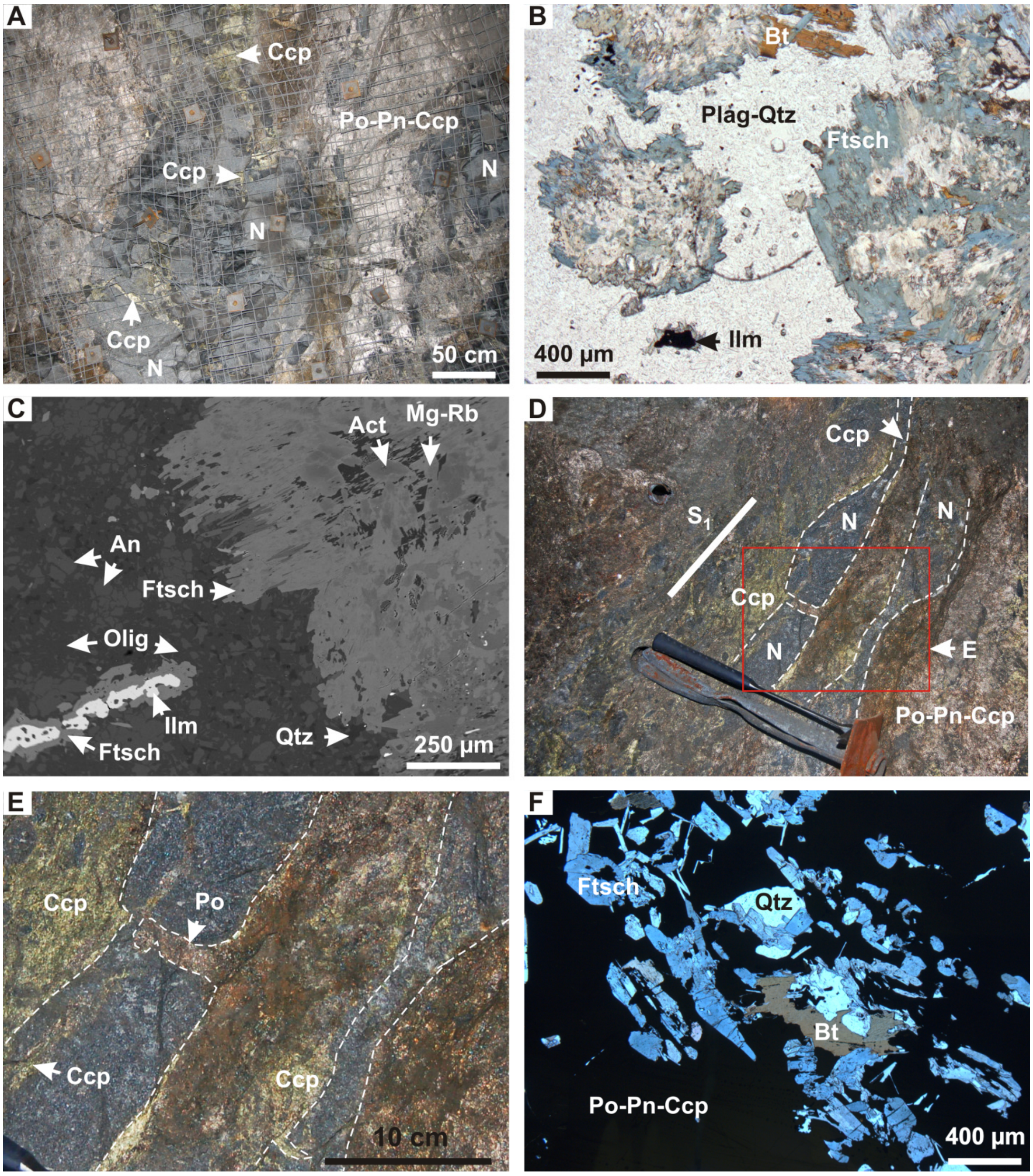

Figure 3.13. D_1 contact breccia ore. (a) Underground photograph showing chalcopyrite segregations in fractures and along margins of norite fragments. (b) Photomicrograph (plane polarized light) and (c) electron back-scatter image of norite fragment showing ferrotschermakite (Ftsch), intergrown with minor biotite (Bt) and ilmenite (Ilm), rimming aggregates of magnesioriebeckite (Mg-Rb) and actinolite (Act). The matrix consists of plagioclase of anorthitic (An) and oligoclase (Olig) composition, and minor quartz (Qtz). (d) Norite fragments boudinaged parallel to L_1. Chalcopyrite (Ccp) and pyrrhotite (Po) occur in necks of the pinch-and-swell boudinage structure. (e) Enlarged portion of (d). (f) Ferrotschermakite-biotite S_1 overgrown by pyrrhotite-rich sulfide matrix. Plag: plagioclase, N: norite.

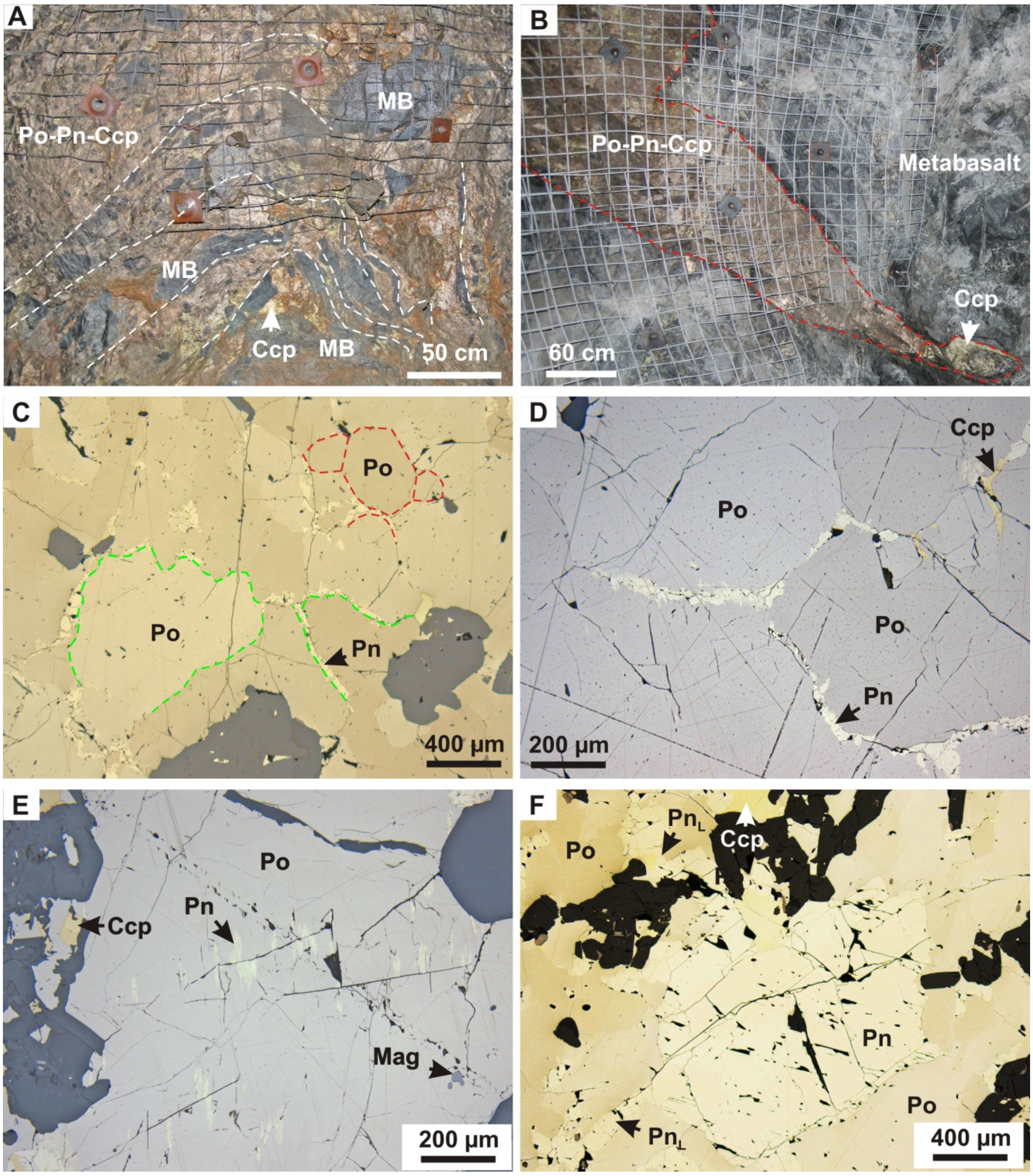

Figure 3.14. D_1-deformed contact breccia ore. (a) Underground photograph showing folded metabasalt (MB) fragments. (b) Underground photograph showing a piercement vein. Looking up on the stope ceiling. (c) Photomicrograph (reflected light, partially crossed nicols) of D_1-deformed contact breccia ore showing anhedral pyrrhotite grains with curved grain boundaries (outlined by green broken lines) coexsting with polygonal pyrrhotite (Po) grains (outlined by red broken lines). Pentlandite (Pn) and minor chalcopyrite (Ccp) occur along grain boundaries of pyrrhotite. (d) Photomicrograph (reflected light, partially crossed nicols) of D_1-deformed contact breccia ore showing polygonal pyrrhotite with pentlandite loops along grain boundaries. (e) Fine exsolution lamellae of pentlandite in pyrrhotite. (f) Granular pentlandite intergrown with randomly-oriented loop pentlandite.

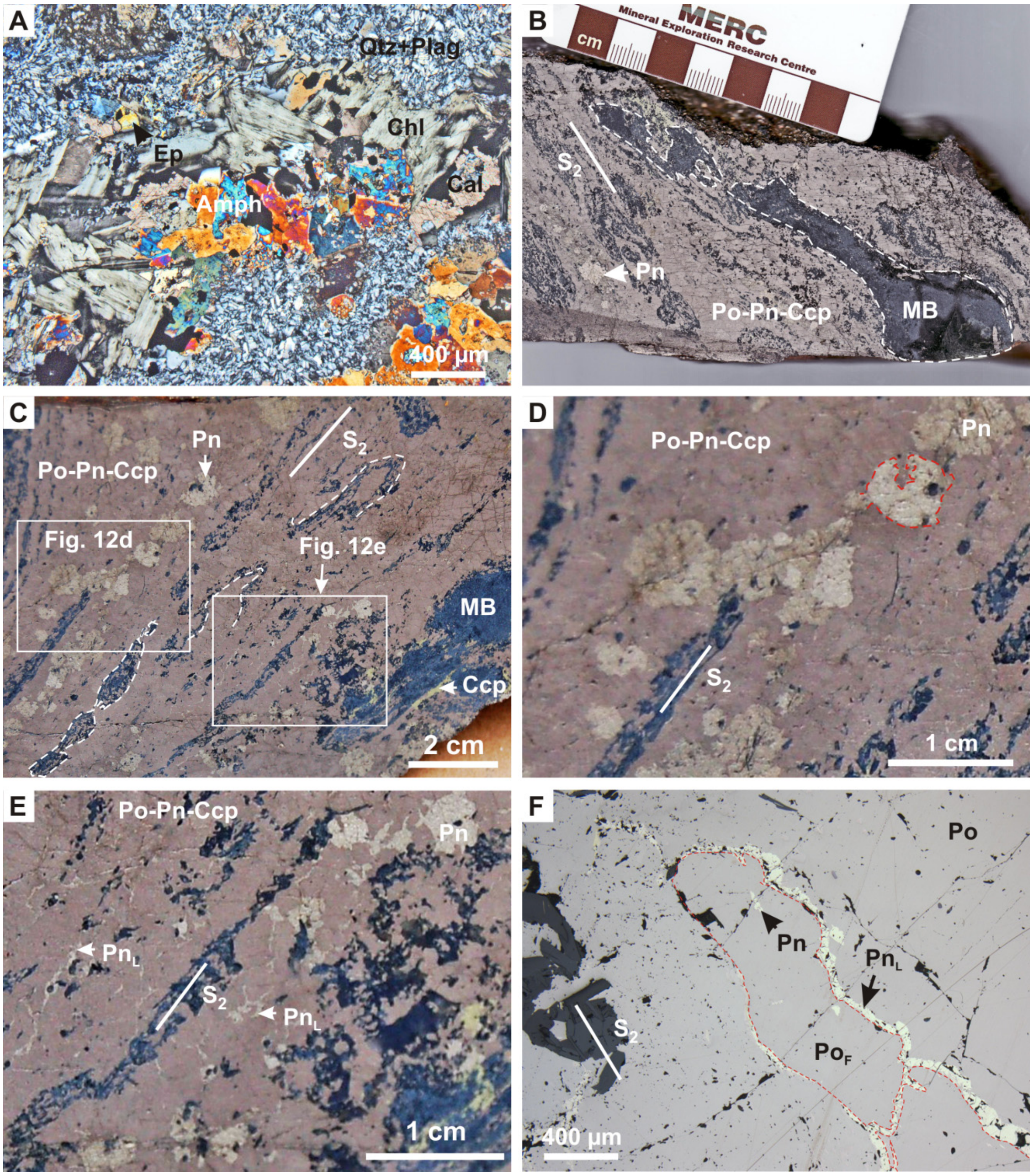

Figure 3.15. D_2-deformed contact breccia ore. (a) Photomicrograph (crossed polars) of norite showing chlorite replacing amphiboles. (b) Polished slab showing boudinaged metabasalt (MB) fragment (outlined by white broken lines) with pyrrhotite and chalcopyrite occuring in the boudin necks. (c) Polished slab showing pentlandite (Pn) grains aligned parallel to boudinaged metabasalt fragments and an internal S_2 chlorite foliation (outlined by white broken lines) that is boudinaged and isoclinally folded. Pyrrhotite occurs in the boudin necks. (d) Zoomed in photograph of (c) showing pentlandite overgrowing and terminating S_2 foliation. (e) Zoomed in photograph of (c)

showing sub-millimeter pentlandite loops aligned parallel to foliation. (f) Photomicrogragh (reflected light, partially crossed nicols) showing loop pentlandite along grain boundaries of flattened pyrhotite (Po_F: outlined by red broken lines) grains that are aligned parallel to S_2.

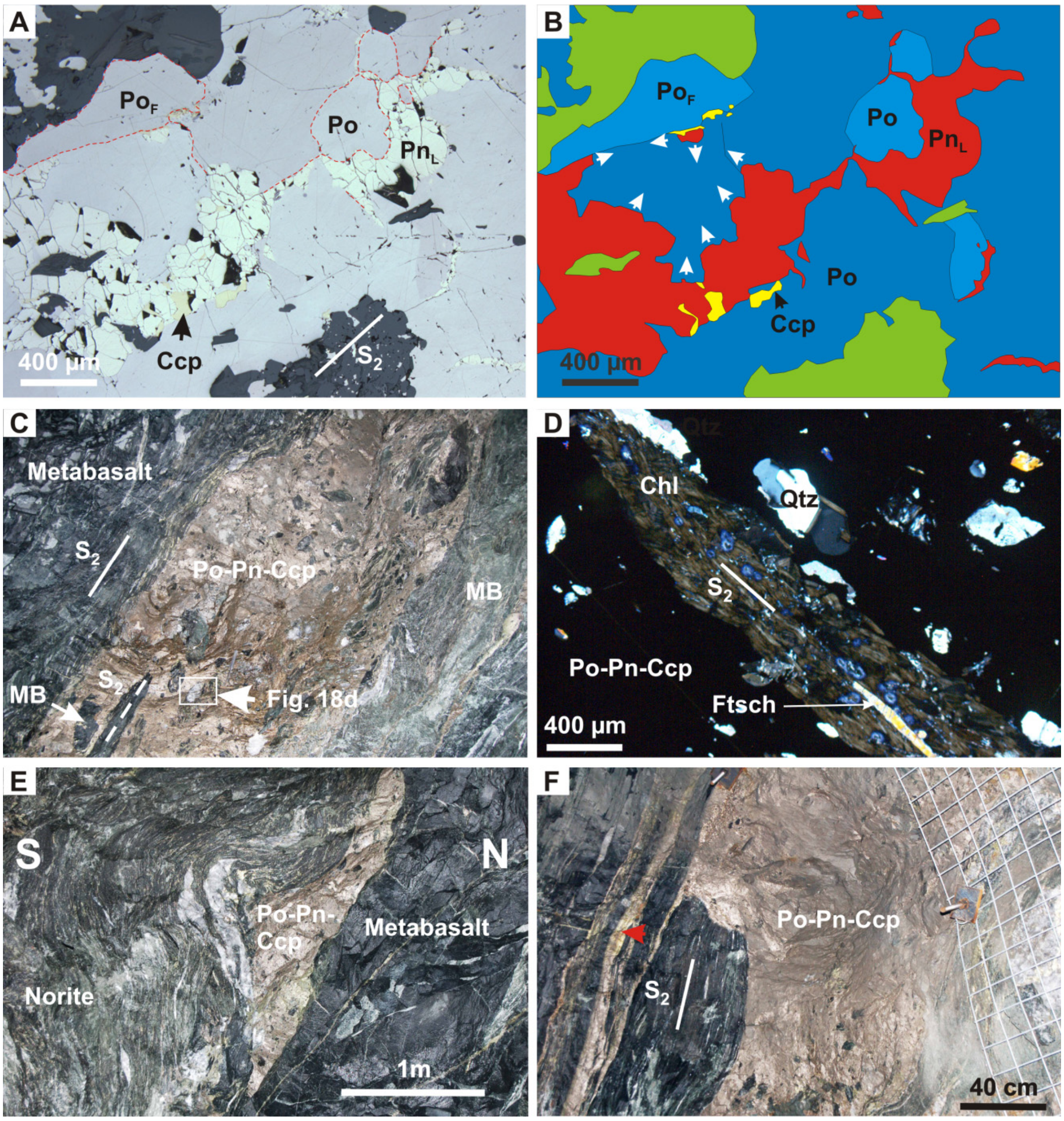

Figure 3.16. (a) Photomicrogragh (reflected light, partially crossed nicols) of D_2-deformed contact breccia ore showing loop pentlandite (Pn_L) aligned parallel to rare flattened pyrrhotite (Po_F) grains that are aligned parallel to an internal S_2 chlorite foliation in metabasalt fragments. (b) Sketch of photomicrograph in (a). White arrows illustrate how continued growth of pentlandite loops from grain boundaries inwards could lead to formation of pentlandite grains. (c) Underground photograph of tabular D_2-deformed fault breccia ore zone with metabasalt (MB) fragments defining a foliation parallel to S_2 in wallrocks. Rectangle shows location of Fig. 3.18d. (d) Photomicrograph (crossed polars) showing S_2 chlorite (Chl) foliation overgrown by a pyrrhotite-rich sulfide matrix in D_2-deformed fault breccia ore. (e) Underground photograph showing thickening of D_2-deformed fault breccia ore in the hinge zone of a N-verging F_2 fold. (f) Underground photograph showing pyrrhotite-rich massive sulfide ore truncating S_2 in D_2-deformed fault breccia ore. Red arrow show some chalcopyrite (Ccp)-rich segregations.

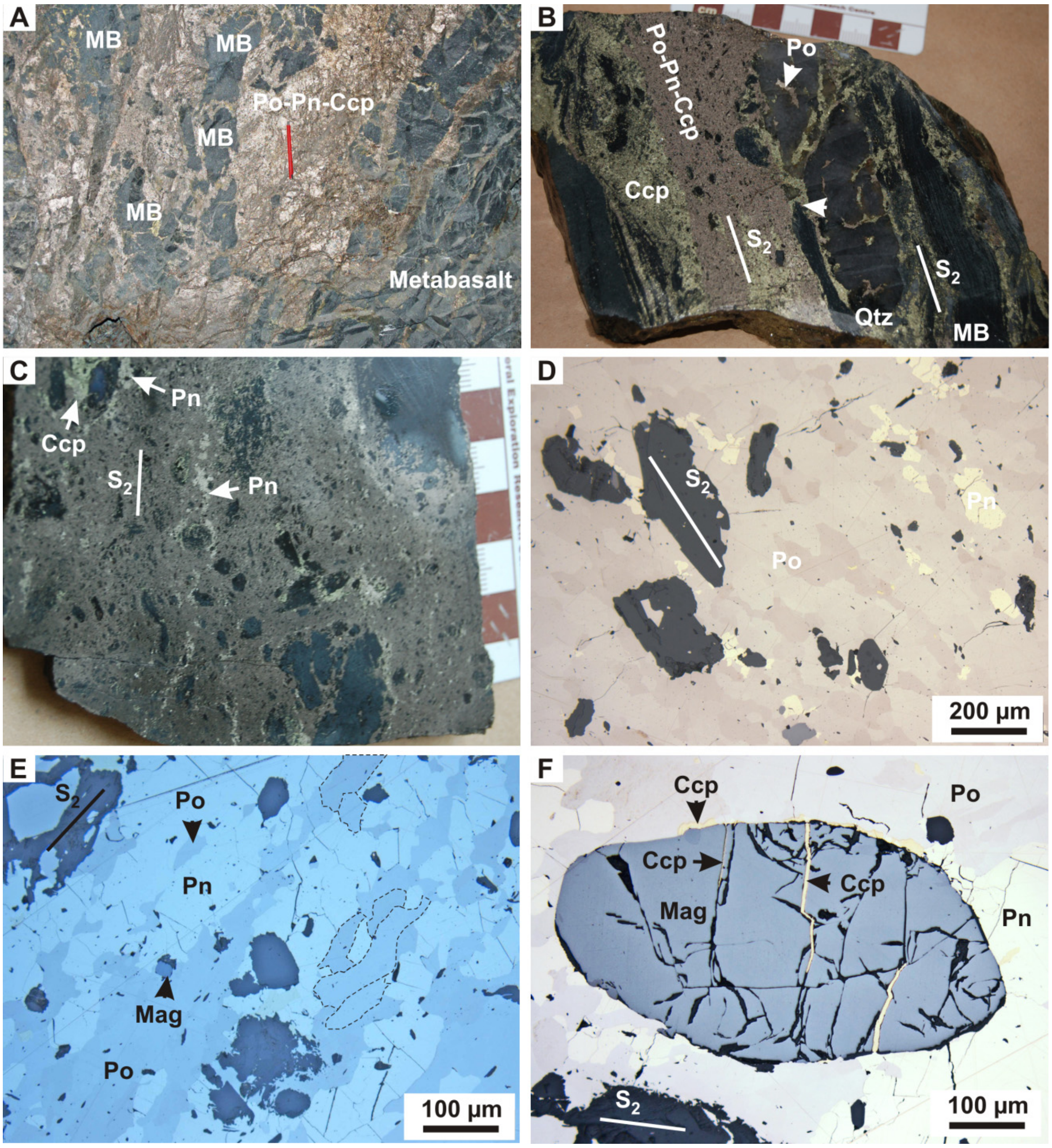

Figure 3.17. D_2-deformed fault breccia ore. (a) Underground photograph showing pyrrhotite-rich massive ore penetrating metabasalt (MB) wall rocks along fractures. (b) Polished slab of boudinaged quartz (Qtz) fragment in a sulfide matrix. Chalcopyrite (Ccp), and minor pyrrhotite (Po) occur along fractures in the boudin. (c) Polished slab showing thin pentlandite bands oriented parallel to S_2. (d) Photomicrogragh of pyrrhotite foliation oriented parallel to a S_2 internal chlorite foliation in metabasalt. (e) Photomicrogragh of anastomosing pentlandite loops oriented parallel to flattened pyrrhotite grains (outlined by broken lines) that are parallel to an internal S_2 chlorite foliation in metabasalt fragments. (f) Photomicrogragh of fractured magnetite (Mag). Chalcopyrite occurs along tensile fractures that are oriented perpendicular to L_2.

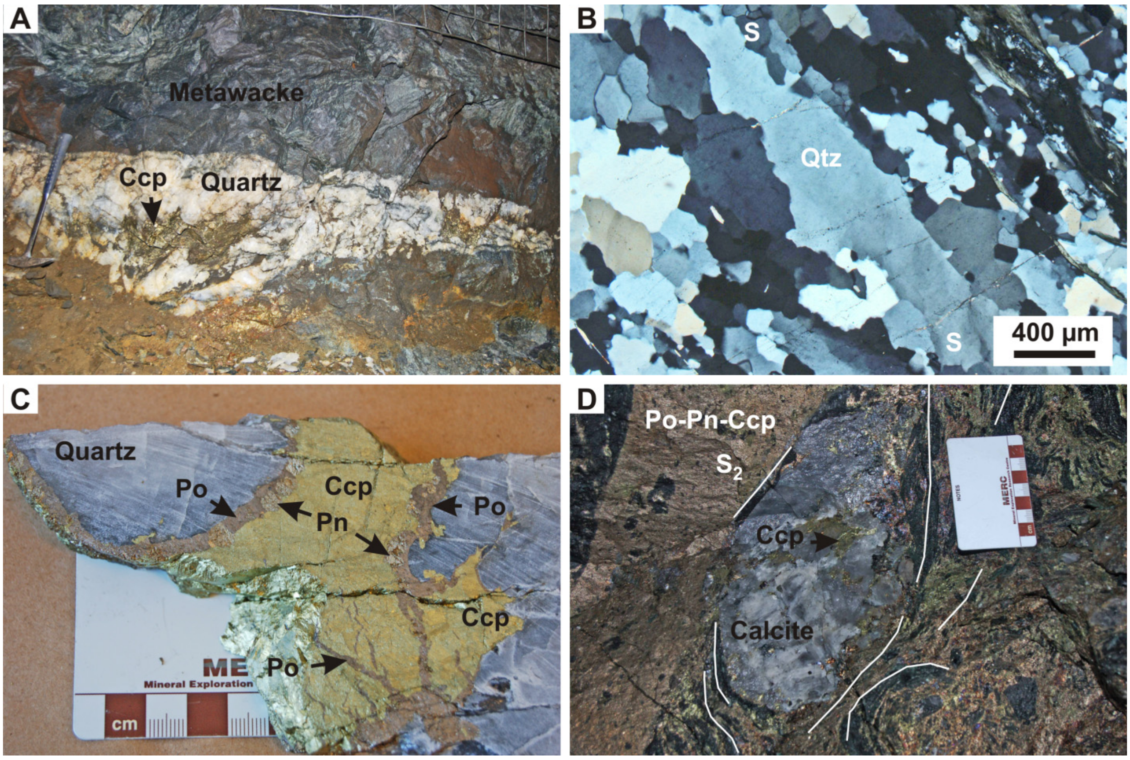

Figure 3.18. Quartz-calcite-sulfide veins. (a) Underground photogragh of extensional chalcopyrite (Ccp)-rich quartz vein. (b) Photomicrogragh (crossed polars) of sheared quartz (Qtz) vein oriented parallel to S_2. Elongate grains have subgrains (S) at their margins. (c) Polished slab of quartz vein showing chalcopyrite associated with minor pyrrhotite and pentlandite. (d) Underground photograph showing stretched calcite fragment mineralized Ccp-rich sulfides. Location for this figure is shown in Fig. 3.16.

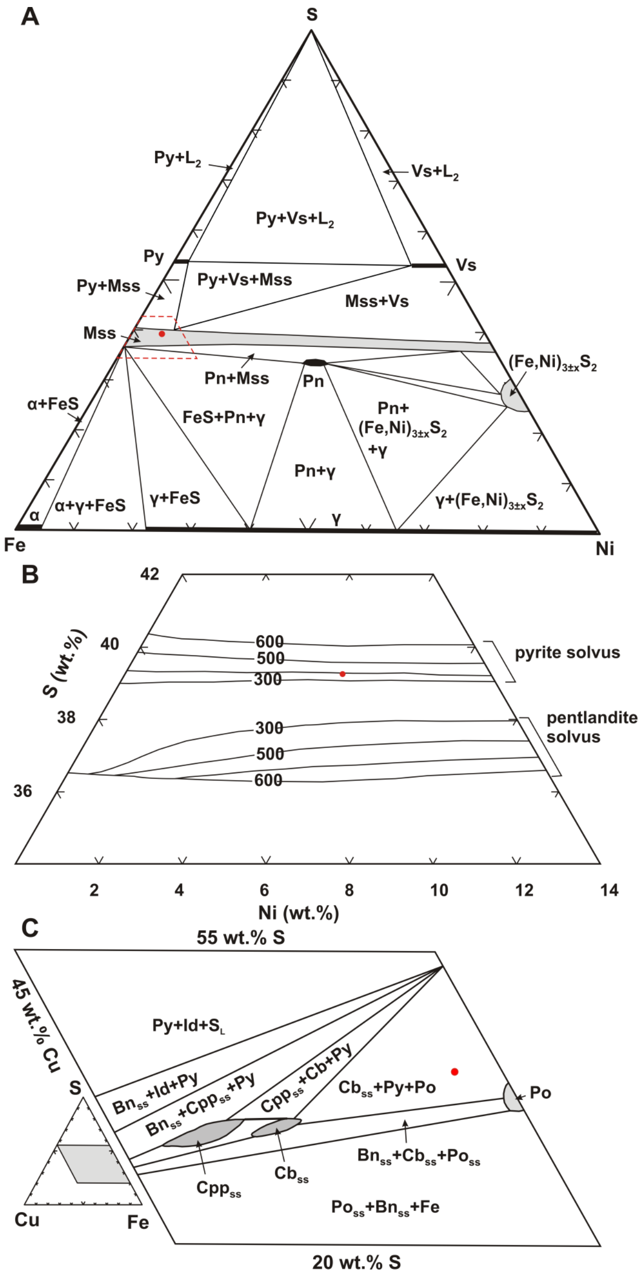

Figure 3.19. (a) Phase relations in the Fe-Ni-S system showing the bulk composition of the Garson ores at 550°C. Modified after Kullerud et al. (1969). (b) Enlargement of the Fe-rich portion of the monosulfide solid solution outlined in (a) by red broken lines. The limits of the monosulfide solid solution (Mss) are shown at 600°C, 500°C, 400°C, and 300°C. Modified after Naldrett et al. (1967). (c) Phase relations in Cu-Fe-S system showing the bulk composition of the Garson ores at 500°C. Insert shows the position of (c) in a Cu-Fe-S ternary diagram. Modified after Kullerud et al. (1969). The red dot represents the bulk composition of the Garson deposit. Py: pyrite, Pn: pentlandite, Po: pyrrhotite, Cb: cubanite, Bn: bornite, Vs: vaesite.

Chapter 4: Geochemistry of Deformed and Hydrothermally-Mobilized Magmatic Ni-Cu-PGE Ores at the Garson Mine, Sudbury

JOSHUA MUKWAKWAMI, C. MICHAEL LESHER and BRUNO LAFRANCE

Mineral Exploration Research Centre, Department of Earth Sciences, Laurentian University, 933 Ramsey Lake Road, Sudbury, Ontario P3E 2C6, Canada

4.1 Abstract

The Garson Ni-Cu-platinum group element (PGE) deposit is a deformed, overturned, contact-type deposit along the contact between the Sudbury Igneous Complex (SIC) and underlying rocks of the Huronian Supergroup in the South Range of the 1850 Ma Sudbury structure. The main Garson ore bodies occur along steeply south-dipping ductile shear zones, which initially formed as D_1 south-over-north amphibolite facies thrust zones that were rotated and overturned during buckling of the SIC. The shear zones were reactivated as south-over-north greenschist facies reverse shear zones during D_2. The mineralization primarily includes pyrrhotite-pentlandite-chalcopyrite-magnetite, occurring as four main types: 1) disseminated to matrix-textured sulfide mineralization in Main Mass norite and slivers of norite within shear zones, 2) semi-massive breccia ore within the shear zones, 3) quartz-calcite-sulfide veins spatially associated with breccia ores, and 4) Cu-Pd-Pt-Au-rich "footwall-type" mineralization in the nearby Garson Ramp deposit. Garson disseminated sulfides and breccia ores have relatively low Pd/Ir ratios

and restricted ranges of Ni tenors and Fe/Ni ratios, very similar to those of undeformed disseminated sulfides and contact-type massive ores at the less-deformed Creighton deposit. This suggests that the mobilization of the breccia ores by ductile plastic flow during D_1 and D_2 did not significantly alter their original magmatic geochemical signatures. Garson breccia ores are slightly depleted in Cu-Pt–Pd–Au and slightly enriched in Rh-Ru-Ir relative to disseminated sulfides, similar to other contact-type deposits at Sudbury. In contrast, the quartz-calcite-sulfide veins at Garson are characterized by very low Rh-Ru-Ir abundances and very high Pd/Ir ratios, consistent with their mobilization and deposition from metamorphic-hydrothermal fluids. Despite being strongly enriched in Cu-Pd–Pt–Au, there are too few of these veins to account for the broad depletion in Cu-Pd–Pt-Au from the main mass of breccia ores, suggesting that the breccia ores are monosulfide solid solution cumulates that left a residual sulfide melt represented by the Cu-Pd-Pt-Au-rich ores in the Garson Ramp deposit.

4.2 Introduction

Although magmatic Ni-Cu-platinum group element (PGE) deposits formed by primary igneous processes, all have been modified to some degree by post-magmatic deformation, metamorphism, and/or hydrothermal alteration (e.g. Barrett et al., 1977; Maiden et al., 1986; Cowden and Archibald, 1987; McQueen, 1987; Stone et al., 2004; Duuring et al., 2007). These secondary processes may mobilize sulfides and alter the geochemical compositions of the ores to varying degrees and on varying scales (e.g., Heath et al., 2001; Stone et al. 2004; Duuring et al., 2007; Layton-Matthews et al., 2011), so it is critical to understand the nature and scale of metal mobilization (see review and discussion by Lesher and Barnes, 2009). Sulfide/metal mobilization during deformation and metamorphism are commonly subdivided into four end-member mechanisms: 1) diffusive mobilization, which is most effective at magmatic temperatures (e.g., Lesher and Keays, 1984, 2002; Layton-Matthews et al., 2011), 2) mechanical mobilization, which involves ductile plastic flow of relatively low-strength sulfides (e.g., Barrett et al., 1977; McQueen, 1987), 3) metamorphic-hydrothermal mobilization, which involves dissolution and precipitation of sulfides (Vokes and Craig, 1993), and 4) metamorphic partial melting, which may involve mobilization of a sulfide-sulfosalt melt (Frost et al., 2002; Sparks and Mavrogenes, 2005; Baile and Reid, 2005; Tomkins et al., 2007).

Metal mobilization by diffusive processes has been evaluated experimentally (McDougall et al., 1961; Klotsman et al., 1963; Condit et al., 1974), but has only been interpreted to have occurred in metal-enriched sulfide-rich metasedimentary rocks adjacent to normal magmatic ores (e.g., Paterson et al., 1984; Lesher and Keays, 1984; Layton-Matthews et al., 2011). There is no evidence of this process having occurred at Garson, so it will not be discussed further.

During deformation and metamorphism, progressive dissolution of pentlandite into a Fe-Ni-(Cu) monosulfide solid solution (*mss*) and chalcopyrite into a Fe-Cu intermediate solid solution (*iss*) begins at ~300°C and complete conversion to a homogeneous *mss* can be attained at medium to high-grade metamorphic conditions (500-800°C), depending on the time available for diffusion and bulk composition of the ore (Ewers, 1972; McQueen, 1979, 1987; Barrett et al., 1977). Ores with lower Cu contents (e.g., Kambalda and Thompson) will revert to a single-phase *mss* at lower temperatures than those with higher

Cu contents (e.g., Duluth, Noril'sk, and Sudbury). Massive sulfide ores mobilized by ductile plastic flow as a homogeneous *mss* will exhibit limited ranges of Fe/Ni/Cu ratios and Ni/Cu tenors (Barrett et al., 1977; McQueen, 1987) and geochemical variations matching typical magmatic *mss* differentiation trends (Barnes and Miller, 2010). In contrast, massive sulfide ores mobilized by ductile plastic flow of polymineralic pyrrhotite-pentlandite-chalcopyrite aggregates will exhibit large-scale variations in Fe/Ni/Cu ratios and Ni/Cu tenors due to segregation of very ductile chalcopyrite and moderately ductile pyrrhotite from less ductile pentlandite (Barrett et al., 1977; McQueen, 1987).

Metamorphic-hydrothermal fluids can modify the compositions of deformed sulfides through dissolution and subsequent re-precipitation of metals during or after post-metamorphic peak conditions (e.g., Keays et al., 1982; Lesher and Keays, 1984; Cook et al., 1993; Vokes and Craig, 1993). Bailey et al. (2006) suggested that the Ni depletion in the deformed sulfide ores at the Thayer Lindsley mine (Fig. 4.1) were caused by the replacement of pentlandite by pyrrhotite, and subsequent mobilization of the liberated Ni by metamorphic hydrothermal fluids during amphibolite facies metamorphism. Cu, Pt, Pd, Au, Ag, Bi, As, and Te are also readily mobilized by hydrothermal fluids and may be re-precipitated into veins (McCallum et al., 1976; Bavinton and Keays, 1978; Groves and Keays, 1979; Keays et al., 1982; Fyfe and Kerrich, 1984; Lesher and Keays, 1984; Gilligan and Marshall, 1987; Keays, 1987; Farrow and Watkinson, 1994; Marshall et al., 2000; Magyarosi et al., 2002; Szentpéteri et al, 2002; Hanley, 2005) or dispersed more widely (e.g., Layton-Matthews et al., 2011). Although Au-Pd-Pt can be very soluble in hydrothermal fluids (e.g., Wood, 2002; Hanley, 2005), Ir is much less soluble, and thus, hydrothermal mobilization of PGE normally results in decoupling Pd from Ir, very low Ir contents, and high, but variable Pd/Ir ratios in hydrothermal sulfides (Keays et al., 1982; Lesher and Keays, 1984, 2002).

Partial melting of massive sulfides and subsequent mobilization of the melt has been an important mechanism of mobilization in some Pb-Zn deposits (e.g., Broken Hill, Australia; Montauban, Canada; Lengenbach, Switzerland; Bleikvassli, Norway) deformed at moderate to high metamorphic temperatures ranging between 520 and 850°C (e.g., Lawrence, 1967; Vokes, 1971; Mavrogenes et al., 2001; Frost et al, 2002; Tomkins, 2007; Tomkins et al., 2007). Whereas Pb-Zn systems may produce a partial melt enriched in Ag, As, Au, Bi, Hg, Sb, Se, Sn, Tl, and Te between 500 and 600°C depending on pressure conditions (Frost et al., 2002), Ni-Cu-PGE ores would exist as *mss* ± *iss* at those temperatures and would only start melting at temperatures above ~900°C for an average Sudbury ore composition (Kullerud et al, 1969). Recently, Tomkins et al. (2007) suggested that the crystallization products of small quantities of low-temperature, late-stage magmatic melts, which are variably enriched in sulfarsenides and sulfosalts in Ni-Cu-PGE deposits, may be subject to melting and mobilization during amphibolite- to granulite-facies metamorphism. However, the maximum amount of partial melt that can be generated even during granulite-facies metamorphism from most sources is less than 0.05% because most Ni-Cu-PGE deposits contain only very small quantities of sulfarsenide minerals (Tomkins et al., 2007).

Whereas deposits in the North Range are relatively undeformed, the Garson deposit and many others in the South Range (e.g., Falconbridge, Creighton, and Thayer Lindsley: Fig. 4.1), underwent a complex history of modification by deformation, metamorphism, and metamorphic-hydrothermal fluids (e.g., Davidson, 1948; Lochhead, 1955; Owen and Coats, 1984; Binney et al., 1994; Bailey et al., 2004; Ames and Farrow, 2007; Dare et al., 2010; Mukwakwami et al., 2012). In order to evaluate the influence of deformation, metamorphism, and metamorphic-hydrothermal fluids on the compositions of deformed ores at Garson, we present geochemical data for 60 representative ore samples collected from the #1 and #4 shear ore bodies on the 3560, 4800, 4900, 5000, and 5100 levels, and 5 samples from the footwall-type mineralization in the contiguous #600 ore body in the Garson Ramp deposit. These data are supplemented by geochemical data from the Vale geochemical assay database. Comparisons of the geochemical variations between and within these ores and to other similar South Range deposits indicate that secondary processes did not significantly alter the magmatic geochemical signatures of the deformed ores. The geochemistry of the #1 shear, #4 shear, and #600 ore bodies are best explained by segregation of *mss* and residual sulfide melt, as observed in other contact-type deposits at Sudbury. Only locally have metals been mobilized by metamorphic-hydrothermal fluids.

4.3 Geologic Setting

The 1850 Ma (Krogh, 1984) Sudbury Igneous Complex (SIC) straddles the boundary between Archean granitic and gneissic rocks of the Superior Province to the north, and Paleoproterozoic metasedimentary and metavolcanic rocks of the Southern Province to the south. The SIC formed as an impact melt sheet at the center of a peak-ring impact structure with an estimated original diameter of ~200-260 km (see review by Grieve et al., 2008). Upon cooling, the "Main Mass" of the SIC differentiated into a lower norite unit, a middle quartz gabbro unit, and an upper granophyre unit (Fig. 4.1). The Main Mass is underlain by a discontinuous layer of Sublayer norite, representing the basal unit of the SIC, and overlain by fall-back breccias, phreatomagmatic volcanic deposits, and sedimentary rocks of the Whitewater Group (Dressler, 1984; Ames, 1999; Ames et al., 2002; Lightfoot et al., 1997, 2001; Grieve et al., 2010). The SIC and overlying Whitewater Group are folded into a 60 km x 30 km doubly-plunging elliptical synform, which is surrounded by impact-related breccias (Sudbury breccia) in the country rocks below the SIC and by radial and concentric quartz dioritic dikes that extend from the SIC into the country rocks. The southern limb of the synform is transected by multiple shear zones, the South Range Shear Zone system, which strikes roughly parallel to the long axis of the synform (Fig. 4.1 and insert).

Sudbury is one of the largest Ni-Cu-PGE mining camps in the world with a pre-mining resource (past production + current resource) conservatively estimated at over 1648 million metric tons grading ~1.2 percent Ni and ~1.0 percent Cu (Naldrett and Lightfoot, 1993). The mineralization occurs as 1) massive pyrrhotite-pentlandite-(chalcopyrite)-rich deposits that occur within and immediately below the discontinuous inclusion-rich Sublayer norite in embayments along the footwall contact of the SIC, 2) chalcopyrite-pentlandite-pyrrhotite-(bornite)-(millerite)-rich veins within brecciated footwall rocks, and 3) coarse disseminated to semi-massive pyrrhotite-pentlandite-chalcopyrite-rich deposits within radial and concentric quartz-diorite dikes (Farrow and Lightfoot 2002; Ames, 2007).

The geology of the Garson Mine is described in Mukwakwami et al. (2012) and is summarized below. The geology of the #600 ore body in the Garson Ramp mine, which is located ~500m meters to the SW of the Garson mine, has not been previously published and it is described below. Our description of this area is based on a few days of underground work, supplemented by mine reports and 3D wireframes of the ore body.

4.3.1 Garson Deposit

The Garson deposit is located along the contact between SIC norite and metabasalt associated with metagabbro, pelitic schist, quartzite, and metawacke of the Elsie Mountain Formation of the Elliot Lake Group, Huronian Supergroup (Young et al., 2001; Long, 2004; Ames et al., 2005). These rocks were partially melted and brecciated immediately below the SIC contact forming an anatectic metabreccia that is up to 65m thick above the 4000 level (Figs. 4.2 and 4.3). The deposit consists of 4 major ore bodies that are coincident with steeply south-dipping shear zones and splays after which named (#1, #2, #3, and #4 shear ore bodies: Figs. 4.3, 4.4). The #1 shear ore body occurs along the sheared contact between Huronian rocks and either the SIC or metabreccia. Below a depth of 1280m, the #1 shear ore body diverges from this contact and continues into the footwall Huronian rocks (Fig. 4.3). The #2, #3, and #4 shear ore bodies occur at the contact between SIC norite and slivers of Huronian rocks and metabreccia. The #2 and #3 shear ore bodies are coincident with splays that truncate the SIC and merge with the #1 shear zone. The #2 shear ore body can be traced from surface to below the 1000 level where it converges and merges with the #1 shear ore body. The #3 shear ore body can be traced from below the 1600 level to less than 50 feet above the 2800 level where it also converges and merges with the #1 shear ore body. The #4 shear ore body occurs within the Main Mass Norite above 4000 level. It converges to within ~50m of the #1 shear ore body on the 4000 level, and continues into footwall Huronian rocks below this level, where it is sub-parallel to the #1 shear zone.

The ore bodies are generally bounded by penetratively foliated wall rocks that record two major deformation events, D_1 and D_2. D_1 structures in the shear zones formed during amphibolite facies metamorphism and are characterized by a strong schistose S_1 fabric and a down-dip L_1 mineral lineation defined by ferrotschermakite and green magnesiohornblende in metabasalt and norite, respectively. The Garson shear zones formed as south-over-north D_1 thrusts that formed due to flexural slip along the SIC-footwall contact during regional buckling of the SIC and overlying Whitewater Group (Mukwakwami et al., 2012). The shear zones imbricated the SIC, its ore zones and the underlying Huronian rocks, and emplaced slivers of Huronian rocks and anatectic metabreccia into the overlying norite. The D_1 shear zones were later reactivated during syn-D_2 greenschist facies metamorphism as high angle reverse, south-over-north D_2 shear zones following overturning of the SIC-Huronian contact during buckling (Mukwakwami et al., 2012). Syn-D_2 metamorphic titanite crystallized at ca. 1849 ± 6 Ma, suggesting that D_1 and D_2 occurred immediately after crystallization of the SIC during the Penokean Orogeny (Mukwakwami et al., *submitted*). The effects of the subsequent 1.7-1.6 Ga Yavapai-Labradorian (Davidson et al., 1992; Bailey et al., 2004; Piercey et al., 2007) and

1.45 Ga Chieflakian (Fueten and Redmond, 1997; Szentpéteri, 2009) orogenies, which affected other parts of the South Range, have not been observed at Garson.

Three main types of Ni-Cu-PGE mineralization occur in the Garson deposit: 1) disseminated to matrix-textured sulfides, 2) breccia ore, and 3) quartz-calcite-sulfide veins (Fig. 4.5). The characteristics of these ore types have been described by Mukwakwami et al. (*submitted*) and are summarized in Table 4.1. Disseminated to matrix textured sulfides in undeformed norite contain 5 to 25% polycrystalline sulfide grains that fill interstices between plagioclase, green magnesiohornblende, quartz, and biotite (Fig. 4.5a). Where deformed, sulfides occur as bands aligned parallel to the foliation (Fig. 4.5a). Breccia ore contains up to 50% rock fragments in a pyrrhotite-rich matrix (Figs. 4.5c-f) and can be subdivided into three subtypes: 1) D_1 contact breccia ore, 2) D_2 contact breccia ore, and 3) D_2 fault breccia ore. The contact breccia ores occur in thicker segments (8-50m wide) of the #1 and #4 ore bodies and contain fragments of Huronian rocks and Sublayer norite, suggesting that the ores formed in embayments or depressions at the base of the SIC and were later deformed during D_1 and D_2 (Mukwakwami et al., 2012; *submitted*). In contrast, fault breccia ores are tabular and contain fragments of Huronian rocks exclusively, suggesting that they represent ores that were extruded from the embayments and mobilized by ductile plastic flow along the shear zones (Mukwakwami et al., 2012; *submitted*). Both contact and fault breccia ores within and along the margins of the #1 and #4 shear ore bodies contain chalcopyrite-rich segregations (Fig. 4.5f: Mukwakwami, *submitted*). The quartz-calcite-sulfide veins, which represent the third mineralization type at Garson, were emplaced as sub-horizontal extensional- and steeply south-dipping shear veins during D_2 (Fig. 4.5g).

4.3.2 Garson Ramp - #600 Ore Body

The east-west trending #600 ore body occurs along a steeply south-dipping shear zone within footwall metavolcanic-metasedimentary rocks of the Elsie Mountain Formation, ~500m meters SW of the #1 shear ore body (Fig. 4.4). Similar to the situation at the Garson mine, the Huronian rocks and the Main Mass norite are generally massive, but are characterized by a strong, steeply south-dipping, schistose foliation with a down-dip mineral lineation within ~5 to 20m of the SIC/Huronian contact. The foliation and lineation are defined predominantly by S_2 chlorite that extensively replaced S_1 green magnesiohornblende and ferrotschermakite in norite and metabasalt, respectively. S-C-C′ fabrics are observed in norite on multiple mine levels, and they consistently indicate a south-over-north reverse displacement during D_2 (Fig. 4.6a).

The ore body generally occurs as 0.5-3m-wide vein-like tabular bodies containing fragments of Huronian rocks in a matrix of massive sulfides (Fig. 4.6b). The tabular bodies plunge parallel to the mineral lineation and they are commonly bounded by sheared wall rocks as observed at the main Garson mine (Mukwakwami et al., 2012). The fragments of Huronian rocks are boudinaged and have a shape-preferred orientation, defining a foliation that is parallel to the penetrative schistose S_2 foliation in the wall rocks and pyrite-rich bands (Figs. 4.5h, 4.6b), suggesting that the tabular bodies were sheared during D_2 and presumably D_1. Chalcopyrite-rich sulfide veins infill fractures within massive wall rocks, indicating that the ore was mobilized by ductile plastic flow, but the presence of hydrothermal veins indicate that fluids may have also affected the ore (Krstic and Vandenberg, 2005).

Because of its stratigraphic location in the footwall rocks below the SIC and its very high Cu-PGE content (total Pt+Pd+Au ~21.5 g/t: Krstic and Vandenberg, 2005), the #600 ore body is interpreted as a footwall-type deposit. The mineralization consists predominantly of chalcopyrite, pyrrhotite, and violarite with secondary pyrite and marcasite (Fig. 4.5h). Associated minor phases include pentlandite, sphalerite, millerite, and cubanite (Krstic and Vandenberg, 2005).

4.4 Sampling and Analytical Methods

Sixty-five representative samples, weighing 2-5 kg, were analyzed to determine the geochemical compositions of the different ore types. Sixty samples were collected from the #1 and #4 shear ore bodies in accessible stopes on the 3560, 4800, 4900, 5000, and 5100 mine levels. Five samples, including two from norite near the SIC-Huronian contact and three representative samples from the #600 ore body, were collected from the Garson Ramp footwall deposit with the assistance of the mine geologists. Samples were sawn perpendicular to foliation and parallel to lineation using a standard diamond-bonded rock saw, grounded with a diamond-bonded steel lap to remove saw marks, and washed with a nylon brush in tap and distilled water. They were crushed using a small jaw crusher using steel plates known to have low PGE contents, pulverized using an agate ball mill, and analyzed at the Ontario Geoscience Laboratories in Sudbury using aqua regia digestion and flame atomic absorption spectrometry for Ni, Cu, and Ag, pressed pellet wavelength dispersive X-ray fluorescence spectrometry for As, Cr, Co, Ti and Pb, open-vessel mixed acid digest and solution inductively-coupled plasma atomic emission spectrometry for Fe and Zn, open-vessel mixed acid digest and solution ICP–mass spectrometry for Sb, Se, Te, Mo, In, Cd, Sn and Bi, NiS fire-assay pre-concentration, Te co-precipitation, and ICP-MS for Au, Pt, Pd, Rh, Ru, and Ir, and infrared absorption spectrometry using a Leco® S analyzer for S. In samples with Fe contents above the upper detection limit, as was the case in many breccia ores, the Fe tenor was calculated by adding the tenors (wt% metal in 100 wt% sulfides) of all other metals and subtracting this sum from 100%.

Our data are supplemented by 21658 analyses of Garson samples in the Vale Ltd. drill core assay database. The samples were collected from diamond drill cores that intersected the #1 and #4 shear ore bodies between the ~3000 to 6500 levels, and the #600 ore body. The #2 and #3 shear ore bodies were mined out and their assay data were not available in the database, but this would not markedly change the calculated average ore composition of the Garson deposit, because the mineralogy of the main ore zones (#1, #2, #3 and #4 shear ore bodies) is similar (Aniol and Brown, 1979). Vale samples were analyzed at ALS Minerals, Sudbury, Ontario, using ICP–AES for Cu, Ni, Fe, and S, and PbS fire assay ICP–MS for PGE. About 2% of assay duplicates from pulp were sent to SGS Minerals, Lakefield, Ontario, where Cu, Ni, Fe, Co, Pb and Zn were determined using wavelength-dispersive X-ray-fluorescence spectrometry, S was analyzed by Leco®, and PGE and Au were determined by PbS fire assay ICP-AES.

In order to permit comparison of whole rock analyses of samples containing different contents of gangue minerals, metal tenors were calculated to 100% chalcopyrite $CuFeS_2$, pentlandite $Fe_{4.5}Ni_{4.5}S_9$, and pyrrhotite $Fe_{0.9}S$ (Naldrett et al., 1979, 1981). Our data are plotted on binary diagrams and, where available, compared with data from the mine database.

4.5 Results

Nickel and Co show positive correlations with S in samples from the #1 and #4 shear ore bodies, whereas Cu and Zn positively correlate with S in samples only from the footwall-type mineralization (#600 ore body) and hydrothermal veins (Fig. 4.7). Samples from the #1 and #4 shear ore bodies have relatively low whole-rock PGE concentrations, with Pd+Pd concentrations rarely exceeding 3000 ppb, whereas the #600 ore body has high PGE concentrations, with Pd+Pt generally ranging from 300 ppb to over 10 ppm. The #1 and #4 shear ore bodies show striking similarities in metal tenors. Ag_{100}, Au_{100}, Pt_{100}, Pd_{100}, Zn_{100}, Sn_{100}, Cd_{100}, and In_{100} show moderate to strong positive correlations with Cu_{100} all ore types, except quartz-calcite-sulfide veins, whereas Ni_{100} shows a strong negative correlation with Cu_{100} in all ore types (Fig. 4.8). The #600 ore body is characterized by very high tenors of Cu-Pt-Pd. Ruthenium and Ir tenors are very low in quartz-calcite-sulfide veins, generally less than 1 ppb, whereas they are up to 670 ppb and 400 ppb, respectively, in breccia ores.

In order to compare the element distributions among the different ore types at Garson and other South Range deposits, we present our data (metals in 100% sulfides) in primitive mantle-normalized chalcophile multi-element variation diagrams (Fig. 4.9). The order of compatibility is similar to that suggested by Lesher and Keays (2002), which was chosen to highlight variations attributable to differences in magma composition and partitioning during ore formation, but we rearranged the semi-metals (Bi, S, Te, and Se) and Ag to reduce some of the anomalies. Deformed and undeformed disseminated to net-textured sulfides at Garson have broadly similar multi-element chalcophile patterns, which are similar but slightly enriched in Ag-Te-Au-Pd-Pt-Cu-Zn compared to those of undeformed disseminated sulfides at the Creighton mine (Fig. 4.9a: see Fig. 4.1 for location of Creighton mine). D_1 and D_2 contact and D_2 fault breccia ores at Garson exhibit similar multi-element chalcophile patterns to undeformed contact ores at the Creighton mine (Figs. 4.9b-d). However, one sample of D_2 fault breccia ore collected from chalcopyrite-rich segregations on the periphery of the #1 shear ore body (GA183: Fig. 4.5f) contain very high Au-Pd and low Ru-Ir compared to the other fault breccia samples (Fig. 4.9d). Garson Ramp footwall-type ore and quartz-calcite-sulfide veins from the Garson mine have similar element distribution patterns, but the footwall-type ore has higher Au-Pd-Pt abundances than the quartz-calcite-sulfide veins (Fig. 4.9e). A sample of the selvedge surrounding a calcite-sulfide vein at the Garson Mine has significantly higher abundances of Ir-Ru-Rh-Pt than the quartz-calcite-sulfide veins (Fig. 4.9e).

As the composition of the disseminated sulfides appears to represents the composition of undeformed magmatic ore, we have normalized all of the other ore types to average disseminated sulfides at Garson (Fig. 4.9f). Anomalous values for individual elements in individual samples were excluded in calculating the average compositions of each of the mineralization types. Figure 9f shows that the D_1 and D_2 contact breccia ores, and D_2 fault breccia ores exhibit similar element distribution patterns. Whereas deformed contact massive sulfide ore at the nearby Thayer Lindsley mine are depleted in Ni (Bailey et al., 2006), deformed contact and fault breccia ores at Garson have Ni abundances similar to those of the disseminated sulfides (Fig. 4.9e) and approximately similar S-Se-Ru-Ni-Ir-Co-Fe-(Rh) abundances compared to the disseminated sulfides. However, these Garson ores are significantly depleted in Au-Pt-Pd, similar to contact ores at the Strathcona deposit in the North Range, and the Creighton and Falconbridge deposits in the South Range (e.g., Naldrett et al., 1982; Dare et al., 2010). In addition, Garson breccia ores are moderately depleted in Cr-Au-Zn-Ag-Te-Sb-Pb-Mo-Au-Cu and enriched in As. The chalcopyrite-rich segregation (GA183 Fig.: 4.5f) is depleted moderately in Cr-Ir-Ru-Rh and slightly in Pb-Mo-Bi-Fe, and is enriched strongly in As-Sb-Pd, moderately in Cu, and slightly in Au-Pt-Co-Ni (Fig. 4.9f). Garson Ramp footwall-type ore shows some similarities with the quartz-calcite-sulfide veins in that they are both strongly depleted in Rh-Ru-Cr-Ir-Mo and moderately enriched in Cu-Zn-Pd-Au-Ag (Fig.9f). However, they are different in that the quartz-calcite-sulfide veins are strongly depleted in Pt and moderately depleted in Sb-As-Bi whereas the footwall-type ore is enriched in these elements. The calcite vein selvedge is enriched in As-Cu-Pt-Pd-Ag-Rh-Mo-Ir-Sb-Zn-Ru, and is depleted in Ni-Bi-Pb-Cr-Co-Te (Fig. 4.9f).

Pd/Ir ratios are generally low (<10) for all contact and fault breccia ores, which also have higher Ni/Cu ratios compared to the other mineralization types (Fig. 4.10a). In sharp contrast, quartz-calcite-sulfide veins have distinctly very low absolute Ir_{100} (Figs. 4.10c, d), high Pd/Ir ratios (~500-30000: Fig. 4.10a), and very low Ni/Cu ratios. A plot of Pt_{100} against Pd_{100} show a good correlation for all mineralization types from all ore bodies, except that Pt is clearly decoupled from Pd in the quartz-calcite-sulfide veins plot (Fig. 4.10b). Ir_{100} is very strongly correlated with Ru_{100} and Rh_{100} in all of the breccia ore types, but not in quartz-calcite-sulfide veins, and is moderately negatively correlated with Pt_{100} in all of the breccia ores (Figs. 4.10c-e).

Ni tenors and Fe/Ni ratios provide information relevant to the possible segregation of pyrrhotite from pentlandite in breccia ores, which occurs when massive sulfides are mobilized by ductile plastic flow as an aggregate of mixed sulfide phases (Barrett et al., 1977; McQueen, 1987). All ore types, except for the quartz-calcite-sulfide veins, show restricted ranges of Ni tenors and Fe/Ni ratios (Figs. 4.10d, 4.11). The S-weighted average Ni tenors for the #1 and #4 shear ore bodies calculated from the mine drill assay database are 5.1 ± 3.6 wt% and 4.9 ± 3.3 wt%, respectively (Mukwakwami et al., *submitted*), similar to the Sudbury average (e.g., Naldrett, 2004). Contact breccia ores and disseminated sulfides at Garson have restricted ranges of Ni tenors that range predominantly from ~4 to 6 Ni wt%, and Fe/Ni ratios that vary slightly from 9 to 14 (Fig. 4.10f). The highest Ni tenors range from ~6 to 9.5 wt% and are found in only three D_2 contact breccia samples. Quartz-calcite-sulfide veins generally have lower Ni tenors (<2 wt%) and higher Fe/Ni ratios (Fig. 4.10f) compared to the disseminated to matrix textured sulfides and breccia ores, which is consistent with their low modal pentlandite content.

When our data are plotted together with data from the mine database against depth, they clearly show that the Ni tenor in both ore bodies at the Garson mine does not vary significantly with depth between the ~3000 and 6500 levels (Fig. 4.11a). Approximately 72% and 78% of the analyses (mine database) from the #1 and #4 shear ore bodies, respectively, lie within the 4 to 8 wt% Ni tenor range (Fig. 4.11b), suggesting that the majority of the ore within the #1 and #4 ore bodies has a composition similar to the sampled contact and fault breccia ores. The low Ni tenors below 4 wt% coincide with fault breccia samples with a high chalcopyrite content and quartz-calcite-sulfide veins (Fig. 4.11a), suggesting that these ores account for the lower Ni tenor ores within the #1 and #4 ore bodies.

4.6 Discussion

The compositions of deformed magmatic Ni-Cu-PGE ores may vary not only with the intensity of deformation and metamorphic grade during deformation (e.g., Barrett et al., 1977; McQueen, 1987), but also with original magmatic variations resulting from equilibration with different compositions or masses of silicate magma (e.g., Campbell and Naldrett, 1979, Lesher and Campbell, 1993) and any late-magmatic fractional crystallization of the sulfide melt (e.g., Ebel and Naldrett, 1996, 1997). In order to evaluate if metal variations between ore types are due to magmatic processes, we must first determine if their concentrations have been modified by metamorphic or hydrothermal processes.

4.6.1 Hydrothermal Mobilization

The presence of chalcopyrite-pyrrhotite-pentlandite in syn-D_2 quartz-calcite-sulfide shear veins and extensional veins indicates that some metals have been at least locally mobilized by metamorphic-hydrothermal fluids. The elements enriched in the veins (Cu > Zn > Pb > Au > Ag > Pd > Te) have been shown in numerous experimental studies to be soluble in HS^- and Cl^--rich fluids (see reviews by Wood, 2002; Hanley, 2005; Reed and Palandri, 2006). Given the S-rich, Cl-poor environment, HS^- complexing seems most likely, with the abundances of the various elements in the veins depending on the abundances of the elements, their solubility at the source, and the mechanism of deposition. The source is most likely the then actively-deforming contact breccia ores, which are depleted in many of the same elements. However, the enrichments are too low and there are too few veins to account for the broader depletion of these metals in the contact breccia ores, suggesting wider dispersion of some or all of these elements into the wall rocks. Because Garson ores are not milled separately from other Sudbury ores we were not able to obtain mill feeds or concentrates on which to refine the scale of dispersion (e.g., Keays et al. 1981; Layton-Matthews et al., 2011), but a future analysis of this type would help constrain the scale of mobilization.

The elements that are 'depleted' in the veins (Ir > Pt-Ru >> Rh > Cr > Mo > Ni-As > Co > Bi > Sb > Fe) fall into two categories: 1) elements that appear to have low solubilities in hydrothermal fluids (Ir-Ru-Rh-Cr-Ni-Co) except under exceptional conditions and that were likely left behind in the source, and 2) elements that are known to be soluble in hydrothermal fluids under many conditions (Pt-Mo-As-Bi-Sb-Fe-Se) and may have been mobilized further into the footwall rocks. Ni and Co are mobile in As-rich fluids (e.g., Cobalt, Ontario: Andrews et al., 1986), but do not appear to have been mobilized out of (or into) Garson breccia ores. Because breccia ores contain significant amounts of As-Bi-Sb (Gammel et al., 2004; Ames and Farrow, 2007; this study), it seems likely that these elements were also retained in the source. The abundance of As in Thayer Lindsley ores is not known, but this may be one of the reasons why Ni was more mobile during deformation at Thayer Lindsley (Bailey et al. 2006) than at Garson.

The very low abundances of Pt in the quartz-calcite-sulfide veins indicates that it was 1) hosted in phases that were resistant to hydrothermal dissolution and was therefore relatively immobile compared to Pd (e.g., Barnes and Liu, 2012) or that it was 2) dispersed more widely into the wall rocks. The veins only occur on a local scale and extend into the wall rocks within ~5 meters of the shear zone boundaries (Mukwakwami, 2012), but this does not preclude dispersion via a less focused mechanism and the peripheral wall rocks were not sampled. However, the veins constitute a very small proportion of the Garson ores and they are brecciated and form part of the D_2 breccia ore. The veins do not appear to account for the missing Pt and Pd in the contact and fault breccia ores because Pt_{100} in these breccia ores exhibit a moderate negative correlation with Ir_{100} (Figs 10d, e), suggesting that it was not extensively mobilized by hydrothermal fluids.

The similarity of Garson disseminated sulfides and pyrrhotite-rich breccia ores to their undeformed counterparts at Creighton and the absence of major depletions in any of the above elements, indicate that the Garson ores retain more-or-less primary magmatic compositions. Garson Ramp footwall-type ore samples are enriched in Cu-Zn-Pd-Pt-Au-Ag and depleted in Rh-Ru-Cr-Ir-Mo relative to disseminated sulfides and pyrrhotite-rich breccia ores, but have similar Pt/Pd and Ru/Ir ratios suggesting that their compositions have been controlled by other than hydrothermal processes. The chalcopyrite segregation, which has similar enrichments/depletions patterns as the footwall-type ore, likely represent physical accumulation of metamorphic *iss* or an originally more Cu-rich ore.

4.6.2 Deformation and Metamorphism

The breccia ores at Garson underwent plastic ductile flow during amphibolite and greenschist facies metamorphism (Mukwakwami, *submitted*). Depending on the bulk ore composition, temperature and rates of diffusion (which influence mineralogy), deformation of polymineralic aggregates can lead to variations in chalcopyrite/pyrrhotite/pentlandite ratios within an ore shoot due to physical segregation of very ductile chalcopyrite, moderately ductile pyrrhotite, and less ductile pentlandite during ductile mechanical flow of the sulfides (Barrett et al., 1977; McQueen, 1987). The consistent Fe/Ni ratios and Ni tenors in all breccia ore suggest that the sulfides were not ductilely segregated during deformation and, consequently, that the Garson ores deformed as a homogeneous *mss* during D_1 and D_2. As there is no consistent variation of Ni tenors with position in each of the #1 and #4 shear ore bodies, and there is no significant variation in the distribution of Ni tenors between them (Fig. 4.10b), the Ni tenors do not appear to have been modified by deformation and metamorphism (e.g., Barrett et al, 1977; McQueen, 1981, 1987).

Together with the observations of Gammell et al. (2004) and Dare et al. (2010), this study provides additional evidence that As was incorporated into some Sudbury ores at the magmatic stage. Because As is much more abundant in ores on the South Range than in the ores on the North Range (Ames and Farrow, 2007), this suggests that it was incorporated from Huronian metavolcanic rocks and provides additional evidence for models involving post-impact thermomechanical erosion of footwall rocks (e.g., Prevec and Cawthorn, 2002).

Contrary to studies claiming otherwise (e.g., Heath et al., 2004; Stone et al., 2004), the recognition that most of the breccia ores in the Garson deposit retain magmatic geochemical trends and have been only very locally modified by metamorphic-hydrothermal processes confirms other studies showing that careful sampling and analysis of even highly tectonized magmatic sulfide ores can provide valuable information on the genesis of the ore deposits (e.g., Ross and Keays, 1979; Keays et al., 1981; McQueen, 1981; Lesher and Campbell, 1993; Barnes, 2004; Barnes and Miller, 2010; Layton-Matthews et al., 2011).

4.6.3 R Factor

The compositions of magmatic Ni-Cu-PGE sulfide ore are strongly controlled by the amount of silicate magma that they interact with (e.g., Campbell and Naldrett, 1979; Lesher and Burnham, 2001). Campbell and Naldrett (1979) demonstrated that the final concentration of a chalcophile element in a sulfide melt (Y_i) is related to the initial concentration of the element in the silicate melt (X_i^o), the magma:sulfide mass ratio (R), and the sulfide melt/silicate melt partition coefficient (D_i) by the following expression:

$$Y_i = \frac{X_i^o D_i (R+1)}{R + D_i} \ ,$$

which shows that Y_i is controlled primarily by R when $R > 10D_i$.

Disseminated sulfides often have higher metal tenors than massive sulfides in the same deposit because disseminated sulfides often equilibrate with a larger proportion of silicate melt (Lesher and Campbell, 1993; Barnes and Lightfoot, 2005). Contact and fault breccia ores at Garson have similar Ni tenors to- and are slightly enriched in Rh-Ru-Ir relative to the disseminated sulfides (Fig. 4.10f), suggesting that the R factor is unlikely to have controlled the variation in the tenors of chalcophile elements at Garson. The contact massive sulfide ores are often depleted in Au-Pd-Pt-Cu (Keays and Crocket, 1970; Naldrett et al., 1982; 1999; Li et al., 1992, 1993; Mungall et al., 2005; Mungall, 2007), suggesting that they contain a significant component of accumulated *mss* that settled quickly at the base of the SIC via a gravity filtration process (J.P. Golightly, *pers. comm.*, 1999) or incorporated via a dynamic remelting process (Lesher et al., 2009).

In order to model the potential effects of variations in R on the Pt, Pd, Ni, Cu, and Zn contents of Garson ores, we calculated the Y_i values at different R values using starting compositions (X_i^o) estimated from the composition of the Onaping Formation and marginal quartz diorite phase of the quartz diorite offset dykes (Table 4.2), which are thought to represent the initial bulk composition of the SIC (e.g., Ames et al., 2002; Keays and Lightfoot, 2004). Plots of Ni_{100}, Pd_{100} and Pt_{100} against Cu_{100}, do not show agreement between the observed trends and the simulated Y_i trends (Figs. 4.12a-c), further indicating that the variations in the concentration of chalcophile elements at Garson are likely not controlled by the R factor.

4.6.4 Fractional Crystallization of Monosulfide Solid Solution

Fractional crystallization of a sulfide liquid will concentrate Os-Ir-Ru-Rh-Co-(Ni) in *mss* and Cu-Pd-Pt-Au-As-Sb-Bi-Te-Pb-Ag in the residual sulfide liquid (e.g., Fleet et al., 1993; Naldrett et al., 1982, 1999; Li et al., 1996; Ebel and Naldrett, 1996, 1997; Barnes et al., 1997, 2005; Ballhaus et al., 2001; Barnes, 2004; Mungall et al., 2005; Mungall, 2007), as is observed in the D_1-D_2 contact and D_2 fault breccia ores at Garson. This plus the similarities in chalcophile element patterns of D_1-D_2 contact and D_2 fault breccia ores at Garson and undeformed contact-style pyrrhotite-rich sulfides that were interpreted as *mss* cumulates at Creighton mine (Dare et al., 2010) suggest that these Garson breccia ores are *mss* cumulates.

In order to model the potential effects of *mss* fractionation and accumulation on the Pt, Pd, Ni, and Cu contents of Garson ores, we modeled the process using a finite difference numerical model similar to that of Golightly and Lesher (1999) and Mungall (2007), whereby the composition of *mss* in equilibrium with the sulfide melt is calculated, small amounts of *mss* (with or without trapped sulfide melt in this case) are removed, and the sulfide melt composition is then recalculated. The process is repeated until the melt reaches the chalcopyrite-pentlandite tie line, which approximates the thermal minimum in this system. *Mss*/sulfide melt partition coefficients are recalculated at each step using an experimentally-derived function that is dependent on temperature, liquid composition, and solid composition. The abundances of Ni, Cu, Pt, Pd, and Ir in the initial sulfide melt and the *mss*/sulfide melt partition coefficient constants are given in Table 4.3. Except for Ir, which required a significantly lower *mss*/sulfide melt partition coefficient than suggested by experimental studies, the calculated fractionation trends closely match the variations in the natural trends defined by samples of all the breccia and footwall ores and the mine assay database (Fig. 4.13). Thus, we interpret the pyrrhotite-rich, Cu-Pt-Pd-poor contact and fault breccia samples as *mss* cumulates, and the Cu-Pt-Pd-rich fault breccia ore and footwall mineralization as residual sulfide liquid.

4.7 Conclusions

1) The restricted range in Fe/Ni ratios and Ni tenors in highly deformed breccia ores at Garson indicate that Ni was not significantly mobilized during polyphase deformation and amphibolite-greenschist facies metamorphism.

2) The multi-element chalcophile patterns of deformed and undeformed disseminated to matrix net-textured sulfides at Garson are similar, indicating that the disseminated sulfides at Garson were not significantly modified by deformation and metamorphic hydrothermal fluids.

3) Disseminated sulfides, D_1-D_2 contact breccia ores, and D_2 fault breccia ores at Garson are compositionally similar to undeformed disseminated sulfides and contact massive sulfide ore, respectively, at Creighton mine, suggesting a magmatic origin for these Garson ore types.

4) The distribution of Cu, Ni and PGE in the #1 and #4 shear, and #600 ore bodies is best explained by *mss* fractionation. The numerical *mss* fractionation model trends on diagrams of Ni_{100}, Ir_{100}, Pd_{100}, Rh_{100} and Pt_{100} versus Cu_{100} are remarkably similar to those generated by data from the breccias ore samples and the mine dataset. The

contact and D_2 fault breccia ores, which are depleted in Pd and Pt, are *mss* cumulates, whereas the chalcopyrite-segregations and the footwall-type ore represent residual sulfide melt.

5) The only evidence for significant amounts of metal mobility in Garson ores has been the very local mobilization of Cu > Zn > Pb > Au > Ag > Pd > Te into hydrothermal quartz-carbonate-sulfide veins.

4.8 Acknowledgements

The paper is part of a PhD research undertaken by the first author at Laurentian University. The project was funded by a Vale-NSERC-CRD grant to BL and CML, NSERC Discovery grants to BL and CML, and an SEG Foundation Canada grant to JM. We thank Vale for providing access to geological data, mine exposures, and diamond drill cores and for their approval for publication. S. Lowen, D. Hodder, C. Gauld, S. Kedzierski, L. Desjardins, D. Butt, B.Gauvreau, J. Letto and D. Bellefeuille are thanked for logistical assistance and many beneficial discussions on the geology of the Garson

Table 4.1. Mineralogy, metamorphic grade, textures, fabrics, and effects of deformation and metamorphism on major ore types in the Garson deposit.

Ore Types	Sulfide Mineralogy	Metamorphic Facies	Description of Ore Zones ,Textures and Fabrics	Effects of Deformation and Metamorphism	Depletions	Enrichments
Disseminated to net - textured sulfides	Po (80-90%), Pn (5-15%), Ccp (5-10%), Mag (<5%), and minor gersdorffite, cobaltite, niccolite, and rare sperrylite	Amphibolite or greenschist facies	Undeformed: 5 to 25% polycrystalline sulfide grains interstitial to green magnesiohornblende, plagioclase, and quartz in metamorphosed norite (Fig. 4.5a). Deformed: Sulfide bands aligned parallel to an amphibole S_1 or a chlorite S_2 foliation (Fig. 4.5b)	Po and Ccp mobilized by ductile plastic flow into parallelism with S_1 or S_2. Pn was exsolved from Po after deformation because Pn is undeformed.		
D_1 contact breccia ore	Same as in disseminated sulfides	Amphibolite facies with minor greenschist overprint	Occur in thick segments (8 to 50 m) wide of the ore bodies. Contain fragments of norite and Huronian rocks in a sulfide matrix. D_1 fabrics in ore zones: fragments define a foliation and lineation parallel to S_1 and L_1 and, are boudinaged parallel to L_1. Polygonal Po aggregates are associated with veinlets of Pn along grain boundaries, and with randomly distributed large Pn grains.	Massive sulfide ore mobilized by ductile plastic flow as a homogeneous monosulfide solid solution. Polygonal Po recrystallized during and after deformation and exsolved Pn after cessation of D_1.	Au > Cr-Zn > Pb-Bi-Te > Cu > Sb-Pt-Ag > Pd > Mo > Se > Co > Ni	As >> Rh > Ru-Ir > Fe > S
D_2 contact breccia ore	Same as in disseminated sulfides	Greenschist	Occur in thick segments (8 to 50 m) wide of the ore bodies. Contain fragments of norite and Huronian rocks in a sulfide matrix. D_2 fabrics in ore zones: fragments define a foliation and lineation parallel to S_2 and L_2 and, are boudinaged parallel to L_2. Pn layers and elongate grains are oriented parallel to a foliation defined by elongate Po grains and to an internal S_2 chlorite foliation in metabasalt fragments. Pn grains overgrow S_2.	Massive sulfide ore mobilized by ductile plastic flow within embayments as a homogeneous monosulfide solid solution. Po dynamically recrystallized during deformation, but rare flattened Po grains are preserved. Po exsolved Pn after cessation of D_2.	Au > Pb-Cr > Zn > Sb-Bi > Te-Cu-Ag > Pd > Pt > Mo > Se > Co > As	Rh > Ir > Ni > Fe > Ru > S
D_2 fault breccia ore	Same as in disseminated sulfides	Greenschist facies	Ore zones are narrow are tabular. Contain fragments of exclusively Huronian rocks in a sulfide matrix. D_2 fabrics are as in D_2 contact type breccia ore (above).	Massive sulfide ore externally mobilized by ductile plastic flow along shear zones as a homogeneous monosulfide solid solution to form narrow tabular ore zones. Po dynamically recrystallized during deformation, but rare flattened Po grains are	Cr-Pb-Au-Zn > Cu > Bi-Ag > Te-Mo > Sb > Pd-Pt > Se > Co > Ni	As >> Rh > Ir > Ru > Fe > S

				preserved. Po exsolved Pn after cessation of D$_1$.		
Syn-D$_2$ quartz-calcite-sulfide vein	Ccp (80-90%), Po (5-15%), Pn (<5%), Sph (≤1%),	Greenschist facies	Ccp-rich sulfides associated with quartz and/or calcite veins in walls rocks and ore zones. Veins are strongly folded, boudinaged and broken-up in ore zones..	Metamorphic-hydrothermal fluids mobilized ore by dissolution and reprecipitation in syn-D$_2$ quartz-calcite veins.	Ir > Pt-Ru >> Rh > Cr > Mo > Ni-As > Co > Bi > Sb > Fe > Se > S	Cu > Zn > Pb > Au > Ag > Pd > Te
Footwall-type (Garson Ramp)	Ccp-Po- Py-Viol-(Pn)-(Sph)-(Mil)-Cub	Greesnschist facies overprinting earlier amphibolite facies event	Fragments of Huronian rocks in a chalcopyrite-rich sulfide matrix. Pyrite-rich bands are parallel to S$_2$	Massive sulfides mobilized by plastic ductile flow	Ru >> Ir-Cr > Rh > Mo > Co > Ni > Fe > Pb > S	As > Pd >> Au > Cu > Te > Sb > Ag > Pt > Bi > Se > Zn

Enrichments and depletions are relative to the average Garson disseminated sulfides. **Po:** pyrrhotite, **Pn:** pentlandite, **Ccp:** chalcopyrite, **Mag:** magnetite, **Sph:** sphalerite, **Viol:** violarite, **Py:** pyrite, **Mil:** Millerite, **Cu:** Cubanite, **Ge**: gersdorffite, **Co**: cobaltite, **Nic**: niccolite, and rare **Sp**: sperrylite.

Table 4.2. Starting magma compositions (X_i^o) and sulfide melt/silicate melt partition coefficients (D_i) used in R factor model (from Ames et al., 2002; Keays and Lightfoot 2004).

	Ni (ppm)	**Cu (ppm)**	**Pd (ppm)**	**Pt (ppm)**
X_i^o	61	59	3.85	4.01
D_i	1000	1000	100000	100000

Table 4.3. Starting sulfide melt composition (Co) compositions and mss/sulfide melt partition coefficient constants (ao, aFe, aNi, aCu, aS, aT), and range of Ds used in sulfide crystallization modeling. Constants for Ni and Cu are modified from regressions of published experimental data by J.P. Golightly using a database compiled by S-J Barnes. Constants for PGE are modified from Mungall (2007).

	Ni	**Cu**	**Pd**	**Pt**	**Rh**	**Ir**
C_o	5.0 wt%	5.0 wt%	3000 ppm	2500 ppm	300 ppm	150 ppm
a_o	18.12	2.180	-16.77	-22.45	-15.25	-9.12
a_{Fe}	-0.260	-0.057				
a_{Ni}	-0.232	-0.057				
a_{Cu}	-0.194	-0.060				
a_S	-0.082	0.000	0.3027	0.4758	0.4567	0.4073
a_T			-0.00284	-0.00450	-0.00907	-0.01189
D	0.82-9.55	0.29-0.30	0.031-0.22	0.21-4.4	0.54-40	0.67-93

$\log D_{Ni}, D_{Cu} = a_o + a_{Fe} * \text{mol Fe} + a_{Ni} * \text{mol Ni} + a_{Cu} * \text{mol Cu} + a_S * \text{mol Fe}$

$\log D_{PGE} = a_o + a_S * \text{mol S} + a_T * T(^oC)$

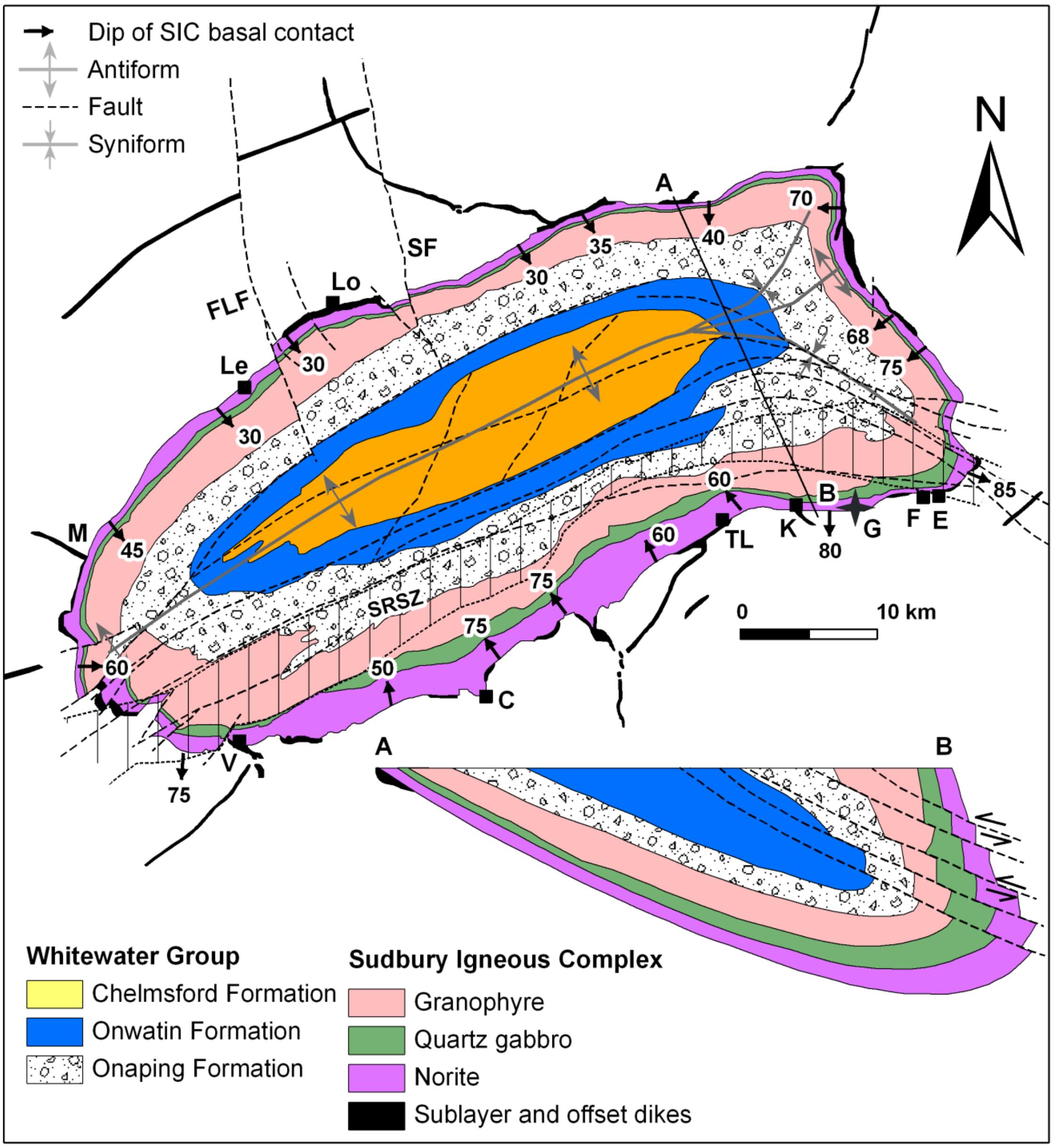

Figure 4.1. Geological map and schematic section (insert) of the Sudbury structure showing the distribution of the Main Mass, Sublayer and offset dikes of the SIC and overlying formations of the Whitewater Group. Modified after Dressler et al.(1991); Ames et al. (2005); Riller (2005); Klimczak et al. (2007); Mukwakwami et al. (2012). SRSZ: South Range Shear Zone, TL: Thayer Lindsley Mine, K: Kirkwood Mine, G: Garson Mine, F: Falconbridge Mine, E: East Mine, C: Creighton Mine, FLF: Fecunis Lake Fault, SF: Sandcherry Fault, HS: Huronian Supergroup.

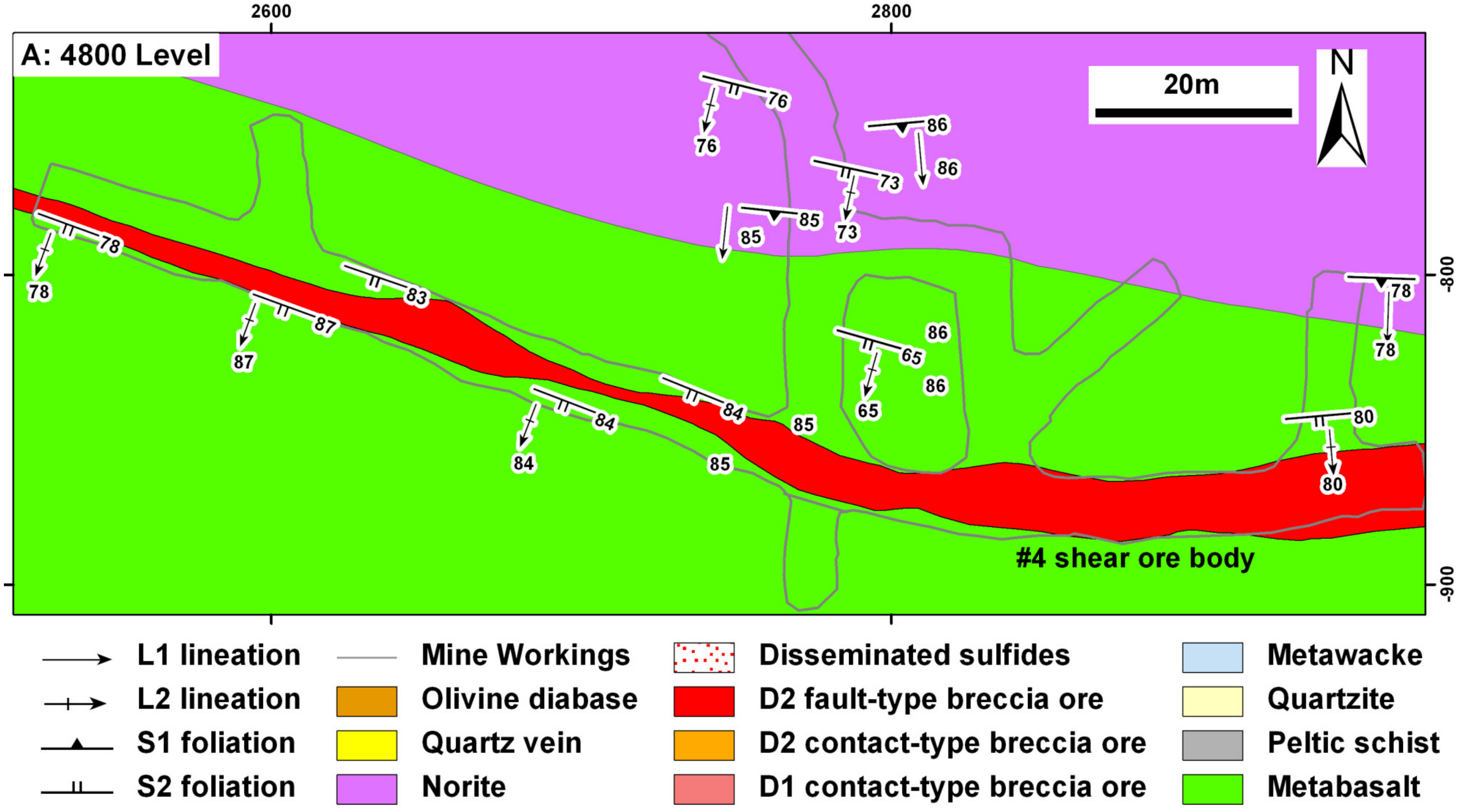
A: 4800 Level
2600
2800
-800
-900
20m
N
#4 shear ore body
76
76
86
86
73
73
85
85
78
78
83
87
87
86
65
65
86
84
84
84
85
85
78
78
80
80
L1 lineation
L2 lineation
S1 foliation
S2 foliation
Mine Workings
Olivine diabase
Quartz vein
Norite
Disseminated sulfides
D2 fault-type breccia ore
D2 contact-type breccia ore
D1 contact-type breccia ore
Metawacke
Quartzite
Peltic schist
Metabasalt

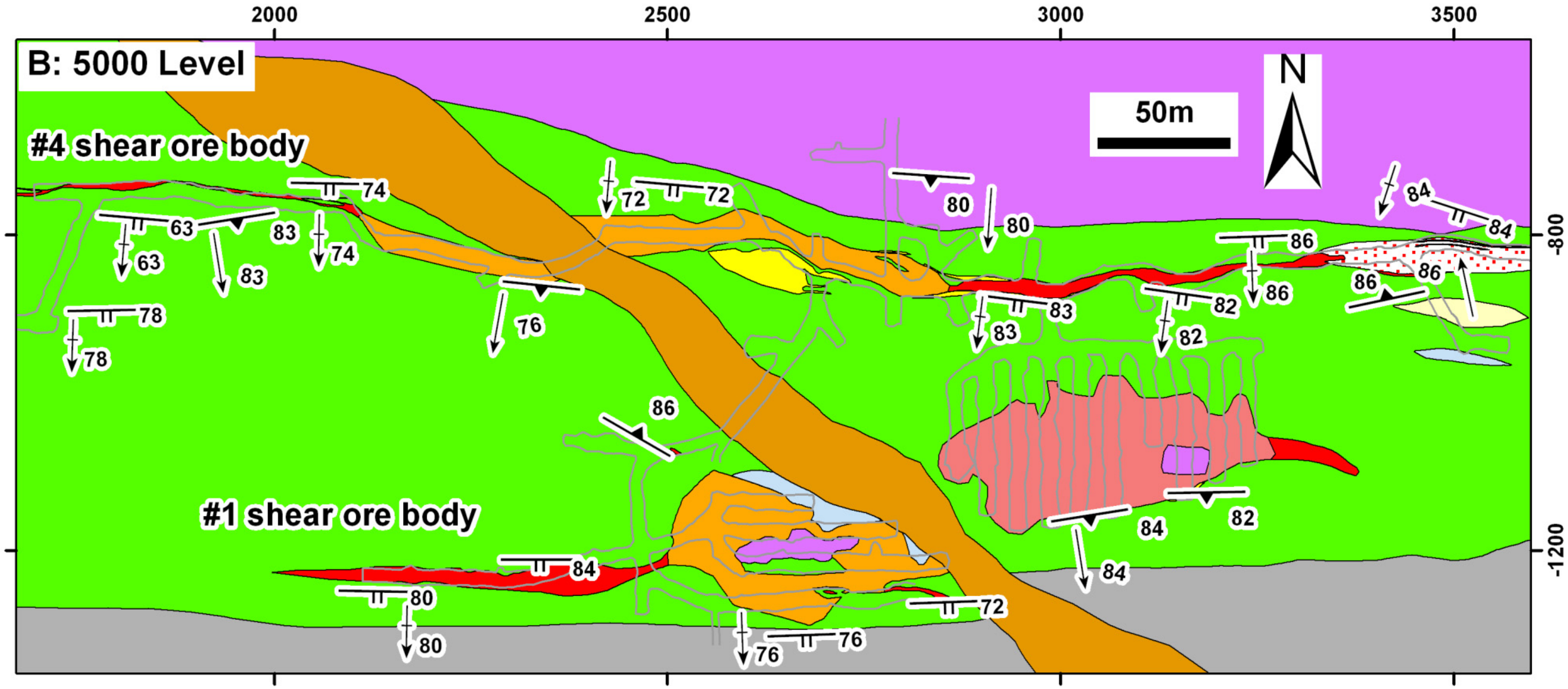

Figure 4.2. Geological maps of the (a) 5000 ft level and (b) 4800 ft level of the Garson Mine (from Mukwakwami et al., submitted) showing the #4 and #1 shear ore bodies.

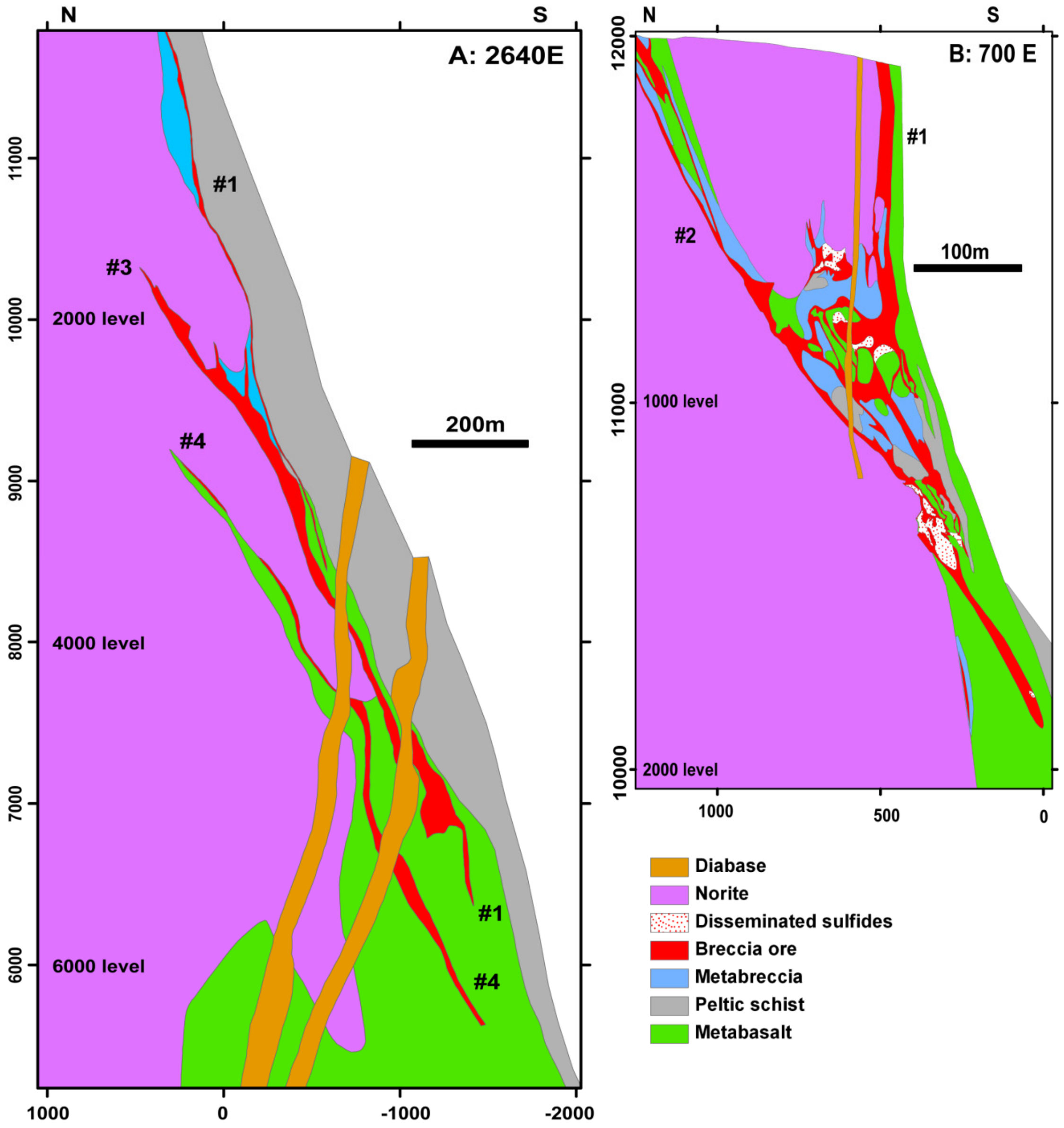

Figure 4.3. Cross sections (looking east) of the Garson ore bodies along sections (a) 2640 E and (b) 700E (from Mukwakwami et al., 2011, as modified from Aniol and Brown, 1979).

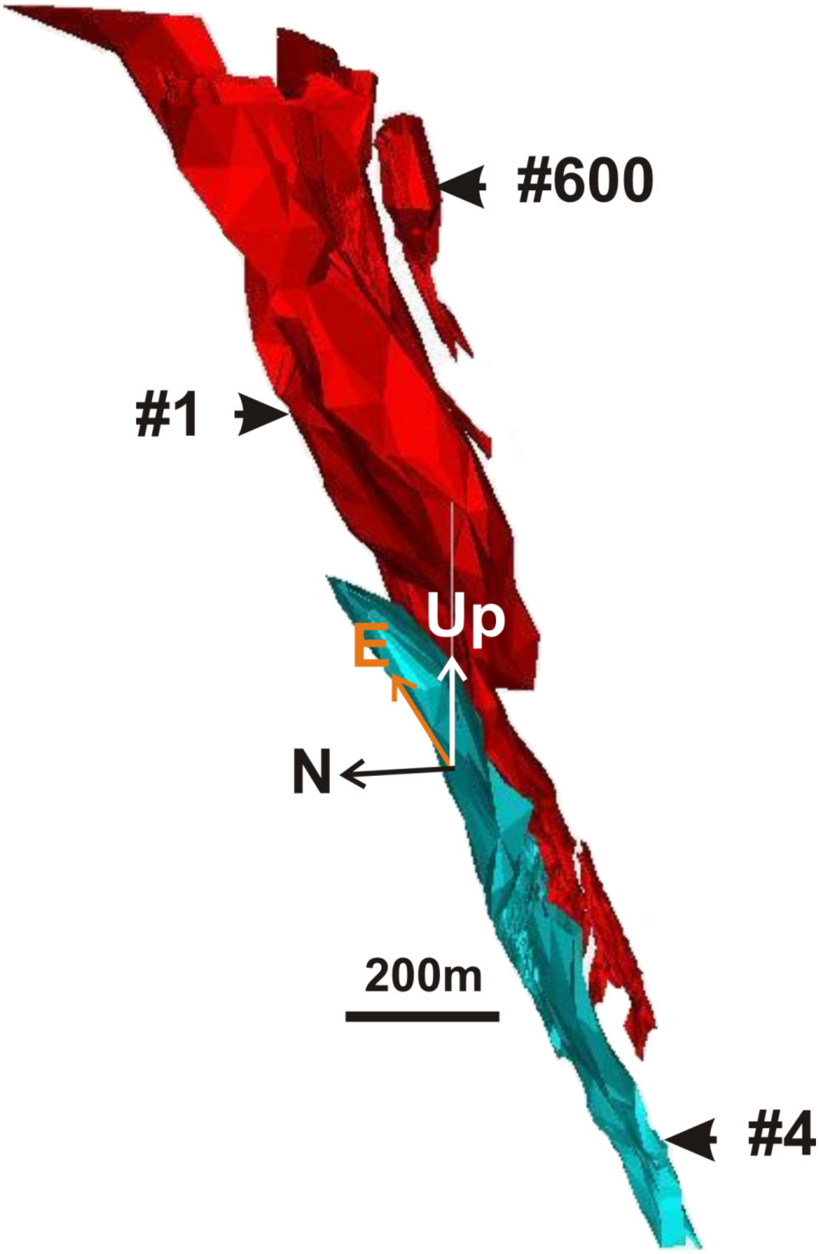

Figure 4.4. Wireframes showing 3D geometry of the #1 and #4 shear ore bodies at the Garson mine and the #600 ore body at the Garson Ramp mine (looking east). The ore bodies have a southerly down-dip plunge.

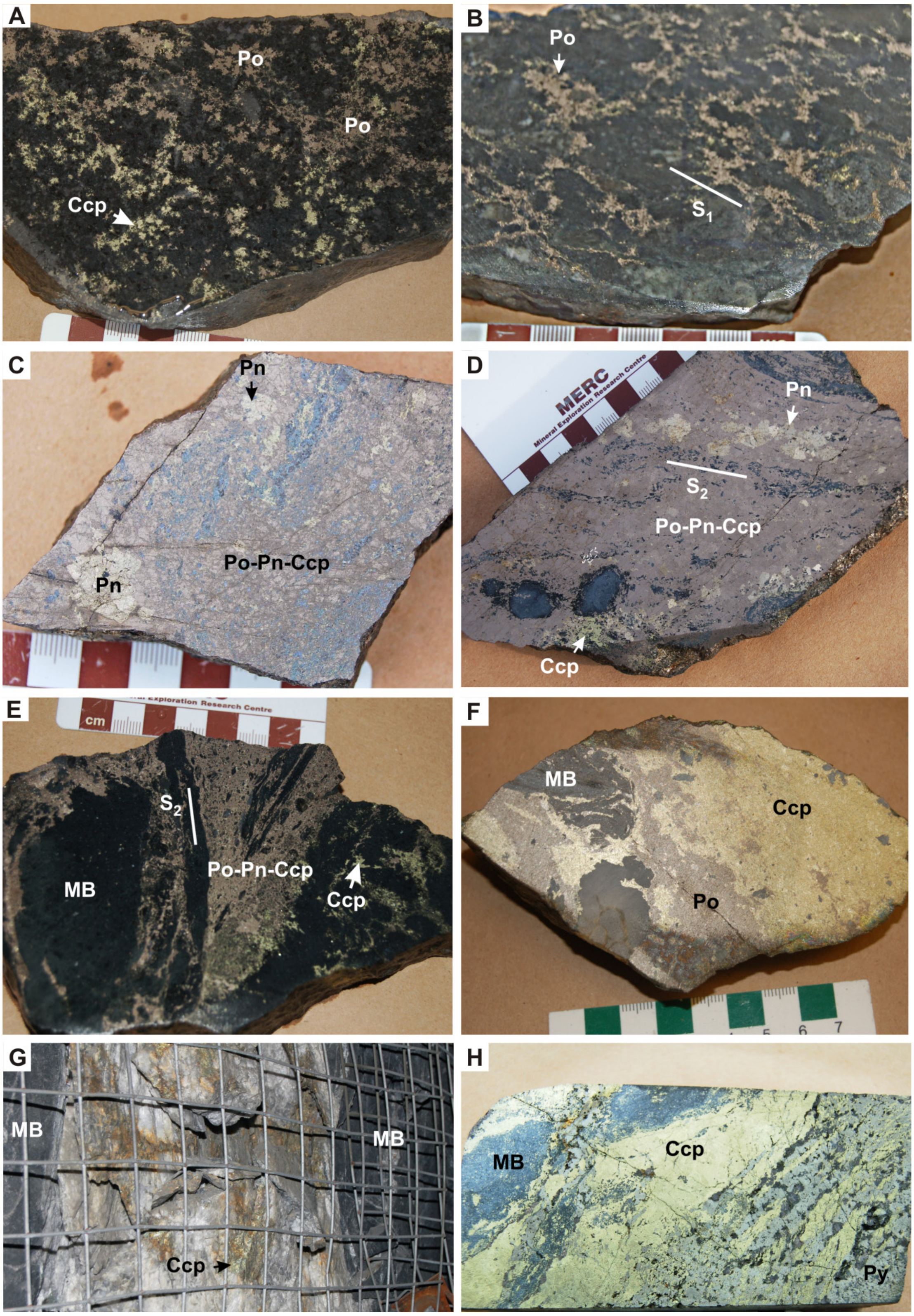
A
Po
Po
Ccp
B
Po
S_1
C
Pn
Pn
Po-Pn-Ccp
D
MERC
Mineral Exploration Research Centre
Pn
S_2
Po-Pn-Ccp
Ccp
E
Exploration Research Centre
cm
S_2
MB
Po-Pn-Ccp
Ccp
F
MB
Ccp
Po
5
6
7
G
MB
MB
Ccp
H
MB
Ccp
Py

Figure 4.5. (a) Polished slabs of representative samples of ore types from the #1 and #4 shear ore bodies at the Garson mine and the #600 ore body at the Garson Ramp mine. (a) undeformed disseminated sulfide mineralization from the Garson Ramp showing pyrrhotite-pentlandite-chalcopyrite blebs in Main Mass norite near the contact with Huronian metabasalt. (b) Deformed disseminated sulfide mineralization from the #4 shear zone showing pyrrhotite-pentlandite-chalcopyrite bands aligned parallel to S_1 in a sheared sliver of norite. (c) D_1 contact breccia ore from the #1 shear ore body showing large pentlandite grain in a matrix of pyrrhotite-rich Fe-Ni-Cu sulfides. (d) D_2 contact breccia ore from the #1 shear ore body showing pentlandite bands aligned parallel to S_2. (e) D_2 fault breccia ore from the #4 shear ore body showing loop pentlandite aligned parallel to S_2. (f) D_2 fault breccia ore from the #1 shear ore body showing chalcopyrite-rich segregations. (g) Subvertical shear quartz-chalcopyrite-pyrrhotite-pentlandite-sphalerite vein. (h) Chalcopyrite-rich footwall-type ore from the Garson ramp pyrite-rich bands aligned parallel to boudinaged metabasalt fragments. Po: pyrrhotite, Pn: pentlandite, Ccp: chalcopyrite, Py: pyrite; MB: metabasalt.

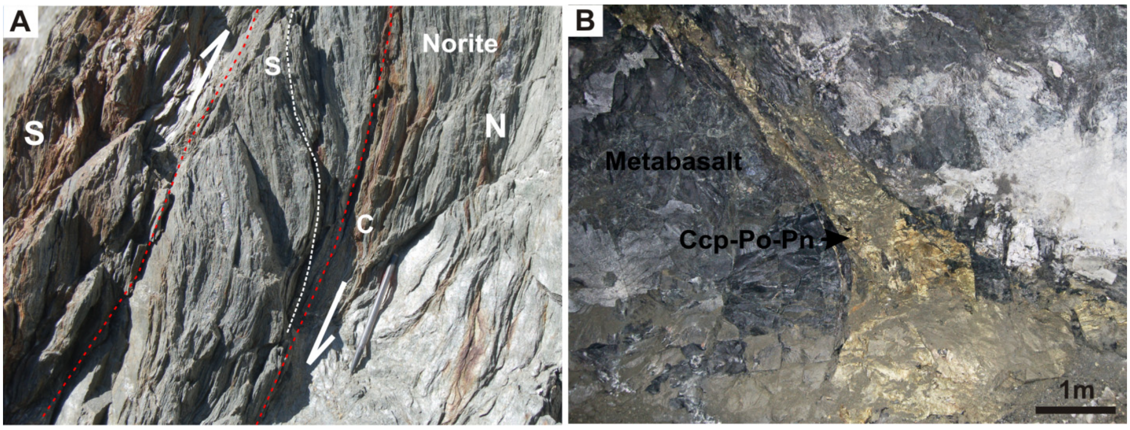

Figure 4.6. Garson Ramp mine photographs of (a) S-C-C′ fabrics indicating south-over-north reverse displacement in norite near the SIC/Huronian contact. (b) Moderately south-dipping tabular ore zone (#600 ore body).

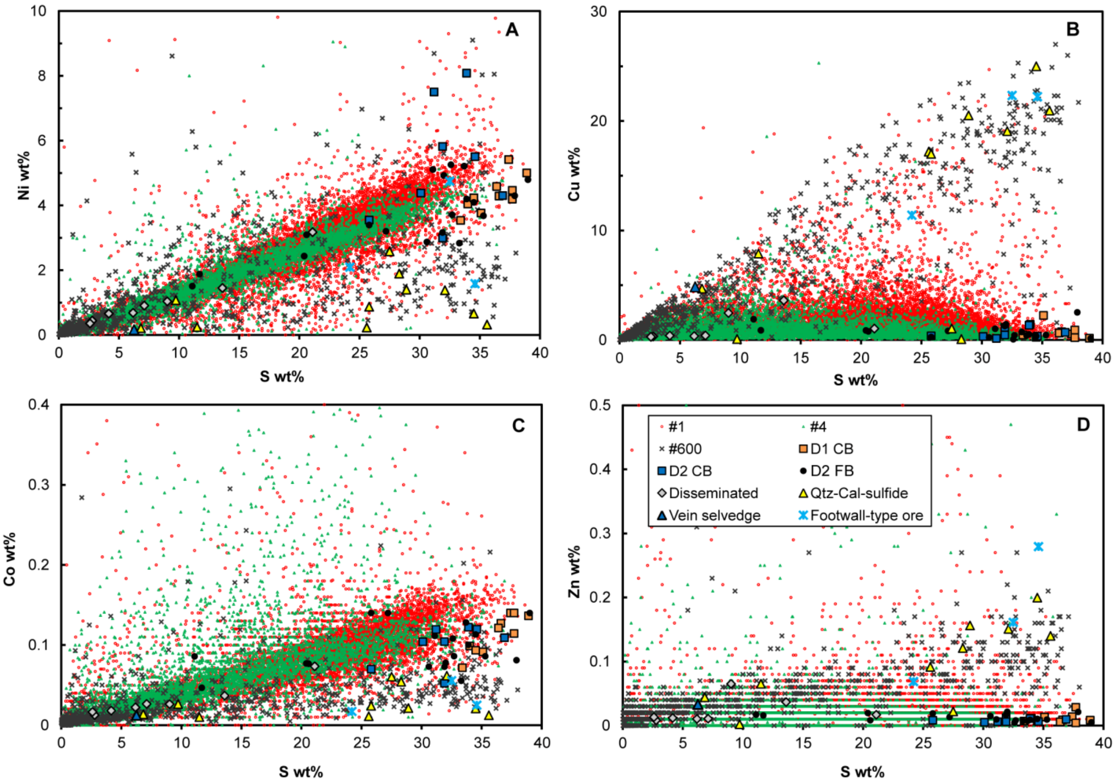

Figure 4.7. Ni, Cu, Co, and Zn *versus* S diagrams for collected samples of disseminated sulfides, D_1 and D_2 deformed contact breccia ore, D_2 fault breccia ore, quartz-calcite-sulfide veins, Garson Ramp footwall-type ore, as well as drill core assay data for the #1 and #4 shear ore bodies at the Garson Mine and #600 ore body at the Garson Ramp mine. #1, #4 and #600 represent #1 and #4 shear and #600 ore bodies. CB: contact breccia ore, FB: fault breccia ore, Qtz-cal: quartz-calcite.

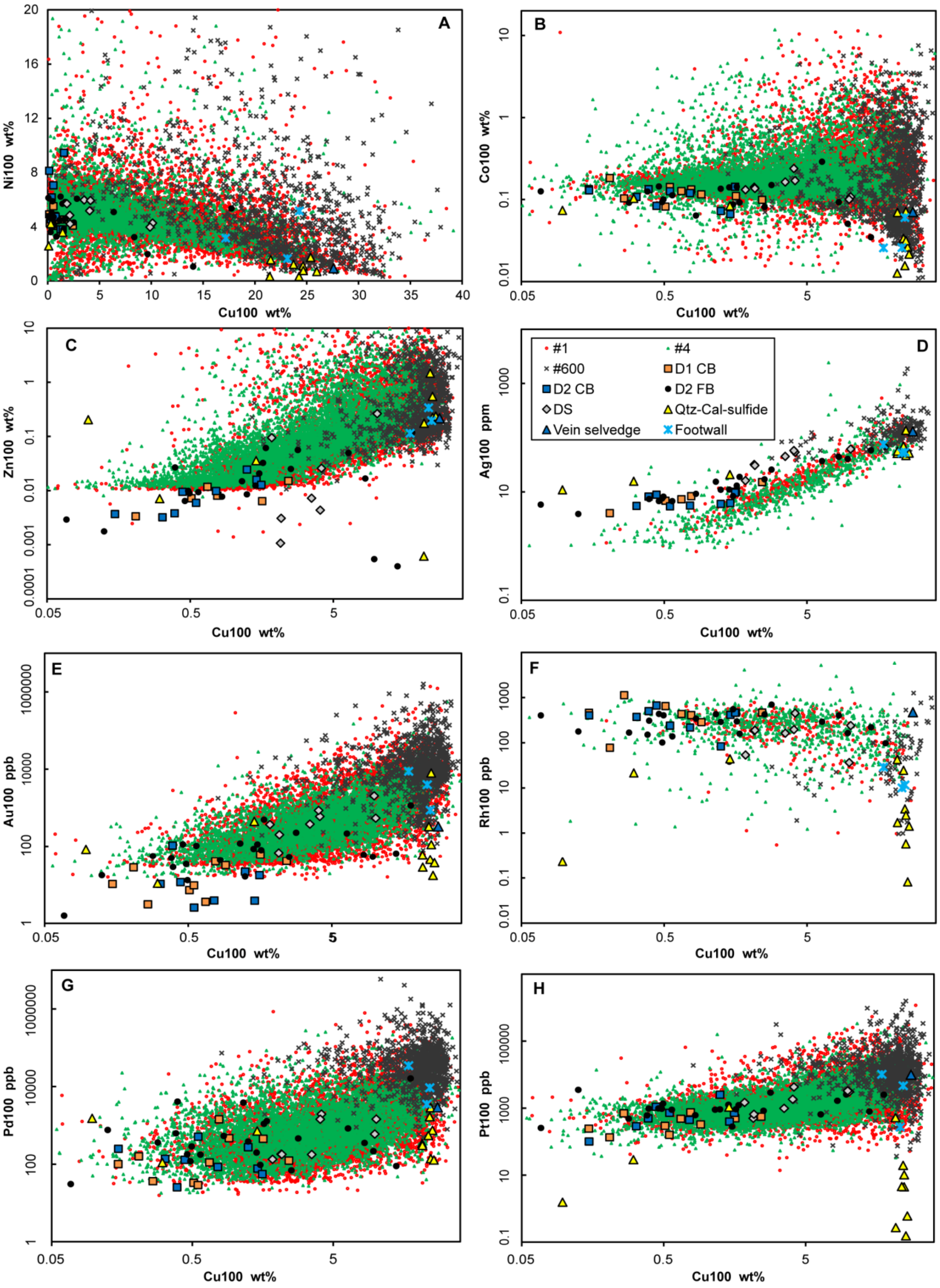

Figure 4.8. Binary plots of Ni, Co, Zn, Ag, Au, Rh, Pt, and Pt tenors *versus* Cu tenor for disseminated sulfides, D$_1$ and D$_2$ contact breccia ore, D$_2$ fault breccia ore, quartz-calcite-sulfide veins, footwall-type ore, and drill core assay data for the #1 and #4 shear, and

#600 ore bodies. #1, #4 and #600 represent #1 and #4 shear and #600 ore bodies. CB: contact breccia ore, FB: fault breccia ore, Qtz-cal: quartz-calcite, DS: disseminated sulfides.

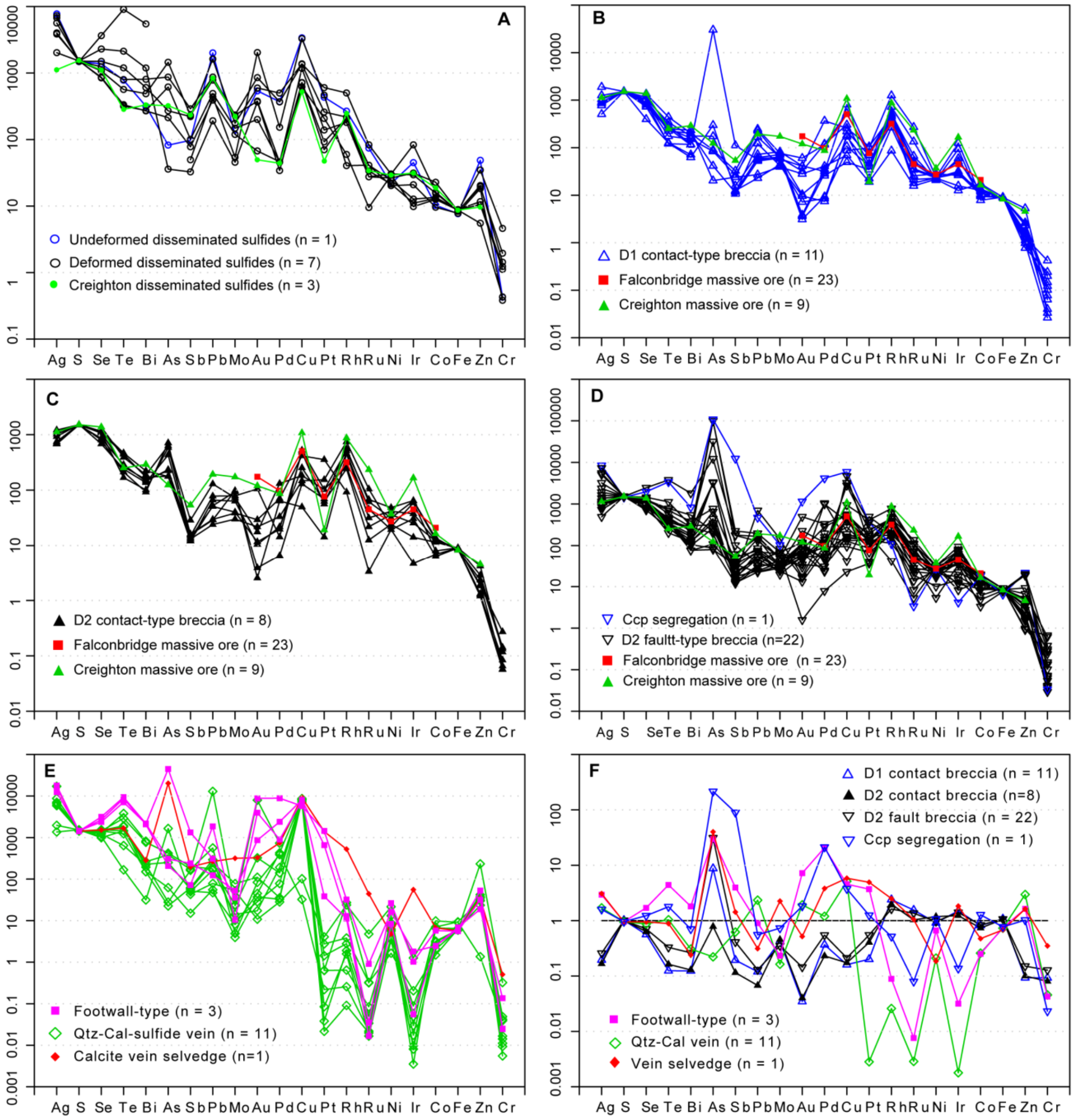

Figure 4.9. Mantle-normalized multi-element distribution patterns of (a) disseminated sulfides from the Creighton and Garson mines; (b)–(d) contact-type massive ore from the Falconbridge mine, contact-type massive ore from the Creighton mine, D_1 contact breccia ore from the Garson mine in (b), D_2 deformed contact breccia ore from the Garson Mine in (c) and (d); (e) Garson Ramp footwall-type ore, quartz-calcite-sulfide veins at the Garson Mine, and calcite vein selvedge at the Garson mine; (f) Multi-element diagram showing the distribution of elements for D_1 contact breccia ore, D_2 deformed contact breccia ore, and D_2 fault-type breccias ore at the Garson mine normalized to the average compositions of Garson disseminated sulfides. Qtz-cal: quartz-calcite.

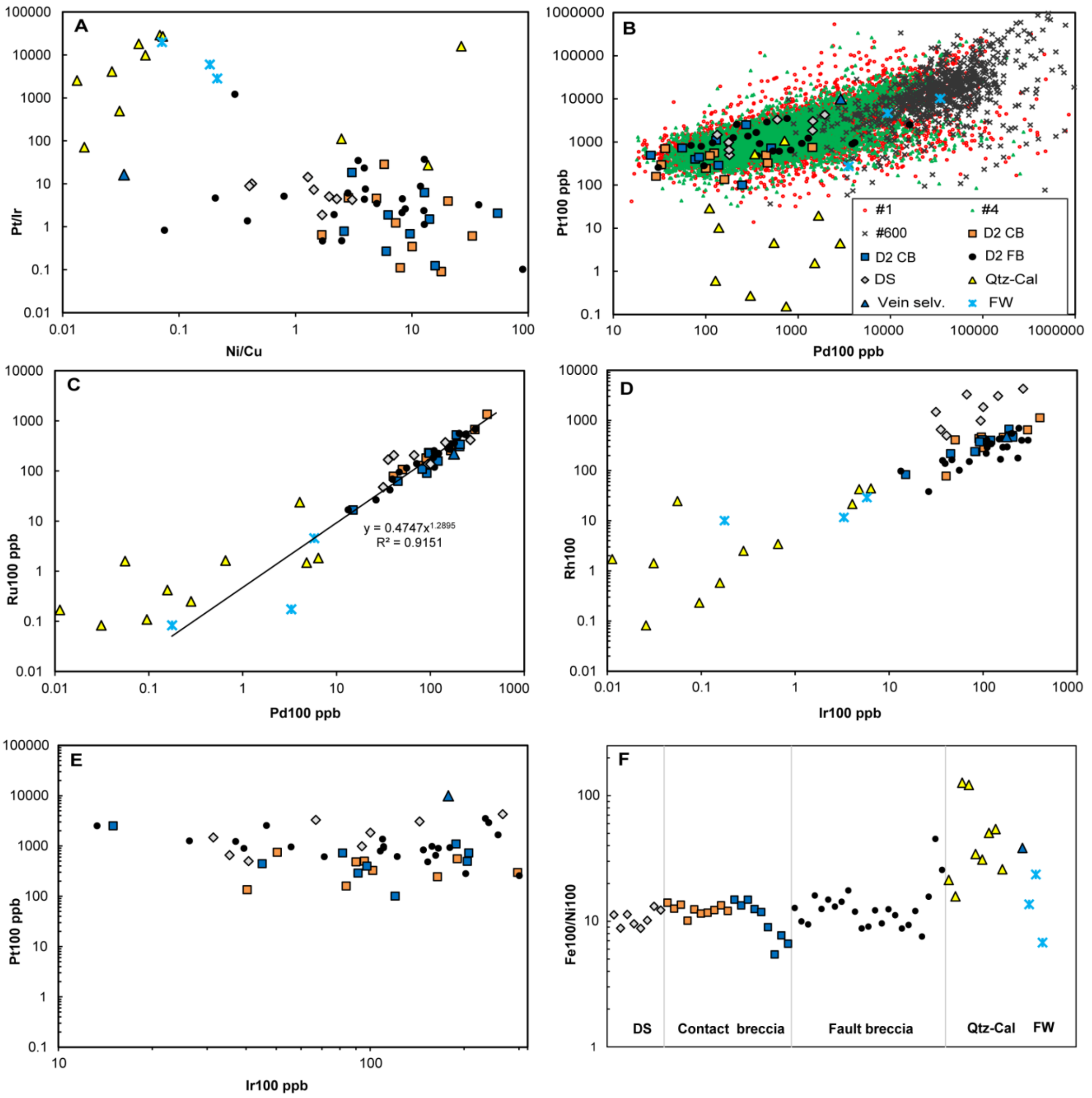

Figure 4.10. Plots of (a) Pd/Ir *versus* Ni/Cu, (b) Pt_{100} *versus* Pd_{100}, (c) Ru_{100} *versus* Ir_{100}, and (d) Rh_{100} *versus* Ir_{100}, (e) Pt_{100} *versus* Ir_{100}, (f) Fe/Ni ratios for Garson ores. #1, #4 and #600 represent #1 and #4 shear and #600 ore bodies. CB: contact breccia ore, FB: fault breccia ore, Qtz-cal: quartz-calcite, DS: disseminated sulfides, vein-selv: vein selvedge, FW: footwall mineralization.

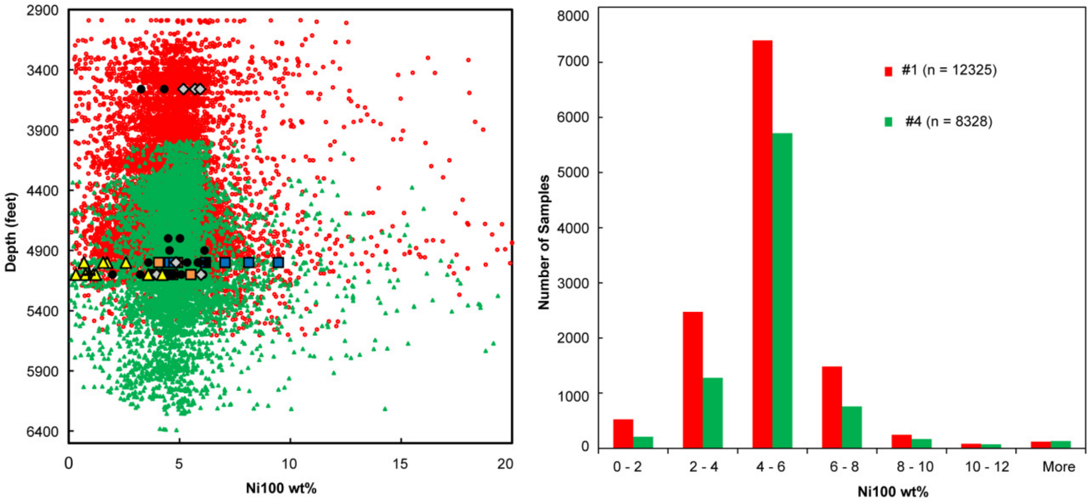

Figure 4.11. (a) Plot of Ni tenors against depth for the #1 and #4 shear ore bodies. (b) Histogram of Ni tenor for the #1 and #4 shear ore bodies.

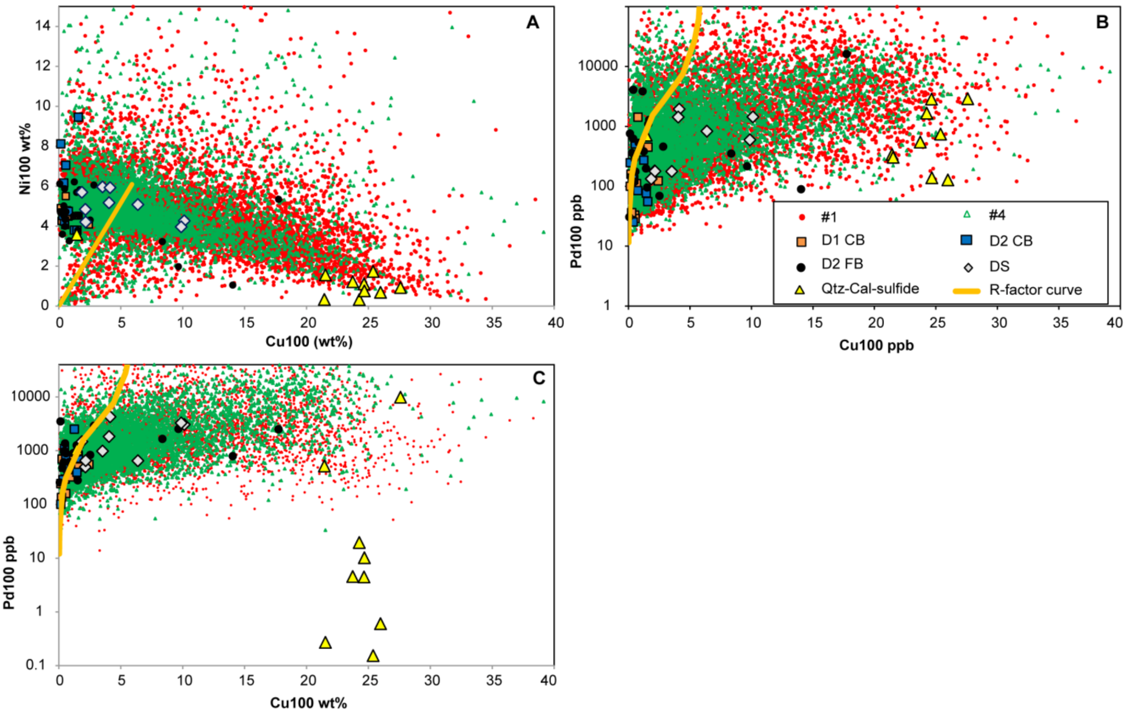

Figure 4.12. Plots of Ni, Rh, Pt, Pd, and Ir tenors *versus* Cu tenor for ores from the #1 and #4 shear and #600 ore bodies compared against models curves calculated for varying magma:suldfide ratios (R factors). #1, #4 and #600 represent #1 and #4 shear and #600 ore bodies. CB: contact breccia ore, FB: fault breccia ore, Qtz-cal: quartz-calcite, DS: disseminated sulfides.

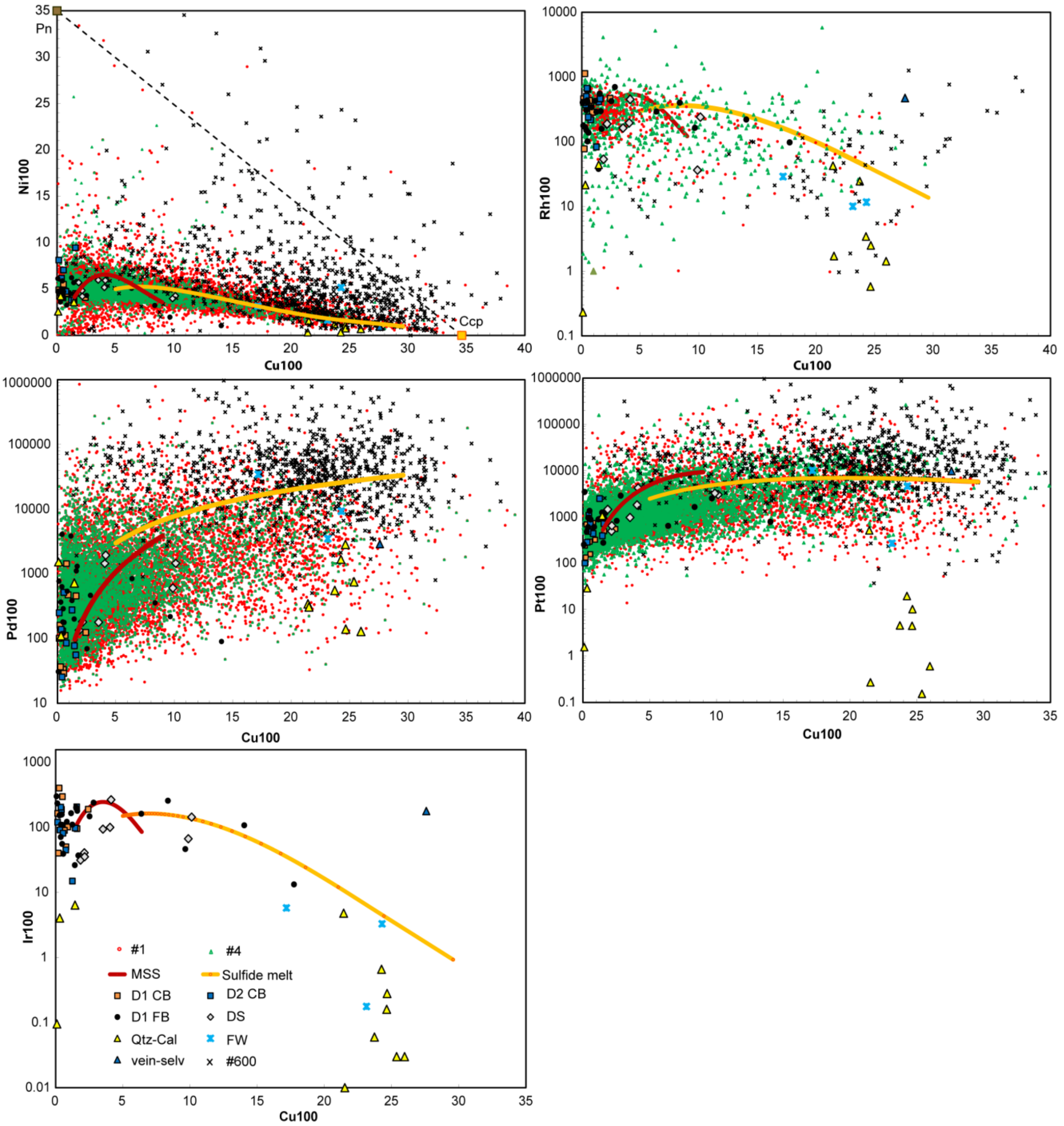

Figure 4.13. Plots of Ni, Rh, Pt, Pd and Ir tenors *versus* Cu tenor for ores from the #1 and #4 shear and #600 ore bodies compared against model curves calculated for fractionation of *mss* (method described in text). #1, #4 and #600 represent #1 and #4 shear and #600 ore bodies. CB: contact breccia ore, FB: fault breccia ore, Qtz-cal: quartz-calcite, DS: disseminated sulfides, FW: footwall mineralization.

Chapter 5: Conclusions

The Garson magmatic Ni-Cu-PGE deposit is a deformed contact-type deposit. It is located along the SE limb of the 1850 Ma SIC (Krogh et al, 1984) at the contact between the Main Mass SIC norite and underlying Paleoproterozoic metabasalt and metasedimentary rocks of the Huronian Supergroup. It comprises four main ore bodies that are coincident with steeply south-dipping shear zones and splays that formed and were reactivated during two major deformation events, D_1 and D_2. The shear zones are characterized by a steeply south-dipping S_1 schistose foliation containing a strong down-dip L_1 mineral lineation defined by ferrotschermakite and green magnesiohornblende in metabasalt and norite, respectively. The amphiboles coexist with oligoclase, ilmenite and quartz, indicating syn-D_1 amphibolite facies metamorphism. In addition, metabasalt locally contains garnet. The average T method (Powell and Holland, 1994) and the Fe-Mg exchange geothermometer (Ravna, 2000) yielded syn-D_1 metamorphic temperatures ranging from ~550°C to 590°C for coexisting garnet-amphibole pairs in metabasalt from the Garson shear zones. D_2 is characterized by a S_2 schistose foliation, containing steeply south-plunging, down-dip, ductile slickenlines and a parallel L_2 chlorite mineral lineation. S_2 and L_2 are coplanar and colinear with S_1 and L_1, respectively. Chlorite coexists with epidote, titanite, calcite and quartz, suggesting syn-D_2 greenschist metamorphic conditions. Dynamic recrystallization of quartz in syn-D_2 shear quartz veins by subgrain rotation and grain boundary migration, suggests a minimum temperature of approximately 400°C (e.g., Hirth and Tullis, 1992; Stipp et al., 2002, 2010) during D_2.

The Garson shear zones formed as layer-parallel, north-dipping D_1 thrusts in response to flexural slip during buckling of the SIC (Mukwakwami et al., 2012). The SIC norite, the underlying Huronian rocks, and the ore zones were imbricated along these thrusts. Together with the underlying basement rocks, the thrusts were overturned as the SE limb of the SIC was steepened and overturned in the vicinity of the Garson mine. The D_1 thrusts were then reactivated as steeply south-dipping reverse shear zones during D_2. The shear zones are cut by unstrained olivine diabase dikes of the ~1240 Ma Sudbury swarm (Krogh et al., 1987; Dudás et al., 1994). Syn-D_2 metamorphic titanite grains yielded ID-TIMS U-Pb ages between ca. 1849 Ma, which suggest that D_1 and D_2 part of a single progressive Penokean deformation. The D_1 Garson shear zones were coeval with the moderately SE-dipping reverse South Range Shear Zones, which formed due to localization of folding-induced strain near the hinge zone during progressive folding of the SIC during the 1.9-1.8 Ga Penokean Orogeny (Cowan and Schwerdtner, 1994; Riller et al., 2010). This questions the significance of other younger deformation events, such as the 1.7-1.6 Ga Mazatzal-Labradorian event (Bailey et al., 2004; Piercey et al., 2007), ca. 1.4 Ga Chieflakian event (Fueten and Redmond, 1997; Szentpéteri, 2009) and ca. 1.3-1.0 Ga Grenville Orogeny (Brocoum and Dalaziel, 1974; Rivers, 1997), in the deformation of the Sudbury impact structure.

The ore shoots have a down-dip southerly plunge parallel to the colinear L_1 and L_2 lineations, suggesting structural controls on the geometry of the ore bodies. The ore bodies consist predominantly of breccia ore, minor disseminated sulfides and quartz-calcite-sulfide veins. Undeformed disseminated sulfide mineralization is characterized by polycrystalline sulfides filling interstices between silicate minerals, whereas the deformed ore has pyrrhotite-rich bands that are parallel to S_1 or S_2. The disseminated sulfides consist predominantly of pyrrhotite (80-90%), pentlandite (5-15%), and chalcopyrite (5-10%) in association with minor magnetite (<5%), trace gersdorffite, cobaltite and niccolite, and rare sperrylite (Gammell et al., 2004). The breccia ores are subdivided into contact and fault breccia ores. Contact breccia ore occurs in thicker portions of the ore zones, and it contains fragments of Sublayer norite, indicating that it formed in embayments at the base of the SIC. In contrast, the fault breccia ore occurs as narrow, tabular ore bodies that are devoid of Sublayer norite fragments. Pyrrhotite and chalcopyrite occupy fold hinges and piercement structures that truncate S_1 and S_2, suggesting that these sulfides were ductile during D_1 and D_2. The absence of Sublayer norite fragments, the strong ductility of the sulfides, and the tabular shape of the ore bodies, suggest that the fault breccia ore formed by ductile plastic flow and injection of the sulfides into shear zones.

The mineralogy of the breccia ores is similar to that of the disseminated sulfides, but the breccia ores are locally rich in chalcopyrite. Silicate rock fragments in the breccia ores define pervasive foliations and are highly stretched parallel to L_1 and L_2, indicating that the ore zones are zones of high strain. Although the silicate rock fragments are strongly deformed, pyrrhotite in breccia ores that were deformed during D_1 and to a greater extent during D_2 generally have polygonal shapes due to recrystallization of the grains either during or immediately after D_1 and D_2. Other breccia ores that were deformed during D_2 have a pyrrhotite foliation defined by elongate pyrrhotite grains. Pentlandite was exsolved along pyrrhotite grain boundaries and therefore occurs as S_2-parallel layers in deformed ore with elongate pyrrhotite grains and as variably-oriented loops in deformed ore with polygonal pyrrhotite grains. These observations suggest that the ore zones deformed as a *mss* during D_1 and D_2 and exsolved pentlandite after cessation of D_1 and D_2. Because D_1 occurred after the deposition of the Whitewater Group and cooling of the SIC, the ore reverted to a *mss* with increasing temperatures during D_1.

When the Garson bulk ore composition is projected on to the Fe-Ni-S ternary diagram, it falls within the *mss* field at 500°C, suggesting that the Garson ores reverted to and were deformed as a homogeneous *mss* at syn-D_1 metamorphic temperatures of 550 to 600°C, in agreement with the textural observations described above. The restricted range of Ni tenors (4 to 8 wt%) and Fe/Ni ratios (9-14) in the breccia ores at Garson are also consistent with ores that are deformed as a homogeneous *mss* because ores that are deformed as pyrrhotite-pentlandite-chalcopyrite aggregates result in segregation of the more ductile pyrrhotite from pentlandite, which in turn leads to large-scale variations in Fe/Ni ratios and Ni tenors within an ore shoot (Barrett et al., 1977; McQueen, 1987).

As the mobilized breccia ores in the main ore bodies consist predominantly of pyrrhotite-pentlandite-chalcopyrite, which melts at temperatures exceeding ~900°C (Kullerud et al., 1969), mobilization of the ores in the Garson shear zones as a partial sulfide melt is unlikely at syn-D_1 mid-amphibolite facies metamorphic temperatures recorded at Garson (~550-600°C). Quartz-calcite-sulfide veins consist of chalcopyrite and minor pyrrhotite and pentlandite, suggesting that the deposit was, to some degree, affected by hydrothermal fluids. The veins have very low Ir concentrations, very high Pd/Ir ratios, consistent with their mobilization by hydrothermal fluids, whereas the disseminated sulfides and breccia ores have low Pd/Ir ratios, suggesting that they are of magmatic origin (e.g., Keays et al., 1982; Lesher and Keays, 1984). The disseminated sulfides and breccia ores have multi-element chalcophile patterns that are similar to undeformed disseminated sulfides and contact massive ores, respectively, at Creighton mine, further suggesting a magmatic origin for these ores. Footwall-type mineralization is observed at the Garson Ramp mine, which is located ~500m SW within the basement footwall rocks of the Garson Mine. It consists of chalcopyrite, pyrrhotite and pentlandite, with secondary pyrite and marcasite, and minor violarite, sphalerite, millerite and cubanite (Krstic and Van den Berg, 2005). It has high Pd/Ir ratios, similar to the hydrothermal veins, but it is strongly enriched in Pt and there is a strong positive correlation between Pt_{100} and Pd_{100}. In contrast, the quartz-calcite-sulfide veins are strongly depleted in Pt, and Pt is decoupled from Pd. This suggests that the footwall-type mineralization and breccias ore are magmatic in origin and that they were not significantly modified by the hydrothermal mobilization that produced the quartz-calcite-sulfide veins.

Because R-factor and *mss* fractionation typically control the variations in metal tenors within magmatic ore bodies (e.g., Campbell and Naldrett, 1979; Naldrett, 2004), the significance of these processes at Garson mine were evaluated. The disseminated sulfides typically have a higher R-factor than massive ore in the same deposit because the disseminated sulfides interacted and equilibrated with larger volumes of silicate melt (Campbell and Naldrett, 1979; Lesher and Campbell, 1993). However, disseminated sulfides at Garson have similar Ni tenors as the breccia ores. This, together with Rh-Ru-Ir enrichment in the breccia ores relative to the disseminated sulfides suggest that the variations in metal tenors at Garson ores are likely not controlled by R-factor. In addition, the observed trends are not in agreement with the simulated trends on plots of Pd_{100}, Pt_{100}, and Ni_{100} *versus* Cu_{100}, further suggesting that the R-factor does not control the metal tenors.

When normalized to the average Garson disseminated sulfides, the breccia ores are enriched in Ir-Ru-Rh and are depleted in Cu-Pd-Pt-Au, whereas Ir-Ru-Rh and Cu-Pd-Pt-Au are depleted and enriched, respectively, in the footwall-type mineralization. These depletions and enrichments at are attributed to *mss* fractionation from an immiscible sulfide melt to form Cu-Pd-Pt-Au-poor contact-type cumulate ore, and Cu-Pd-Pt-Au-rich footwall-type ore (e.g., Naldrett et al., 1982, 1999; Li et al., 1992; Barnes and Lightfoot, 2005; Dare et al., 2010). On plots of Ni_{100}, Rh_{100}, Ir_{100}, Pt_{100} and Pd_{100} *versus* Cu_{100}, breccia ores and footwall-type mineralization fall along *mss* fractionation and sulfide melt model curves, further suggesting that these two ore types are related by *mss* fractionation. Thus the breccia ores at Garson are typical *mss* cumulates that were mobilized by plastic ductile flow of the sulfides, and their bulk geochemistry was not significantly affected by hydrothermal fluids, metamorphism and deformation.

References

Ames D. E., 1999. Geology and regional hydrothermal alteration of the crater-fill Onaping Formation: Association with Zn-Pb-Cu mineralization. Unpublished PhD. Thesis, Carleton University, Canada, 460 p.

Ames, D.E. and Gibson, H.L., 1995. Controls on and geological setting of regional hydrothermal alteration within the Onaping Formation, footwall to the Errington and Vermilion base metal deposits, Sudbury structure, Ontario. In: Current Research, Geological Survey of Canada, 161–173.

Ames, D.E. and Farrow, C.E.G., 2007. Metallogeny of the Sudbury mining camp, Ontario. In: Goodfellow, W.D. (Ed.), Mineral Deposits of Canada. A Synthesis of Major Deposit-Types, District Metallogeny, the Evolution of Geological Provinces, and Exploration Methods. Geological Association of Canada, Mineral Deposits Division Special Publication 5, pp. 329–350.

Ames, D.E., Golightly, J.P., Lightfoot, P.C. and Gibson, H.L., 2002. Vitric compositions in the Onaping Formation and their relationship to the Sudbury Igneous Complex, Sudbury structure. Economic Geology 97, 1541–1562.

Ames, D.E., Davidson, A., Buckle, J.L. and Card, K.D. 2005. Geology, Sudbury bedrock compilation, Ontario. Geological Survey of Canada, Open File 4570, scale 1:50 000.

Ames, D.E., Jonasson, I.R., Gibson, H.L. and Pope, K.O., 2006. Impact-generated hydrothermal system-constraints from the large Paleoproterozoic Sudbury crater, Canada. In: Cockell, C., Gilmour, I., Koeberl, C. (Eds.), Biological Processes Associated with Impact Events: Impact Studies. Berlin-Heidelberg, Springer-Verlag, pp. 55–100.

Anderson, E.M., 1905. The dynamics of faulting. Edinburgh Geological Society Transactions 8, 393–402.

Andrews, A.J., Owsiacki, L., Kerrich, R. and Strong, D.F., 1986. The silver deposits at Cobalt and Gowganda, Ontario: I. Geology, petrography and whole-rock geochemistry. Canadian Journal of Earth Sciences 23, 1480–1506.

Aniol., G.Z. and Brown, D.L., 1979. Garson mine ore body characteristics. Unpublished report for Vale., 69 pp.

Atkinson, B. K., 1975. Experimental deformation of polycrystalline pyrite: effects of temperature, confining pressure, strain rate, and porosity. Economic Geology 70, 47–457.

Baile, R.H. and Reid, D.L., 2005. Ore textures and possible sulphide partial melting at Broken Hill, Aggeneys, South Africa I: Petrography. South African Journal of Geology 108, 51–70.

Bailey, J., Lafrance, B., McDonald, A.M., Fedorowich, J.S., Kamo, S. and Archibald, D.A., 2004. Mazatzal–Labradorian-age (1. 7–1.6 Ga) ductile deformation of the South

Range Sudbury impact structure at the Thayer Lindsley mine, Ontario. Canadian Journal of Earth Sciences 41, 1491–1505.

Bailey, J., McDonald, A.M., Lafrance, B. and Fedorowich, J.S., 2006. Variations in Ni content in sheared magmatic sulfide ore at the Thayer Lindsley mine, Sudbury, Ontario. The Canadian Mineralogist 44, 1063–1077.

Ballhaus C., Tredoux M. and Späth A., 2001. Phase relations in the Fe–Ni–Cu–PGE–S system at magmatic temperature and application to massive sulphide ores of the Sudbury Igneous Complex. Journal of Petrology 42, 1911–1926.

Barnes, S.J., 2004. Komatiites and nickel sulfide ores of the Black Swan area, Yilgarn Craton, Western Australia. 4. Platinum group element distribution in the ores, and genetic implications. Mineralium Deposita 39, 752–765.

Barnes, S.J. and Miller, J.M., 2010. Platinum-group elements and gold in highly deformed and metamorphosed komatiite-hosted nickel deposits of the Lake Johnston greenstone belt, Yilgarn Craton. 11th International Platinum Symposium, Sudbury.

Barnes, S.J. and Liu, W., 2012. Pt and Pd mobility in hydrothermal fluids: Evidence from komatiites and from thermodynamic modelling. Ore Geology Reviews 44, 49-58.

Barnes, S-J., Makovicky, E., Makovicky, M., Rosehansen, J. and Karupmoller S., 1997. Partition coefficients for Ni, Cu, Pd, Pt, Rh, and Ir between monosulfide solid solution and sulfide liquid and the formation of compositionally zoned Ni–Cu sulfide bodies by fractional crystallization of sulfide liquid. Canadian Journal of Earth Sciences 3, 366–374.

Barnes, S-J. and Lightfoot, P., 2005. Formation of magmatic nickel-sulfide ore deposits and processses affecting their copper and platinum-group element contents. In: J.W. Hedenquist, J.F.H. Thompson, R.J. Goldfarb, J.P. Richards, (Eds.), Economic Geology 100th Anniversary Volume, pp. 179–213.

Barrett, F.M., Binns, R.A., Groves, D.I., Marston, R.J. and McQueen, K.G., 1977. Structural history and metamorphic modification of Archean volcanic-type nickel deposits, Yilgarn Block, Western Australia. Economic Geology 72, 1195–1223.

Bavinton, O.A. and Keays, R.R., 1978. Precious metal values from interflow sedimentary rocks from the komatiite sequence at Kambalda, Western Australia. Geochimica et Cosmochimica Acta 42, 1151–1163.

Belkabir, A., Hubert, C., 1995. Geology and structure of a sulfide-rich gold deposit: An example from the Mouska Gold Mine, Bousquet District, Canada. Economic Geology 90, 1064–1079.

Bell, T.H., 1986. Foliation development and refraction in metamorphic rocks: reaction of earlier foliations and decrenulation due to shifting patterns of deformation partitioning. Journal of Metamorphic Geology 4, 421–444.

Bethune, K.M., 1997. The Sudbury dyke swarm and its bearing on the tectonic development of the Grenville Front, Ontario, Canada. Precambrian Research 85, 117–146.

Binney, W.P., Poulin, R.Y., Sweeny, J.M. and Halladay, S.H., 1994. The Lindsley Ni-Cu-PGE deposit and its geological setting. In: Lightfoot, P.C., Naldrett, A. (Eds.), Proceedings of the Sudbury-Noril'sk Symposium. Ontario Geological Survey Special Volume 5, pp. 91–103.

Bleeker, W. 1990. Evolution of the Thompson nickel belt and its nickel deposits, Manitoba, Canada. Unpublished PhD. thesis, University of New Brunswick, Canada, 400 p.

Blonde, J., 1996. Petrology and metamorphism of Nipissing diabase of May Township, Ontario. Unpublished M.Sc. thesis, Carleton University, 160 p.

Boast, M. and Spray, J.G., 2006. Superimposition of a thrust-transfer fault system on a large impact structure: Implications for Ni-Cu-PGE exploration at Sudbury. Economic Geology 101, 1583–1594.

Boerner, D.E. and Milkereit, B., 1999. Structural evolution of the Sudbury impact structure in the light of seismic reflection data. In: Dressler, B.O. and Sharpton, V.L. (Eds.), Large Meteorite Impact and Planetary Evolution. Boulder, Colorado, Geological Society of America Special Paper 339, pp. 419–429.

Bowring, S.A. and Karlstrom. K.E., 1990. Growth, stabilization, and reactivation of Proterozoic lithosphere in the southwestern United States. Geology 18, 1203–1206.

Brocoum, S.J. and Dalziel, I.W.D., 1974. The Sudbury Basin, the Southern Province, the Grenville Front, and the Penokean Orogeny. Geological Society of America Bulletin 85, 1571-1580.

Buchan, K.L. and Ernst, R.E., 1993. Onaping fault system: age constraints on deformation of the Kapuskasing structural zone and units underlying the Sudbury structure. Canadian Journal of Earth Sciences 31, 1197-1205.

Cabri, L., 1973. New data on phase relations in the Cu-Fe-S system. Economic Geology 6, 443-454.

Campbell, I.H. and Naldrett A.J., 1979. The influence of silicate:sulfide ratios on the geochemistry of magmatic sulfides. Economic Geology 74, 503-1505.

Card, K.D., 1978. Geology of the Sudbury-Manitoulin Area, Districts of Sudbury and Manitoulin. Ontario Geological Survey, Report 166, 238 p.

Card, K.D., Church, W.R., Franklin, J.M., Robertson, J.A. West, G.F. and Young, G.M., 1972. The Southern Province. In: Price, R.A. and Douglas, R.J.W. (Eds.), Variations in Tectonic Styles in Canada. Geological Association of Canada Special Paper 11, pp. 335-580.

Card, K.D., Gupta, V.K., McGrath, P.H. and Grant, F.S., 1984. The Sudbury structure: Its regional geological and geophysical setting. In: Pye, E.G., Naldtrett, A.J., Giblin, P.E.

(Eds.), The Geology and Ore Deposits of the Sudbury Structure. Ontario Geological Survey Special Volume 1, pp. 25–44.

Carr, S.D., Easton, R.M., Jamieson, R.A. and Culshaw, N.G., 2000. Geologic transect across the Grenville orogen of Ontario and New York. Canadian Journal of Earth Sciences 37, 193-216.

Chivas, A.R., 1981. Geochemical evidence for magmatic fluids in porphyry copper mineralization Part I. Mafic silicates from the Koloula Igneous Complex. Contributions to Mineralogy and Petrology 78, 389-403.

Clark, B.R. and Kelly, W.C., 1973. Sulfide deformation: I. Experimental deformation of pyrrhotite and sphalerite to 2000 bars and 500°C. Economic Geology 68, 332-352.

Coats, C.J.A. and Snajdr, P., 1984: Ore deposits of the North Range, Onaping-Levack Area, Sudbury. In: Pye, E.G., Naldtrett A.J. and Giblin, P.E. (Eds.), The Geology and Ore Deposits of the Sudbury Structure. Ontario Geological Survey Special Volume 1, pp. 327-346.

Cochrane, L.B., 1991. Analysis of the structural and tectonic environments associated with rock-mass failures in the mines of the Sudbury District. Unpublished Ph.D. thesis, Queen's University, Canada, 264 p.

Condit, R. H., Hobbins, R. R. and Birchenall, C. E., 1974. Self-diffusion of iron and sulfur in ferrous sulfide. Oxidation of Metals 8, 409-455.

Cook, N.J., Halls, C. and Boyle, A.P., 1993. Deformation and metamorphism of massive sulfides at Sulitjelma, Norway. Mineralogical Magazine 57, 67-81.

Cook, N.J., Halls, C. and Boyle, A.P., 1993. Deformation and metamorphism of massive sulfides at Sulitjelma, Norway. Mineralogical Magazine 57, 67-81.

Corfu, F. and Andrews, A., 1986. A U–Pb age for mineralized Nipissing diabase, Gowganda, Ontario. Canadian Journal of Earth Sciences 23, 107–112.

Corfu, F. and Stone, D., 1998. The significance of titanite and apatite U–Pb ages: constraints for the post-magmatic thermal–hydrothermal evolution of a batholithic complex, Berens River area, northwestern Superior Province, Canada. Geochimica et Cosmochimica Acta 62, 2979–2995.

Corfu, F. and Easton, R.M., 2000. U-Pb evidence for polymetamorphic history of Huronian rocks within the Grenville front tectonic zone east of Sudbury, Ontario, Canada. Chemical Geology 172, 149-171.

Cowan, E.J. and Schwerdtner, W.M., 1994. Fold origin of the Sudbury basin. In: Lightfoot, P.C., Naldrett, A. (Eds.), Proceedings of the Sudbury-Noril'sk Symposium. Ontario Geological Survey Special Volume 5, pp. 45–55.

Cowan, E.J., Riller, U. and Schwerdtner, W.M., 1999. Emplacement geometry of the Sudbury Igneous Complex: Structural examination of a proposed impact melt-sheet. In: Dressler, B.O. and Sharpton, V.L. (Eds.), Large Meteorite Impacts and Planetary

Evolution II. Boulder, Colorado, Geological Society of America Special Paper 339, pp. 399–418.

Cowden, A. and Archibald, N.J., 1987. Massive-sulfide fabrics at Kambalda and their relevance to theinferred stability of monosulfide solid-solution. Canadian Mineralogist 25, 37–50.

Cox, S.F., 1987. Flow mechanisms in sulphide minerals. Ore Geology Reviews 2, 133-171. In Marshall, B., Gilligan, L.B. (Eds.), Mechanical and Chemical (Re)mobilization of Metalliferous Mineralization. Ore Geology Reviews 2, pp. 269-286.

Cox, S.F. and Etheridge, M.A., 1984. Deformation microfabric development in chalcopyrite in fault zones, Mt. Lyell, Tasmania. Journal of Structural Geology 6, 167–182.

Craig, J.R., 1973. Pyrite·pentlandite assemblages and other low temperature relations in the Fe-Ni-S system. American Journal of Mineralogy 273–A, 496–510.

Craig, J.R. and Kullerud, G., 1969. Phase relations in the Cu-Fe-Ni-S system and their application to magmatic ore Deposits. In: Wilson, H.D.B. (Ed), Magmatic Ore Deposits; a Symposium. Economic Geology Monographs 4, pp. 344-358.

Daniel, C.G., Hollister, L.S., Parrish, R.R. and Grujic, D., 2003. Exhumation of the main Central Thrust from lower crustal depths, eastern Bhutan Himalaya. Journal of Metamorphic Petrology 21, 317–334.

Dare, S.A.S., Barnes, S-J. and Prichard, H.M., 2010. The distribution of platinum group elements (PGE) and other chalcophile elements among sulfides from the Creighton Ni–Cu–PGE sulfide deposit, Sudbury, Canada, and the origin of palladium in pentlandite. Economic Geology 45, 765–793.

Davidson, A. and van Breemen, O., 1994. U-Pb ages of granites near the Grenville Front, Ontario. In: Radiogenic age and isotopic studies. Geological Survey of Canada Current Research 1994–F, Report 8, 107–114.

Davidson, A., van Breemen, O. and Sullivan, R.W., 1992. Circa 1.75 Ga ages for plutonic rocks from the Southern Province and adjacent Grenville Province: what is the expression of the Penokean Orogeny? In: Radiogenic age and isotopic studies, Report 6. Geological Survey of Canada Paper 92–2, 107–118.

Davidson, S., 1948. Falconbridge mine. In: Structural geology of Canadian ore deposits. Montreal, Canadian Institute of Mining and Metallurgy, pp. 618–626.

Davis, B.K and Forde, A., 1994. Regional slaty cleavage formation and fold axis rotation by re-use and reactivation of pre-existing foliations: the Fiery Creek Slate Belt, North Queensland. Tectonophysics 230, 161–179.

Davis, D.W., 2008. Sub-million-year age resolution of Precambrian igneous events by thermal extraction–thermal ionization mass spectrometer Pb dating of zircon: Application to crystallization of the Sudbury impact melt sheet. Geology 36, 383–386.

Davis, G.C., 1984. Little Stobie mine: A South Range contact deposit. In: Pye, E.G., Naldtrett A.J. and Giblin, P.E. (Eds.), The Geology and Ore Deposits of the Sudbury Structure. Ontario Geological Survey Special Volume 1, pp. 361–369.

Davis, T.P., 2005. Mine-scale structural controls on the Mount Isa Zn-Pb-Ag and Cu orebodies. Economic Geology 99, 543–559.

Davis, W.J., McNicoll, V.J., Bellerive, D.L., Santowski, K. and Scott, D.J., 1997. Modified chemical procedures for the extraction and purification of U from titanite, allanite and rutile in the Geochronology Laboratory, Geological Survey of Canada. In: Radiogenic Age and Isotopic Studies: Report 9. Geological Survey of Canada, Current Research 1997-F, pp. 33–35.

Dickin, A.P. and McNutt, R.H., 1989. Nd model age mapping of the southeast margin of the Archean foreland in the Grenville province of Ontario. Geology 17, 299–302.

Diener, J.F.A., Powell, R., White, R.W. and Holland, T.J.B., 2007. A new thermodynamic model for clino- and orthoamphiboles in Na_2O-CaO-FeO-MgO-Al_2O_3-SiO_2–H_2O-O. Journal of Metamorphic Geology 25, 631–656.

Dressler, B.O., 1984. General geology of the Sudbury area. In: Pye, E.G., Naldtrett A.J. and Giblin, P.E. (Eds.), The Geology and Ore Deposits of the Sudbury Structure. Ontario Geological Survey Special Volume 1, pp. 57–82.

Dressler, B.O., Gupta, V.K. and Muir, T.L., 1991. The Sudbury Structure. In: Thurston, P.C., Williams, H.R., Sutcliffe R.H., and Stott G.M. (Eds.), Geology of Ontario. Ontario Geological Survey Special Volume 4, Part l, pp. 593–625.

Dudás, F.Ö., Davidson, A. and Bethune, K.M., 1994. Age of the Sudbury dikes and their metamorphism in the Grenville Province. In: Radiogenic and isotopic studies. Geological Survey of Canada Report 8, 97–106.

Duuring, P., Bleeker, W. and Beresford, S.W., 2007. Structural modification of the komatiite-associated Harmony nickel sulfide deposit, Leinster, Western Australia. Economic Geology 102, 277–297.

Duuring, P., Bleeker, W., Beresford, S.W. and Hayward, N., 2010. Towards a volcanic–structural balance: relative importance of volcanism, folding, and remobilisation of nickel sulphides at the Perseverance Ni–Cu–(PGE) deposit, Western Australia. Mineralium Deposita 45, 281–311.

Easton, R.M., 2000. Metamorphism of the Canadian shield, Ontario, Canada. II. Proterozoic metamorphic history. The Canadian Mineralogist 38, 319–344.

Ebel, D.S. and Naldrett, A.J., 1996. Fractional crystallization of sulfide ore liquids at high temperature. Economic Geology 91, 607–621.

Ebel, D.S. and Naldrett, A.J., 1997. Crystallization of sulfide liquids and the interpretation of ore composition. Canadian Journal of Earth Science 34, 352–365.

Ernst, R.E. and Buchan, K.L., with samples from Aspler, L.B., Barager, W.R.A., Corkery, M.T., Davidson, A., Emslie, R.F., Fahrig, W.F. (archives), Gandhi, S.S., Goutier, J., Halls, H.C., Hamilton, M.A., Hanes, J.A., Kjarsgaard, B.A., LeCheminant, A.N., Palmer, H.C., Percival, J.A., Peterson, T., Phinney, W.C., Sandeman, H.A., Smyk, M.C. and Williamson, M.-C., 2010. Geochemical database of Proterozoic intraplate mafic magmatism in Canada. Geological Survey of Canada, Open File 6016.

Ewers, W.E., 1972. Nickel-iron exchange in pyrrhotite. Proceedings of the Australasian Institute of Mining and Metallurgy 241, 19–25.

Faleiros, F.M., da Cruz Campanha, G.A., da Silveira Bello, D.M. and Fuzikawa, K., 2010. Quartz recrystallization regimes, c-axis texture transitions and fluid inclusion reequilibration in a prograde greenschist to amphibolite facies mylonite zone (Ribeira Shear Zone, SE Brazil), Tectonophysics 485, 193–214.

Farrow, C.E.G. and Watkinson, D.H., 1997. Diversity of precious-metal mineralization in footwall Cu-Ni-PGE deposits, Sudbury, Ontario: Implications for hydrothermal models of formation. The Canadian Mineralogist 35, 817–839.

Farrow, C.E.G. and Lightfoot, P.C., 2002. Sudbury PGE revisited: Toward an Integrated model. In: Cabri, L.J. (Ed.), The Geology, Geochemistry, Mineralogy and Mineral Beneficiation of Platinum Group Element. Canadian Institute of Mining, Metallurgy and Petroleum Special Volume 54, pp. 13–130.

Fleet, M.E. and Bernett, R.L., 1978. Al^{IV}/Al^{VI} partitioninig in calciferous amphiboles from the Frood mine, Sudbury, Ontario. Canadian Mineralogist 16, 527–532.

Fleet, M.E., Barnett, R.L. and Morris, W.A., 1987. Prograde metamorphism of the Sudbury Igneous Complex. The Canadian Mineralogist 25, 499–514.

Fleet, M.E., Chryssoulis, S.L., Stone, W.E. and Weisener, C.G., 1993. Partitioning of platinum-group elements and Au in the Fe-Ni-Cu-S system: Experiments on the fractional crystallization of sulphide melt. Contributions to Mineralogy and Petrology 115, 36−44.

Francis, C.A., Fleet, M.E., Misra, K. and Craig, J.R., 1976. Orientation of exsolved pentlandite in natural and synthetic nickeliferous pyrrhotite. American Mineralogist 61, 913–920.

Frost, B.R., Chamberlain, K.R. and Schumacher, J.C., 2000. Sphene (titanite): phase relations and role as a geochronometer. Chemical Geology 172, 131–148.

Frost, B.R., Mavrogenes, J. A. and Tomkins, A. G., 2002. Partial melting of sulfide ore deposits during medium- and high-grade metamorphism. Canadian Mineralogist 40, 1–18.

Fueten, F. and Redmond, D.J., 1997. Documentation of a 1450 Ma contractional orogeny preserved between the 1850 Ma Sudbury impact structure and the 1 Ga Grenville orogenic front, Ontario. Geological Society of America Bulletin 109, 268–279.

Fyfe, W.S., Kerrich, R., 1984. Gold: natural concentration processes. In: R.P. Foster (Ed.), Gold 82: The Geology, Geochemistry and Genesis of Gold Deposits. Balkema, Rotterdam, pp. 99–127.

Gammell, R.R., Lesher, C.M., McDonald, A.M., Farrow, C.E.G. and Weresczynksky, M., 2004. As-rich Ni-Cu-(PGE) mineralization in the Garson mine, Sudbury, Ontario. Geological Association of Canada-Mineralogical Association of Canada Annual Meeting, St. Catherines.

Getty, S.R. and Gromet, L.P., 1992. Geochronological constraints on ductile deformation, crustal extension, and doming around a basement-cover boundary, New England Appalachians. American Journal of Science 292, 359–397.

Gibbins, S.F.M., 1994. Geology, Geochemistry, stratigraphy and mechanisms of emplacement of the Onaping Formation, Dowling area, Sudbury structure, Ontario, Canada. Unpublished M.Sc. thesis, Laurentian University, Sudbury, Canada, 314 p.

Gill., J.E., 1969. Experimental deformation and annealing of sulfides and interpretation of ore textures. Economic Geology 64, 500–508.

Gilligan, L.B. and Marshall, B., 1987. Textural evidence for remobilization in metamorphic environments. In: Marshall, B. and Gilligan, L.B. (Eds.), Mechanical and Chemical (Re) Mobilization of Metalliferous Mineralization. Ore Geology Reviews 2, pp. 205–229.

Gilligan, L.B. and Marshall, B., 1987. Textural evidence for remobilization in metamorphic environments. In: Marshall, B. and Gilligan, L.B. (Eds.), Mechanical and Chemical (Re) mobilization of Metalliferous Mineralization. Ore Geology Reviews 2, pp. 205-229.

Golightly, J.P., 1994. The Sudbury Igneous Complex as an impact melt: Evolution and ore genesis. In: Lightfoot, P.C., and Naldrett, A. (Eds.), Proceedings of the Sudbury-Noril'sk Symposium. Ontario Geological Survey Special Volume 5, pp. 105-117.

Golightly, J.P. and Lesher, C.M., 1999. MSS fractionation, volatile-enhanced partitioning, and sulphide liquid immiscibility in magmatic Fe-Ni-Cu-(PGE) sulphide deposits. Geological Association of Canada-Mineralogical Association of Canada Annual Meeting, Sudbury.

Grant, R.W. and Bite, A. 1984. Sudbury quartz diorite offset dikes. In: Pye, E.G., Naldtrett A.J. and Giblin, P.E. (Eds.), The Geology and Ore Deposits of the Sudbury Structure. Ontario Geological Survey Special Volume 1, pp. 275-300.

Grieve, R.A.F., 1987. Terrestrial impact structure. Annual Review of Earth and Planetary Sciences 15, 245–270.

Grieve, R.A.F., Stöffler, D. and Deutsch, A., 1991. The Sudbury Structure: controversial or misunderstood? Journal of Geophysical Research 96, 22753–22764.

Grieve, R.A.F, Reimold, W.U., Morgan, J., Riller, U. and Pilkington, M., 2008. Observations and interpretations at Vredefort, Sudbury, and Chicxulub: Towards an empirical model of terrestrial impact basin formation. Meteoritics and Planetary Science 43, 855–882.

Grieve, R.A.F., Ames, D.E., Morgan, J.V. and Artemieva, N., 2010. The evolution of the Onaping Formation at the Sudbury impact structure. Meteoritics and Planetary Science 45, 1–24.

Groves, D.I., Barrett, F.M. and McQueen, K.G., 1979. The relative roles of magmatic segregation, volcanic exhalation and regional metamorphism in the generation of volcanic·associated nickel ores of Western Australia. Canadian Mineralogist 17, 319–336.

Ham, A.P. and Bell, T.H., 2004. Recycling of foliations during folding. Journal of Structural Geology 26, 1989–2009.

Hammarstrom, J.M. and Zen, E., 1986. Aluminum in hornblende: An empirical igneous geobarometer. American Mineralogist 71, 1297–1313.

Hanley, J., 2005. The aqueous geochemistry of the platinum-group elements (PGE) in surficial, low T hydrothermal and high-T magmatic hydrothermal environments. Mineralogical Association of Canada Short Course 35, 35–56.

Hawley, J.E., 1962. The Sudbury ores, their mineralogy and origin; Part 3, interpretations; the history and origin of the Sudbury ores. The Canadian Mineralogist 7, 146–207.

Hawley, J.E., 1965. Upside-Down Zoning at Frood, Sudbury, Ontario. Economic Geology 60, 529–575.

Hawley, J.E. and Stanton, R.L., 1962. The Sudbury ores, their mineralogy and origin; Part 2, the facts; the ores, their minerals, metals and distribution. The Canadian Mineralogist 7, 30–145.

Heath, C., Lahaye, Y., Stone, W.E. and Lambert, D.D., 2001. Origins and variations in nickel tenor along the strike of the Edwards lode nickel sulfide orebody, Kambalda, Western Australia. The Canadian Mineralogist 39, 655–671.

Hirth, G. and Tullis, J., 1992. Dislocation creep regimes in quartz aggregates. Journal of Structural Geology 14, 145–159.

Holland, T.J.B. and Powell, R., 1998. An internally consistent thermodynamic data set for phases of petrological interest. Journal of Metamorphic Geology, 16, 309–343.

Hollister, L.S., 1966. Garnet zoning: an interpretation based on the Rayleigh fractionation model. Sceince 154, 1647–1651.

Hollister, L.S., 1969. Contact metamorphism in the Kwoiek area of British Columbia: an end member of the metamorphic process. Geological Society of America Bulletin 80, 2465–2494.

Ivanov, B.A. and Deutsch, A., 1999. Sudbury impact event: Cratering mechanics and thermal history. In: Dressler, B.O., Sharpton, V.L. (Eds.), Large Meteorite Impacts and Planetary Evolution II. Geological Society of America Special Paper 339, pp. 389–397.

Keays, R.R., 1987. Principles of mobilization (dissolution) of metals in mafic and ultramafic rocks – The role of immiscible magmatic sulphides in the generation of hydrothermal gold and volcanogenic massive sulphide deposits. In: B. Marshall and L.B. Gilligan (Eds.), Mechanical and Chemical (Re)mobilization of Metalliferous Mineralization. Ore Geology Reviews 2, pp. 47–63.

Keays, R.R. and Crocket, J.H., 1970. A study of precious metals in the Sudbury nickel irruptive ores. Economic Geology 65, 438–450.

Keays, R.R. and Lightfoot, P.C., 2004. Formation of Ni-Cu platinum group element sulphide mineralisation in the Sudbury impact melt sheet. Mineralogy and Petrology 82, 217–258.

Keays, R.R., Nickel, E.H., Groves, D.I. and McGoldrick, P.J., 1982. Iridium and palladium as discriminants of volcanic-exhalative, hydrothermal, and magmatic nickel sulfide mineralization. Economic Geology 77, 1555–1547.

Keays, R.R., Ross, J.R. and Woolrich, P., 1981. Precious metals in volcanic peridotite-associated nickel sulfide deposits in Western Australia. II: Distribution within the ores and host rocks at Kambalda. Economic Geology 76, 1645–674.

Kelly, W.C. and Clark, B.R., 1975. Sulfide deformation: III. Experimental deformation of chalcopyrite to 2000 bars and 500°C. Economic Geology 70, 431–453.

Klimczak, C., Wittek, A., Doman, D. and Riller, U., 2007. Fold origin of the NE-lobe of the Sudbury Basin, Canada: Evidence from heterogeneous fabric development in the Onaping Formation and the Sudbury Igneous Complex. Journal of Structural Geology 29, 1744–1756.

Klotsman, S. M., Timofeyev, A. N. and Trakhtenberg, 1. Sh., 1963. Investigation of the diffusion properties of the chalcogenides of transition metals IV. Temperature dependence of the anisotropy of nickel and sulphur self-diffusion in nickel monosulphide. Physics Metals Metallography 16, 92-98.

Krstic, S. and Vandenberg, B., 2005. Garson 600 ore body: Mineralogical characterization. Unpublished report for Vale, 69 p.

Krogh, T. E., 1994. Precise U-Pb ages for Grenvillian and pre-Grenvillian thrusting of Proterozoic and Archean metamorphic assemblages in the Grenville Front tectonic zone, Canada. Tectonics 13, 963–982.

Krogh, T.E., Davis, D.W. and Corfu, F., 1984. Precise U–Pb zircon and baddeleyite ages for the Sudbury Structure. In: Pye, E.G., Naldtrett, A.J., Giblin, P.E. (Eds.), The Geology and Ore Deposits of the Sudbury Structure. Ontario Geological Survey Special Volume 1, pp. 431–446.

Krogh, T.E., Corfu, F., Davis, D.W., Dunning, G.R., Heaman, L.M., Machado, N., Greenough, J.D. and Nakamura, E., 1987. Precise U-Pb isotopic ages of diabase dykes and mafic to ultramafic rocks using trace amounts of baddeleyite and zircon. In: Halls, H.C. and Fahring, W.F. (Eds.), Mafic Dyke Swarms. Geological Association of Canada Special Paper 34, pp. 147–152.

Kuenen, P.H. and de Sitter, L.U., 1938. Experimental investigation into the mechanism of folding. Leidsche Geologische Mededeelingen 10, 217–239.

Kullerud, G., Yund, R.A. and Moh, G.H., 1969. Phase relations in the Cu-Fe-S, Cu-Ni-S, and Fe-Ni-S systems. In: Wilson, H.D.B. (Ed.), Magmatic Ore Deposits; a Symposium. Economic Geology Monographs 4, 323-343.

Lacroix, S. and Darling, R., 1991. Tectonized Cu-Ni deposits of the Aulneau-Redcliff area, Central Labrador Trough, Quebec. Economic Geology 86, 718-739.

Lakomy, R., 1990. Implications for cratering mechanics from a study of the Footwall Breccia of the Sudbury impact structure, Canada. Meteoritics 25, 195-207.

Lawrence, L.J., 1967. Sulphide neomagmas and highly metamorphosed sulphide deposits. Mineralium Deposita 2, 5–10.

Layton-Matthews, D., Lesher, C.M., Burnham, O.M., Liwanag, J., Halden, N.M., Hulbert, L. and Peck, D.C., 2007. Magmatic Ni-Cu-platinum-group element deposits of the Thompson Nickel Belt. In: Goodfellow,W.D. (Ed.), Mineral Deposits of Canada: A Synthesis of Major Deposit-Types, District Metallogeny, the Evolution of Geological Provinces, and Exploration Methods. Geological Association of Canada, Mineral Deposits Division, Special Publication 5, pp. 409-432.

Layton-Matthews, D.M., Lesher, C.M., Liwanag, J., Halden, N., Burnham, O.M., Hulbert, L., Peck, D.C. and Keays, R.R., 2011. Mineralogy, geochemistry, and genesis of komatiite-associated Ni-Cu-(PGE) mineralization in the Thompson Nickel Belt, Manitoba. Reviews in Economic Geology 17. 123–143.

Leake, B.E., 1971. On aluminous and edenitic hornblendes. Mineralogical Magazine 38, 389–406.

Leake, B.E.,Wooley, A.R., Arps, C.E.S., Birch, W.D., Gilbert, M.C., Grice, J.D., Hawthorne, F.C., Kato, A., Kisch, H.J., Krivovichev, V.G., Linthout, K., Laird, J., Mandarino, J.A., Maresch, W.V., Nickel, E.H., Rock, N.M.S., Schumacher, J.C., Smith, D.C., Stephenson, N.C.N., Ungaretti, L., Whittaker, E.J.W., Guo, Y., 1997. Nomenclature of amphiboles: report of the subcommittee on amphiboles of the International Mineralogical Association, Commission on New Minerals and Mineral Names. The Canadian Mineralogist 35, 219-233.

Lee, C. and Siddorn, J., 2006. Garson structural geology review. Unpublished SRK report for Vale, 12 p.

Lesher, C.M. and Keays, R.R., 1984. Metamorphically and hydrothermally mobilized Fe-Ni-Cu sulphides at Kambalda, Western Australia. In Buchanan, D.L. and Jones, M.J. (Eds.), Sulphide deposits in mafic and ultramafic rocks. London, UK, Institution of Mining and Metallurgy, pp. 62–69.

Lesher, C.M. and Campbell, I.H., 1993. Geochemical and fluid dynamic modeling of compositional variations in Archean komatiite-hosted nickel sulfide ores in Western Australia. Economic Geology 88, 804–816

Lesher, C.M. and Burnham, O.M., 2001. Multicomponent elemental and isotopic mixing in Ni-Cu-(PGE) ores at Kambalda, Western Australia. The Canadian Mineralogist 39, 421–446.

Lesher, C.M. and Keays, R.M., 2002. Komatiite-associated Ni-Cu-(PGE) deposits: mineralogy, geochemistry, and genesis. In: Cabri, L.J. (Ed.), The Geology, Geochemistry, Mineralogy, and Mineral Beneficiation of the Platinum-Group Elements. Canadian Institute of Mining, Metallurgy and Petroleum 54, pp. 579-617.

Lesher, C.M., and Barnes, S.J., 2009. Komatiite-associated Ni-Cu-(PGE) deposits. In: Li, C. and Ripley, E.M. (Eds.), Magmatic Ni-Cu-PGE Deposits: Genetic Models and Exploration. Geological Publishing House of China, pp. 27-101.

Lesher, C.M., Golightly, J.P., Gregory, S.K., Huminicki, M.A. and Pattison, E.F., 2009. Genesis of Ni-Cu-PGE mineralization associated with the 1.85 Ga Sudbury impact event. Geological Association of Canada-Mineralogical Association of Canada Annual Meeting, Toronto.

Li, C., Naldrett, A.J., Coats, C.J.A. and Johannessen, P., 1992. Platinum, palladium, gold, and copper-rich stringers at the Strathcona mine, Sudbury: Their enrichment by fractionation of a sulfide liquid: Economic Geology 87, 1584–1598.

Li, C., Naldrett, A.J., Rucklidge, J.C. and Kilius, L.R., 1993. Concentration of platinum-group elements and gold in sulfides from the Strathcona deposit, Sudbury, Ontario. The Canadian Mineralogist 31, 523–531.

Li, C., Barnes, S-J., Makovicky, E., Rose-Hansen, J. and Makovicky, M., 1996. Partitioning of Ni, Cu, Ir, Rh, Pt and Pd between monosulfide solid solution and sulfide liquid: effects of composition and temperature. Geochimica et Cosmochimica Acta 60, 1231–1238.

Lightfoot, P.C., Keays, R.R., Morrison, G.G., Bite, A. and Farrell, K., 1997. Geologic and geochemical relationships between the contact sublayer, inclusions, and the Main Mass of the Sudbury Igneous Complex: A case study of the Whistle mine embayment. Economic Geology 92, 647–673.

Lightfoot, P.C., Keays, R.R. and Doherty, W., 2001. Chemical evolution and origin of nickel sulfide mineralization in the Sudbury Igneous Complex, Ontario, Canada. Economic Geology 96, 1855–1875.

Liwanang, J. 2001. Post-magmatic modification of the sulphide deposits from the Thompson Nickel Belt, Manitoba, Canada. Unpublished MSc. Thesis, University of Manitoba, Canada, 207 p.

Lochhead, D.R., 1955. The Falconbridge ore deposit, Canada. Economic Geology 50, 42–50.

Long, D.G.F, 2004. The tectonostratigraphic evolution of the Huronian basement and the subsequent basin fill: geological constraints on impact models of the Sudbury event. Precambrian Geology 129, 203–233.

Long, S., McQuarrie, N., Tobgay, T. and Hawthorne, J., 2011. Quantifying internal strain and deformation temperature in the eastern Himalaya, Bhutan: Implications for the evolution of strain in thrust sheets. Journal of Structural Geology, 579-608.

Lusk, J. and Ostwald, J., 1983. Analysis of pyrrhotite properties accompanying recrystallization of metamorphosed nickel sulfide ore from Kambalda, Western Australia. Canadian Journal of Earth Sciences 20, 113–119.

Magyarosi, Z., Watkinson, D.H. and Jones, P.C., 2002. Mineralogy of Ni-Cu platinum-group element sulfide ore in the 800 and 810 orebodies, Copper Cliff South mine, and P-T-X conditions during the formation of platinum-group minerals. Economic Geology 97, 1471–1486.

Maiden, K.J., 1984. Metamorphic features of stratiform gold ores in the Barberton greenstone belt, eastern Transvaal. In: R.P. Foster (Ed.), Gold 1982: The Geology, Geochemistry and Genesis of Gold Deposits. Geological Society of Zimbabwe Special Publication 1, 325–338.

Maiden, K.J., Chimimba, L.R., and Smalley, T.J., 1986. Cuspate ore-wall rock interfaces, piercement structures, and the localization of some sulfide ores in deformed sulfide deposits. Economic Geology 81, 1464–1472.

Mancini, F., Papunen, H., 2000. Metamorphism of Ni–Cu sulfides in mafic-ultramafic intrusions: The Svecofennian Saaksjarvi complex, southern Finland. In: Spry, P.G., Marshall, B. and Vokes, F.M. (Eds), Metamorphosed and Metamorphogenic ore Deposits. Reviews in Economic Geology 11, pp. 217–232.

Marshall, B. and Gilligan, L.B., 1987. An introduction to remobilization: Information from orebody geometry and experimental considerations. In: Marshall, B. and Gilligan, L.B. (Eds.), Mechanical and Chemical (Re) mobilization of Metalliferous Mineralization. Ore Geology Reviews 2, pp. 87–131.

Marshall, B. and Gilligan, L.B., 1993. Remobilization, syn-tectonic processes and massive sulphide deposits. In: Groves, D.I. and Bennett, J.M. (Eds.), Structural Setting and Controls on Mineral Deposits. Ore Geology Reviews 8, pp. 39–64.

Marshall, B., Vokes, M.V. and Larocque, A.C.L., 2000. Regional metamorphic remobilization: upgrading and formation of ore deposits. In Spry, P.G., Marshall, B. and Vokes F.M. (Eds), Metamorphosed and Metamorphogenic ore Deposits. Reviews in Economic Geology 11, pp. 19-38.

Marshall, D., Watkinson, D., Farrow, C., Moln´ar, F. and Fouillac, A-M., 1999. Multiple fluid generations in the Sudbury Igneous Complex: fluid inclusion, Ar, O, H, Rb and Sr evidence. Chemical Geology 154, 1-19.

Mavrogenes, J.A., MacIntosh, I.W. and Ellis, D.J., 2001. Partial melting of the Broken Hill galena-sphalerite ore: Experimental studies in the system PbS-FeS-ZnS-(Ag_2S). Economic Geology 96, 205–210.

McCallum, M.E., Loucks, R.R., Carlson, R.R., Cooley, E.F., Doerge, T.A., 1976. Platinum metals associated with hydrothermal copper ores of the New Rambler Mine, Medicine Bow Mountains, Wyoming. Economic Geology 71, 1429–1450.

McCormick, K.A., Fedorowich, J.S., McDonald, A.M. and James, R.S., 2002. A textural, mineralogical, and statistical study of the Footwall Breccia within the Strathcona Embayment of the Sudbury Structure. Economic Geology 97, 125-143.

McDonough, W.F. and Sun, S.-S., 1995. The composition of the Earth. Chemical Geology 120, 223–254.

McDougall, T. F., Meikle, B. K., Guy-Bray, T. V., Saul, V. A. and Gill, J. E., 1961. Experimental investigation of solid diffusion and volatilization of certain metallic sulfides. Economic Geology 56. 362-391

McQueen, K.G., 1979. Experimental heating and diffusion effects in Fe-Ni sulfide ore from Redross, Western Australia. Economic Geology 74, 140–148.

McQueen, K.G., 1981. The nature and metamorphic history of the Wannaway nickel deposit, Western Australia. Economic Geology 76, 1444–1468.

McQueen, K.G., 1987. Deformation and remobilization in some Western Australian nickel ores. In: Marshall, B. and Gilligan, L.B. (Eds.), Mechanical and Chemical (Re)mobilization of Metalliferous Mineralization. Ore Geology Reviews 2, pp. 269–286.

Means, W. D. 1987. A newly recognized type of slickenside striation. Journal of Structural Geology 9, 585–590.

Menard, T., Lesher, C.M., Stowell, H.H., Price, D.P., Pickell, J.R., Onstott, T.C. and Hubert, L., 1996. Geology, genesis, and metamorphic history of the Namew Lake Ni-Cu deposit, Manitoba. Economic Geology 91, 1394–1413.

Milkereit, B., Green, A., Berrer, E., Boerner, D., Broome, J., Cosec, M, Cowan, J., Davidson, A., Dressler, B., Fueten, F., Grieve, R., James, R., Krause, B., McGrath, P., Meyer, W., Moon, W., Morris, W., Morrison G., Naldrett, A., Peredery, W., Rousell, D., Salisbury, M., Schwerdtner, W., Snajdr, P., Thomas, M. and Watts, A., 1992. Deep geometry of the Sudbury structure from seismic reflection profiling. Geology 20, 807–811.

Misra, K.C. and Fleet, M.E., 1973. The chemical compositions of synthetic and natural pentlandite assemblages. Economic Geology 68, 518–539.

Muir, T.L. and Peredery, W.V., 1984. The Onaping Formation In: Pye, E.G., Naldtrett, A.J., Giblin, P.E. (Eds.), The Geology and Ore Deposits of the Sudbury Structure. Ontario Geological Survey, Special Volume 1, 139–210.

Mukwakwami, J., Lafrance, B. and Lesher, C.M., 2012. Back-thrusting and overturning of the southern margin of the 1.85 Ga Sudbury Igneous Complex at the Garson mine, Sudbury, Ontario. Precambrian Research 196–197, 81–105.

Mungall, J.E., 2007. Crystallization of magmatic sulfides: An empirical model and application to Sudbury ores; Geochimica et Cosmochimica Acta 71, 2809–2819.

Mungall, J.E., Andrews, D.R.A., Cabri, L.J., Sylvester, P.J. and Tubrett, M., 2005. Partitioning of Cu, Ni, Au, and platinum-group elements between monosulfide solid solution and sulfide melt under controlled oxygen and sulfur fugacities. Geochimica et Cosmochimica Acta 69, 4340–4360.

Naldrett, A.J., 1981. Nickel sulfide deposits: classification, composition, and genesis. Economic Geology 75th Anniversary Volume, 628-685.

Naldrett, A. J., 1984a. Ni-Cu ores of the Sudbury Igneous Complex - Introduction. In: Pye, E.G., Naldrett, A.J., and Giblin, P.E. (Eds.), The Geology and Ore Deposits of the Sudbury Structure. Ontario Geological Survey, Special Volume 1, pp. 309−307.

Naldrett, A. J., 1984b. Mineralogy and composition of the Sudbury ores. In: Pye, E.G., Naldrett, A.J., and Giblin, P.E. (Eds.), The Geology and Ore Deposits of the Sudbury Structure. Ontario Geological Survey, Special Volume 1, pp. 309–325.

Naldrett, A.J., 2004. Magmatic sulfide deposits. Geology, geochemistry and exploration. Berlin, Springer, 727 p.

Naldrett, A.J. and Lightfoot, P.C., 1993. Ni-Cu-PGE ores of the Noril'sk region, Siberia: A model for giant magmatic ore deposits associated with flood basalts. Society of Economic Geologists Special Publication 2, 81–123.

Naldrett, A.J., Craig, J.R. and Kullerud, G., 1967. The central portion of the Fe-Ni-S system and its bearing on pentlandite exsolution in iron-nickel sulfide ores. Economic Geology 62, 826-847.

Naldrett, A.J., Bray, J.G., Gasparrini, E.L., Podolsky, T. and Rucklidge, J.C., 1970. Cryptic variation and the petrology of the Sudbury Nickel Irruptive. Economic Geology 65, 122–155.

Naldrett, A.J., Hoffman, E.L., Green, A.H., Chou, C.-L., Naldrett, S.R. and Alcock, R.A., 1979. The composition of Ni-sulfide ores, with particular reference to their content of PGE and Au. Canadian Mineralogist 17, 403–416.

Naldrett, A.J., Innes, D.G., Sowa, J. and Gorton, M.P., 1982. Compositional variations within and between five Sudbury ore deposits. Economic Geology 77, 1519-1534.

Naldrett, A.J., Hewins, R.H., Dressler, B.O. and Rao, B.V., 1984. The Contact Sublayer of the Sudbury Igneous Complex. In: Pye, E.G., Naldtrett A.J. and Giblin, P.E. (Eds.), The Geology and Ore Deposits of the Sudbury Structure. Ontario Geological Survey Special Volume 1, pp. 253–274.

Naldrett, A.J., Asif, M., Schandl, E., Searcey, T., Morrison, G.G., Binney, W.P. and Moore, C., 1999. Platinum-group elements in the Sudbury ores: Significance with respect to the origin of different ores zones and to the exploration for footwall orebodies. Economic Geology 94, 185–210.

Ostwald, J. and Lusk, J., 1978. Sulfide fabrics in some nickel sulfide ores from Kambalda, Western Australia. Canadian Journal of Earth Sciences 15, 501–515.

Owen, D.L., and Coats, C.J.A., 1984. Falconbridge and east mines. In: Pye, E.G., Naldtrett, A.J. and Giblin, P.E. (Eds.), The Geology and Ore Deposits of the Sudbury Structure. Ontario Geological Survey Special Volume 1, pp. 371–378.

Palmer, H.C., Merz, B.A. and Hayatsu, A., 1977. The Sudbury dikes of the Grenville Front: paleomagnetism, petrochemistry, and K-Ar age studies. Canadian Journal of Earth Sciences 14, 1867–1887.

Parrish, R.R., Bellerive, D.L., Sullivan, R.W., 1992. U–Pb chemical procedures for titanite and allanite in the Geochronology Laboratory, Geological Survey of Canada. In: Radiogenic Age and Isotopic Studies: Part 5. Geological Survey of Canada Paper 91-2, pp. 187–190.

Pavlis, T.L., Serpa, L.F. and Keener, C., 1993. Role of seismogenic processes in fault-rock development: An example from Death Valley, California. Geology 21, 267–270.

Pe-Piper, G., 1988. Calcic amphiboles of mafic rocks of the Jeffers Brook plutonic complex, Nova Scotia, Canada. American Mineralogist 73, 993–1006.

Peredery W.V., 1972. Chemistry of fluidal glasses and melt bodies in the Onaping formation. In: Guy-Bray, J. (Ed.), New developments in Sudbury Geology. Geological Association of Canada Special Paper 10, 49–59.

Piercey, P., Schneider, D.A. and Holm, D.K., 2007. Geochronology of Proterozoic metamorphism in the deformed Southern Province, northern Lake Huron region, Canada. Precambrian Research 157, 127–143.

Powell, R. and Holland, T., 1994. Optimal geothermometry and geobarometry. American Mineralogist 79, 120-133.

Prevec, S.A. and Cawthorn, R.G., 2002. Thermal evolution and interaction between impact melt sheet and footwall: a genetic model for the contact sublayer of the Sudbury Igneous Complex, Canada. Journal of Geophysical Research 107, 10.1029/2001JB000525.

Raase, P., 1974. A1 and Ti contents of hornblende, indicators of pressure and temperature of regional metamorphism. Contributions to Mineralogy and Petrology 45, 231–236.

Ramsay, J.G., 1967. Folding and Fracturing of Rocks. McGraw-Hill Book Company, New York, 568 p.

Ramsay, J.G., 1974. Development of chevron folds. Geological Society of America Bulletin 85, 1741–1754.

Ravna, E.K., 2000. Distribution of Fe^{2+} and Mg between coexisting garnet and hornblende in synthetic and natural systems: an empirical calibration of the garnet–hornblende Fe–Mg geothermometer. Lithos 53, 265–277.

Read, A.S, Karlstrom, K.E., Jeffrey A., Grambling, J.A., Bowring, S.A., Heizler, M. and Daniel, C., 1999. A middle-crustal cross section from the Rincon Range, northern New Mexico: Evidence for 1.68 Ga, pluton-influenced tectonism and 1.4 Ga regional metamorphism. Rocky Mountain Geology, 34, 67–91.

Reed, M.H. and Palandri, J., 2006. Sulfide mineral precipitation from hydrothermal fluids. Reviews in Mineralogy and Geochemistry 61, 609–631.

Rickard, D.T. and Zweifel, H., 1975. Genesis of Precambrian sulfide ores, Skellefte District, Sweden. Economic Geology 70, 255–274.

Riller, U., 2005. Structural Characteristics of the Sudbury impact structure, Canada: impact-induced versus orogenic deformation – a review. Meteoritics and Planetary Science 40, 1723–1740.

Riller, U. and Schwerdtner, W.M., 1997. Mid-crustal deformation at the southern flank of the Sudbury Basin, central Ontario, Canada. Geological Society of America Bulletin 109, 841–854.

Riller, U., Schwerdtner, W.M., Halls, H.C. and Card, K.D., 1999. Transpressive tectonism in the eastern Penokean orogen, Canada: Consequences for Proterozoic crustal kinematics and continental fragmentation. Precambrian Research 93, 51–70.

Riller, U., Boutelier, D., Schrank, C., Cruden, A.R., 2010. Role of kilometer-scale weak circular heterogeneities on upper crustal deformation patterns: evidence from scaled analogue modeling and the Sudbury Basin, Canada. Earth and Planetary Earth Science Letters 297, 587–597.

Rivers, T., 1997. Lithotectonic elements of the Grenville Province: review and tectonic implications. Precambrian Research 86, 117–154.

Robert, F., Boulier, A. M. and Firdaous, K., 1995. Gold-quartz veins in metamorphic terranes and their bearing on the role of fluids in faulting. Journal of Geophysical Research 100, 12861–12879.

Roscoe, W.E., 1975. Experimental deformation of natural chalcopyrite at temperatures up to 300°C over the strain rate range 10^{-2} to 10^{-6} sec^{-1}. Economic Geology 70, 454–472.

Ross, J.R. and Keays, R.R., 1979. Precious metals in volcanic-type nickel sulfide deposits in Western Australia: I. Relationships with the composition of the ores and host rocks. Canadian Mineralogist 17, 417–436.

Rousell, D.H., 1984. Structural Geology of the Sudbury Basin. In: Pye, E.G., Naldtrett, A.J., and Giblin P.E. (Eds.), The Geology and ore deposits of the Sudbury structure. Ontario Geological Survey Special Volume 1, pp. 83–95.

Rubio Pascual, F.J., Arenas, R., Díaz García, F., Martínez Catalán, J.R. and Abati, J., 2002. Contrasting high-pressure metabasites from the Santiago unit (Ordenes

Complex, northwestern Iberian Massif, Spain). In: Martínez Catalán, J.R., Hatcher, R.D., Jr., Arenas, R., and Díaz García, F. (Eds.), Variscan-Appalachian Dynamics: The Building of the Late Paleozoic Basement. Boulder, Colorado, Geological Society of America Special Paper 364, pp. 105–124.

Schumacher, R., 1991. Compositions and phase relations of calcic amphiboles in epidote- and clinopyroxene-bearing rocks of the amphibolites and lower granulite facies, central Massachusetts, USA. Contributions to Mineralogy and Petrology 108, 196–211.

Shanks, W.S. and Schwerdtner, W.M., 1991a. Structural analysis of the central and southwestern Sudbury Structure, Southern Province, Canadian Shield. Canadian Journal of earth Sciences 28, 411–430.

Shanks, W.S. and Schwerdtner, W.M., 1991b. Crude quantitative estimates of the original northwest-southeast dimension of the Sudbury Structure, south-central Canadian Shield. Canadian Journal of earth Sciences 28, 1677–1686.

Shewman, R.W. and Clark, L.A., 1970. Pentlandite phase relations in the Fe-Ni-S system and notes on the monosulfide solid solution. Canadian Journal of Earth Sciences 7, 67-85.

Sibson, R. H., Robert, F. and Poulsen, H. K., 1988. High-angle reverse faults, fluid-pressure cycling, and mesothermal gold-quartz deposits. Geology 16, 551–555.

Siddorn, J.P. and Ham, A., 2006. Review of Garson mine phase 3 exploration program. Unpublished SRK report for Vale, 53 p.

Sims, P.K., Van Schmus, W.R., Schulz, K.J. and Peterman, Z.E., 1989. Tectono-stratigraphic evolution of the Early Proterozoic Wisconsin magmatic terranes of the Penokean Orogen. Canadian Journal of Earth Sciences 26, 2145–2158.

Snelling, P.E., 2009. The influences of stress and structure on mining-induced seismicity in Creighton mine, Sudbury, Canada. Unpublished MSc. thesis, Queen's University, Canada, 209 p.

Sparks, H.A. and Mavrogenes, J.A., 2005. Sulfide melt inclusions as evidence for the existence of a sulfide partial melt at Broken Hill, Australia. Economic Geology 100, 773–779.

Spear, F.C., 1993. Metamorphic Phase Equilibria and Pressure-Temperature-Time Paths. Mineralogical Society of America, 799 p.

Spear, F.S., 1988. Metamorphic fractional crystallization and internal metasomatism by diffusional homogenization of zoned garnets. Contributions to Mineralogy and Petrology 99, 507–517.

Stipp, M., Stünitz, H., Heilbronner, R. and Schmid, S.M., 2002. The eastern Tonale fault zone: a 'natural laboratory' for crystal plastic deformation of quartz over a temperature range from 250 to 700°C. Journal of Structural Geology 24, 1861–1884.

Stipp, M., Tullis, J., Scherwath, M. and Behrmann, J.M., 2010. A new perspective on paleopiezometry: Dynamically recrystallized grain size distributions indicate mechanism changes. Geology 38; 759–762.

Stöckhert, B., Brix, M.R., Kleinschrodt, R., Hurford, A.J. and Wirth, R., 1999. Thermochronometry and microstructures of quartz-a comparison with experimental flow laws and predictions on the temperature of the brittle-plastic transition. Journal of Structural Geology 21, 351–369.

Stockwell, C.H., 1982. Proposals for the time classification and correlation of Precambrian rocks and events in Canada and adjacent areas of the Canadian Shield. Geological Survey of Canada Paper 80–19, 135 p.

Stone, W.E., Heydari, M. and Seat, Z., 2004. Nickel tenor variations between Archaean komatiite-associated nickel sulphide deposits, Kambalda ore field, Western Australia: the metamorphic modification. Mineralogy and Petrology 82, 295–316.

Stupavsky, M. and Symons, D.T.A., 1982. Extent of Grenvillian remanence components in rocks of the Southern Province. Canadian Journal of Earth Sciences 19, 698–707.

Sullivan, R. W. and Davidson, A., 1993, Monazite age of 1747 Ma confirms post-Penokean age for the Eden Lake complex, Southern Province. In: Radiogenic Age and Isotopic Studies: Report 7: Geological Survey of Canada Paper 93-2, 45–48.

Szabó, E. and Halls, H.C., 2006. Deformation of the Sudbury Structure: paleomagnetic evidence from the Sudbury Breccia. Precambrian Research 150, 27–48.

Szentpéteri, K., 2009. Geology and mineralization of the proximal Worthington offset area in the Sudbury Igneous Complex, Canada. Unpublished PhD thesis. Eötvös Loránd University, Hungary, 145 p.

Szentpéteri, K., Watkinson, D.H., Molnar, F. and Jones, P.C., 2002. Platinum-group elements-Co-Ni-Fe sulfarsenides and mineral paragenesis in Cu-Ni-platinum-group element deposits, Copper Cliff north area, Sudbury, Canada. Economic Geology 97, 1459−1470.

Therriault, A.M., Fowler, A.D. and Grieve, R.A.F., 2002. The Sudbury Igneous Complex: differentiated impact melt sheet. Economic Geology 97, 1521–1540.

Thompson, M.L., Bernett, R.L., Fleet, M.E. and Kerrich, R., 1985. Metamorphic assemblages in the South Range norite and footwall mafic rocks near the Kirkwood mine, Sudbury, Ontario. Canadian Mineralogist 23, 173–186.

Tilton, G.R., 1960. Volume diffusion as a mechanism for discordant lead ages. Journal of Geophysical Research 65, 2933-2945.

Tomkins, A.G., 2007. Three mechanisms of ore remobilization during amphibolite facies metamorphism at the Montauban Zn–Pb–Au–Ag deposit. Mineralium Deposita 42, 627–637.

Tomkins, A.G., Pattison, D.R.M. and Frost, R.B., 2007. On the initiation of metamorphic sulfide anatexis. Journal of Petrology 48, 511–535.

Tucker, R.D. and Gower, C.F., 1994. A U-Pb geochronological framework for Pinware terrane, Grenville Province, southeast Labrador. Journal of Geology 102, 67–78.

Van Schmus, W.R., 1976. Early and Middle Proterozoic history of the Great Lakes area. Royal Society London Philosophical Transactions 280, 605–628.

Van Schmus, W.R., Bickford, M.E. and Turek, A., 1996. Proterozoic geology of the east-central Midcontinent basement. In: van der Pluijm, B.E. and Catacosinos, P.A. (Eds.), Basement and Basins of Eastern North America. Boulder, Colorado, Geological Society of America Special Paper 308, pp. 7–32.

Van Schmus, W.R., Bickford, M.E., Anderson, J.L., Bender, E.E., Anderson, R.R., Bauer, P.W., et al. 1993. Transcontinental Proterozoic Provinces. In: Reed Jr., C., Bickford, M.E., Houston, R.S., Link, P.K., Rankin, D.W., Sims. P.K., and Van Schmus, W.R. (Eds), Precambrian: Coterminous U.S., the Geology of North America. The Geological Society of America C–2, pp. 171-334.

Vokes, E.M., 1971. Some aspects of the regional metamorphic mobilization of preexisting sulphide deposits. Mineralium Deposita 6, 122–129.

Vokes, E.M. and Craig, J.R., 1993. Post-crystallization mobilization phenomena in metamorphosed stratabound sulfide ores. Mineralogical Magazine 57, 19–28.

Wakefield, J., 1976. The structural and metamorphic evolution of the Pikwe Ni-Cu Sulfide deposit, Selebi-Pikwe, Eastern Botswana. Economic Geology 71, 988–1005.

Wasserburg, G.J., 1963. Diffusion processes in lead-uranium systems. Journal of Geophysical Research 68, 4823-4846.

Wasteneys, H.A., Kamo, S.L., Moser, D., Krogh, T.E., Gower, C.E. and Owen, J.V., 1997. U-Pb geochronological constraints on the geological evolution of the Pinware terrane and adjacent areas, Grenville Province, southeast Labrador, Canada. Precambrian Research 81, 101–128.

White, R.W., Powell, R. and Holland, T.J.B., 2007. Progress relating to calculation of partial melting equilibria for metapelites and felsic gneisses. Journal of Metamorphic Geology 25, 511–527.

Wilson, M.R., 1973. The geological setting of the Sulitjelma ore bodies, Central Norwegian Caledonides. Economic Geology 68, 309–316.

Wood, S.A., 2002. The aqueous geochemistry of the platinum-group elements with applications to ore deposits. In Cabri, L.J. (Ed.), The Geology, Geochemistry, Mineralogy and Mineral Beneficiation of Platinum-Group Elements. Montreal, Canadian Institute of Mining, Metallurgy and Petroleum, 211–249.

Woodsworth, G.J., 1977. Homogenization of zoned garnets from peltic schists. The Canadian Mineralogist 15, 230–242.

Young, G.M., Long, D.G.F., Fedo, C.M. and Nesbitt, H.W., 2001. Paleoproterozoic Huronian basin: product of a Wilson cycle punctuated by glaciations and a meteorite impact. Sedimentary Geology 141–142, 233–254.

Yund, R.A. and Kullerud. G., 1966. Thermal stability of assemblages in the Cu-Fe-S system. Journal of Petrology 7, 454–488.

Zenk, M. and Schulz, B., 2004. Zoned Ca-amphiboles and related P-T evolution in metabasites from the classical Barrovian metamorphic zones in Scotland. Mineralogical Magazine 68, 769–786.

Zieg M. J. and Marsh B. D., 2005. The Sudbury Igneous Complex: Viscous emulsion differentiation of a superheated impact melt sheet. Geological Society of America Bulletin 117, 1427–1450.

Appendices

Appendix A. Electron Microprobe Analyses of Amphiboles

Electron microprobe analyses of amphiboles in Garson metabasalt, Main Mass SIC norite, norite inclusions in massive sulfide ore and metagabbro. The analyses were obtained using a Cameca SX-100 electron probe microanalyzer equipped with WDS detectors in the Ontario Geoscience Laboratories in Sudbury. Operating conditions were 20 kV accelerating voltage and 20 nA beam current. Dave Crabtree helped with the analyses.

Appendix A

Sample #	Amph. Color	Rock Type	SiO_2	TiO_2	Al_2O_3	Cr_2O_3	MgO	CaO	MnO	FeOt	Na_2O	K_2O	F	Cl	Total
GA101-1-1c	Bl-Gr	MB	40.8	0.3	16.9	0.1	5.4	11.3	0.2	21.6	1.3	0.5	0.0	0.0	98.4
GA101-1-1r	Bl-Gr	MB	42.1	0.2	16.1	0.0	6.3	11.0	0.2	20.4	1.6	0.4	0.0	0.0	98.2
GA101-1-2c	Bl-Gr	MB	41.2	0.3	16.0	0.1	5.4	11.3	0.2	21.7	1.2	0.5	0.1	0.1	98.1
GA101-1-2r	Bl-Gr	MB	40.7	0.4	17.6	0.0	5.3	11.1	0.2	20.8	1.6	0.5	0.0	0.0	98.2
GA101-1-1	Bl-Gr	MB	24.9	0.0	22.9	0.1	12.2	0.0	0.2	29.6	0.0	0.0	0.0	0.0	90.0
GA101-1-3c	Bl-Gr	MB	41.0	0.3	15.9	0.1	5.4	11.4	0.2	22.0	1.4	0.5	0.0	0.1	98.2
GA101-1-3r	Bl-Gr	MB	40.7	0.2	17.6	0.0	5.4	11.1	0.3	20.9	1.7	0.4	0.0	0.0	98.4
GA101-1-4c	Bl-Gr	MB	41.3	0.1	17.2	0.0	5.2	11.2	0.2	21.3	1.5	0.4	0.0	0.0	98.5
GA101-1-4r	Bl-Gr	MB	40.9	0.2	18.0	0.0	5.3	11.1	0.2	20.9	1.6	0.4	0.0	0.0	98.8
GA101-1-5c	Bl-Gr	MB	40.6	0.3	16.3	0.0	5.1	11.4	0.2	21.7	1.3	0.6	0.0	0.1	97.6
GA101-1-5r	Bl-Gr	MB	41.0	0.3	16.9	0.0	5.2	11.2	0.2	21.4	1.4	0.4	0.0	0.0	98.1
GA101-5-1c	Bl-Gr	MB	41.2	0.3	15.8	0.0	5.3	11.4	0.2	22.2	1.4	0.5	0.0	0.1	98.5
GA101-5-1r	Bl-Gr	MB	40.6	0.3	17.2	0.0	5.4	11.4	0.2	21.2	1.5	0.6	0.0	0.1	98.6
GA101-5-2c	Bl-Gr	MB	40.5	0.3	16.6	0.0	5.1	11.4	0.2	21.5	1.4	0.6	0.0	0.1	97.6
GA101-5-2r	Bl-Gr	MB	40.6	0.3	17.1	0.0	5.1	11.3	0.2	21.3	1.5	0.5	0.1	0.1	98.0
GA101-5-3c	Bl-Gr	MB	41.1	0.3	17.2	0.0	5.7	11.3	0.2	20.3	1.4	0.6	0.0	0.0	98.2
GA101-3-1r	Bl-Gr	MB	40.6	0.3	17.5	0.1	5.6	10.9	0.2	20.8	1.7	0.4	0.0	0.0	98.1
GA101-3-2c	Bl-Gr	MB	41.0	0.3	16.2	0.0	5.2	11.5	0.2	21.9	1.3	0.5	0.0	0.1	98.2
GA101-3-2r	Bl-Gr	MB	40.3	0.3	17.7	0.1	5.3	10.9	0.3	20.7	1.7	0.4	0.0	0.0	97.7
GA101-3-3c	Bl-Gr	MB	40.6	0.3	16.3	0.0	5.1	11.4	0.2	21.7	1.3	0.5	0.0	0.0	97.6
GA101-3-3r	Bl-Gr	MB	40.6	0.3	17.1	0.1	5.4	11.1	0.2	20.5	1.5	0.4	0.0	0.1	97.2
GA101-7-1c	Bl-Gr	MB	41.1	0.3	15.7	0.1	5.4	11.5	0.2	22.2	1.5	0.5	0.0	0.1	98.4
GA101-7-1r	Bl-Gr	MB	41.1	0.3	16.0	0.0	5.4	11.3	0.2	21.7	1.4	0.5	0.0	0.0	98.1
GA101-7-2c	Bl-Gr	MB	40.9	0.3	16.1	0.0	5.5	11.5	0.2	21.4	1.5	0.5	0.1	0.0	98.0
GA101-7-2r	Bl-Gr	MB	40.8	0.3	16.6	0.0	5.7	11.2	0.2	20.7	1.6	0.4	0.0	0.0	97.5
GA101-8-1c	Bl-Gr	MB	40.9	0.3	16.8	0.0	5.2	11.4	0.2	21.7	1.4	0.6	0.0	0.1	98.6
GA101-8-1r	Bl-Gr	MB	40.9	0.3	16.7	0.1	6.0	11.0	0.3	20.6	1.5	0.3	0.0	0.0	97.7
GA101-8-2c	Bl-Gr	MB	41.0	0.2	17.3	0.1	5.6	11.0	0.2	20.7	1.6	0.4	0.0	0.0	98.2
GA101-8-2r	Bl-Gr	MB	42.0	0.3	15.6	0.0	6.5	11.0	0.3	20.1	1.6	0.3	0.1	0.0	97.8
GA161-12-1c	Br	MMN	46.2	2.2	8.5	0.2	13.7	11.7	0.3	13.0	0.8	0.7	0.1	0.0	97.4
GA161-12-1r	Br	MMN	46.7	2.1	8.3	0.2	13.6	11.5	0.2	13.1	0.9	0.6	0.1	0.0	97.4
GA161-12-1	Br	MMN	46.8	1.9	8.9	0.3	12.6	11.6	0.3	14.0	0.9	0.6	0.0	0.0	98.0
GA161-12-2c	Gr	MMN	51.9	0.2	5.7	0.0	14.7	12.3	0.3	13.2	0.5	0.1	0.0	0.2	99.0
GA161-12-2r	Gr	MMN	51.2	0.2	6.2	0.0	14.0	12.1	0.3	13.5	0.7	0.1	0.0	0.0	98.3
GA161-12-3c	Gr	MMN	53.0	0.1	4.2	0.2	15.2	12.0	0.3	12.9	0.4	0.1	0.0	0.0	98.6
GA161-12-3r	Gr	MMN	54.7	0.1	3.0	0.0	16.4	12.3	0.2	11.6	0.3	0.0	0.0	0.0	98.6
GA161-41c	Br	MMN	47.5	2.0	7.8	0.2	14.3	11.4	0.3	12.3	0.7	0.6	0.0	0.0	97.1
GA161-41r	Br	MMN	47.2	2.0	7.8	0.2	13.7	11.3	0.2	13.6	1.0	0.6	0.0	0.0	97.6
GA161-4-2c	Gr	MMN	51.9	0.1	4.6	0.1	14.9	12.1	0.3	13.0	0.5	0.1	0.0	0.0	97.7
GA161-4-2r	Gr	MMN	47.6	0.3	9.4	0.0	12.2	11.8	0.3	14.6	1.1	0.2	0.0	0.0	97.5
GA161-4-3	Gr	MMN	50.6	0.2	6.4	0.1	14.1	10.7	0.4	13.8	0.8	0.1	0.0	0.0	97.1
GA161-5-1	Br	MMN	46.8	2.2	8.5	0.2	14.4	11.9	0.2	11.9	0.9	0.6	0.0	0.0	97.6
GA161-5-2	Gr	MMN	48.8	0.2	9.2	0.0	12.6	11.9	0.3	13.8	1.0	0.2	0.0	0.0	98.3
GA161-5-3	Gr	MMN	47.8	0.3	9.9	0.0	12.2	11.6	0.3	14.4	1.1	0.2	0.0	0.0	97.8
GA161-5-4	Gr	MMN	51.2	0.2	5.8	0.0	14.3	12.1	0.3	12.9	0.6	0.1	0.0	0.0	97.6
GA161-13-1c	Br	MMN	50.0	1.3	5.9	0.2	15.8	11.9	0.2	11.2	0.7	0.4	0.1	0.0	97.6
GA161-13-1r	Br	MMN	49.4	1.4	6.4	0.2	13.7	11.8	0.3	12.6	0.5	0.4	0.1	0.0	96.8
GA161-13-2c	Gr	MMN	51.7	0.1	5.2	0.1	14.7	12.2	0.3	13.0	0.6	0.1	0.0	0.0	97.9

GA161-13-3c	Gr	MMN	47.2	0.2	10.2	0.1	11.8	11.7	0.3	14.6	1.0	0.2	0.1	0.0	97.4
GA161-6-1	Gr	MMN	53.9	0.1	2.7	0.1	15.8	12.0	0.3	12.4	0.3	0.1	0.0	0.0	97.6
GA104-8-1	Gr	NI	55.3	0.0	1.8	0.1	17.6	11.9	0.3	11.0	0.2	0.0	0.0	0.0	98.3
GA104-8-2	Gr	NI	53.9	0.0	0.6	0.0	15.5	0.6	0.9	26.1	0.0	0.0	0.0	0.0	97.8
GA104-8-3	Gr	NI	41.1	0.2	17.7	0.0	6.6	11.3	0.2	18.8	1.5	0.3	0.0	0.3	98.1
GA104-8-4	Gr	NI	41.5	0.1	17.3	0.0	7.1	11.1	0.3	18.1	1.6	0.3	0.0	0.4	97.9
GA104-8-5	Gr	NI	39.6	0.3	19.4	0.0	4.9	10.9	0.3	20.4	1.7	0.5	0.0	0.7	98.7
GA104-10-1	Gr	NI	51.0	0.3	5.7	0.4	14.8	11.7	0.2	13.0	0.5	0.3	0.0	0.0	97.9
GA104-10b-2	Gr	NI	53.5	0.0	0.9	0.1	16.1	1.2	0.9	24.7	0.0	0.0	0.0	0.0	97.4
GA104-10b-3	Gr	NI	51.6	0.2	5.6	0.1	15.9	11.8	0.2	11.6	0.5	0.1	0.0	0.0	97.7
GA104-10b-4	Gr	NI	52.9	0.0	1.8	0.1	15.3	1.3	0.9	24.9	0.1	0.0	0.0	0.1	97.4
GA104-10b-5	Gr	NI	41.7	0.2	17.6	0.0	7.2	11.3	0.3	17.7	1.5	0.3	0.0	0.4	98.2
GA108-7b-1r	Bl-Gr	MG	41.7	0.0	15.6	0.1	7.9	10.8	0.3	18.8	1.6	0.3	0.0	0.2	97.4
GA108-7b-1c	Gr	MG	53.1	0.0	3.2	0.1	14.9	12.4	0.3	13.0	0.2	0.1	0.0	0.0	97.3
GA108-7b-2	Bl-Gr	MG	42.1	0.3	16.7	0.2	6.9	11.6	0.3	17.8	1.5	0.3	0.1	0.0	97.8
GA108-7b-3	Gr	MG	53.0	0.0	3.0	0.0	14.6	12.5	0.2	13.3	0.2	0.1	0.0	0.0	97.0
GA108-7b2-4	Gr	MG	50.6	0.0	3.6	0.0	8.4	11.0	0.5	23.4	0.3	0.0	0.0	0.0	98.1
GA108-2-1	Bl-Gr	MG	41.3	0.3	17.1	0.5	6.7	11.7	0.3	18.4	1.2	0.4	0.0	0.0	98.0
GA108-2-2c	Bl-Gr	MG	42.2	0.3	16.1	0.4	7.2	11.5	0.3	18.1	1.3	0.4	0.0	0.1	97.9
GA108-2-2r1	Bl-Gr	MG	42.1	0.1	17.1	0.4	11.0	11.9	0.3	12.6	1.6	0.1	0.0	0.0	97.2
GA108-2-2r2	Bl-Gr	MG	45.1	0.0	13.9	0.2	10.2	11.6	0.3	15.1	0.9	0.1	0.0	0.0	97.3
GA108-2-3	Bl-Gr	MG	42.0	0.3	15.8	0.0	7.5	11.6	0.3	18.2	1.4	0.4	0.0	0.1	97.6
GA108-2-4c	Bl-Gr	MG	41.7	0.3	17.6	0.3	6.7	11.6	0.3	18.2	1.3	0.5	0.0	0.1	98.7
GA108-2-4r	Bl-Gr	MG	41.5	0.4	17.2	0.3	7.0	11.5	0.3	17.7	1.5	0.4	0.0	0.0	97.7

Oxides are in wt.%. FeOt = FeO total. MB: metabasalt, MMN: Main Mass SIC norite, MG: metagabbro, NI:norite inclusions (NI) in massive sulfide ore.

Appendix B. Electron Microprobe Analyses of Plagioclase

Electron microprobe analyses of plagioclase in Garson metabasalt, Main Mass SIC norite, metagabbro, and norite inclusions in massive sulfide ore. The analyses were obtained using a Cameca SX-100 electron probe microanalyzer equipped with WDS detectors in the Ontario Geoscience Laboratories in Sudbury. Operating conditions were 20 kV accelerating voltage and 20 nA beam current. Dave Crabtree helped with the analyses.

Appendix B

Sample Label	Rock Type	SiO_2	TiO_2	Al_2O_3	MgO	CaO	MnO	FeOt	SrO	BaO	Na_2O	K_2O	Total
GA-101-1-1c	MB	62.4	0.0	23.3	0.0	5.0	0.0	0.3	0.1	0.0	8.8	0.1	100.0
GA-101-1-1r	MB	61.8	0.0	23.8	0.0	5.3	0.0	0.3	0.2	0.0	8.7	0.1	100.2
GA-101-1-2c	MB	61.5	0.0	24.1	0.0	5.8	0.0	0.4	0.1	0.0	8.3	0.1	100.5
GA-101-1-3a	MB	62.5	0.0	23.6	0.0	5.2	0.0	0.3	0.1	0.0	8.7	0.1	100.4
GA-101-1-3b	MB	66.5	0.0	20.2	0.0	1.6	0.0	0.4	0.0	0.0	10.8	0.1	99.6
GA-101-5-1c	MB	62.0	0.0	23.6	0.0	5.2	0.0	0.2	0.1	0.0	8.7	0.1	100.0
GA-101-3-1	MB	62.6	0.0	23.4	0.0	5.1	0.0	0.4	0.1	0.0	8.8	0.1	100.4
GA-101-3	MB	62.6	0.0	23.3	0.0	5.0	0.0	0.3	0.0	0.0	8.9	0.1	100.1
GA-101-3	MB	62.1	0.0	23.6	0.0	5.2	0.0	0.2	0.0	0.0	8.8	0.1	100.0
GA-101-7-1	MB	62.2	0.0	23.7	0.0	5.4	0.0	0.3	0.1	0.0	8.6	0.1	100.5
GA-101-7-2a	MB	62.4	0.0	23.5	0.0	5.2	0.0	0.3	0.1	0.0	8.8	0.1	100.4
GA-101-7-2b	MB	64.6	0.0	22.0	0.0	3.5	0.0	0.4	0.1	0.0	9.7	0.0	100.5
GA-161-12-1	MMN	54.0	0.0	28.6	0.0	11.1	0.0	0.1	0.2	0.0	5.0	0.2	99.2
GA-161-12-2c	MMN	55.7	0.0	27.0	0.3	9.3	0.0	0.4	0.2	0.1	5.4	0.9	99.3
GA-161-12-2r	MMN	58.9	0.0	25.6	0.0	7.6	0.0	0.3	0.1	0.0	7.3	0.1	100.0
GA-161-4-1c	MMN	53.5	0.1	28.9	0.0	11.6	0.0	0.2	0.1	0.0	4.9	0.1	99.4
GA-161-4-1i	MMN	57.2	0.0	26.6	0.0	9.1	0.0	0.1	0.2	0.0	6.5	0.1	99.9
GA-161-4-1r	MMN	64.6	0.0	22.2	0.0	3.7	0.0	0.2	0.2	0.0	9.8	0.0	100.8
GA-161-5-1c	MMN	54.2	0.0	28.5	0.0	11.1	0.0	0.3	0.2	0.0	5.2	0.1	99.6
GA-161-5-1r	MMN	55.2	0.0	28.0	0.0	10.3	0.0	0.1	0.2	0.0	5.7	0.1	99.7
GA-161-13-1r	MMN	55.1	0.0	28.1	0.0	10.5	0.0	0.2	0.2	0.0	5.5	0.1	99.7
GA-161-13-2c	MMN	53.6	0.0	28.4	0.0	11.5	0.0	0.1	0.1	0.0	5.0	0.1	99.0
GA-161-13	MMN	62.6	0.0	23.3	0.0	4.8	0.0	0.0	0.2	0.0	8.9	0.1	99.9
GA-161-13	MMN	63.2	0.0	22.7	0.0	4.3	0.0	0.0	0.3	0.0	9.2	0.1	99.7
GA-161-6-1c	MMN	55.0	0.0	27.7	0.0	10.5	0.0	0.2	0.1	0.0	5.6	0.1	99.3
GA-161-6-1r	MMN	55.0	0.0	28.1	0.0	10.6	0.0	0.3	0.1	0.0	5.4	0.1	99.6
GA-161-6-2c	MMN	53.5	0.0	28.9	0.0	11.8	0.0	0.3	0.2	0.0	4.8	0.1	99.6
GA-161-6-2r	MMN	54.7	0.0	28.4	0.0	10.2	0.0	0.2	0.2	0.1	5.2	0.5	99.4
GA-104-8-1	NI	60.6	0.0	24.4	0.0	6.2	0.0	0.2	0.3	0.0	8.1	0.0	99.9
GA-104-8-2	NI	46.7	0.0	33.2	0.0	16.9	0.0	0.3	0.2	0.0	1.8	0.0	99.2
GA-104-8-3	NI	45.7	0.0	34.4	0.0	18.0	0.0	0.0	0.1	0.0	1.2	0.0	99.5
GA-104-8-4	NI	45.8	0.0	34.1	0.0	18.0	0.0	0.0	0.0	0.0	1.3	0.0	99.2
GA-104-8-5	NI	60.8	0.0	24.7	0.0	6.5	0.0	0.0	0.2	0.0	8.1	0.0	100.4
GA-104-8-6	NI	60.5	0.0	24.4	0.0	6.1	0.0	0.0	0.2	0.0	8.1	0.0	99.4
GA-104-10b-1	NI	45.2	0.0	34.2	0.0	18.3	0.0	0.1	0.0	0.0	1.0	0.0	99.0
GA-104-10b-2	NI	60.3	0.0	24.7	0.0	6.5	0.0	0.2	0.2	0.0	8.0	0.0	100.0
GA-104-10-1	NI	45.3	0.0	34.4	0.0	18.4	0.0	0.0	0.0	0.0	1.1	0.0	99.2

GA-104-10-2	NI	61.6	0.0	24.1	0.0	6.0	0.0	0.0	0.3	0.0	8.2	0.0	100.3
GA-104-10-3	NI	45.5	0.0	33.7	0.0	16.9	0.0	0.1	0.1	0.0	1.3	0.3	97.9
GA-108-7b-1c	MG	52.6	0.0	29.7	0.0	12.8	0.0	0.1	0.0	0.0	4.3	0.1	99.7
GA-108-7b-1r	MG	51.9	0.0	30.1	0.0	13.1	0.0	0.2	0.0	0.0	4.2	0.1	99.7
GA-108-7b-1r2	MG	49.3	0.0	31.6	0.0	15.3	0.0	0.2	0.1	0.0	2.9	0.0	99.4
GA-108-7b-1r3	MG	64.7	0.0	22.0	0.0	3.4	0.0	0.1	0.1	0.0	9.9	0.1	100.3
GA-108-7b-1r3	MG	61.9	0.0	23.8	0.0	5.4	0.0	0.2	0.1	0.0	8.7	0.1	100.1
GA-108-7b2-2c	MG	52.7	0.0	29.4	0.0	12.3	0.0	0.1	0.1	0.0	4.6	0.1	99.3
GA-108-7b2-2r	MG	53.0	0.0	29.4	0.0	12.3	0.0	0.2	0.1	0.0	4.6	0.1	99.7
GA-108-7b2	MG	48.2	0.0	32.8	0.0	16.2	0.0	0.3	0.1	0.0	2.3	0.0	100.0
GA-108-2-1	MG	60.0	0.1	22.9	0.7	6.3	0.1	2.0	0.1	0.1	8.0	0.1	100.3
GA-108-2-2	MG	58.9	0.0	25.6	0.2	8.0	0.0	0.7	0.0	0.0	7.2	0.0	100.7

Oxides are in wt.%. FeOt = FeO total. MB: metabasalt, MMN: Main Mass SIC norite, MG: metagabbro, NI:norite inclusions (NI) in massive sulfide ore.

Appendix C. Electron Microprobe Analyses of Amphibole and Epidote

Electron microprobe analyses of amphibole and epidote in Garson metabasalt (sample GA 181). The analyses were obtained using a Cameca SX-100 electron probe microanalyzer equipped with WDS detectors in the Ontario Geoscience Laboratories in Sudbury. Operating conditions were 20 kV accelerating voltage and 20 nA beam current. Dave Crabtree helped with the analyses.

Appendix C

Sample #	SiO_2	TiO_2	Al_2O_3	Cr_2O_3	MgO	CaO	MnO	FeOt	NiO	Na_2O	K_2O	F	Cl	Total
1-Amp1-1	38.2	0.2	19.6	0.0	2.5	11.3	0.4	22.7	0.0	0.9	0.8	0.1	0.1	96.8
1-Amp1-2	39.3	0.2	20.3	0.0	2.5	11.6	0.3	22.6	0.0	0.9	0.7	0.0	0.0	98.4
1-Amp1-3	39.1	0.2	20.4	0.0	2.5	11.3	0.3	22.4	0.0	1.1	0.6	0.0	0.1	97.9
1-Amp1-4	39.1	0.2	20.5	0.0	2.4	11.2	0.3	22.4	0.0	1.0	0.7	0.0	0.0	98.0
1-Amp1-5	39.3	0.2	20.6	0.0	2.5	11.4	0.3	22.4	0.0	1.1	0.6	0.0	0.0	98.5
1-Amp2-1	39.3	0.2	20.3	0.0	2.5	11.3	0.3	22.6	0.0	1.0	0.7	0.0	0.0	98.4
1-Amp2-2	39.3	0.2	20.0	0.0	2.5	11.5	0.3	22.9	0.0	1.0	0.7	0.1	0.0	98.6
1-Amp2-3	39.0	0.2	20.5	0.0	2.5	11.5	0.4	22.7	0.0	1.0	0.7	0.0	0.0	98.6
1-Amp2-4	39.1	0.2	19.9	0.0	2.6	11.5	0.3	22.7	0.0	0.9	0.7	0.0	0.1	98.0
1-Amp3	39.4	0.3	20.2	0.0	2.6	11.4	0.3	22.6	0.0	0.9	0.7	0.0	0.0	98.5
1-Amp4-1	38.9	0.2	20.5	0.0	2.5	11.5	0.3	22.5	0.0	1.0	0.7	0.0	0.0	98.1
1-Amp4-2	39.2	0.2	20.1	0.0	2.6	11.5	0.3	22.6	0.0	0.7	0.7	0.0	0.0	97.9
1-Amp4-3	39.1	0.2	20.3	0.0	2.5	11.6	0.3	22.7	0.0	1.0	0.7	0.0	0.0	98.5
1-Amp5	39.2	0.3	20.4	0.0	2.6	11.5	0.3	22.5	0.0	0.9	0.7	0.0	0.0	98.4
1-Amp6-1	38.6	0.2	19.9	0.0	2.5	11.4	0.3	22.3	0.0	0.9	0.6	0.0	0.0	96.8
1-Amp6-2	38.8	0.2	19.8	0.0	2.5	11.4	0.3	22.3	0.0	1.0	0.7	0.0	0.0	97.1
1-Epi1-1	37.9	0.1	27.4	0.0	0.0	23.1	0.2	8.3	0.0	0.0	0.0	0.0	0.0	97.0
1-Epi1-2	38.2	0.0	27.0	0.0	0.0	22.9	0.2	8.9	0.0	0.0	0.0	0.0	0.0	97.2
1-Epi1-3	38.0	0.1	28.3	0.0	0.0	22.6	0.2	7.0	0.0	0.0	0.0	0.0	0.0	96.3
1-Epi1-4	38.5	0.1	27.2	0.0	0.0	22.9	0.1	8.6	0.0	0.0	0.0	0.0	0.0	97.4
1-Epi1-5	38.0	0.1	26.0	0.0	0.0	23.1	0.2	10.0	0.0	0.0	0.0	0.0	0.0	97.4
2-Amp1-1	39.2	0.2	20.5	0.0	2.5	11.3	0.3	22.4	0.0	1.1	0.7	0.0	0.0	98.2
2-Amp1-2	39.1	0.2	20.2	0.0	2.5	11.3	0.3	22.7	0.0	1.0	0.7	0.0	0.1	98.0
2-Amp1-3	39.0	0.4	20.6	0.0	2.5	11.3	0.4	22.6	0.0	1.1	0.7	0.1	0.1	98.7
2-Amp1-4	39.1	0.2	20.0	0.0	2.5	11.4	0.3	23.0	0.0	1.0	0.8	0.0	0.1	98.5
2-Amp1-5	39.2	0.3	20.3	0.0	2.6	11.4	0.3	22.5	0.0	1.0	0.7	0.0	0.0	98.2
2-Amp2-1	38.8	0.2	20.1	0.0	2.5	11.3	0.3	22.6	0.0	1.0	0.7	0.0	0.0	97.7
2-Amp2-2	38.8	0.2	20.3	0.0	2.4	11.4	0.3	22.6	0.0	1.0	0.7	0.0	0.0	97.8
2-Amp2-3	39.0	0.2	20.3	0.0	2.5	11.2	0.3	22.6	0.0	1.0	0.7	0.0	0.0	97.8
2-Amp2-4	38.9	0.2	20.5	0.0	2.5	11.4	0.3	22.5	0.0	1.0	0.7	0.0	0.0	98.1
2-Amp2-5	38.9	0.2	20.6	0.0	2.5	11.4	0.3	22.5	0.0	1.0	0.7	0.0	0.0	98.1
2-Amp2-6	39.4	0.2	19.8	0.0	2.5	11.3	0.3	22.5	0.0	1.0	0.7	0.0	0.1	97.7
2-Amp3-1	38.7	0.2	20.1	0.0	2.4	11.5	0.3	22.7	0.0	1.0	0.7	0.0	0.0	97.7
2-Amp3-2	38.7	0.2	20.3	0.0	2.5	11.4	0.4	22.5	0.0	1.0	0.7	0.0	0.0	97.5
4-Amp1-1	39.4	0.2	20.3	0.0	2.6	11.5	0.3	22.7	0.0	1.0	0.7	0.0	0.0	98.8
4-Amp1-2	39.1	0.2	20.2	0.0	2.5	11.4	0.3	22.4	0.0	0.7	0.7	0.0	0.0	97.6
4-Amp1-3	39.2	0.2	20.3	0.0	2.4	11.4	0.3	22.7	0.0	1.0	0.7	0.0	0.1	98.2
4-Amp2-1	38.8	0.2	20.4	0.0	2.4	11.4	0.3	22.5	0.0	1.0	0.7	0.0	0.0	97.6
4-Amp2-2	38.7	0.2	20.3	0.0	2.3	11.4	0.3	22.7	0.0	1.0	0.7	0.0	0.1	97.7
4-Amp3-1	39.2	0.2	20.8	0.0	2.4	11.3	0.3	22.5	0.0	1.1	0.7	0.0	0.1	98.4
4-Amp3-2	39.2	0.2	20.7	0.0	2.4	11.3	0.3	22.4	0.0	1.0	0.7	0.1	0.0	98.3
4-Amp4-1	39.3	0.2	20.1	0.0	2.5	11.4	0.3	22.8	0.0	1.0	0.7	0.0	0.0	98.3
4-Amp4-2	39.4	0.2	20.4	0.0	2.4	11.4	0.3	22.7	0.0	1.0	0.7	0.1	0.0	98.7
4-Epi1-1	38.6	0.2	28.5	0.0	0.0	23.0	0.3	7.2	0.0	0.0	0.0	0.0	0.0	97.8
4-Epi1-2	38.6	0.2	27.9	0.0	0.0	22.7	0.2	7.6	0.0	0.0	0.0	0.0	0.0	97.2
4-Unk-1	24.2	0.1	21.8	0.0	8.2	0.1	0.4	35.0	0.0	0.0	0.0	0.0	0.0	89.8

Oxides are in wt.%. FeOt = FeO total. Amp: amphibole, Epi: epidote

Appendix D. Electron Microprobe Analyses of Garnet

Electron microprobe analyses of garnet in Garson metabasalt (sample GA 181). The analyses were obtained using a Cameca SX-100 electron probe microanalyzer equipped with WDS detectors in the Ontario Geoscience Laboratories in Sudbury. Operating conditions were 20 kV accelerating voltage and 20 nA beam current. Dave Crabtree helped with the analyses.

Appendix D

Sample #	SiO_2	TiO_2	Al_2O_3	Cr_2O_3	MgO	CaO	MnO	FeOt	Na_2O	K_2O	Total
Gnt1-1	36.5	0.1	20.7	0.01	0.53	8.6	6.1	27.2	0.0	0.0	100
Gnt1-2	36.6	0.1	20.6	0.00	0.57	8.8	6.1	27.2	0.0	0.0	100
Gnt1-3	36.7	0.1	20.7	0.00	0.55	8.7	6.2	27.1	0.0	0.0	100
Gnt1-4	36.6	0.1	20.7	0.00	0.54	8.2	6.6	27.5	0.0	0.0	100
Gnt1-5	36.8	0.1	20.8	0.00	0.55	8.2	6.6	27.2	0.0	0.0	100
Gnt1-6	36.8	0.1	20.7	0.00	0.58	7.2	7.0	28.2	0.0	0.0	100
Gnt1-7	36.7	0.1	20.6	0.01	0.59	7.7	6.8	27.5	0.0	0.0	100
Gnt1-8	36.9	0.1	20.5	0.00	0.54	8.5	6.5	27.1	0.0	0.0	100
Gnt1-9	36.8	0.1	20.7	0.00	0.52	9.6	6.0	26.4	0.0	0.0	100
Gnt1-10	36.8	0.1	20.9	0.01	0.50	9.0	6.1	26.9	0.0	0.0	100
Gnt1-11	36.9	0.1	20.8	0.00	0.56	8.6	6.1	27.3	0.0	0.0	100
Gnt1-12	37.0	0.1	20.7	0.01	0.55	8.9	6.0	27.2	0.0	0.0	100
Gnt1-13	37.0	0.1	20.7	0.00	0.54	8.8	5.9	27.1	0.0	0.0	100
Gnt1-14	36.9	0.1	20.9	0.00	0.52	8.3	6.2	27.4	0.0	0.0	100
Gnt1-15	37.0	0.1	20.8	0.00	0.52	8.5	6.3	27.3	0.0	0.0	100
Gnt1-16	36.9	0.0	20.8	0.00	0.53	8.5	6.2	27.4	0.0	0.0	100
Gnt1-17	37.1	0.1	20.7	0.02	0.51	8.9	6.2	26.8	0.0	0.0	100
Gnt1-18	36.9	0.1	20.8	0.00	0.45	8.9	6.2	27.2	0.0	0.0	100
2-Gnt2-1	36.4	0.1	20.7	0.02	0.53	8.5	6.3	27.3	0.0	0.0	100
2-Gnt2-2	36.8	0.1	20.6	0.00	0.53	9.1	6.0	26.9	0.0	0.0	100
2-Gnt2-3	36.6	0.1	20.8	0.00	0.49	9.0	6.0	26.9	0.0	0.0	100
2-Gnt2-4	36.8	0.1	20.8	0.01	0.52	8.9	6.0	27.1	0.0	0.0	100
2-Gnt2-5	36.7	0.1	20.9	0.02	0.54	8.8	6.1	27.1	0.0	0.0	100
2-Gnt2-6	36.5	0.1	20.9	0.00	0.55	8.6	6.2	27.0	0.0	0.0	100
2-Gnt2-7	37.1	0.1	20.9	0.00	0.53	9.4	6.0	26.6	0.0	0.0	101
2-Gnt2-8	36.7	0.1	20.9	0.01	0.53	8.8	6.1	26.9	0.0	0.0	100
2-Gnt2-9	36.9	0.1	20.7	0.00	0.56	8.7	6.1	27.0	0.0	0.0	100
2-Gnt2-10	36.7	0.1	20.9	0.01	0.53	8.4	6.4	27.2	0.0	0.0	100
2-Gnt2-11	37.0	0.1	20.8	0.00	0.53	8.7	6.1	27.2	0.0	0.0	100
2-Gnt2-12	36.9	0.1	20.9	0.00	0.50	8.3	6.1	27.5	0.0	0.0	100
2-Gnt2-13	37.0	0.1	20.9	0.00	0.53	8.6	6.1	27.1	0.0	0.0	100
2-Gnt2-14	36.9	0.1	21.0	0.00	0.55	8.4	6.1	27.4	0.0	0.0	100
2-Gnt2-15	37.0	0.1	20.8	0.00	0.51	8.2	6.4	27.4	0.0	0.0	100
2-Gnt2-16	36.6	0.1	20.8	0.00	0.54	8.6	6.2	27.2	0.0	0.0	100
2-Gnt2-17	36.3	0.1	20.7	0.00	0.51	8.6	6.2	27.1	0.0	0.0	100
2-Gnt2-18	36.6	0.1	20.7	0.00	0.52	8.6	6.2	27.1	0.0	0.0	100
2-Gnt2-19	36.6	0.1	20.7	0.00	0.53	8.6	6.2	27.3	0.0	0.0	100
2-Gnt2-20	36.8	0.1	20.8	0.01	0.52	9.0	6.0	27.1	0.0	0.0	100
2-Gnt2-21	36.8	0.1	20.7	0.00	0.49	8.8	6.0	27.1	0.0	0.0	100
2-Gnt2-22	36.8	0.3	20.9	0.00	0.55	8.4	6.2	27.4	0.0	0.0	101
2-Gnt2-23	37.1	0.2	20.9	0.00	0.53	8.7	6.1	27.1	0.0	0.0	101
2-Gnt2-24	37.0	0.3	20.8	0.00	0.50	8.8	6.0	27.0	0.0	0.0	100
2-Gnt2-25	37.2	0.3	21.0	0.00	0.52	8.9	6.0	26.9	0.0	0.0	101
4-Gnt1-1	36.9	0.1	20.9	0.00	0.47	9.2	6.3	26.3	0.0	0.0	100
4-Gnt1-2	36.9	0.1	20.9	0.00	0.48	9.2	6.1	26.6	0.0	0.0	100
4-Gnt1-3	37.1	0.1	20.9	0.00	0.51	10.0	5.7	26.3	0.0	0.0	101
4-Gnt1-4	37.0	0.1	21.0	0.00	0.52	9.8	5.7	26.5	0.0	0.0	101
4-Gnt1-5	37.0	0.1	21.0	0.01	0.56	9.1	5.8	27.0	0.0	0.0	101
4-Gnt1-6	36.9	0.1	20.9	0.00	0.54	8.9	5.9	27.0	0.0	0.0	100

4-Gnt1-7	36.7	0.1	20.9	0.00	0.55	8.9	6.0	27.1	0.0	0.0	100
4-Gnt1-8	36.7	0.1	20.8	0.01	0.57	9.2	6.0	26.5	0.0	0.0	100
4-Gnt1-9	36.6	0.1	20.9	0.00	0.51	8.8	6.2	26.9	0.0	0.0	100
4-Gnt1-10	37.0	0.1	20.9	0.00	0.52	9.1	6.2	26.6	0.0	0.0	100
4-Gnt1-11	36.8	0.1	20.8	0.01	0.57	8.7	6.4	27.0	0.0	0.0	100
4-Gnt1-12	36.7	0.1	21.0	0.00	0.54	9.0	6.2	26.7	0.0	0.0	100
4-Gnt1-13	37.0	0.1	20.7	0.00	0.52	9.5	6.1	26.4	0.0	0.0	100
4-Gnt1-14	36.9	0.2	20.8	0.01	0.51	8.9	6.2	26.9	0.0	0.0	100
4-Gnt1-15	36.8	0.3	20.8	0.00	0.51	9.6	6.0	26.1	0.0	0.0	100
4-Gnt1-16	37.1	0.2	20.7	0.00	0.49	10.3	5.7	25.8	0.0	0.0	100
4-Gnt1-17	37.0	0.1	20.8	0.00	0.48	8.9	6.1	26.8	0.0	0.0	100
4-Gnt1-18	36.8	0.1	20.8	0.01	0.51	8.6	6.2	27.0	0.0	0.0	100
4-Gnt1-19	36.9	0.1	20.9	0.00	0.51	9.3	5.8	26.8	0.0	0.0	100
4-Gnt1-20	36.7	0.1	20.6	0.00	0.49	8.6	6.2	27.2	0.0	0.0	100
4-Gnt1-21	36.9	0.1	21.0	0.00	0.49	8.4	6.6	27.1	0.0	0.0	100
4-Gnt1-22	36.9	0.1	20.9	0.01	0.48	8.4	6.8	26.8	0.0	0.0	100
4-Gnt1-23	37.0	0.0	21.0	0.02	0.43	8.4	6.9	26.9	0.0	0.0	101
4-Gnt1-24	36.5	0.2	20.8	0.00	0.53	7.9	6.8	27.6	0.0	0.0	100
4-Gnt1-25	36.8	0.2	20.7	0.00	0.52	8.3	6.7	27.0	0.0	0.0	100

Oxides are in wt.%. FeOt = FeO total. Grt: garnet

Appendix E. Electron Microprobe Analyses of Ilmenite

Electron microprobe analyses of ilmenite in Garson metabasalt (sample GA 181). The analyses were obtained using a Cameca SX-100 electron probe microanalyzer equipped with WDS detectors in the Ontario Geoscience Laboratories in Sudbury. Operating conditions were 20 kV accelerating voltage and 20 nA. Dave Crabtree helped with the analyses.

Appendix E

Sample #	SiO_2	TiO_2	Al_2O_3	Cr_2O_3	Nb_2O_3	MgO	CaO	MnO	FeOt	NiO	Total	Fe_2O_3	FeO	Total
Oxi1-1	0.1	52.3	0.0	0.0	0.1	0.1	0.1	2.2	45.1	0.0	99.9	0.5	44.7	100
Oxi1-2	0.1	52.3	0.0	0.0	0.1	0.1	0.1	2.2	45.0	0.0	99.8	0.4	44.6	100
Oxi1-3	1.4	50.7	0.8	0.0	0.1	0.2	0.4	2.1	44.4	0.0	100.1	0.2	44.2	100
2-Oxi1-1	0.0	51.7	0.0	0.0	0.1	0.0	0.2	2.4	45.1	0.0	99.5	1.4	43.9	100
2-Oxi1-2	0.0	51.8	0.0	0.0	0.1	0.0	0.1	2.4	45.1	0.0	99.5	1.2	44.0	100
2-Oxi2-1	0.1	52.5	0.1	0.0	0.1	0.1	0.1	2.1	45.4	0.0	100.4	0.6	44.9	100
2-Oxi2-2	0.0	52.5	0.0	0.0	0.1	0.0	0.1	2.1	45.4	0.0	100.2	0.6	44.9	100
4-Oxi-1	0.1	51.6	0.0	0.0	0.1	0.0	0.1	1.6	46.0	0.0	99.6	1.6	44.6	100
4-Oxi-2	0.1	51.7	0.0	0.0	0.1	0.0	0.2	1.5	46.0	0.0	99.5	1.5	44.7	100
4-Oxi-3	0.1	52.0	0.0	0.0	0.1	0.0	0.1	1.5	45.9	0.0	99.8	0.9	45.1	100

Oxides are in wt.%. FeOt = FeO total

Appendix F. Electron Microprobe Analyses of Titanite

Scanning electron microscope analyses of titanite in Garson Huronian gabbro (samples GA115 and GA188) and SIC norite (GA187). The analyses were obtained using a Zeiss EVO-50 SEM equipped with EDS detectors in the Ontario Geoscience Laboratories in Sudbury. Operating conditions were 20 kV accelerating voltage, 0.75 nA beam current and 50s count time. Sandra Clarke helped with the analyses.

Appendix F

Sample#	SiO_2	TiO_2	Al_2O_3	Cr_2O_3	MgO	CaO	MnO	FeOt	Total
187-1-rim1	30.75	38.09	1.40	0.00	0.00	28.55	0.00	0.50	99.29
187-1-core 1	30.76	37.88	1.46	0.16	0.00	28.64	0.00	0.37	99.27
187-1-core 2	30.63	38.14	1.51	0.00	0.00	28.68	0.11	0.43	99.50
187-1-rim2	30.58	38.91	1.07	0.00	0.00	28.49	0.00	0.45	99.49
187-2-rim	30.30	38.02	1.36	0.09	0.00	28.25	0.00	0.61	98.63
187-2-core	30.90	38.54	1.22	0.00	0.00	28.57	0.00	0.42	99.65
187-3-rim1	30.62	38.82	1.21	0.00	0.00	28.66	0.00	0.38	99.69
187-3-core1	30.62	38.20	1.37	0.14	0.00	28.77	0.00	0.34	99.45
187-3-core2	30.62	38.44	1.30	0.00	0.00	28.73	0.00	0.31	99.39
187-3-rim2	30.78	38.46	1.42	0.10	0.00	28.75	0.00	0.43	99.93
187-4-rim1	30.86	39.33	1.25	0.00	0.00	28.61	0.00	0.44	100.49
187-4-rim2	31.04	38.54	1.57	0.12	0.00	28.93	0.00	0.47	100.66
187-4-rim3	30.92	38.85	1.20	0.00	0.00	28.75	0.00	0.50	100.22
187-4-rim4	30.92	38.70	1.38	0.00	0.00	28.65	0.00	0.51	100.16
187-5-core	30.67	38.84	1.09	0.00	0.00	28.67	0.09	0.47	99.84
187-5-rim2	30.65	38.75	1.05	0.00	0.00	28.62	0.00	0.53	99.60
187-5-3z	30.48	37.99	1.37	0.09	0.00	28.49	0.11	0.54	99.07
187-6-core1	30.92	38.58	1.31	0.09	0.00	28.45	0.00	0.81	100.16
187-6-core2	30.81	38.13	1.38	0.11	0.00	28.57	0.00	0.83	99.84
187-7-rim	30.62	37.97	1.61	0.15	0.00	28.65	0.00	0.50	99.50
187-7-core	30.49	38.37	1.29	0.11	0.00	28.65	0.00	0.39	99.31
187-8-rim1	30.26	38.45	1.08	0.00	0.00	28.51	0.00	0.36	98.67
187-8-core	30.56	39.02	0.94	0.16	0.00	28.83	0.00	0.26	99.76
187-8-rim2	30.72	38.66	1.22	0.00	0.00	28.83	0.00	0.35	99.77
187-9-rim1	30.23	36.81	1.70	0.00	0.29	26.86	0.00	1.28	97.15
187-9-core	30.78	38.32	1.25	0.00	0.00	28.70	0.00	0.42	99.48
187-9-rim 2	31.32	38.01	1.54	0.00	0.00	28.69	0.00	0.62	100.18
187-10-rim	30.99	38.26	1.41	0.14	0.13	28.31	0.00	0.49	99.72
187-10-core	31.05	38.09	1.58	0.00	0.00	28.74	0.00	0.48	99.95
115-1-rim	30.46	38.96	1.03	0.18	0.00	28.73	0.00	0.46	99.82
115-1-core	30.62	38.29	1.23	0.19	0.00	28.77	0.00	0.44	99.54
115-2-rim	30.35	38.10	1.43	0.27	0.00	28.88	0.00	0.43	99.47
115-2-core	30.55	38.66	1.10	0.12	0.00	28.69	0.00	0.26	99.36
115-3-rim	30.43	38.66	1.09	0.15	0.00	28.52	0.00	0.44	99.29
115-3-core	30.58	38.53	1.39	0.16	0.00	28.70	0.00	0.39	99.75
115-4-rim	30.54	38.69	0.84	0.00	0.00	28.39	0.00	0.41	98.87
115-4-core	30.56	38.54	1.11	0.15	0.00	28.54	0.00	0.39	99.28
115-5-1	30.55	38.26	1.00	0.23	0.00	28.44	0.00	0.40	98.87
115-5-2	30.49	37.97	1.23	0.34	0.00	28.69	0.00	0.29	99.02

115-5-3	30.76	38.12	1.30	0.33	0.00	28.55	0.00	0.36	99.41
115-5-4	30.64	38.87	0.97	0.19	0.00	28.45	0.00	0.32	99.44
115-5-5	30.88	38.73	1.04	0.29	0.00	28.64	0.00	0.44	100.02
115-5-6	30.54	38.76	0.95	0.30	0.00	28.67	0.00	0.50	99.73
115-6-1	30.70	38.58	1.34	0.25	0.00	28.96	0.00	0.50	100.32
115-6-2	30.70	38.03	1.34	0.32	0.00	28.76	0.00	0.60	99.74
115-6-3	30.85	38.16	1.45	0.31	0.00	28.81	0.00	0.63	100.22
115-6-4	30.76	38.23	1.36	0.45	0.00	28.91	0.00	0.55	100.27
115-6-5	30.54	38.59	0.90	0.14	0.00	28.45	0.00	0.49	99.10
115-7-rim-1	30.84	38.29	1.42	0.11	0.00	28.62	0.00	0.54	99.83
115-7-core	31.00	38.35	1.51	0.14	0.00	28.82	0.00	0.36	100.19
115-7-rim-2	30.68	38.56	1.32	0.00	0.00	28.60	0.00	0.37	99.54

Oxides are in wt.%. FeOt = FeO total

Appendix G. Whole Rock Geochemistry - Analytical Procedures

Whole rock sulfide samples were crushed using a small jaw crusher using steel plates with low PGE contents, pulverized using an agate ball mill, and analyzed at the Ontario Geoscience Laboratories in Sudbury using flame atomic absorption spectrometry (AAS) for Ni, Cu, and Ag, WD–XRF for As, Cr, Co, Ti and Pb, solution ICP–AES–open vessel digest for Fe and Zn, solution ICP–MS for Sb, Se, Te, Mo, In, Cd, Sn and Bi, NiS fire-assay with an ICP-MS finish for Au, Pt, Pd, Rh, Ru, and Ir, and infrared absorption for S.

Appendix G

Sample #	Units	L.D.L.	GA003	GA023	GA024	GA025	GA027	GA039	GA040	GA041	GA056	GA098	GA011	GA012
Ore body			**#4**	**#1**	**#1**	**#1**	**#1**	**#1**	**#1**	**#1**	**#4**	**#4**	**#4**	**#4**
Type			**D_1 CB**	**D_1 CB**	**D_1 CB**	**D_1 CB**	**D_1 CB**	**D_1 CB**	**D_1 CB**	**D_1 CB**	**D_1 CB**	**D_1 CB**	**D_2 CB**	**D_2 CB**
Fe	**wt%**	**0.004**	>38	>38	>38	>38	>38	>38	>38	>38	>38	>38	31.6	35.2
Ni	**wt%**	**0.0006**	3.5	4.3	3.8	5.4	4.5	5.0	4.6	4.0	4.2	4.2	2.6	3.5
Cu	**wt%**	**0.0003**	0.45	0.74	2.24	0.54	0.90	0.15	0.63	1.42	0.21	0.24	0.84	0.37
S	**wt%**	**0.01**	33.4	36.6	35.1	37.4	37.7	38.9	36.4	34	37.7	34.5	25.8	31.9
Ag	**ppm**	**2**	6	8	14				7	9	4		5	5
Au	**ppb**	**0.22**	6	39	38	9	32	11	3	54	28	3	20	18
Ir	**ppb**	**0.01**	259.30	48.27	175.57	82.34	100.68	167.45	85.97	85.56	39.71	362.70	10.11	157.16
Pd	**ppb**	**0.12**	29	1372	114	28	462	102	106	403	157	33	185	108
Pt	**ppb**	**0.17**	259.5	718.5	513.5	157.1	322.3	248.9	461.2	445.3	132.9	634.2	1700.6	914.3
Rh	**ppb**	**0.02**	565.5	392.4	430.6	234.2	282.6	469.3	414.0	416.6	76.5	1019.4	56.2	557.7
Ru	**ppb**	**0.08**	586.58	102.66	308.56	126.04	168.46	261.65	172.25	207.53	77.15	1222.23	11.27	437.45
Cr	**ppm**	**4**	454	101	356	86	165	208	306	238	624	997	208	596
Co	**ppm**	**6**	717	1272	916	1400	1144	1364	1213	988	1400	935	490	700
Zn	**ppm**	**4**	71	89	134	139	287	85	59	114	42	65	156	84
Pb	**ppm**	**3**	3	8	10	18	34	8	24	33	4	8	3	3
As	**ppm**	**1**	13	1448	8				4	4	1		6	18
Sb	**ppm**	**0.06**	<0.06	0.59	0.08	<0.06	0.13	<0.06	0.14	0.16	0.13	<0.06	<0.06	<0.06
Se	**ppm**	**0.4**	48	83	73	65	74	62	64	61	55	27	55	43
Te	**ppm**	**0.01**	1.3	3.4	3.8	1.4	2.9	3.1	2.0	2.4	3.0	1.4	3.6	2.4
Mo	**ppm**	**0.03**	1.9	2.8	3.8	2.1	3.0	3.1	3.0	3.4	1.9	2.9	1.3	1.3
Bi	**ppm**	**0.01**	1.4	2.8	4.1	2.9	4.0	2.9	3.6	4.5	5.7	1.6	2.9	2.9

Sample #	**Units**	**L.D.L.**	**GA014**	**GA037**	**GA093**	**GA120**	**GA121**	**GA123**	**GA184**	**GA015**	**GA047**	**GA049**	**GA070**	**GA071**
Ore body			**#4**	**#1**	**#1**	**#1**	**#4**	**#1**	**#1**	**#1**	**#4**	**#4**	**#4**	**#4**
Type			**D_2 CB**	**D_2 CB**	**D_2 CB**	**D_2 CB**	**D_2 CB**	**D_2 CB**	**D_2 CB**	**D_2 FB**	**D_2 FB**	**D_2 FB**	**D_2 FB**	**D_2 FB**
Fe	**wt%**	**0.004**	37.2	>38	>38	>38	>38	>38	>38	>38	>38	>38	>38	>38
Ni	**wt%**	**0.0006**	3.0	4.4	4.3	5.5	8.1	5.8	7.5	4.3	5.2	2.9	4.1	3.2
Cu	**wt%**	**0.0003**	1.14	0.31	0.69	0.35	1.34	0.45	0.14	2.52	0.41	0.23	0.34	1.27
S	**wt%**	**0.01**	30.1	36.9	34.6	33.9	31.9	31.2	34.8	37.9	33.7	30.6	34.5	31.9
Ag	**ppm**	**2**	7	6	5	5	7	8	5	17	6			7
Au	**ppb**	**0.22**	9	4	9	3	90	15	2	52	100	44	45	93
Ir	**ppb**	**0.01**	76.90	88.27	40.86	183.00	177.00	67.30	111.00	147.75	140.00	122.03	64.33	169.15
Pd	**ppb**	**0.12**	61	133	77	23	48	422	229	69	159	289	564	80
Pt	**ppb**	**0.17**	313.5	279.0	403.5	441.0	621.0	599.0	93.1	832.4	871.7	385.4	552.1	235.5
Rh	**ppb**	**0.02**	326.5	360.4	197.9	448.0	395.0	198.0	373.0	423.5	385.8	133.9	136.4	460.6
Ru	**ppb**	**0.08**	178.76	87.34	56.84	275.00	290.00	90.00	146.00	350.64	242.35	227.78	126.67	470.32
Cr	**ppm**	**4**	295	67	156	197	298	125	137	324	160	151	89	290
Co	**ppm**	**6**	524	1041	1091	1197	1223	1043	1194	811	1282	730	1132	729
Zn	**ppm**	**4**	124	52	96	63	110	60	61	213	74	149	105	170
Pb	**ppm**	**3**	6	9	9	7	10	16	4	15	3	9	3	3
As	**ppm**	**1**	28	2	8	10	10	26	27	7	29			11
Sb	**ppm**	**0.06**	0.06	<0.06	0.06	<0.06	0.07	0.13	0.08	0.13	<0.06	0.23	0.17	0.08
Se	**ppm**	**0.4**	47	98	79	74	55	85	74	56	73	60	74	44
Te	**ppm**	**0.01**	2.0	5.1	5.1	2.8	3.0	3.9	1.9	3.8	3.2	4.5	3.8	2.7
Mo	**ppm**	**0.03**	1.6	3.5	2.9	4.2	3.4	3.0	4.5	2.7	1.4	1.3	1.3	1.6
Bi	**ppm**	**0.01**	1.8	4.9	5.0	3.5	3.1	3.9	2.3	4.1	3.0	4.5	4.2	2.1

Sample #	**Units**	**L.D.L.**	**GA072**	**GA075**	**GA077**	**GA099**	**GA103**	**GA136**	**GA143**	**GA144**	**GA157**	**GA158**	**GA170**	**GA205**
Ore body			**#4**	**#4**	**#1**	**#4**	**#4**	**#4**	**#4**	**#4**	**#4**	**#4**	**#1**	
Type			**D_2 FB**	**D_2 FB**	**D_2 FB**	**D_2 FB**	**D_2 FB**	**D_2 FB**	**D_2 FB**	**D_2 FB**	**D_2 FB**	**D_2 FB**	**D_2 FB**	**D_2 FB**
Fe	**wt%**	**0.004**	>38	>38	>38	>38	23.4	>38	31.5	31.5	>38	36.4	>38	>38
Ni	**wt%**	**0.0006**	3.7	3.7	2.8	4.2	1.9	5.3	2.4	3.1	3.2	3.4	5.1	4.8
Cu	**wt%**	**0.0003**	0.42	0.45	0.72	0.51	0.88	0.06	0.86	0.78	0.82	0.27	1.02	0.13
S	**wt%**	**0.01**	32.7	35.3	33.3	33.9	11.7	32.6	20.4	20.6	27.2	25.8	31.1	39
Ag	**ppm**	**2**	7	7	8	6	8	5	7	6	11	5	9	4
Au	**ppb**	**0.22**	11	32	38	91	70	1	43	46	85	19	13	18
Ir	**ppb**	**0.01**	93.73	51.42	106.01	34.97	74.51	258.00	96.50	14.30	118.00	74.70	90.70	239.00
Pd	**ppb**	**0.12**	245	110	463	156	143	26	588	108	2754	2772	315	776
Pt	**ppb**	**0.17**	1171.3	883.6	535.5	796.1	904.1	220.0	498.0	686.0	641.0	658.0	755.0	3592.0
Rh	**ppb**	**0.02**	346.9	93.5	296.6	122.8	217.0	346.0	159.0	20.7	307.0	208.0	238.0	181.3
Ru	**ppb**	**0.08**	217.10	105.57	194.76	60.92	170.28	586.00	194.00	14.40	248.00	153.00	97.80	546.00
Cr	**ppm**	**4**	140	94	344	87	253	538	866	399	524	243	89	1802
Co	**ppm**	**6**	861	860	554	1002	467	1081	770	766	1400	1400	1114	1400
Zn	**ppm**	**4**	81	94	74	90	158	46	196	83	133	190	97	51
Pb	**ppm**	**3**	6	4	6	7	4	9	3	12	21	13	4	107
As	**ppm**	**1**	138	4	15	142	12	19	849	6	3551	3352	8	16
Sb	**ppm**	**0.06**	0.08	<0.06	0.11	0.10	0.07	0.07	0.30	0.11	0.88	0.65	0.06	0.11
Se	**ppm**	**0.4**	66	68	59	79	28	46	48	51	56	51	85	111
Te	**ppm**	**0.01**	3.3	3.0	2.1	4.7	2.6	2.7	2.6	5.1	3.2	2.4	5.7	13.8
Mo	**ppm**	**0.03**	1.0	1.9	2.9	1.3	0.5	2.7	0.7	0.8	2.4	1.7	3.4	7.3
Bi	**ppm**	**0.01**	3.5	2.4	2.7	5.0	3.0	2.6	3.6	7.4	4.6	2.8	5.7	7.7

Sample #	Units	L.D.L.	GA085	GA086	GA087	GA182	GA183	GA204	GA018	GA048	GA146	GA145	GA150	GA019
			#4	#4	#4	#1	#1	MMN	#4	#4	MMN	MMN	MMN	#4
Type			D_2 FB	D_2 FB	D_2 FB	D_2 FB	D_2 FB	U DS	D_1 DS	D_1 DS	D_1 DS	D_1 DS	D_1 DS	D_2 DS
Fe	**wt%**	**0.004**	20.1	23.6	23.4	>38	30.3	15.9	10.6	14.4	30.9	10.8	11.5	17.2
Ni	**wt%**	**0.0006**	0.9	0.8	1.5	4.9	3.9	1.0	0.7	0.9	3.2	0.4	0.4	1.5
Cu	**wt%**	**0.0003**	2.45	10.54	7.12	1.43	13.08	2.46	0.39	0.40	1.03	0.31	0.28	1.89
S	**wt%**	**0.01**	11	27.9	27.7	32	26.6	9.02	4.16	7.11	21.1	2.78	2.6	11.1
Ag	**ppm**	**2**	13	44	30	16	>50	15	5	6	9	4	4	11
Au	**ppb**	**0.22**	18	49	39	415	847	131	42	13	205	44	59	64
Ir	**ppb**	**0.01**	75.47	80.93	34.32	31.30	9.81	35.00	10.40	7.63	17.50	19.70	6.91	48.10
Pd	**ppb**	**0.12**	103	67	160	1091	11916	351	20	34	74	144	99	247
Pt	**ppb**	**0.17**	487.6	595.9	1884.7	1040.0	1856.0	746.0	109.0	93.5	822.0	317.0	127.0	193.0
Rh	**ppb**	**0.02**	117.7	165.3	121.1	134.0	72.0	58.3	18.0	34.7	29.9	33.4	13.5	86.7
Ru	**ppb**	**0.08**	124.97	139.97	69.99	35.50	12.40	90.30	15.20	38.52	26.50	30.80	9.47	80.40
Cr	**ppm**	**4**	292	201	105	65	65	272	566	549	630	278	835	228
Co	**ppm**	**6**	273	261	375	779	1400	262	181	265	735	126	165	858
Zn	**ppm**	**4**	323	785	751	215	877	651	119	108	169	83	132	170
Pb	**ppm**	**3**	7	8	8	21	52	73	13	11	16	18	9	30
As	**ppm**	**1**	49	3	4	517	4000	1	8	2	1	1	3	4000
Sb	**ppm**	**0.06**	0.10	0.14	0.11	0.83	>50	0.13	0.14	0.08	0.10	0.09	0.11	9.72
Se	**ppm**	**0.4**	23	43	45	156	109	25	9	12	96	8	6	22
Te	**ppm**	**0.01**	1.2	3.7	3.2	38.4	29.9	2.3	0.8	0.8	14.2	1.1	0.7	2.4
Mo	**ppm**	**0.03**	0.7	0.9	0.7	2.1	3.8	1.5	1.3	1.1	1.3	0.7	0.8	2.1
Bi	**ppm**	**0.01**	0.8	1.4	1.4	38.3	15.3	1.9	1.4	1.3	16.6	1.1	1.4	2.4

Sample #	**Units**	**L.D.L.**	**GA057**	**GA096**	**GA017**	**GA080A**	**GA084**	**GA122**	**GA065**	**GA126**	**GA127**	**GA066**	**GA067**
Ore body			**#4**	**#4**	**#1**	**#1**	**#4**	**#1**	**#4**	**#1**	**#1**	**#4**	**#4**
Type			**D_2 DS**	**D_2 DS**	**Qtz-Cal**	**Qtz-Cal**	**Qtz-Cal**	**Qtz-Cal**	**Qtz-Cal**	**Qtz-Cal**	**Qtz-Cal**	**Qtz-Cal**	**Qtz-Cal**
Fe	**wt%**	**0.004**	13.2	29.0	27.2	24.4	8.2	27.3	11.6	34.1	34.8	32.8	24.6
Ni	**wt%**	**0.0006**	0.7	1.5	1.4	0.2	0.2	0.9	0.2	0.7	1.4	2.6	0.3
Cu	**wt%**	**0.0003**	0.35	3.61	20.51	17.20	4.68	17.00	7.88	25.00	19.07	1.04	20.95
S	**wt%**	**0.01**	6.18	13.6	28.9	25.6	6.83	25.8	11.5	34.5	32.1	27.5	35.6
Ag	**ppm**	**2**	5				26	>50	15	>50	>50	15	>50
Au	**ppb**	**0.22**	33	744	14	32	1511	233	35	36	25	320	58
Ir	**ppb**	**0.01**	5.75	24.47	0.02	0.47	0.03	0.04	0.09	0.03	0.01	4.60	4.69
Pd	**ppb**	**0.12**	29	218	602	1181	543	393	44	123	270	513	332
Pt	**ppb**	**0.17**	106.6	1203.7	0.1	13.9	0.9	3.3	3.3	0.6	0.2	770.8	508.4
Rh	**ppb**	**0.02**	30.7	13.3	0.1	2.4	0.1	17.6	0.8	1.4	1.5	31.7	41.6
Ru	**ppb**	**0.08**	27.31	75.24	<0.08	1.16	<0.08	1.14	<0.08	<0.08	0.15	1.32	1.45
Cr	**ppm**	**4**	525	367	30	31	21	607	41	14	26	120	82
Co	**ppm**	**6**	222	368	213	111	136	241	101	208	617	604	124
Zn	**ppm**	**4**	104	367	1563	915	441	9163	652	1997	1509	220	1400
Pb	**ppm**	**3**	12	24	20	5	5	1388	12	8	39	7	8
As	**ppm**	**1**	5				4	1	4	3	1	50	6
Sb	**ppm**	**0.06**	0.09	0.10	0.22	0.20	0.21	0.64	0.10	0.08	0.30	0.13	0.11
Se	**ppm**	**0.4**	10	100	78	79	21	65	37	104	91	71	86
Te	**ppm**	**0.01**	0.6	39.7	36.8	16.3	6.6	5.5	5.6	14.3	19.4	7.8	9.9
Mo	**ppm**	**0.03**	1.2	1.0	0.6	0.3	0.2	0.8	1.2	0.2	0.5	0.6	0.7
Bi	**ppm**	**0.01**	1.1	>50	16.6	3.5	3.7	3.9	1.8	3.6	3.3	5.1	2.6

Sample #	**Units**	**L.D.L.**	**GA053**	**GA105**	**GA080B**	**GA196**	**GA202**	**GA210**
Ore body			**#4**	**#1**	**#1**	**#600**	**#600**	**#600**
Type			**Qtz-Cal**	**Qtz-Cal**	**VS**	**FW**	**FW**	**FW**
Fe	**wt%**	**0.004**	14.4	25.3	16.1	28.1	29.3	32.0
Ni	**wt%**	**0.0006**	1.1	1.9	0.2	2.1	1.6	4.7
Cu	**wt%**	**0.0003**	0.08	0.07	4.85	11.39	22.22	22.33
S	**wt%**	**0.01**	9.73	28.3	6.26	24.2	34.6	32.5
Ag	**ppm**	**2**	4	8	23	>50	>50	>50
Au	**ppb**	**0.22**	3	61	57	5820	3806	795
Ir	**ppb**	**0.01**	1.03	0.07	31.31	3.84	0.17	3.03
Pd	**ppb**	**0.12**	28	1112	510	22930	3375	8574
Pt	**ppb**	**0.17**	7.3	1.1	1743.0	6780.4	262.9	4292.3
Rh	**ppb**	**0.02**	5.5	0.2	83.2	19.2	9.7	10.7
Ru	**ppb**	**0.08**	6.05	<0.08	38.82	3.02	0.08	0.16
Cr	**ppm**	**4**	26	18	234	237	63	59
Co	**ppm**	**6**	263	542	124	171	250	555
Zn	**ppm**	**4**	19	1207	332	687	2794	1611
Pb	**ppm**	**3**	3	62	7	31	268	17
As	**ppm**	**1**	21	14	178	1480	10	14
Sb	**ppm**	**0.06**	<0.06	0.70	0.19	4.83	0.38	1.21
Se	**ppm**	**0.4**	20	54	20	118	193	217
Te	**ppm**	**0.01**	0.5	12.8	3.5	56.5	99.8	103.3
Mo	**ppm**	**0.03**	0.7	0.2	2.8	1.2	0.5	2.4
Bi	**ppm**	**0.01**	0.2	4.8	1.2	35.5	>50	>50

CB: contact breccia ore, FB: fault breccia ore, DS: disseminated sulfides, Qtz-Cal: quartz-calcite-sulfide vein, VS: vein selvedge, FW: footwall-type ore, L.D.L: lower detection limit.